Guidebook to the Geology of Central Arizona

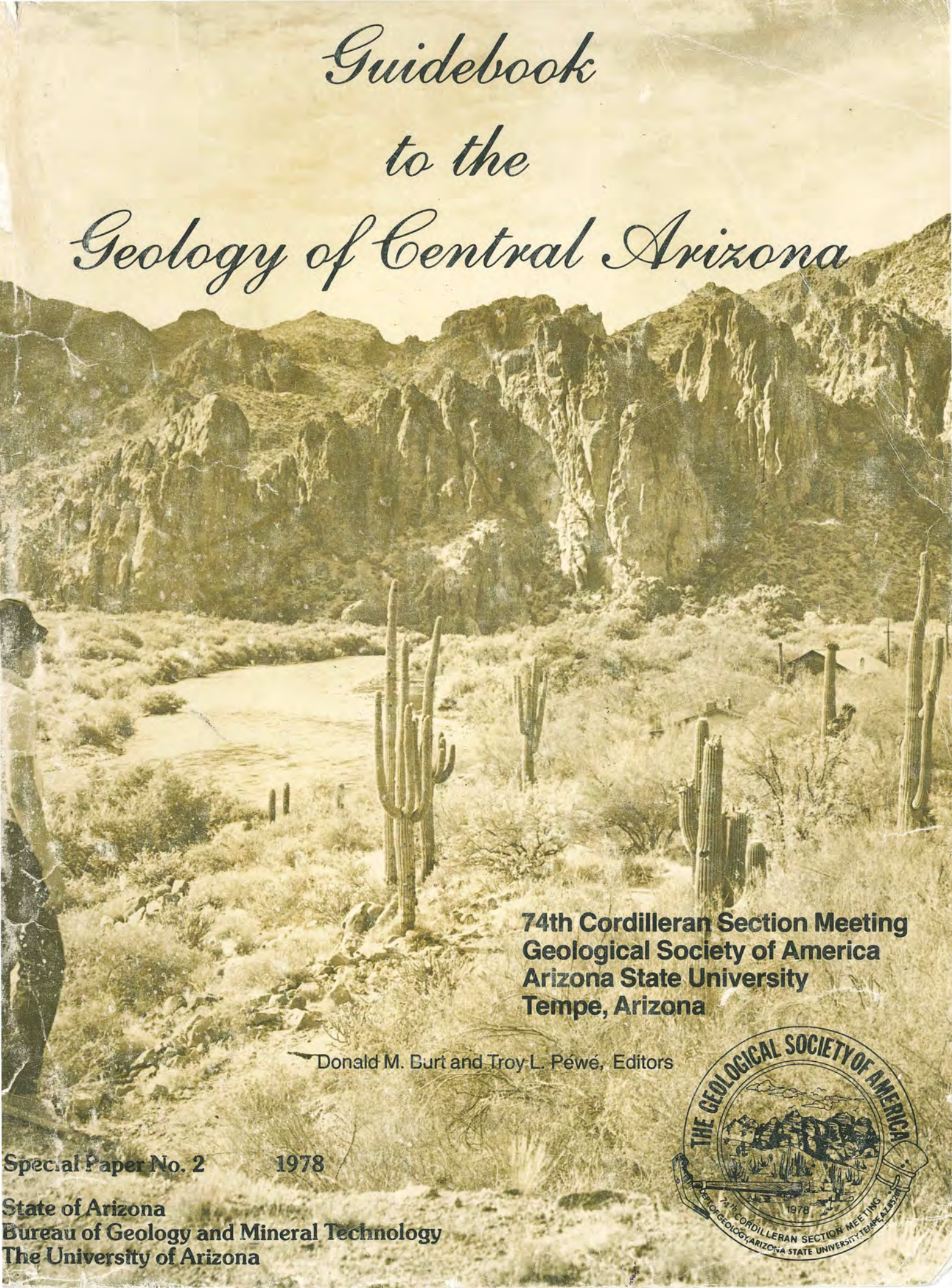

74th Cordilleran Section Meeting
Geological Society of America
Arizona State University
Tempe, Arizona

Donald M. Burt and Troy L. Péwé, Editors

Special Paper No. 2 1978

State of Arizona
Bureau of Geology and Mineral Technology
The University of Arizona

This guidebook, edited for content and style at Arizona State University, Tempe, Arizona, is being printed and distributed by the Bureau of Geology and Mineral Technology as Special Paper No. 2.

This and other publications may be purchased over-the-counter at the distribution center located at 845 N. Park Avenue, Tucson, Arizona. Mail orders will be accepted and should be sent to the following address:

PUBLICATIONS
BUREAU OF GEOLOGY AND MINERAL TECHNOLOGY
845 N. PARK AVENUE
TUCSON, AZ 85719

Remittance in the form of check or money order payable to the Bureau of Geology and Mineral Technology, must accompany all publication orders. (Stamps will not be accepted.)

In addition to the cost of the publication A HANDLING CHARGE OF 10 PERCENT OF THE ORDER WILL BE CHARGED, and should be included with the remittance.

Payment in U.S. currency is required on all foreign orders and additional charges will be made to cover foreign postage.

PRICE $6.00

RECEIVED
FEB 4 1981
STRUCTURES SECTION

Cover Photograph. View downstream of Salt River with Goldfield Mountains composed of Tertiary volcanic rocks in distance. Near Stewart Mountain Dam, 30 km east of Phoenix, Arizona. (Photograph No. 2886 by Troy L. Péwé, June, 1969.)

Frontispiece. Detail of alligator-bark juniper. Excellent indicator of semiarid environment on edge of pine forest in Arizona. North edge of White Mountains 5 miles south of Eager, Apache County, Arizona. Photograph by Troy L. Péwé, February 13, 1976.

Guidebook to the Geology of Central Arizona

Donald M. Burt and Troy L. Péwé, Editors
Department of Geology, Arizona State University

1978

Special Paper No. 2

State of Arizona
Bureau of Geology and Mineral Technology

The University of Arizona

Material contained in this Special Paper may be quoted or reproduced without special permission provided appropriate acknowledgment is given to the source.

CONTENTS

Page

1. **Terraces of the Lower Salt River Valley in Relation to the Late Cenozoic History of the Phoenix Basin, Arizona.** *Troy L. Péwé* 1
   Geology field trip log along the Lower Salt River, Arizona from Tempe Butte, Tempe to Saguaro Lake and return 14

2. **Geology of the Pinacate Volcanic Field.** *James T. Gutmann and Michael F. Sheridan* 47
   Road log and stop guide 49

3. **Lithium Pegmatites of the White Picacho District, Maricopa and Yavapai Counties, Arizona.** *David London and Donald M. Burt* 61
   Road log and stop guide 66

4. **Precambrian Pike's Peak Iron-Formation, Central Arizona.** *Roger M. Slatt, Greta M. Heintz, Patrick H. Lowry, and Patrick F. O'Hara* 73

5. **The Sacaton Porphyry Copper Deposit.** *Robert R. Cummings* 83

6. **The Superstition Cauldron Complex.** *Michael F. Sheridan* 85
   Road log and stop guide 89

7. **Groundwater Recharge with Sewage Effluent.** *Herman Bouwer* 97
   Road log and stop guide 98

8. **Precambrian Metavolcanic Rocks of the Squaw Peak Area, Maricopa County, Arizona.** *Douglas G. Thorpe and Donald M. Burt* 101
   Road log 104
   Stop guide 105

9. **Earth Fissures and Land Subsidence, Eastern Maricopa and Northern Pinal Counties, Arizona.** *R. H. Raymond, Carl C. Winikka, and R. L. Laney* 107
   Road log and stop guide 109

10. **Geology of the Palo Verde Nuclear Generating Station and Adjacent Areas, Maricopa County, Arizona.** *K. M. Euge, W. R. Lund, and J. D. Scott* 115
    Road log and stop guide 121
    Return log 125
    Appendices 125

11. **Paleozoic Biostratigraphy and Paleontology Along the Mogollon Rim, Arizona.** 131
    Part I. Paleontology of the Naco Formation in the Kohl Range area, Arizona. *Stanley S. Beus and Douglas C. Brew* 131
    Part II. Stratigraphic and paleomagnetic relations between basal Cambrian and Devonian strata in central Arizona. *D. P. Elston and S. L. Bressler* 138
    Part III. Road log from Tempe to Payson and Diamond Point via Highways 87 and 260. *Prepared by Department of Geology, Arizona State University, Tempe, Arizona* 143

12. **Barringer Meteorite Crater, Coconino County, Arizona.** *Eugene Shoemaker, David Roddy, Carleton Moore, and Robert Dietz* 151
    Road log and stop guide 159

13. **The Eruptive Mechanism of the Peridot Mesa Vent, San Carlos, Arizona.** *K. H. Wohletz* 167
    The San Carlos Alkaline Rock Association. *John R. Holloway and Christina Cross* 171
    Road log and stop guide 173

ILLUSTRATIONS

Figures

Article 1

Page

Figure 1. Index map of the Phoenix Basin, Arizona and adjoining areas 2–3
Figure 2. Physiographic diagram of the Phoenix Basin and adjoining areas 4–5
Figure 3. Diagrammatic transverse profile of paired terraces on the Salt River Valley 6
Figure 4. Converging longitudinal profiles of part of the floodplains and terraces of streams entering the Phoenix Basin from adjoining mountains on the north and east 7
Figure 5. Development stages of caliche surrounding the pebbles and cobbles in gravelly sediment 8
Figure 6. Caliche-split boulder of quartzite on gravel surface of Sawik Terrace 9
Interleaf. Meandering lower Verde River downstream 1 km from Bartlett Dam 11
Figure 7. Index map showing location and number of topographic maps of field trip stops, lower Salt River Valley 14
Figure 8. Field trip log map showing locations of stops 1–2 16–17
Figure 9. Field trip log map showing locations of stops 3–6 and 34 18–19
Figure 10. Field trip log map showing locations of stops 7–12 20–21
Figure 11. View downstream (west) of Blue Point Terrace scarp 22
Figure 12. Cumulative-frequency distribution curves for analyses of sediments of modern floodplain and terraces of the lower Salt River Valley 23
Figure 13. Desert pavement study site no. 4 near Thomas and Higley Roads 25
Figure 14. Field trip log map showing locations of stops 13–15 and 27–29 26–27
Figure 15. Granite Reef Dam on the Salt River; CAP siphon construction 28
Figure 16. Field trip log map showing locations of stops 16–21 30–31
Figure 17. Aerial view of the lower Salt River Valley looking south from Lone Creek to Blue Point 32
Figure 18. View upstream (east) of lower Salt River, NE Sec. 2, T. 2 N., R. 7 E. Scarp of Blue Point Terrace on right in middle ground near river 33
Figure 19. Aerial view of Saguaro Lake and Stewart Mountain Dam, looking south 34
Figure 20. Theodore Roosevelt Dam and Roosevelt Lake on the lower Salt River 35
Figure 21. Stewart Mountain Dam and Saguaro Lake on the lower Salt River 36
Figure 22. Field trip log map showing locations of stops 22–26 38–39
Figure 23. Aerial view of lower Verde River Valley looking west-northwest 40
Figure 24. Block diagram showing alluvial and colluvial deposits shed from the McDowell Mountains overlying terrace deposits on the west side of the lower Verde River 41
Figure 25. Cumulative-frequency distribution curves for analyses of sediments of modern floodplain and terraces of the lower Verde River Valley 41
Figure 26. Field trip log map showing locations of stops 29–33 42–43
Interleaf. Apache Lake and volcanic rocks of the Superstition volcanic field 46

Article 2

Figure 1. Pinacate volcanic field. This is a portion of a NASA photograph taken from Apollo 6 48
Figure 2. Sketch map of Crater Elegante 50
Figure 3. Geologic relationships exposed in southeastern walls of Crater Elegante as seen from the center of the crater floor 52–53
Figure 4. Facies map of Elegante surge deposits 54
Figure 5. Measured sections of typical sandwave (E–1B), massive (E–1E) and planar facies (E–1H) 55
Figure 6. Deflation model of cumulative Elegante surge cloud 55
Figure 7. Compaction of massive bed due to degassing 55
Figure 8. Normal faults cutting lower parts of the cinder section in the flank of the cone at stop 1 56
Figure 9. Sketch map of Cerro Colorado 58
Figure 10. Map of radial dunes at Cerro Colorado 59
Interleaf. Landscape of rounded boulders produced by spheroidal weathering of granite in an arid environment 60

Article 3

Figure 1. View of the Red and White Picachos from the west 61
Figure 2. Map showing the distribution of major rock types in the district 62
Figure 3. Reconnaissance geologic map of the field trip area 63
Figure 4. Low angle fault in the Tertiary sedimentary rocks exposed in San Domingo Wash 67
Figure 5. The North Morning Star pegmatite, viewed from the south 67
Figure 6. Geologic map of the North Morning Star pegmatite 68
Figure 7. Cross sections through the North Morning Star pegmatite 68

Figure 8. The White Ridge pegmatite, viewed from the south 69
Figure 9. View looking southwest down Mitchell Wash Canyon 70
Figure 10. The Lower Jumbo pegmatite viewed from above 70
Figure 11. Isometric plate diagram of the Lower Jumbo pegmatite 71
Figure 12. Tourmalinization of host rocks along pegmatite contact, Mitchell Wash Canyon 72

Article 4

Figure 1. Districution of Yavapai Series and iron-formation in central Arizona 73
Figure 2. Geologic map of the Pike's Peak iron-formation and associated lithologies 74
Figure 3. Various views looking at ridges and associated lithologies of iron formation 75
Figure 4. Photographs showing various laminae, ripple-like features on a bedding plane, fault breccia and side view of folded cherty iron oxide 76
Figure 5. Measured stratigraphic section a–f 77
Figure 6. Measured stratigraphic section g–i 78
Figure 7. Six thin sections showing the deformation, metamorphism, and recrystallization of volcanic and sedimentary structures in Pike's Peak iron-formation 79
Figure 8. Model for the origin of the Pike's Peak iron-formation 81

Article 5

Figure 1. Location map, Sacaton porphyry copper deposit 83

Article 6

Figure 1. Distribution of volcanic rocks associated with the Superstition-Superior field 85
Figure 2. Detail of the three principal cauldrons 85
Figure 3. Stratigraphic columns 86
Figure 4. Chemical variation diagrams for volcanic rocks from the Superstition cauldron complex 86
Figure 5. Location map for field trip stops 88
Figure 6. Typical textures in the breccia of First Water 91
Figure 7. Map of the pyroclastic surge facies of the Coronado Mesa vent 94
Figure 8. Sections of planar facies (S–1) and sandwave facies (S–7) of pyroclastic surge deposits at Coronado Mesa 95

Article 7

Figure 1. Schematic of rapid-infiltration project below 23rd Avenue Sewage Treatment Plant 98
Figure 2. Infiltration basin with secondary sewage effluent and well on center dike pumping renovated sewage water from aquifer 99
Figure 3. Schematic vertical cross section of system in Figure 1 99
Figure 4. Wall of gravel pit northeast of infiltration basins showing sand and gravel layers 100

Article 8

Figure 1. Squaw Peak. View from 24th Street and Lincoln Drive, Phoenix 101
Figure 2. Preliminary geologic map of a portion of Squaw Peak Park 102

Article 9

Figure 1. Map showing distribution of Arizona earth fissures 107
Figure 2. Map showing location of stops on field trip 108
Figure 3. Line of holes along the trace of earth fissure at stop No. 1 109
Figure 4. Aerial view of fissure gullies at stop No. 2 110
Interleaf. A large earthcrack located on the south side of Chandler Heights on Hunt Road 1¼ miles east of Powers Road 111
Figure 5. Offset along fissure gully at stop No. 2 112
Figure 6. Deep fissure gully at stop No. 3 112
Figure 7. Extruded well casing at stop No. 4. The bottom of the concrete pad is 12 inches above the ground surface 113
Interleaf. Dr. Donal M. Ragan and Ms. Susan Anderson taking initial measurements between nails driven into asphalt at corner of 76th Street and Albany Street 114

Article 10

Figure 1. Geologic map of the Palo Verde site area 116–117
Figure 2. Stratigraphic chart of the site area 118
Figure 3. Geologic cross sections through the site vicinity 119

Figure 4. Geologic cross section through the southern portion of the PVNGS site to the Arlington basalt flow 120
Figure 5. Isometric block diagrams of the present ground surface, top of Palo Verde Clay and bedrock surface in the plant site area 121
Figure 6. Location map showing route of travel 122
Figure 7. View from stop 1 to the northwest 123
Figure 8. View of borrow pit cut exposing Gila River gravels overlain by the Gillespie basalt flow 124
Figure 9. View of road cut exposing basin-fill sediments which are overlain by the Arlington basalt flow 124
Figure 10. View of road cut adjacent to Wintersburg Road exposing a Tertiary volcanic flow sequence with sedimentary interbeds 125
Figure 11. Generalized tectonic map of Arizona 126
Figure 12. Earthquake epicenter map of Arizona and adjacent areas 128
Interleaf. Spheroidal weathering of coarse-grained granite bedrock in a semiarid environment 130

Article 11

PART I
Figure 1. Selected Paleozoic stratigraphic and fossil localities below the Mogollon Rim, central Arizona 132
Figure 2. Diagrammatic cross section of the Naco Formation in east-central Arizona. Kohl Ranch columnar section is shown in detail 133
Figure 3. Pennsylvania fauna from Kohl Ranch 134–135
Figure 4. Pennsylvania fauna from Kohl Ranch 136–137

PART II
Figure 1. Stratigraphic relations and polarities for basal Cambrian and Devonian strata in central Arizona 139
Figure 2. Equal-area stereographic projection showing mean directions of magnetization for Cambrian and Devonian strata from northern and central Arizona 142

PART III
Figure 1. Stratigraphic section in the Payson area, Arizona 148

Article 12

Figure 1. Sketch geologic map of Canyon Diablo region, Arizona 152
Figure 2. Geologic map of area around Meteor Crater, Arizona 154
Figure 3. Cross sections of Meteor Crater and nuclear explosion craters 155
Figure 4. Diagrammatic sketches showing sequence of events in formation of Meteor Crater 157
Interleaf. Upturned edges of stratified rock on west side of interior of Meteor Crater, Arizona 162
Interleaf. Upturned edges of stratified rock on southwest side of interior of Meteor Crater 165

Article 13

PART I
Figure 1. Location map of Peridot Mesa and road log for the field trip 167
Figure 2. Geologic map of Peridot Mesa area 168
Figure 3. Pyroclastic surge facies map of Peridot Mesa 169
Figure 4. Schematic diagram illustrating the deflation (loss of gas) of a pyroclastic surge with increasing time (distance) from the vent 170
Figure 5. Illustration of four stages of the eruptive history of the Peridot Mesa vent 171

PART II
Figure 1. Location map of alkaline volcanics in the San Carlos area 172

Tables

Article 1
Table 1. Tentative correlation of terraces of streams entering the Phoenix Basin 6
Table 2. Particle size and weight distribution of material at ASU desert pavement site 4 24

Article 3
Table 1. Some minerals from the White Picacho pegmatites 65

Article 4
Table 1. Comparative chemistry of Pike's Peak and other iron-formations 78

Article 6
Table 1. Symbols for map units 87

Article 13
Table 1. Chemical composition of rocks and minerals from the San Carlos area 172

TERRACES OF THE LOWER SALT RIVER VALLEY IN RELATION TO THE LATE CENOZOIC HISTORY OF THE PHOENIX BASIN, ARIZONA

by
Troy L. Péwé

INTRODUCTION

The terraces of the lower Salt River Valley offer fine examples of physiographic features, along with pediments and caliche formation, that illustrate late Cenozoic events in the Phoenix Basin and adjoining mountains. The Phoenix Basin is a term loosely applied to a series of topographical and structural basins in southcentral Arizona extending from the Bradshaw-Mazatzal-Superstition Mountains area on the north and east to the general area of the Hassayampa River on the west and the Buckeye Hills and the Sierra Estrella Mountains on the west and southwest (fig. 1). The basin is interrupted by several small mountain masses such as the Phoenix, South, and White Tank Mountains and the entire complex is part of the Basin and Range Physiographic Province. The area is characterized by fault-block mountains with intervening basins filled with thousands of feet of unconsolidated sediments shed from the mountains.

All major rivers and most other streams entering the basin from the north and east are flanked by sets of paired river terraces, many of which are strath terraces. The terraces range from 10 to 300 feet above the river, and are floored with coarse, rounded river gravel. The writer has examined such terraces along the Agua Fria (Péwé, 1976), New River, Queen Creek, and Gila River near Florence and near Arlington.

He has studied with associates the terraces on the lower Salt and Verde Rivers (Péwé, 1966; 1970; 1971; 1975; Pope, 1974; Pope and Péwé, 1973; Kokalis, 1970, 1971), the adjacent mountains and alluvial fans draining into the Salt and Verde Rivers (Shank, 1973; Shank and Péwé, 1973; Péwé and Shank, 1973; Péwé, 1974; Christenson, Welsch and Péwé, 1975; Cordy, Holway and Péwé, 1977), and also some aspects of dust being deposited into the area and its possible relationship to caliche (Péwé, et al., 1976; Péwé, et al., in press).

RIVER TERRACES

Terraces which typify the important nonparallel sets and which are at right angles to the trend of the mountain range are those mapped eastward from Tempe to Stewart Mountain Dam along the Salt River (figs. 1, 2). Four paired terraces are present (fig. 3). Reconnaissance work indicates that these same terraces extend farther east to Roosevelt Lake. The lowest terrace, named the Lehi Terrace (Péwé, 1971), is only 5 feet above the present river level near Lehi and rises to about 20 feet above the river 15 miles upstream.

A higher terrace, the Blue Point Terrace, grades from 10 to 80 feet above the river between Tempe and Stewart Mountain Dam. It is a dissected strath terrace upstream from the mountain front and is covered with 10 to 20 feet of sand and gravel. The most prominent terrace is the Mesa Terrace (Péwé, 1971), an old, extensively dissected surface extending from Tempe, where it is 10 feet above the river, to near Stewart Mountain Dam where it is 220 feet above the river, and eastward to Roosevelt Dam where it is more than 300 feet above the river (fig. 4). Here is is believed to be truncated by a fault (Péwé, 1975).

The gravel of the Mesa Terrace is strongly indurated by caliche. Unlike the gravel of the younger Blue Point Terrace, which has cobbles slightly cemented, the older gravel is completely plugged by calcium carbonate and well developed laminar layers are formed.

The Sawik Terrace (Péwé, 1971) is the highest terrace, the most fragmentary, and lies 235 feet above the river at the mountain front. It decreases to an elevation of about 50 feet above the river in Scottsdale where it passes under the alluvial fan deposits shed from the Phoenix and McDowell Mountains. The gravel of the terrace is very strongly calichified. Both the Sawik and the Mesa Terraces have thick, well-calichified gravel layers near or at the surface.

The Verde River joins the Salt River near the west edge of the Mazatzal Mountains at the east side of the Phoenix Basin. The trend of the river is not at right angles to the trend of the mountains. Four paired, well-developed terraces are present on the lower Verde River (Pope, 1974; Pope and Péwé, 1973). Detailed work has been done on these terraces, and they are similar to the terraces on the Salt River and also converge downstream.

The Agua Fria River emanates from the north side of the basin near the Hieroglyphic Mountains, flows onto the sloping Phoenix Basin floor near Lake Pleasant Dam, and then trends southward to join the Gila River near the center of the basin (figs. 1, 2). The Agua Fria displays at least three paired terraces (Péwé, 1976) and, especially south from the Lake Pleasant Dam, they are fill terraces composed of coarse boulder gravel. At Lake Pleasant they are strath terraces. The gravels of the upper two terraces are completely plugged with caliche and laminar layers are present. The upper terrace at the dam site is approximately 130 feet above the river. The flights of terraces converge downstream (fig. 4). Although studied only in reconnaissance, it is evident from the amount of calichification, convergence of terraces in the downstream

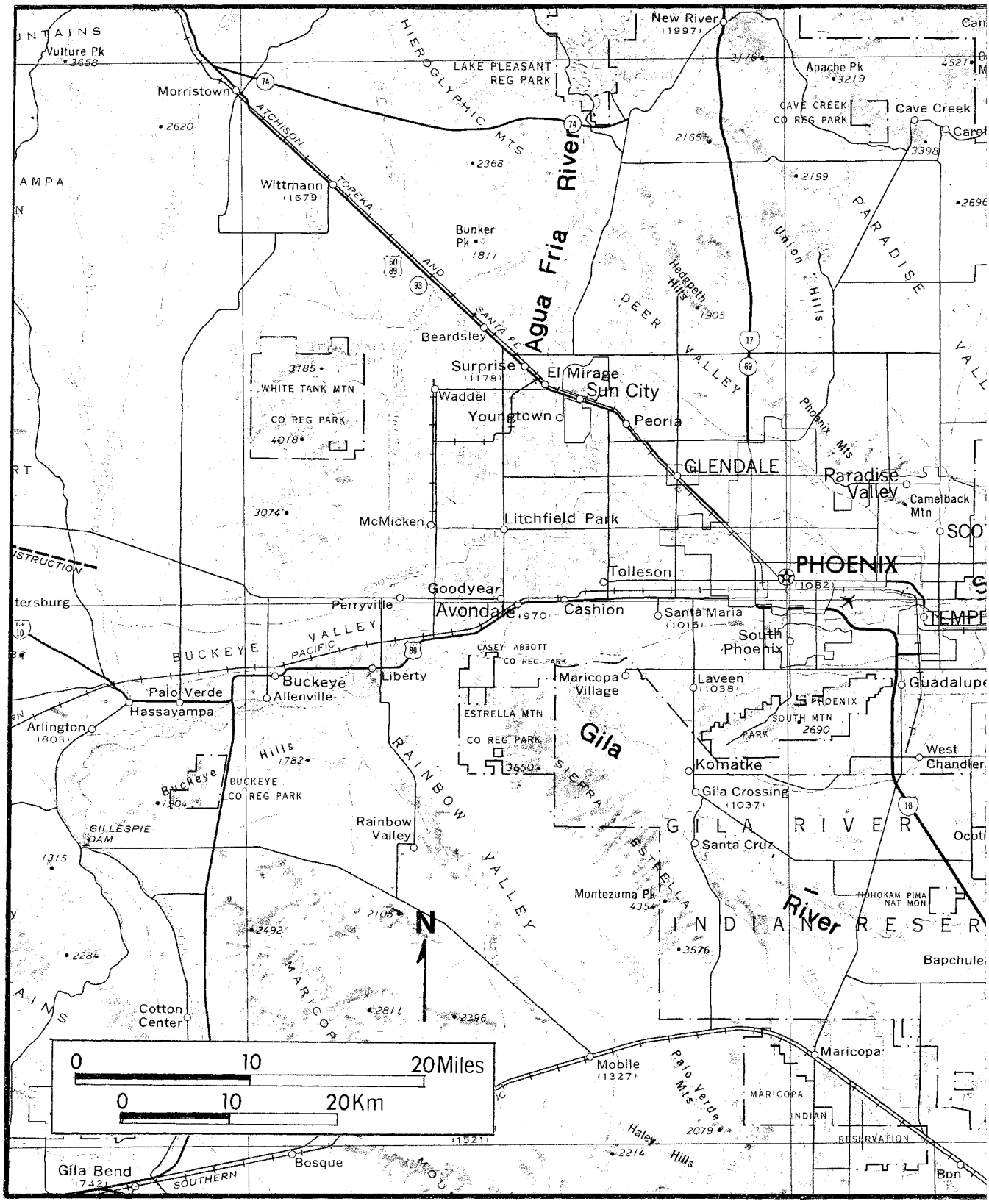

Figure 1. Index map of the Phoenix Basin, Arizona and adjoining areas. (Base from U. S. Geological Survey satellite image map, 1972–1973.)

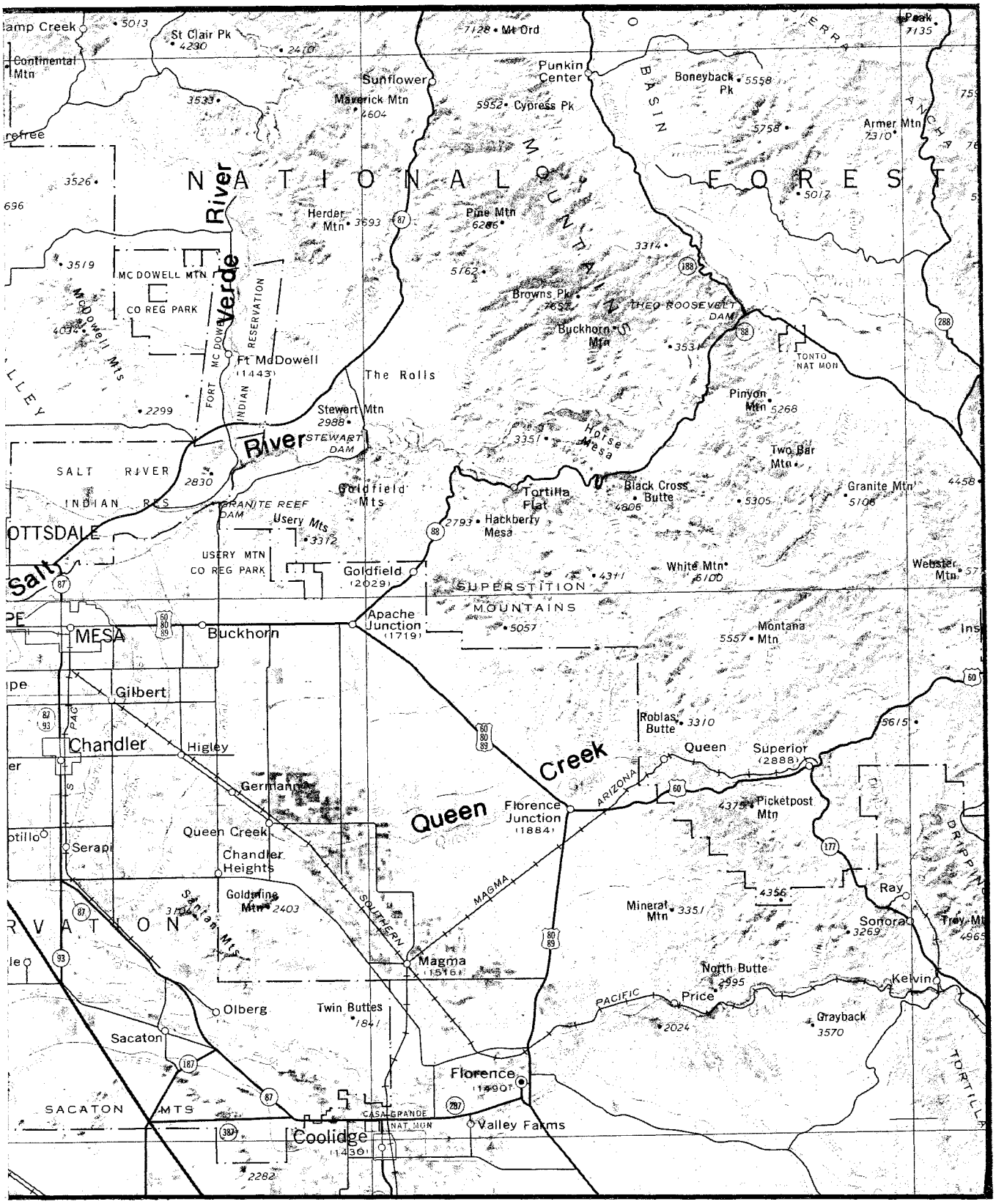
Lamp Creek
St Clair Pk
Continental Mtn
Sunflower
Maverick Mtn
Punkin Center
Cypress Pk
Boneyback Pk
Armer Mtn
NATIONAL FOREST
Verde
River
Herder Mtn
Pine Mtn
MC DOWELL MTN
CO REG PARK
McDowell Mts
Ft McDowell
FORT MC DOWELL INDIAN RESERVATION
The Rolls
Browns Pk
Buckhorn Mtn
THEO ROOSEVELT DAM
TONTO NAT MON
Pinyon Mtn
Stewart Mtn
STEWART DAM
Horse Mesa
Two Bar Mtn
SALT RIVER INDIAN RES
GRANITE REEF DAM
Goldfield Mts
Tortilla Flat
Black Cross Butte
Granite Mtn
Usery Mts
Hackberry Mesa
USERY MTN CO REG PARK
Goldfield
White Mtn
Webster Mtn
Salt
SUPERSTITION MOUNTAINS
Apache Junction
Montana Mtn
MESA
Buckhorn
Gilbert
Chandler
Higley
Roblas Butte
Queen
Superior
Germanna
Queen Creek
Florence Junction
Picketpost Mtn
Queen Creek
Chandler Heights
Goldwing Mtn
Ray
Minerat Mtn
Sonora
Magma
North Butte
Kelvin
Olberg
Twin Buttes
Price
Grayback
Sacaton
Florence
SACATON MTS
CASA GRANDE NAT MON
Valley Farms
Coolidge

Figure 2. Physiographic diagram of the Phoenix Basin and adjoining areas diagrammatically showing sets of converging terraces along river valleys entering the basin. (Base through the courtesy of the Salt River Project, Tempe, Arizona.)

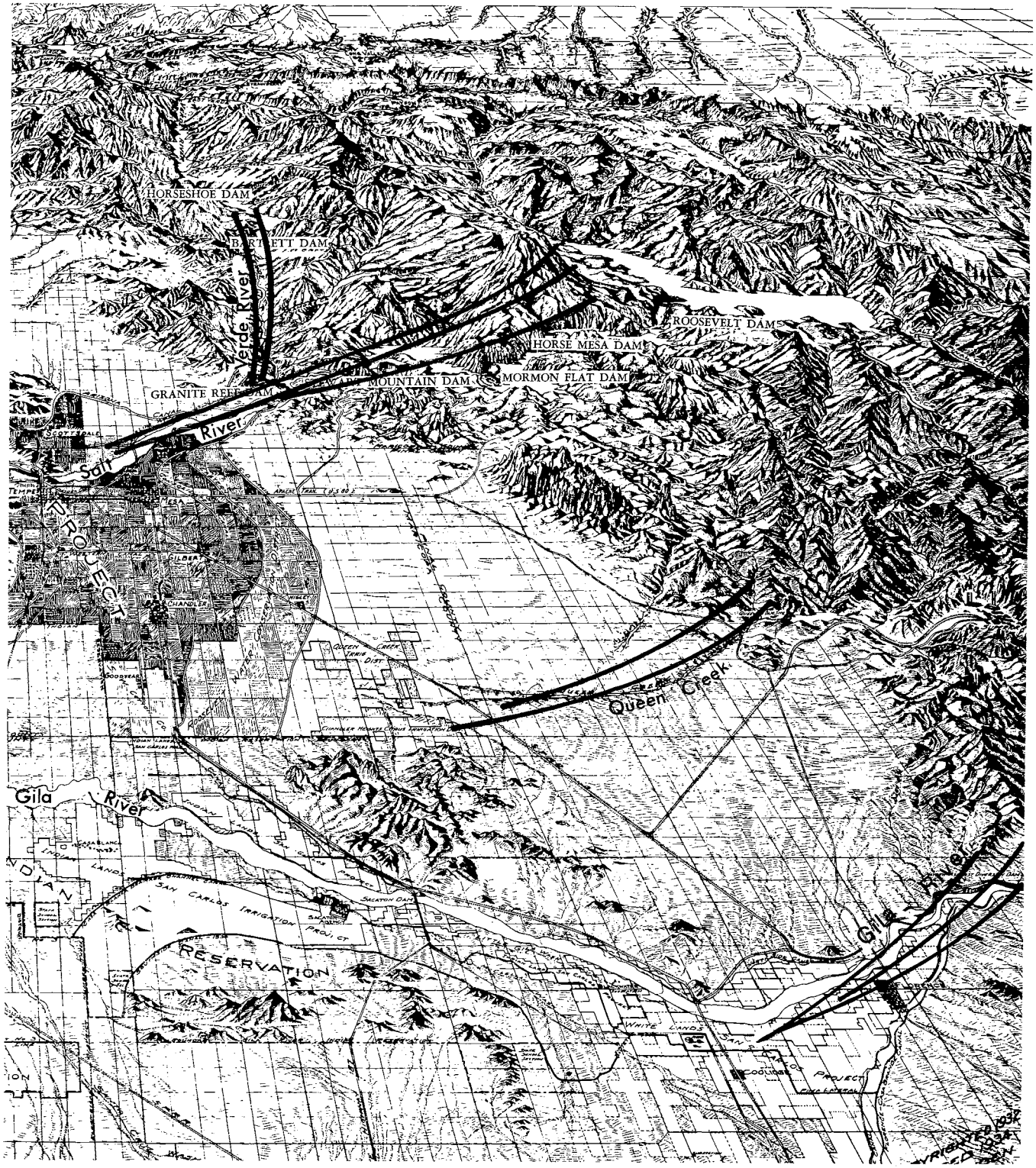
HORSESHOE DAM
BARTLETT DAM
Verde River
ROOSEVELT DAM
HORSE MESA DAM
MORMON FLAT DAM
MOUNTAIN DAM
GRANITE REEF DAM
Salt River
PROJECT
Queen Creek
Gila River
SAN CARLOS IRRIGATION PROJECT
RESERVATION
Gila River

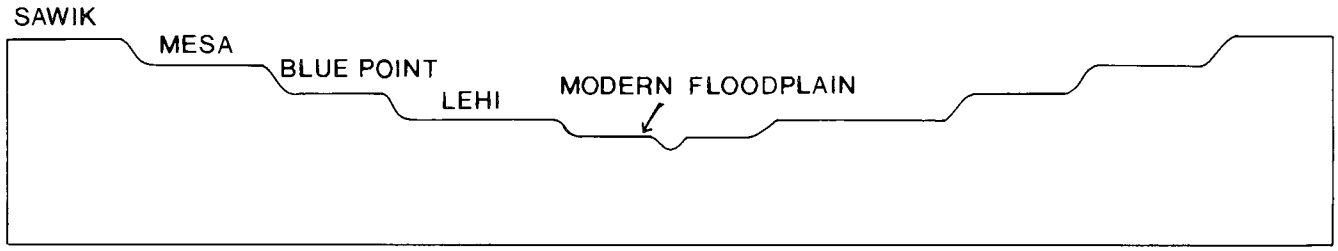

Figure 3. Diagrammatic transverse profile of paired terraces on the lower Salt River Valley.

direction, and size of the gravels that they are very similar to terraces on the lower Verde and lower Salt rivers (table 1). The boulder gravel and rock types from the northern mountains disappear into the center of the basin and only basin-fill silty sediments are exposed in the shallow banks of the river to the south.

Reconnaissance observations on the terraces on New River indicate that high-level strath terraces with gravel 5 to 10 feet thick occur near the village of New River and the terraces converge with the profile of the modern stream downstream. More work is needed to demonstrate existing multiple terraces in this area.

Table 1: Tentative correlation of terraces of streams entering the Phoenix Basin

Agua Fria River	New River	Verde River	Salt River	Queen Creek	Gila River
Péwé, 1973	**This Paper**	**Pope and Péwé, 1973**	**Péwé 1971**	**This Paper**	**This Paper**
Lake Pleasant	Present	"Lousley Hill" Deposit	Sawik	Radio Ridge	1
Landing Field		Mesa	Mesa	Bridge	2
		McDowell			
Canal	?	Blue Point	Blue Point		3
			Lehi		

Prominent converging terraces are displayed on the sides of the Gila River Valley where the river emerges from the mountains into the Phoenix Basin near Florence (fig. 4; table 1). The reconnaissance information available indicates that these terraces converge with the profile of the modern stream to the east (figs. 1, 2; table 1).

About 5 miles northwest of Florence Junction (figs. 1, 2) in the southeastern part of the Phoenix Basin, Queen Creek flows westward from the Superstition Mountains onto the basin floor and disappears in the low land. The creek is flanked by at least two terrace levels that converge with the modern floodplain westward in the valley (figs. 1, 2; table 1). The gravel deposits are strongly indurated with caliche.

These rivers and creeks flow (or used to flow) through the Phoenix Basin but do not exhibit any terraces there except low banks formed where the streams migrate laterally and cut into the alluvial fans composed of Valley Fill material. None of the rock types of the terrace gravels in the mountain edges occur along the Gila, the Salt, and the Agua Fria Rivers toward the west in the basin until in the vicinity of Arlington near the mouth of the Hassayampa River (figs. 1, 2). Here terraces 40 and 80 feet above the modern river are present (Lee and Bell, 1975). The rock types are very similar to those occurring on the Salt River terraces as studied upstream from Tempe and the terrace gravels are extremely well calichified. In the vicinity of Arlington and Gillespie Dam, the terraces are locally covered with basalt flows. From near the mouth of the Hassayampa River to a short distance west of Gila Bend, in the vicinity of Painted Rock Reservoir, the terraces appear parallel to the profile of the modern Gila River.

In the years 1902–1904 Willis T. Lee of the U.S. Geological Survey traveled to the then remote far western region of Phoenix, Arizona to investigate the underground streams and geology of lower Salt River Valley. He was preceded in 1896 by Arthur P. Davis, hydrographer of the U.S. Geological Survey, who studied the growing irrigation district near Phoenix and clearly described it in pioneer Water Supply Paper No. 2 of the U.S. Geological Survey.

Lee traveled the central part of the Phoenix Basin on foot, horse, and wagon as the first geologist to systematically collect geological and hydrological data on all the major wells and most minor wells drilled in the valley. He then studied the geomorphology and investigated the geology of the local bedrock hills and mountains. His classic report, published in 1905, remains the most thorough and accurate report on the subject to date. Later reports are replete with more detailed data on water quantity and quality but the outline presented by Lee is still workable.

From an examination of primitive well records of the time, Lee easily noted that bedrock in the valley was below sea level. Debris shed from the surrounding mountains accumulated in subsiding basins (1905, p. 115). Many "buttes" in the valley are knobs of bedrock projecting above a sea of alluvium. Faulting and block tilting were recognized as important in forming the basic structure of the region.

The coarse-rounded gravel of earlier river times expressed on the edges of the mountains as terrace deposits,

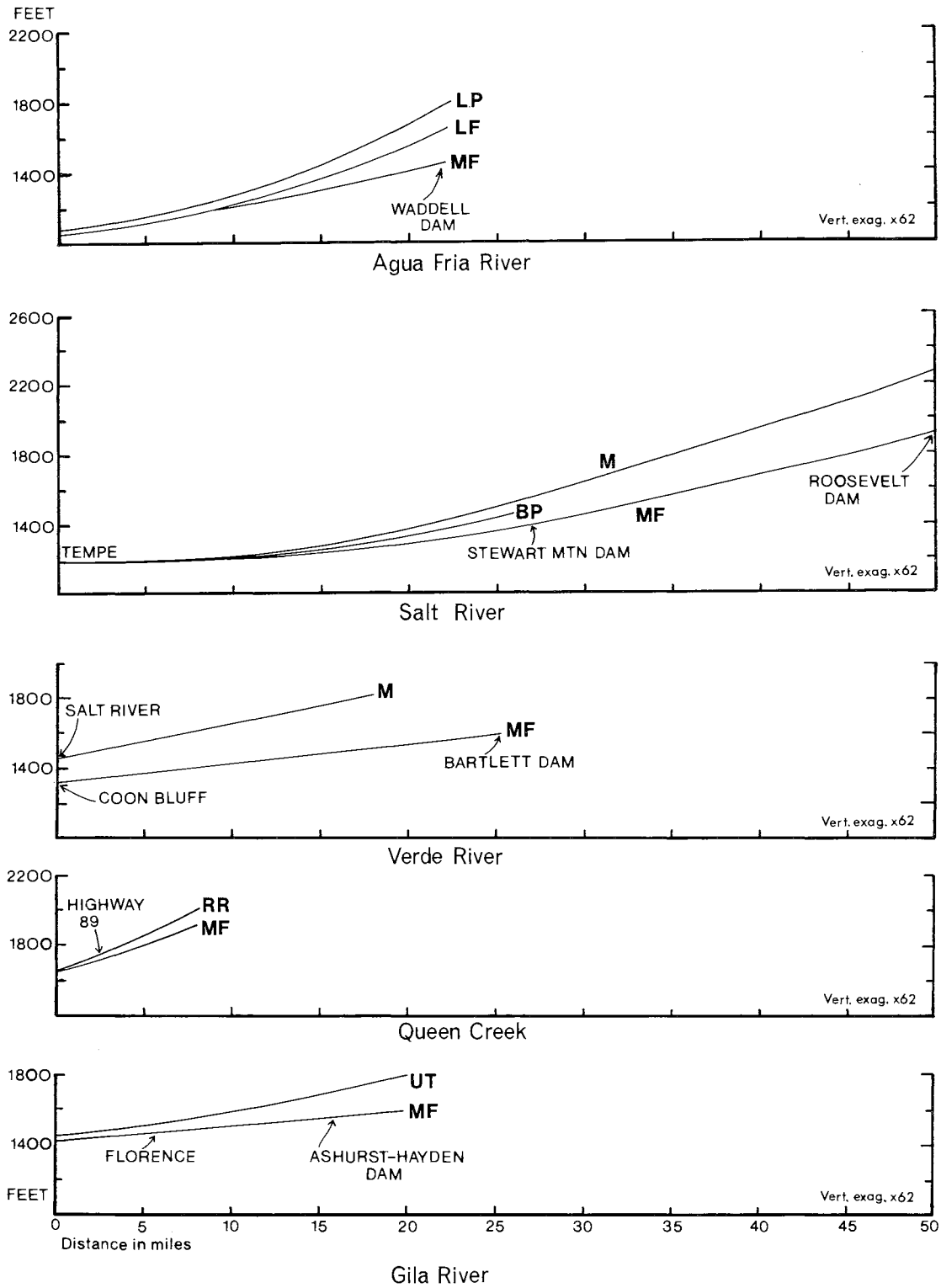

Figure 4. Converging longitudinal profiles of part of the floodplains and terraces of streams entering the Phoenix Basin from adjoining mountains on the north and east. MF—Modern Floodplain; LP—Lake Pleasant Terrace; LF—Landing Field Terrace; UT—Upper Terrace; M—Mesa Terrace; BP—Blue Point Terrace; RR—Radio Ridge Terrace.

disappear into the basin (fig. 4) and are to be found at depth. No clearer report has yet been written on the subject than those by Lee (1904; 1905, p. 125–135) who postulated the ancient Salt River location from gravels that exist to a depth of at least 620 feet (by 1905 records). Lee states,

> "Since it is always the river that is making the deposits of gravel and bowlders through which water passes readily, it naturally follows that the bowlder beds mark the ancient courses of the river. It furthermore follows that the present course of the underflow is in general the course of the ancient river that deposited the gravels and bowlders in which the underflow occurs. It remains, then, to determine the old courses as accurately as possible in order to place the pumping plants in the most advantageous localities. At first thought, this course should be in general down the valley, parallel to the river. But a little reflection indicates that this is not necessarily the case. As the floor of the valley was raised by the deposition of debris, the river shifted from side to side of the valley. When the level of the rising valley floor reached the saddle of some spur or divide, the river might pass over this divide, leaving its former course at one side. This is probably what Salt River has done..."

Drill records indicate that in ancient times (probably Mesa and Sawik Terrace time) the Salt River flowed south through Mesa and joined the Gila River south of South Mountain.

CALICHE

Stream terraces and alluvial fans on the edges of the Phoenix Basin expose sediments cemented by $CaCO_3$–caliche. Caliche is a near-surface accumulation of $CaCO_3$ common to soils of low and middle latitudes in arid and semi-arid regions throughout the world. This "lime" accumulation transforms otherwise unconsolidated sand and gravel to "concrete," much to the disgust of "users of the soil." Although we have no record of the choice language used by ancient man as he hacked irrigation canals with crude implements from the caliche-cemented gravel of the Mesa Terrace, we do know that the first attempt to construct a canal in the Phoenix area by modern man in December of 1867 resulted in failure as red-headed K. W. (Jack) Swilling began construction on the north bank of the Salt River in the hard caliche-cemented colluvium of Papago Pediment opposite the present location of downtown Tempe (Peplow, 1970). He was forced to find a new location 2½ miles downstream at what is now 44th Street and Washington.

Caliche layers form as meteoric water percolates downward into the soil, carrying calcium carbonate in solution, and is stopped and/or drawn upward in its descent by capillary action. In situ evaporation of this water results in precipitation of the calcium carbonate in soil voids. Thus, the permeability of the soil or unconsolidated rock and the amount of rainfall influence the depth of descent of the percolating water, and the depth of caliche development. Climate is a critical factor in caliche development. Hot, dry climates where rainfall occurs in periodic thundershowers followed quickly by renewed sunlight and low humidity promoting evaporation are most favorable. The arid and semi-arid climates of the southwestern United States are extremely conducive to the formation of caliche.

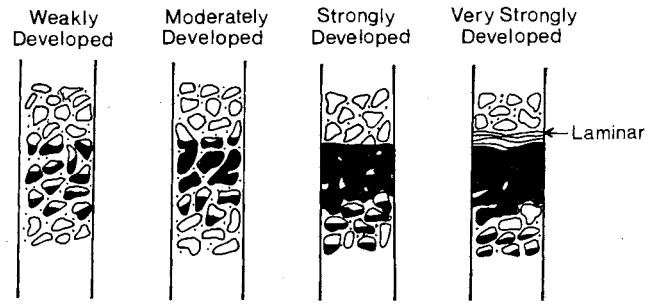

Figure 5. Development stages of caliche surrounding the pebbles and cobbles in gravelly sediment. (After Gile, 1975.)

Caliche deposits in general are sheet-like and form roughly parallel to the ground surface. The deposits undulate with the topography and vary laterally in thickness. These lateral variations in thickness are the result of various factors; including differences in permeability, topography, and nature of the host material.

As illustrated in Figure 5, the caliche layer exhibits a sequence of progressive development with time, beginning as a calcium carbonate coating on the undersides of rock particles (weakly developed). Caliche then builds up and fills in spaces between pebbles as the pebble coatings merge and coalesce (moderately developed), and eventually all interpebble spaces become full and the profile is "plugged," forming a hard, concrete-like layer (strongly developed). This layer is impermeable and will become capped by pure, laminated layers of $CaCO_3$ as water can no longer percolate into the soil (very strongly developed). Thus, in general, the longer the caliche has been forming, the harder and more strongly developed it becomes.

The study of caliche has been extensive throughout the world and detailed work has been done in the southwest United States since the 1920s. Some of the leading papers on the subject are listed in the selected references.

While the general concept is that the $CaCO_3$ is precipitated from rain water moving downward, an older idea is that it was precipitated from ground water moving upward toward and near the surface. The earliest such suggestion for Arizona was by Blake (1901), although Lee (1905) felt that the deposition of caliche from downward-moving water was equally as valid.

The thickness and depth of the caliche profile is thus dependent on the depth of penetration of soil water. Other factors of soil formation include climate, vegetation, topography, age, and parent material. The occurrence of caliche in sediments of various compositions and textures indicates that it is not a primary depositional feature. Caliche deposits progress through a developmental sequence with time, as do soils.

The ultimate source of $CaCO_3$ in caliche in noncarbonate sediments has been a topic of great interest since these occurrences were first observed. In areas of carbonate bedrock or alluvial gravels derived from carbonate bedrock, no real problem is encountered in terms of source. Some of the concepts for noncarbonate rocks include chemical weathering of noncarbonate Ca-bearing parent material with additions of CO_3 from air and rain water, leaching of $CaCO_3$ from dust collected at the surface, and from the accumulation of Ca and CO_3 ions in water.

Over the last few years some observers have suggested an eolian source for the $CaCO_3$. The writer strongly believes in such a source inasmuch as wind-blown dust is quite common and deposited in enormous amounts annually (Péwé, et al., 1976). Analyses of the dust in the Phoenix area based on 15 samples collected over an 18-month period give a percentage of $CaCO_3$ of from 1.2 to 3.8 (Péwé, et al., in press).

Although the details are not completely known, it appears that many of the grains and cobbles and perhaps even boulders in the calichified sand and gravel are in some instances completely surrounded by $CaCO_3$. They float in the matrix of calcite and are not in contact with one another. In most areas the simple fillings of the voids in the parent materials by $CaCO_3$ cannot account for the amount of $CaCO_3$ present. It is believed by many that there is as much as 25% expansion of the unconsolidated sediments with the crystallization of the $CaCO_3$.

A great number of fractured pebbles and cobbles appear on the surface of the older two of the terraces in the Phoenix Basin and on very old alluvial fans (fig. 6). Cobbles on these terraces show postdepositional fracturing in which the $CaCO_3$ apparently invaded previously existing cracks and permeable zones in the cobbles forcing them apart below the surface. Frequently cobbles can be found in place with major cracks revealing as much as 2 inches of separation. This is more normally characteristic of the finer grained rock types. Young (1964) concludes that crystallization forces of $CaCO_3$ which result in a volume increase are responsible, and notes that the role of $CaCO_3$ in the disintegration of bedrock and surface deposits in semi-arid and arid lands may be underestimated.

Figure 6. Caliche-split boulder of quartzite on gravel surface of Sawik Terrace. Near Thomas and Higley Roads, Mesa, Arizona. (Photograph No. 4040 by Troy L. Péwé, September 17, 1977.)

ORIGIN OF THE TERRACES

Of utmost importance to an understanding of the late Cenozoic history of the Phoenix Basin is the origin of the sets of paired river terraces that converge downstream and border the basin on the north and east. The terraces represent periodic rejuvenation of the streams. The increase in the power of the streams and subsequent downcutting could be the result of climatic change (increased runoff) or tectonic disturbance of the mountains and the basins. The uplift of the mountains with concurrent depression of the basins increases the stream gradient. Although the climate must have changed slightly in this area during the Quaternary (the last 1.8 million years), such changes probably would have produced some terraces that would be parallel to the profile of the modern stream. However, the convergence of terraces downstream to the Phoenix Basin strongly suggests periodical regional uplift of the ranges over a long period of time.

Convergence of terraces downstream due to tectonic uplift is not unknown. This phenomenon is widespread and important in interpreting and dating tectonic movements. Convergence has been recorded along the Nanana River in the Alaska Range (Wahrhaftig, 1958), for example. Especially clear is the detailed study on the Rangatiki River in New Zealand by Milne (1973). He illustrates convergence of terraces due to uplift of the mountains where the river originates. Although preliminary studies strongly indicate that these terraces are tectonic in origin, climatic effects may also be involved. Another concept is that as the mountains are worn down the streams have less material to carry and so they begin to cut down more rapidly. This would result in the formation of one set of terraces but it is difficult to illustrate multiple paired terraces unless the system were "rejuvenated," probably by uplift. Until otherwise demonstrated, the convergence of terraces downstream to the Phoenix Basin seems to indicate periodic regional uplift of the ranges in relation to the Phoenix Basin over a long period of time.

AGE OF TERRACES

Of critical interest is the age of terraces and therefore the age and rate of supposed tectonic disturbance. No direct, absolute dating is currently available for the ages of terraces. Fragments of the Geronimo Head Tuff, with a minimum age of 16 million years (Stuckless and Sheridan, 1971), occurs in the Sawik and other terrace gravels on the Salt River; therefore, the terraces flowing through the volcanic area of the Goldfield and Superstition Mountains are less than 16 million years old. A study of the distribution of gravels from ancient drainages from the south that used to flow north to the Colorado Plateau, suggests (McKee and McKee, 1972) that the reversal of the drainage occurred no earlier than 10 million years ago and no later than 5 million years ago. Therefore the terraces could be as old as 5 million years.

Several converging lines of qualitative evidence indicate a great antiquity for these land forms. It is apparent that the upper terraces are very old as indicated by the fragmentary nature of their preservation. For example, evidence of great age is indicated by small remnants of strath terraces on granite just south of the Salt River 1 to 4 miles east of Coon Bluff (Péwé, 1971). These remnants are graded to a pediment that formerly extended from the Usery Mountains and sloped northward to the Mesa Terrace level of the Salt River. Subsequently, the pediment area has regraded to the Blue Point and modern floodplain 220 feet below the Mesa Terrace pediment level. It is not known exactly how long it takes to regrade a granite pediment of about 30 square miles to a level 220 feet lower than in the past, but to remove that much bedrock surely took hundreds of thousands of years, if not more than a million years.

A method not yet pursued in depth but which indicates antiquity of the terraces is the development of taffoni in rocks below the level of the Mesa Terrace. Taffoni are hollows or niches a few inches to many yards long produced in bedrock by cavernous weathering in desert areas (Péwé, 1974, p. 46–48). To form below the level of the Mesa Terrace these hollows had to form after downcutting and destruction of the bedrock floodplain floor that existed in Mesa time. Since it is believed that taffoni form slowly we have another qualitative factor indicating that the upper terraces are quite old.

Some of the best evidence for a great age of the upper terraces is the extensive development of caliche. Caliche is an epigenetic accumulation of calcium carbonate derived from soil processes in unconsolidated sediments in climates where moisture is deficient during all seasons. Such deposits are common throughout the Phoenix Basin and the adjoining and intervening ranges. The degree of development of caliche is directly related to age if other determining factors such as topographic setting, rainfall, erosion processes, and composition and texture of parent material are essentially the same. The thickest deposit of caliche occurs in the upper terraces, and in the Salt River area more than 45 feet of heavily cemented gravel occurs in sediments of the Sawik Terrace. The Mesa Terrace is equally well cemented with the extensive development of plugged horizons many feet thick with excellent development of laminar layers. In these upper terraces surface cobbles exhibit caliche rinds up to 4 inches thick. On the younger terraces, such as the Blue Point, there is a less well developed caliche layer and the gravels are less firmly cemented. Cobbles with caliche rinds are present but these rinds may be very thin to no more than ¼ inch thick. Extensive caliche development similar to that found in the upper terraces in the Salt River is common in all of the upper terraces examined

Interleaf. Meandering lower Verde River downstream 1 km east from Bartlett Dam. High terrace gravel on basalt knob on right, middle ground. Low strath terrace gravels on left, middle ground. 35 km east of Phoenix, Arizona. (Photograph No. 3223 by Troy L. Péwé, December 22, 1971.)

in the Phoenix Basin, including extremely old alluvial fans on the flanks of the McDowell Mountains (Christenson, Welsch, and Péwé, 1975) and the Phoenix Mountains (Shank and Péwé, 1973).

Similar caliche deposits have been described in southern New Mexico (Gile, 1975) and in Saudi Arabia (Chapman, 1974) on surfaces with comparable thicknesses and degree of caliche development as in the Phoenix Basin in terms such as very old and up to a million years or more.

Along the Gila River near Arlington, Gillespie Dam, and Gila Bend the 40- and 80-foot terraces of river gravel with rock types similar to the Salt River Terraces are extensively calichified and are firmly cemented. Here the terraces are overlain by lava flows that have been dated at 2 to 3 million years (Lee and Bell, 1975).

TECTONIC SIGNIFICANCE OF TERRACES ALONG STREAMS ENTERING THE PHOENIX BASIN

It is apparent from the study of the converging terraces on the streams flowing out of the mountains and entering the Phoenix Basin from the north and east that the mountain ranges in that area are undergoing a slow regional uplift, apparently periodically. It also is apparent that the stream terraces converge on the edge of the basins and disappear under the valley fill deposits. It would appear that there has been slow down-dropping and filling of the basins over the last 2 or 3 million years, perhaps longer, and the river gravels are present at some depth in the basin. The exact depth is not known, but in the city of Tempe, gravel of the Mesa Terrace is anywhere from 10 to more than 30 feet deep, becoming deeper toward the southern part of the city. South of Mesa the coarse river gravel is at least 600 feet below the surface. No outcrop of the mountain gravels is known along the streams in the basin until the drainage network encounters similar caliche-cemented Salt River-gravel type lithology near the vicinity of the mouth of the Hassayampa River. It is therefore thought that the down-faulting extends westward to the vicinity of the Hassayampa River. From here downriver to Gila Bend the terraces are parallel, based on present reconnaissance work, and are not part of this original down-dropping that occurred or is occurring in the basin.

It is tempting to speculate on the rate of uplift. Assuming that the converging terraces do indicate rising of the mountains; assuming further that the maximum uplift is about 400 feet near Roosevelt Dam; and assuming that a period of 2 million years was involved, one could suggest that the rate of uplift has been about 1 inch/400 years or .0025 inches/year (.0001 mm/yr).

SELECTED REFERENCES

Aldridge, B. N., 1970, Floods of November 1965 to January 1966 in the Gila River Basin, Arizona and New Mexico, and adjacent basins in Arizona: U.S. Geol. Survey Water-Supply Paper 1850-C, 176 p.

Aristarian, L. F., 1970, Chemical analyses of caliche profiles from the High Plains, New Mexico: Jour. Geology, v. 78, p. 201–212.

Blake, W. P., 1901, The caliche of southern Arizona: Trans. Am. Inst. Min. Eng., v. 31, p. 220–226.

Bretz, J. H., and Horberg, L., 1949, Caliche in southeastern New Mexico: Jour. Geology, v. 57, p. 491–511.

Chapman, R. W., 1974, Calcareous duricrust in Al-Hasa, Saudi Arabia: Geol. Soc. Amer. Bull., v. 85, p. 119–130.

Christenson, G. E., 1975, Environmental geology of the McDowell Mountains, Arizona: ground water, waste disposal, construction conditions, and caliche: Arizona Acad. Sci. Bull., v. 10, proc. suppl., p. 49–50.

Christenson, G. E., Welsch, D. G., and Péwé, T. L., 1975, Environmental geology in arid regions—an application in urban planning, Scottsdale, Arizona (abst.): Geol. Soc. America Annual Mtg., Absts., with programs, v. 7, no. 7, p. 1026.

Cooley, M. E., 1961, Description and origin of caliche in the Glen-San Juan Canyon region, Utah and Arizona: Az. Geol. Soc. Digest, v. 4, p. 35–41.

Cooley, M.E., 1973, Map showing distribution and estimating thickness of alluvial deposits in the Phoenix area, Arizona, Map I-845C: U.S. Geol. Survey, scale 1:250,000.

Cordy, G. E., Holway, J. V., and Péwé, T. L., 1977, Geology for land use planning in arid regions, Phoenix, Arizona: (abst.) Geol. Soc. America Cordilleran Section Annual Mtg., Absts., with programs, v. 9, no. 4, p. 404.

Davis, A. P., 1897, Irrigation near Phoenix, Arizona: U.S. Geol. Survey Water-Supply Paper 2, 98 p.

Davis, A. P., 1902, Water storage on Salt River, Arizona: U.S. Geol. Survey Water-Supply Paper 73, 54 p.

Fodor, R. V., 1969, Petrology and petrography of the volcanic rocks in the Goldfield Mountains, Arizona: Ariz. State Univ., unpub. Master's Thesis, 66 p.

Gile, L. H., 1961, A classification of Ca horizons in soils of a desert region, Dona Ana County, New Mexico: Soil Sci. Soc. America Proc., v. 25, p. 52–61.

Gile, L. H., 1975, Holocene soils and soil geomorphic relations in an arid region of southern New Mexico: Quaternary Research, v. 5, p. 321–360.

Gile, L. H., Peterson, F. F., and Grossman, R. B., 1965, The K-horizon: a master soil horizon of $CaCO_3$ accumulation: Soil Sci., v. 99, p. 74–82.

Gile, L. H., Peterson, F. F., and Grossman, R. B., 1966, Morphologic and genetic sequences of carbonate accumulation in desert soils: Soil Sci., v. 101, p. 347–360.

Howard, R. B., Cowen, B., and Inouye, D., 1977, Reappraisal of desert pavement formation: (abst.) Geol. Soc. America Cordilleran Section Annual Mtg., Absts., with programs, v. 9, no. 4, p. 438–439.

Kokalis, P. G., 1970, Terraces of the middle Salt River Valley, Arizona: II—size, shape and lithologic characteristics of the alluvial sediments (abst.): Ariz. Acad. Sci. Journ. Supp., v. 6, p. 64.

Kokalis, P. G., 1971, Terraces of the lower Salt River Valley, Arizona: Ariz. State Univ., unpub. Master's Thesis, 103 p.

Lattman, L. H., 1973, $CaCO_3$ cementation of alluvial fans in southern Nevada: Geol. Soc. America Bull., v. 84, p. 3013–3028.

Lee, W. T., 1904, Underground waters of Gila Valley, Arizona: U.S. Geol. Survey Water-Supply Paper 104, 71 p.

Lee, W. T., 1904, Underground waters of Salt River Valley, Arizona: U.S. Geol. Survey Water-Supply Paper 136, 196 p.

Lee, G. K., and Bell, J., 1975, Late Cenozoic geology along the Gila River near Gillespie Dam, Central Arizona: (abst.) Geol. Soc. America Annual Mtg., Absts., with programs, v. 7, no. 3, p. 340.

McKee, E. D., and McKee, E. H., 1972, Pliocene uplift of the Grand Canyon region—time of drainage adjustment: Geol. Soc. America Bull., v. 83, p. 1923–1932.

Melton, M. A., 1960, Origin of the drainage of southeastern Arizona: Arizona Geol. Soc. Digest, v. 2, p. 113–122.

Merrill, R. K., 1974, The late Cenozoic geology of the White Mountains, Apache County, Arizona: Arizona State Univ., unpub. Ph.D. dissertation, 202 p.

Milne, J. D. G., 1973, Map and sections of river terraces in the Rangitike Basin, North Island, New Zealand: New Zealand Soil Survey Report 4.

Pedersen, E. P., and Royse, C. F., 1970, Late Cenozoic geology of the Payson Basin, Gila County, Arizona: Arizona Acad. Sci., v. 6, p. 168–178.

Peplow, E. H., Jr., 1970, The taming of the Salt: Salt River Project, Tempe, Arizona, p. 143.

Péwé, T. L., 1966, Morphology of the Salt River: Stewart Mountain Dam to Phoenix, Arizona: unpub. report, 8 p.

Péwé, T. L., 1970, Terraces of the middle Salt River Valley, Arizona: I—progress report (abst.): Ariz. Acad. Sci. Jour. Supp., v. 6, p. 64.

Péwé, T. L., 1971, Guidebook to the geology of the lower Salt River Valley: unpub. guidebook, 21 p.

Péwé, T. L., 1974, Geomorphic processes in polar deserts: *in* Smiley, T. L., and Zumberge, J. H., eds., Polar deserts and modern man: Univ. Ariz. Press, Tucson, p. 33–52.

Péwé, T. L., 1975, The late Cenozoic history of the Phoenix Basin, Arizona: an exploratory model: unpub. MS, 14 p.

Péwé, T. L., 1976, Terraces of the lower Agua Fria River Valley, Maricopa County, Arizona (abst.): Jour. Arizona Acad. Sci., v. 11, proc. suppl., p. 93.

Péwé, T. L., Péwé, E. A., and Péwé, R. H., 1976, Rate of desert dust deposition (abst.): Jour., Arizona Acad. Sci., v. 11, proc. suppl., p. 95–96.

Péwé, T. L., Péwé, E. A., and Péwé, R. H., Journaux, A., and Slatt, R. M., 1977, Desert dust: Characteristics and rates of deposition in Central Arizona: in Desert Dust: origin, characteristics and effect on man: (in press).

Péwé, T. L., and Shank, D. C., 1973, Fanhead incision in the Phoenix Basin: Jour. Ariz. Acad. Sci., v. 8, p. 41-42.

Pope, C. W., 1974, Geology of the lower Verde River Valley, Maricopa County, Arizona: Ariz. State Univ. unpub. Master's Thesis, 104 p.

Pope, C. W., and Péwé, T. L., 1973, Geology of the lower Verde River Valley, Maricopa County, Arizona (abst.): Arizona Acad. Sci. Jour., Proc. Supp., v. 8, p. 42.

Price, W. A., 1925, Caliche and pseudo-anticlines: Am. Assoc. Pet. Geol. Bull., v. 9, p. 1009–1017.

Reeves, C. C., Jr., 1970, Origin, classification, and geologic history of caliche in the southern High Plains, Texas and eastern New Mexico: Jour. Geology, v. 78, p. 352–362.

Shank, D. C., 1973, Environmental geology in the Phoenix Mountains, Maricopa County, Arizona: Ariz. State Univ., unpub. Master's Thesis, 39 p.

Shank, D. C., and Péwé, T. L., 1973, Environmental geology in the Phoenix Mountains: Jour. Ariz. Acad. Sci., v. 8, p. 43.

Sharon, D., 1962, On the nature of hamadas in Israel: Zeitschrift für Geomorphologie, v. 6, p. 129–147.

Sheridan, M. F., Stuckless, J. S., and Fodor, R. V., 1970, A Tertiary silicic cauldron complex at the northern margin of the Basin and Range Province, central Arizona, U.S.A.: Bull. Volcanol., v., 34 no. 3, p. 1–14.

Sigalove, J. J., 1968, Carbon-14 content and origin of caliche: unpub. Master's Thesis, University of Arizona.

Springer, M. E., 1958, Desert pavement and vesicular layer of Lahohtan Basin, Nevada: Soil Sci. Soc. America Procds., v. 22, p. 63–66.

Stuckless, J. S., and Sheridan, M. F., 1971, Tertiary volcanic stratigraphy in the Goldfield and Superstition Mountains, Arizona: Geol. Soc. America Bull., v. 82, p. 3235–3240.

Stuckless, J. S., and Naeser, C. W., 1972, Rb-Sr and fission track age determination in the Precambrian basement around the Superstition volcanic field, Arizona: U.S. Geol. Survey Prof. Paper 800B, p. B191-B194.

Tilford, N. R., 1966, Engineering geology—Stewart Mountain Dam Site, Arizona: Ariz. State Univ. unpub. Master's Thesis, 42 p.

Wahrhaftig, C., 1958, Quaternary geology of the Nenana River Valley and adjacent parts to the Alaska Range: U.S. Geol. Survey Prof. Paper 293, 68 p.

GEOLOGY FIELD TRIP LOG ALONG THE LOWER SALT RIVER, ARIZONA FROM TEMPE BUTTE, TEMPE TO SAGUARO LAKE AND RETURN

The numbered stop locations are on topographic maps (fig. 7); these maps should be consulted for a clearer understanding of the discussion.*

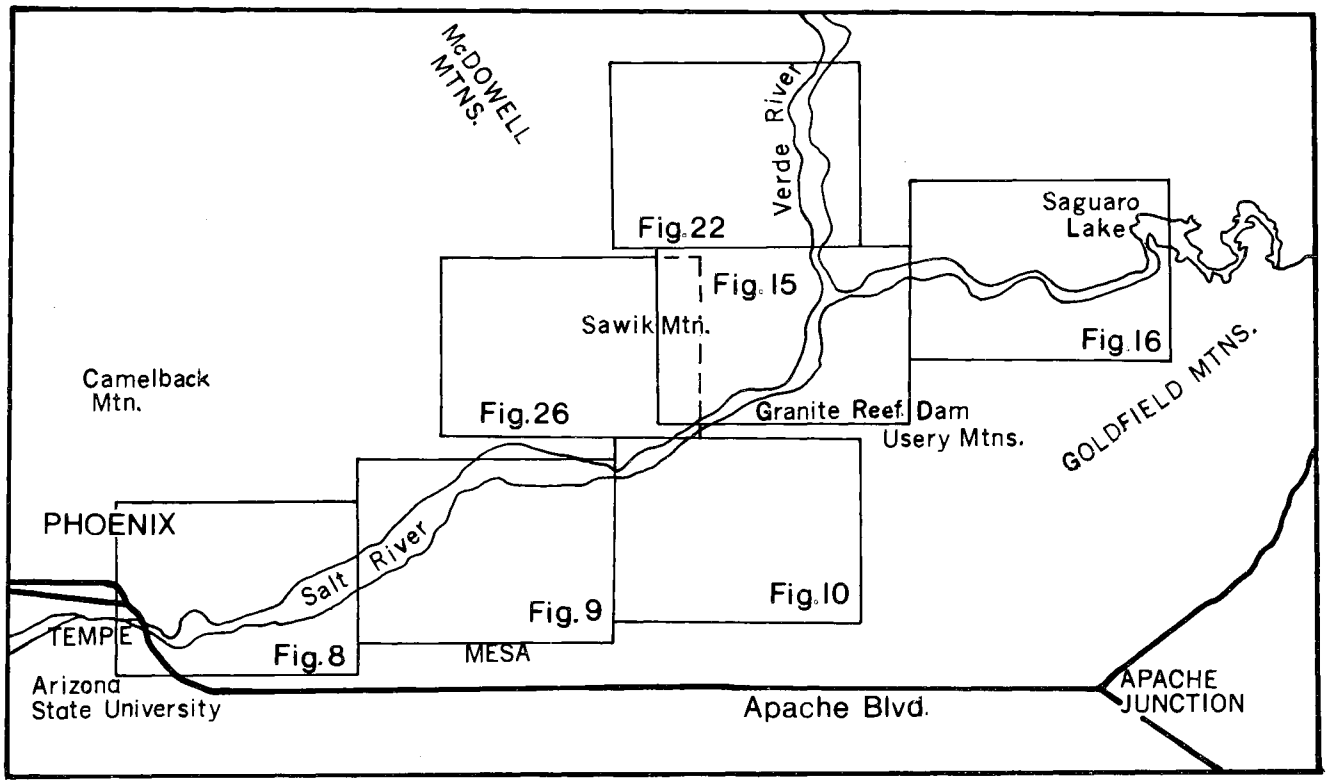

Figure 7. Index map showing location and number of topographic maps of field trip stops, lower Salt River Valley.

STOP 1. ARIZONA STATE UNIVERSITY (Tempe Quadrangle, 1952). On edge of river scarp near railroad track at Arizona State University overlooking fraternity houses (fig. 8). The fraternity houses to the east are on a low terrace of the Salt River which is really part of the floodplain. However they are not on the active part of the floodplain and were not flooded in the flood of December, 1965–January, 1966. The water reached an elevation of about 1,160 feet, about 3 or 4 feet below the level of the terrace and the fraternity houses. The scarp at **STOP 1** is about 10 feet above the active floodplain. The terrace upon which Arizona State University is built is part of the Mesa Terrace which is well displayed at **STOP 2** in Mesa, 3 miles to the east.

At this locality, the modern Salt River flows between Tempe Butte on the south and the Papago Pediment on the north (fig. 8). The bedrock is very shallow at this narrow constriction and actually crops out locally in the bottom of the floodplain. In the geologic past the Salt River flowed to the west by going south of Tempe Butte and South Mountain (figs. 1, 2). At least four terraces are present on the map (fig. 8); they all have low scarps and appear to terminate in the vicinity of the western part of the map (Tempe Butte). No prominent terraces of the Salt River are exhibited downstream. On the ASU campus there is 3 to 6 feet of river silt overlying coarse, rounded river gravel of the Mesa Terrace. This gravel is exposed in the basements of most of the buildings constructed on the campus.

From **STOP 1** proceed east along University Avenue to **STOP 2.**

STOP 2. TERRACE SCARP. One of the best western exposures of the prominent Mesa Terrace that extends unbroken from here eastward 10 miles to the Usery Mountains (figs. 8, 9, 10). Gravel crops out and the terrace scarp here is 20 feet above the active floodplain.

As for all the major terraces, the overbank silt, or silt from the surrounding mountains which overlies the gravel, has been washed away at the terrace scarp, and it is here that the caliche-cemented gravel is well exposed.

*The topographic maps are part of various U.S. Geological Survey Quadrangles as stated in their title.

Proceed through Mesa to Country Club Avenue and then north on Country Club Avenue to terrace scarp at Mesa Country Club.

STOP 3. MESA TERRACE (Mesa Quadrangle, 1952; fig. 9). A road cut exposes the caliche-cemented gravel in the scarp of the Mesa Terrace. The Mesa Terrace was named (Péwé, 1971) from the City of Mesa, established by the Mormons in 1878 on a table land above the river. The Spanish name for table, mesa, was adopted as a name for the settlement. The Mesa Terrace is 40 feet above the modern floodplain at this locality. The scarp is well exhibited and a small colluvial apron extends from the scarp down onto the lower terrace.

The exposure is old and the caliche cementing the terrace gravel is beginning to be weathered. At the top of the scarp, holes dug for a sign that was never erected expose well-developed caliche. The caliche development is the complete plug stage and at places along the edge of the scarp laminar caliche is well formed.

From **STOP 3** proceed across the lower terrace north and east to the village of Lehi.

STOP 4. VILLAGE OF LEHI. This lower terrace is named the Lehi Terrace (Péwé, 1971) from the village of Lehi (fig. 9). The village was established in 1877 by the Mormons and was the first settlement in this immediate area. The term Lehi comes from the Biblical prophet of 600 B.C. who took his family into the wilderness to escape the destruction of Jerusalem. The name has great antiquity but the terrace is undoubtedly older. The terrace here is about 10 feet above the modern floodplain and was not flooded in the flood of December, 1965. However, the flood of 1965 did not reach its possible maximum because of storage provided by the six reservoirs on the Verde and Salt Rivers. Without the reservoirs the peak discharge at Granite Reef Dam would have been about 120,000 cfs (Aldridge, 1970, p. C-27). The largest known flood in the Salt River Basin occurred in February 1891 when a flow of 300,000 cubic feet per second (cfs) was recorded. Flood waters at that time invaded most of the downtown area of Phoenix and covered the Lehi Terrace.

From old records of the towns of Lehi and Mesa we learn that on February 19, 1891, the Salt River reached the highest point that could be remembered by the settlers and did considerable damage to their crops and buildings. However, 3 days later the river rose an additional 3 feet completely engulfing the bottomland. It is reported that five Indians were drowned, but all the white settlers escaped to the mesa where they remained for 2 weeks. Most of the Indians and settlers lost nearly all their personal possessions in the flood and the canals were badly damaged. The water in Lehi was described as being waist deep, or belly deep to a pony.

The Lehi Terrace is a low terrace of the floodplain. Isolated remnants of the terrace are present upstream as far as Stewart Mountain Dam. However, with the establishment of the dams, the possibility of this terrace now being flooded is extremely rare. The top stratum silt is 1 to 10 feet thick and is underlain by sand and gravel.

Two hundred yards southeast from **STOP 4,** on Keal Road, Mr. Roger Sattler came across the remains of a fossil in an excavation for a septic tank. The writer investigated the site and recovered a fine carapace of a box turtle 14 by 10 inches which was at the top of the river gravel beneath 90 inches of top stratum silt. The fossil, which occurred in a silty clay which has tubules and small nodules of caliche, is probably late Quaternary in age; a study is underway.

STOP 5. SCARP OF LEHI TERRACE ABOVE MODERN SALT RIVER FLOODPLAIN. Beneath 3 or 4 feet of top stratum silt is a coarse, rounded river gravel with clasts about 4 inches in diameter. There is no cementation by caliche whatsoever but there is a very thin film of caliche completely surrounding the larger cobbles in the silty matrix. In the upper 2 feet of the section there are characteristic pot sherds of Hohokam culture, as well as lithic artifacts. The Indians probably used this flat area for agriculture 1,000 years ago and it was periodically inundated by the river until the building of the Theodore Roosevelt Dam. At this locality we are about 8 or 9 feet above the low part of the Salt River Channel. On top of the terrace scarp there can also be found a litter of pot sherds.

STOP 6. LOW TERRACE SCARP OF BLUE POINT TERRACE. The gravel terrace scarp, 3 to 6 feet above the Lehi Terrace, appears along the road to the south in this area. This is probably the most western exposure of the Blue Point Terrace. From this STOP one can see ½ mile to the south the prominent scarp of the Mesa Terrace, the top of which is here 60 feet above the modern floodplain. To the north one can see the counterpart of the 60-foot terrace across the Salt River Valley.

From here proceed to **STOP 7** just north of the Southern Canal about 1 mile east of **STOP 6.**

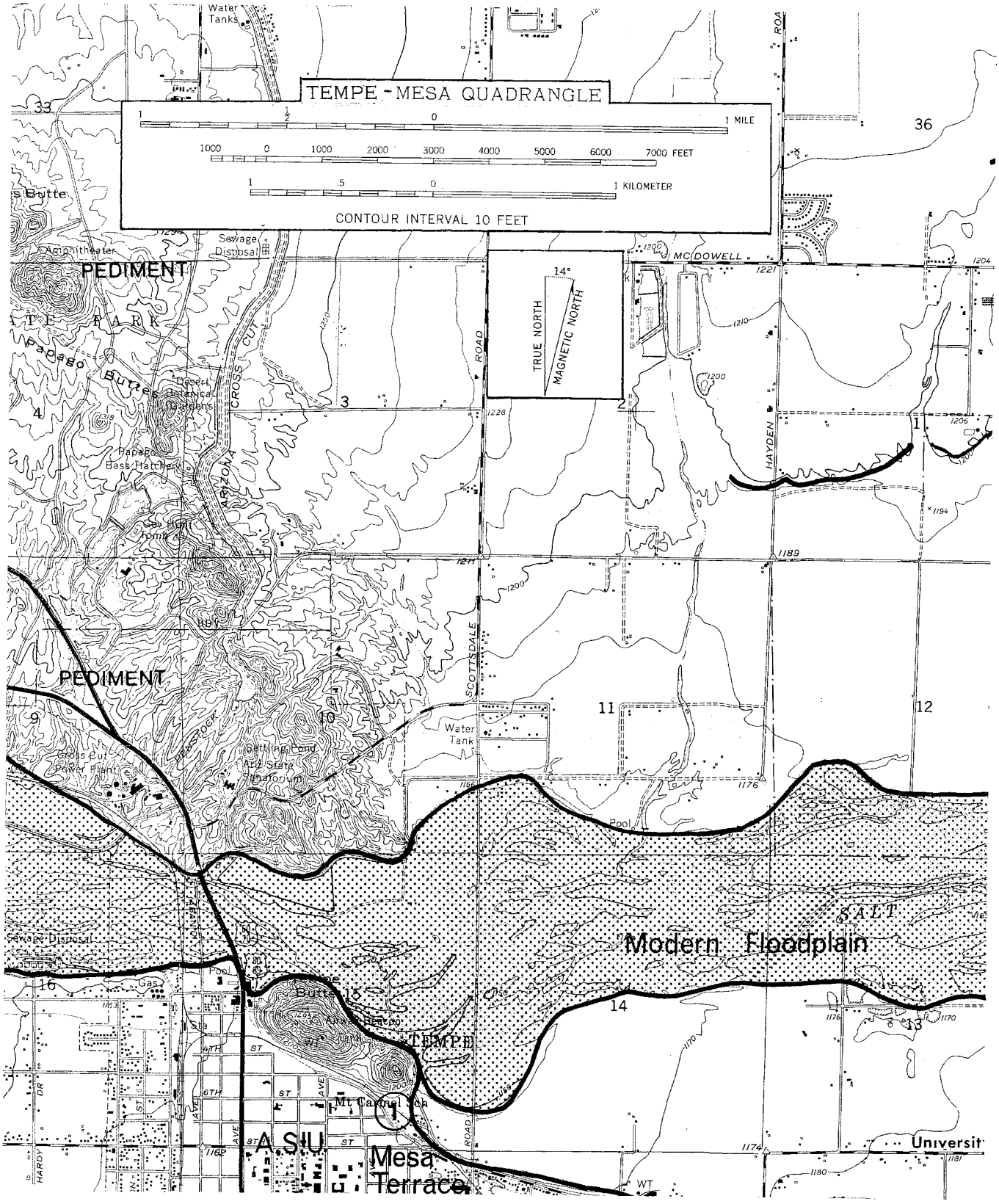

Figure 8. Field trip log map showing locations of STOPS 1–2.

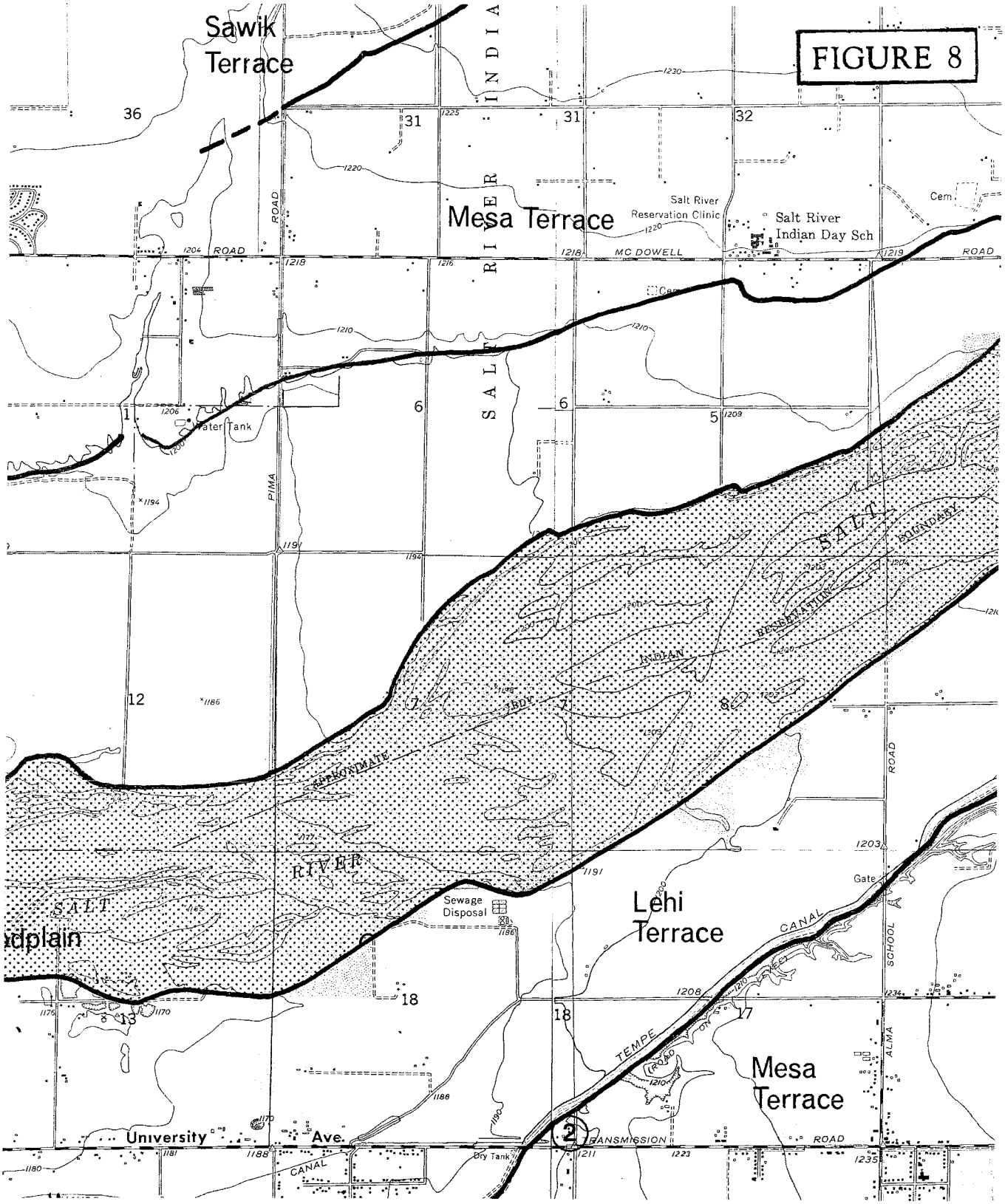
FIGURE 8
Sawik Terrace
Mesa Terrace
Lehi Terrace
Mesa Terrace
SALT RIVER INDIAN
Salt River Reservation Clinic
Salt River Indian Day Sch
Cem
MC DOWELL
ROAD
PIMA
Water Tank
SALT RIVER INDIAN RESERVATION BOUNDARY
APPROXIMATE
Sewage Disposal
Gate
CANAL
TEMPE
SCHOOL
ALMA
University Ave.
TRANSMISSION
Dry Tank
2

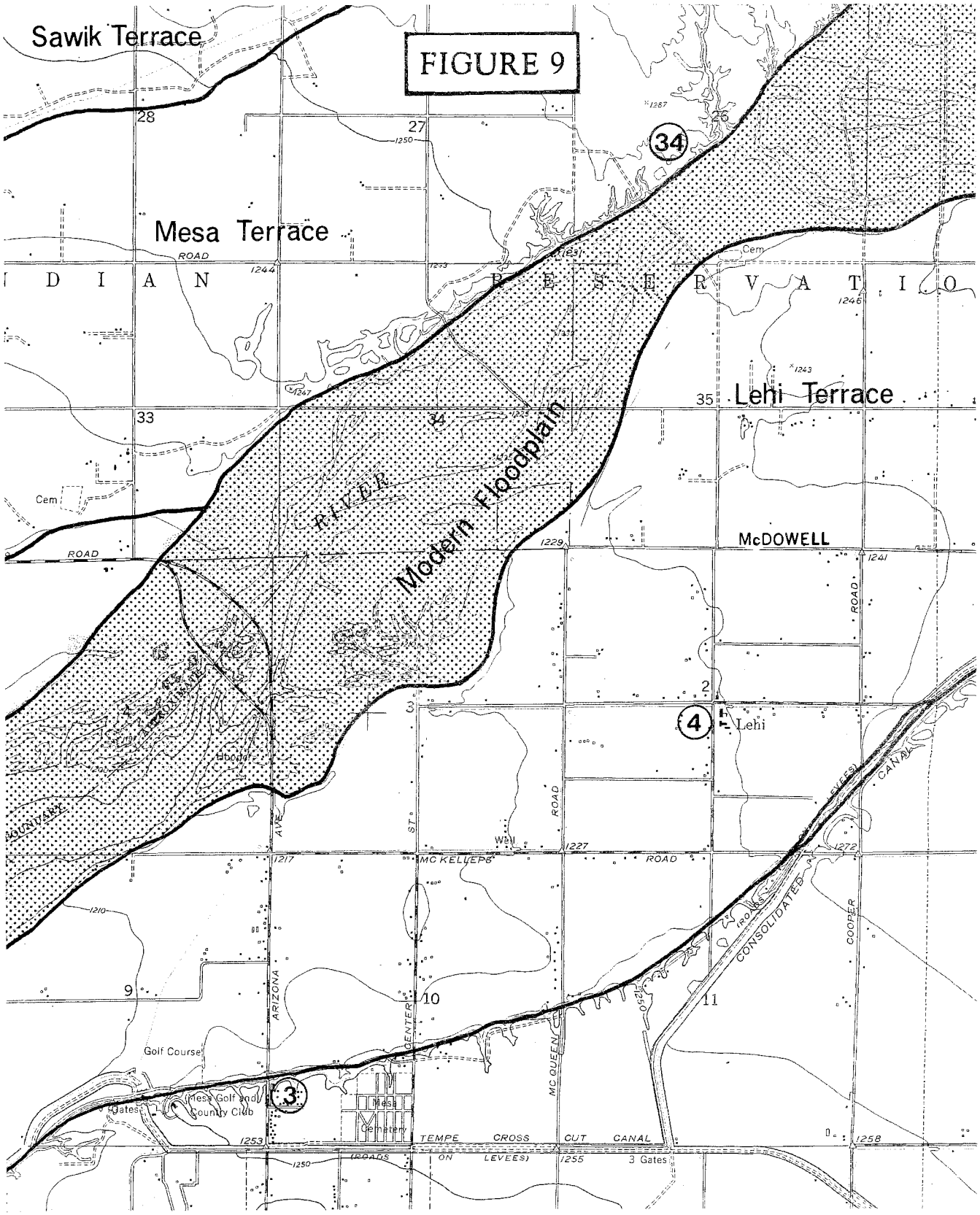

Figure 9. Field trip log map showing locations of STOPS 3–6 and 34.

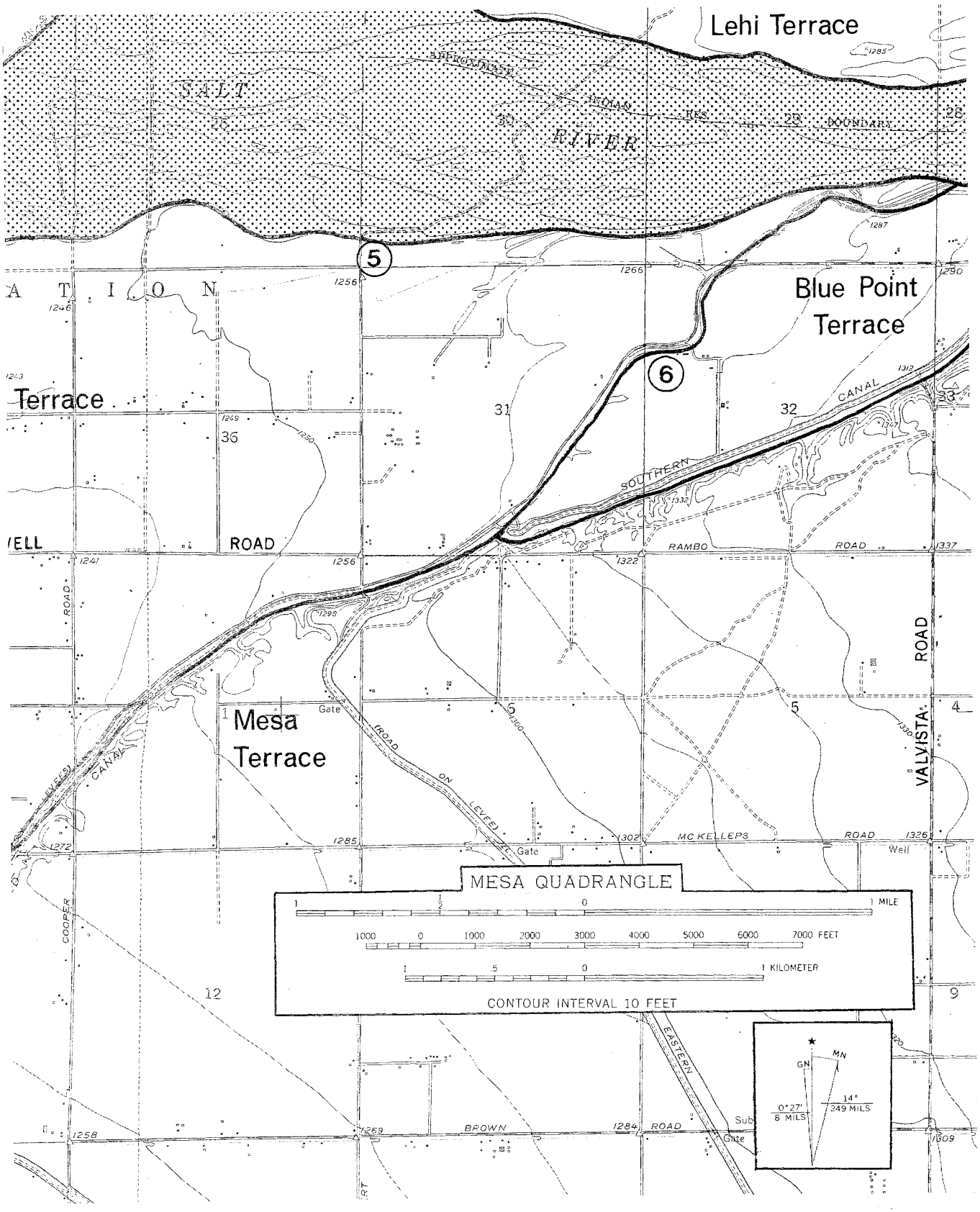
Lehi Terrace
SALT
RIVER
INDIAN
RES.
BOUNDARY
Blue Point
Terrace
Terrace
Mesa
Terrace
SOUTHERN
CANAL
RAMBO
ROAD
MC KELLEPS
ROAD
BROWN
ROAD
VALVISTA
ROAD
COOPER
ROAD
EASTERN
ROAD ON LEVEE
CANAL
MESA QUADRANGLE
1 MILE
7000 FEET
1 KILOMETER
CONTOUR INTERVAL 10 FEET
GN
MN
0°27'
8 MILS
14°
249 MILS

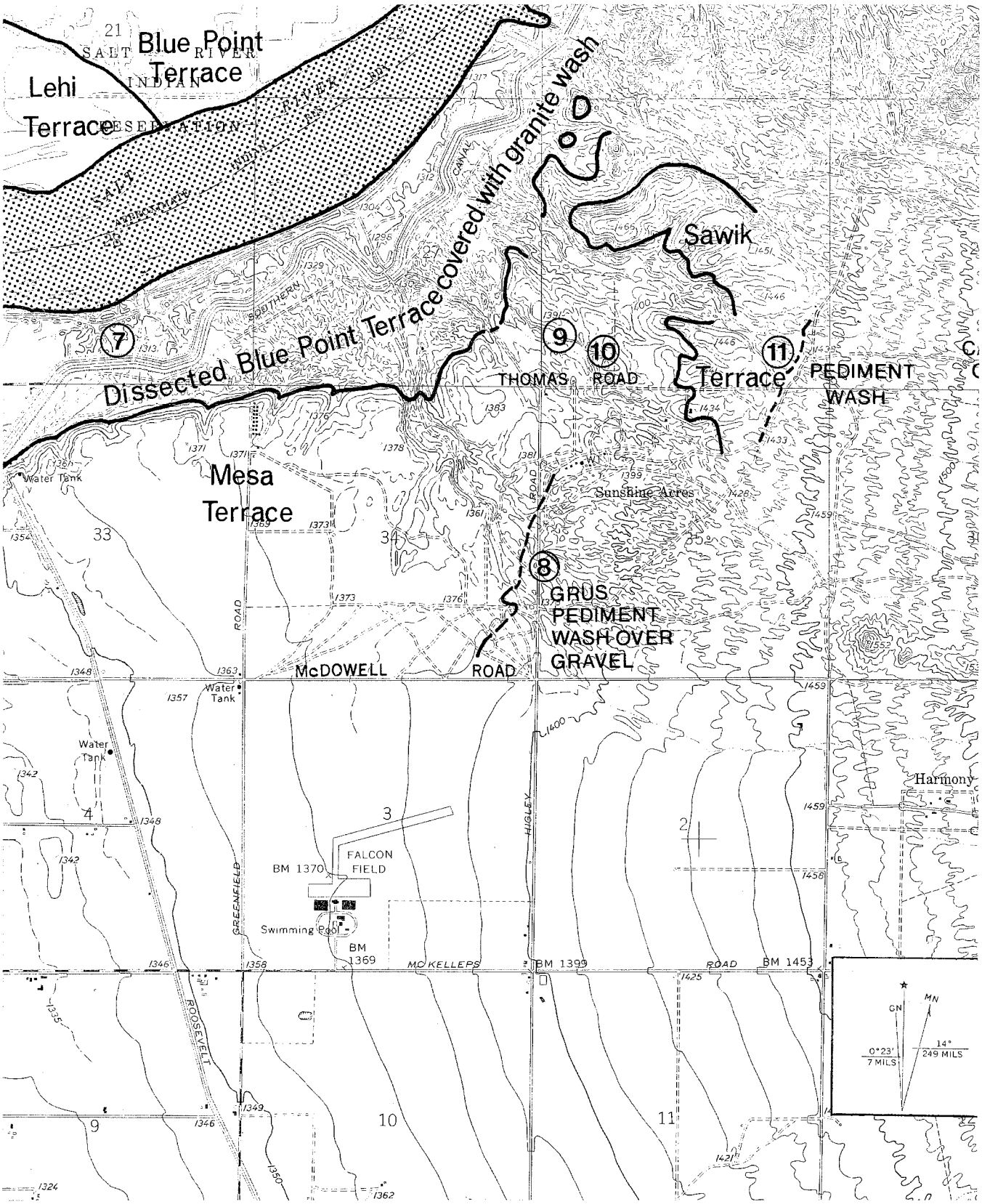

Figure 10. Field trip log map showing locations of STOPS 7–12.

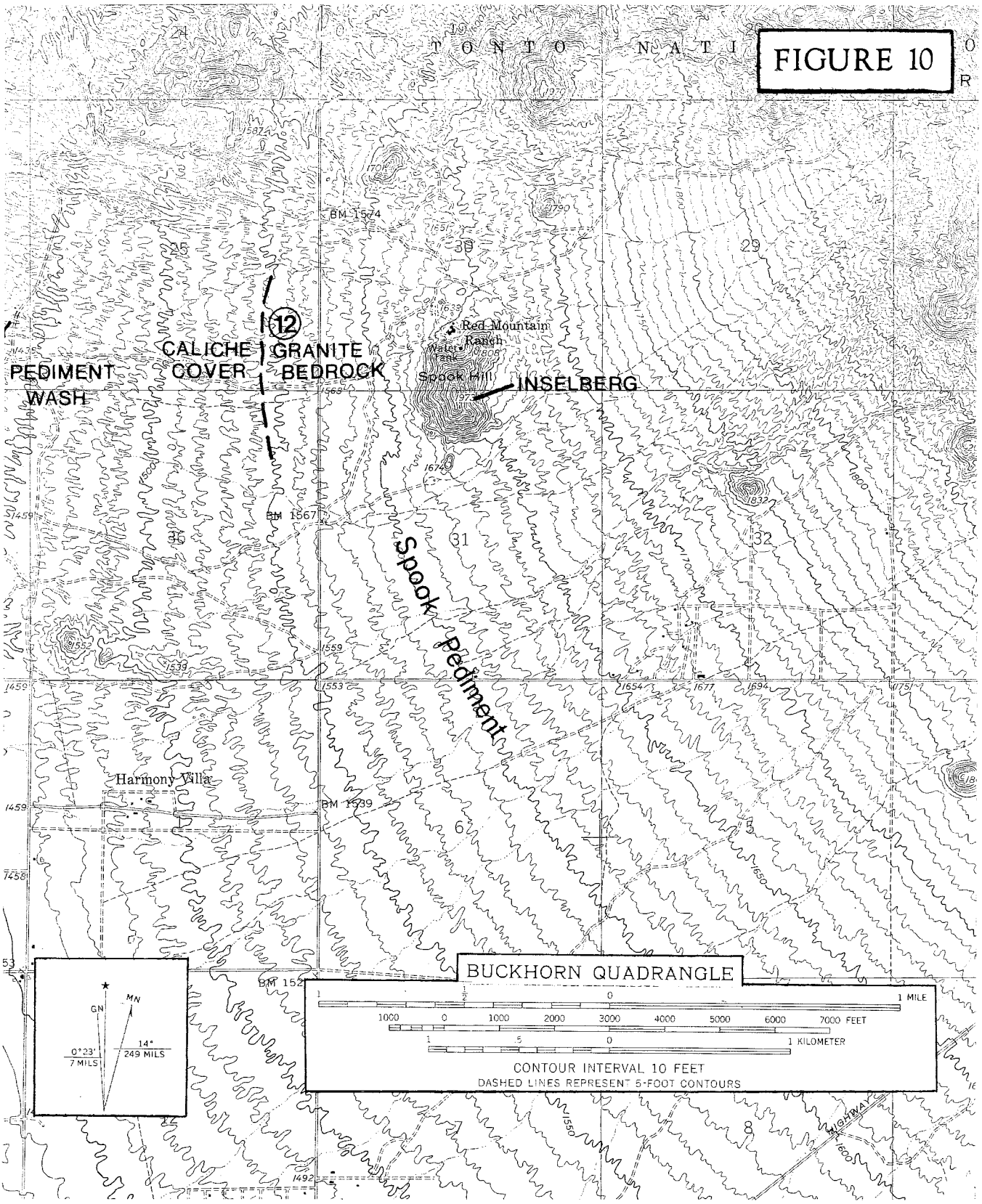
FIGURE 10
TONTO NATI
12
CALICHE COVER
GRANITE BEDROCK
PEDIMENT WASH
INSELBERG
Red Mountain Ranch
Water Tank
Spook Hill
Spook Pediment
Harmony Villa
BM 1574
BM 1567
BM 1539
BUCKHORN QUADRANGLE
1 MILE
7000 FEET
1 KILOMETER
CONTOUR INTERVAL 10 FEET
DASHED LINES REPRESENT 5-FOOT CONTOURS
GN
MN
0°23'
7 MILS
14°
249 MILS
HIGHWAY

Figure 11. View downstream (west) of Blue Point Terrace scarp (SW Sec. 28, T. 2 N., R. 6 E.). Modern flood plain on right; Camelback Mountain on right in far distance. (Photograph No. 14,263 by Troy L. Péwé, March, 1970.)

STOP 7. BLUEPOINT TERRACE SCARP (Buckhorn Quadrangle, 1956; fig. 10). This is the scarp of the Blue Point Terrace. It lies below the Mesa Terrace but above the modern floodplain and the Lehi Terrace. The terrace scarp is about 20 feet above the modern floodplain of the Salt River and at an elevation of 1,300 feet at this spot. The terrace, poorly developed and partly covered with colluvium, is termed (Péwé, 1971) the Blue Point Terrace after Blue Point Picnic Area near where it is well exposed on the south side of the Salt River, 8 to 10 miles upstream from this spot.

Caliche is poorly developed in the gravelly alluvium of this terrace. The cobbles and pebbles may have a caliche rind of about ⅛ inch but there is no massive cementation of the pebbles or cobbles.

Along the Southern Canal at this spot can be found many small snail shells, but they are of little value for determining the age of the sediments. These shells are in the sediments that have been dredged from the canal during periodic cleaning and dumped on the side. The snails were introduced from the Orient by ships entering the Gulf of California and the snails evidently worked their way up the Colorado River and its tributaries, including these canals, in the last 30 years.

A view downstream from **STOP 7** (fig. 11) shows a well-developed terrace scarp in alluvium. At this locality is also an abandoned irrigation canal. A view upstream, as well as an examination of the map, indicates that the Blue Point Terrace is only a few hundred yards wide from here to Granite Reef Dam. From near the Granite Reef Diversion Dam and upstream, the terrace is cut on bedrock and is a strath terrace. Between **STOP 7** and Granite Reef Dam the terrace is covered with a granite alluvium and colluvium from the Usery Mountains to the east. As local base level was lowered (the downcutting of the Salt River), much of this colluvial cover over the terrace was removed and the streams have cut into the surface of the terrace.

Kokalis (1971) made detailed analyses of the size-grade distribution of the sediments of the terraces as well as the modern floodplain. The sediments can be classed as gravels

to sandy gravels. He concluded that the average medium diameter of the terrace sediment is -4.0Φ (fig. 12) and that of the modern floodplain sediments is -3.4Φ. He further states that the average of the most coarse 1 percentile illustrates this difference, as that of the terrace sediments is -7.4Φ while the average for the modern floodplain gravels is -7.0Φ. His analyses indicate that for all practical purposes the size distribution of the sediments on the terrace is the same as that of the floodplain. However, there is a slight difference, and the regimen of the Salt River in the past may have been slightly more rigorous during the time that the

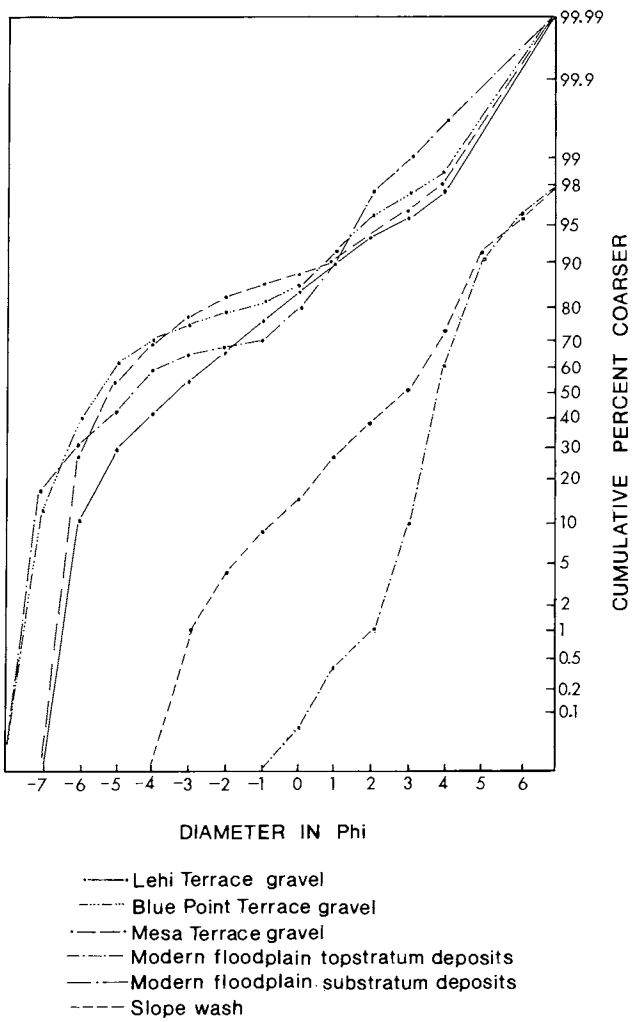

Figure 12. Cumulative-frequency distribution curves for analyses of sediments of modern flood plain and terraces of the lower Salt River Valley, Arizona. (After Kokolis, 1971.)

high terraces were produced than during the time of the modern floodplain.

Kokalis (1971) was able to demonstrate that in the reach of the Salt River from Stewart Mountain Dam to its mouth there was no change in size distribution of the sediments. Also, it was not possible to distinguish one terrace from another by size grade analyses alone.

Return to west along canal to Gilbert Road and south to McKellips Road. Proceed east on McKellips Road through the citrus groves.

At the Junction of Val Vista Road and McKellips Road examination of the soil in the citrus groves indicates that the coarse silt has many pea-sized gravel pieces of angular feldspar, quartz, and granite. This material is washed from Spook Pediment and forms a thin veneer over the underlying Mesa Terrace river gravel. The same type of soil is present in the vicinity of Falcon Field in Section 3 (fig. 10). Proceed north on Higley Road to **STOP 8** in the vicinity of Sunshine Acres.

STOP 8. SUNSHINE ACRES. Along Higley Road in the vicinity of Sunshine Acres one may notice that the grus pediment wash from Spook Pediment to the east thins and the caliche-cemented coarse gravel of the Mesa Terrace is exposed. In the sharp-walled gullies just west of Higley Road in Section 34 at an elevation of 1,361 feet is exposed highly indurated caliche-cemented gravel with no grus wash on the surface. The Mesa Terrace is here at an elevation of about 1,370 feet (fig. 10).

STOP 9. ROAD CUT IN MESA TERRACE ON HIGLEY ROAD. This is the surface of the Mesa Terrace at an elevation of 1,391 feet. The road cut has exposed highly calichified coarse gravel with lenses of silt and sand. The plug stage of the caliche growth is well exhibited on both sides of the road cut and especially on the small new cut on the south end of the east wall of the road. Many fractured cobbles and boulders can be seen with caliche-filled fractures. In many places on Mesa Terrace the fractured parts of the cobbles have been displaced as much as 2 inches. At this locality, laminar caliche is well developed. As much as 1 or 2 feet of laminar caliche can be seen, especially in finer material. The development of caliche indicates great antiquity of the terrace, and, as mentioned earlier, the surface of the Mesa Terrace is surely quite old; very early Pleistocene if not Pliocene.

Proceed south to Thomas Road and east on Thomas Road 100 yards to **STOP 10.**

STOP 10. DESERT PAVEMENT STUDY SITE. The study site is on gravel of the Mesa Terrace. To the north and east a higher level terrace can be seen. The level is well displayed and represents the highest of the series of terraces, the Sawik Terrace, 185 feet above the modern floodplain.

Excellent desert pavement has formed on the terrace gravel surface in many places. Desert pavement is a stone mosaic composed of pebbles which lie flat and adjacent to

each other embedded in a fine matrix, generally silt. If there is a binding agent present such as clay or salt, the material is usually indurated to form a thin, strong carapace. If there is no binding agent, the fine material is loose. The desert pavement is generally very old and the clasts are highly patinated by desert varnish.

In an attempt to learn more about the origin and rate of formation of desert pavement, the writer, assisted by students, established three test sites on alluvial fans near Quartzsite, Arizona in March, 1975, and has periodically studied the sites. Three areas 9 yards square were carefully cleared of stones to study the rate of rejuvenation of the desert pavement. The weight, number, and volume of surface clasts were carefully measured. Also measured were the size, weight, and number of clasts in the silt recovered from a measured pit dug nearby.

To continue studies closer to Arizona State University, Site No. 4 was established near the corner of Higley and Thomas Roads on the surface gravel of the Mesa Terrace (fig. 13). The area is not as ideal as that near Quartzsite, but it is closer to Tempe. Site 4 was initiated by Mr. James Bayles, June 1, 1977, in the same manner as the first three sites. The 9-yard-square area was carefully cleared of stones by hand picking with little disturbance as possible to the underlying material. No clasts were at the surface after the area was cleared. The first step was to clear a 1-yard-square area within the 9-yard-square area. The surface clasts in the one-yard-square area were analyzed for size distribution and weight (table 2).

Table 2. Particle size and weight distribution of material at ASU desert pavement Site 4.

>32mm	>16mm	>8mm	>4mm	<4mm	Total
882gm	7973gm	5078gm	231gm	113gm	14,277gm

To produce a desert pavement it is necessary to concentrate the particles on the surface either by 1) deflation by wind, 2) erosion by water, 3) upward migration of particles from the subsurface material or 4) any combination of these. Many of the sites are in such a position that erosion by water would be relatively minor, nevertheless, some of the material is removed this way. Deflation by wind is always present in desert areas, and surely some contribution of erosion is by this method. At Quartzsite, considerable stone cover has already been regenerated on the cleared surfaces. The different parts of the area have been recleared at different times, and at this writing there are three different degrees of surface desert pavement regeneration present at the sites.

In Israel, Sharon (1962) performed in-place experiments on hamadas, the middle east term for desert pavement. Two different types of hamadas were studied: one was flint, and the other was a limestone cover. Both were carefully cleared of rocks to prevent unnecessary disturbance of the soil; one area was 150 m^2 and the other was 120 m^2. After 5 years the two plots were photographed and the amount of surface lowering was measured. Both hamadas were found to have regenerated nearly identical amounts of cover, estimated to be about 60–80%; and their surface lowering was measured and found to be an average of 15–20 mm. The area outside the plot was also measured for surface lowering and was about 10 mm.

At the time of the writing of this guidebook, Site 4 has just been cleaned (fig. 13) and no information is available regarding regeneration of the surface. However, by measuing the weight, number, and size of pebbles underlying the desert pavement to the depth of one foot it can be calculated that if all the fines were removed (by wind or water) clasts remaining as lag would be enough to completely regenerate (by weight alone) particles to produce an armor similar to that of the original surface if the surface were lowered about 3 inches.

On study sites near Quartzsite preliminary analysis of the data indicate that in 10 or 12 years enough of the fines will be removed to generate an armor similar to the original.

In an attempt to investigate further the origin and time of formation of desert pavement, observations were taken on the intaglio southeast of Chandler, Arizona. An intaglio is an animal or human figure carved in the desert by disturbing the desert pavement. Such figures have been drawn over many years by ancient man in the area.

The exact age is not available for the intaglio southeast of Chandler (the Pima Indian culture's witch Ha-ak Va-ak). However, the area scraped for the figure in the ancient desert pavement has now been replaced by a new armored surface. But the new surface is composed of smaller stones than the original and also the color is not as dark as the original. The short study we have conducted at Quartzsite also indicates that the regenerating surface is composed of smaller clasts than those of the original surface.

The methods by which the clasts reappear are under study. Two of the most obvious methods are by either wind or water deflation of the fines. Another suggestion is that the stones migrate upward by repeated wetting and drying of the silty clay. This has been demonstrated in the laboratory (Springer, 1958) and supported in the field by Howard and others (1977). This upward stone migration is especially true if the clay fraction has expanding lattice clays. X-ray diffraction analysis of the clays near Quartzsite indicate the presence of montmorillonite and a variety of mixed layer clays usually consisting of montmorillonite and illite in all samples. Preliminary x-ray diffraction analysis work has been unable to determine the clay mineralogy in the silty clays at the Mesa Terrace site.

From **STOP 10** proceed eastward along Thomas Road. Here you find probably the only place in the world where a Saguaro cactus is growing in the middle of the road and traffic is detoured to each side. From here the road ascends

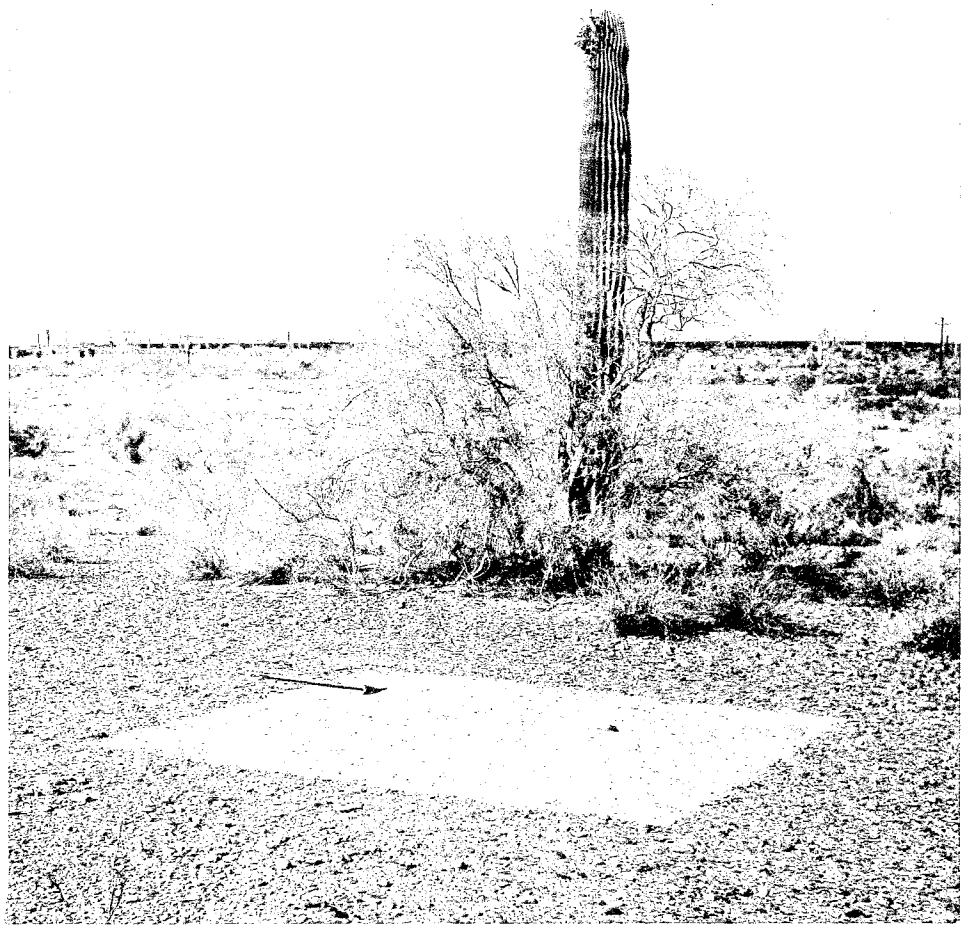

Figure 13. Desert pavement study site No. 4 near Thomas and Higley Roads. (Photograph No. 3946 by Troy L. Péwé, June 18, 1977.)

to the Sawik Terrace level (fig. 10) at an elevation of 1,400–1,450 feet.

STOP 11. PEDIMENT WASH (GRUS) OVERRIDING SAWIK TERRACE GRAVEL. At an elevation of about 1,433–1,438 feet in the southeastern one-quarter of Section 26 (fig. 10), the edge of the "pediment wash" sediments can be seen and the underlying rounded caliche-cemented gravels of the Sawik Terrace are exposed in shallow washes.

Proceed west over calichified pediment wash (grus) on desert trail until it intersects Bush Highway at **STOP 12.**

STOP 12. SPOOK PEDIMENT. The broad pediment cut on granite rocks is named the Spook Pediment (Péwé, 1971) from Spook Hill, a well developed inselberg projecting 300 feet above the gently sloping pediment surface in the northern part of the Buckhorn Quadrangle (fig. 10). Part of the pediment is graded to remnants of the Sawik Terrace, but most is graded to the Mesa Terrace in this area. Bedrock crops out along the Bush Highway at this locality and stream cuts to the east and west. The typical gently sloping, smooth-looking pediment is gullied with shallow stream incisions 1 to 5 feet deep. The surface of the Spook Pediment in this area slopes about 100 feet per mile to the west and southwest.

STOP 13. GRANITE REEF DIVERSION DAM (Granite Reef Dam Quadrangle, 1964; fig. 14). A view of Salt River 2 miles downstream from the mouth of Verde River near Granite Reef Diversion Dam. From this locality the river and the low Granite Reef Dam can be seen (fig. 15).

Granite Reef Diversion Dam is one of the many facilities of the Salt River Project, an organization that brings power and irrigation water to the Salt River Valley. The Salt River project is the nation's oldest and most successful multi-purpose reclamation development, providing a dependable supply of water and power for the greater Phoenix valley. The Project delivers water to 250,000 acres of land and electricity to approximately 240,000 customers (1976). The Salt River Project began

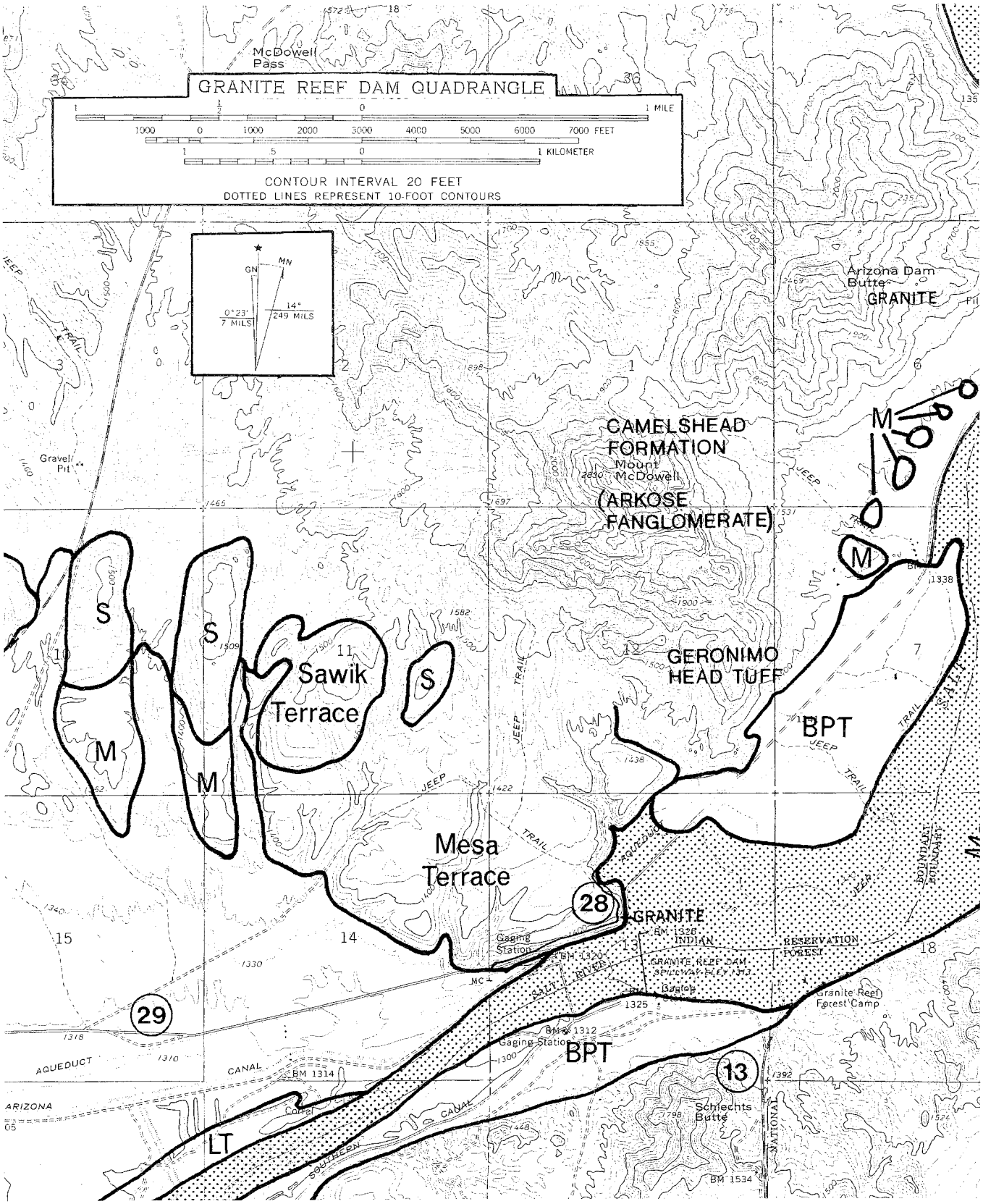

Figure 14. Field trip log map showing locations of STOPS 13–15 and 27–29.

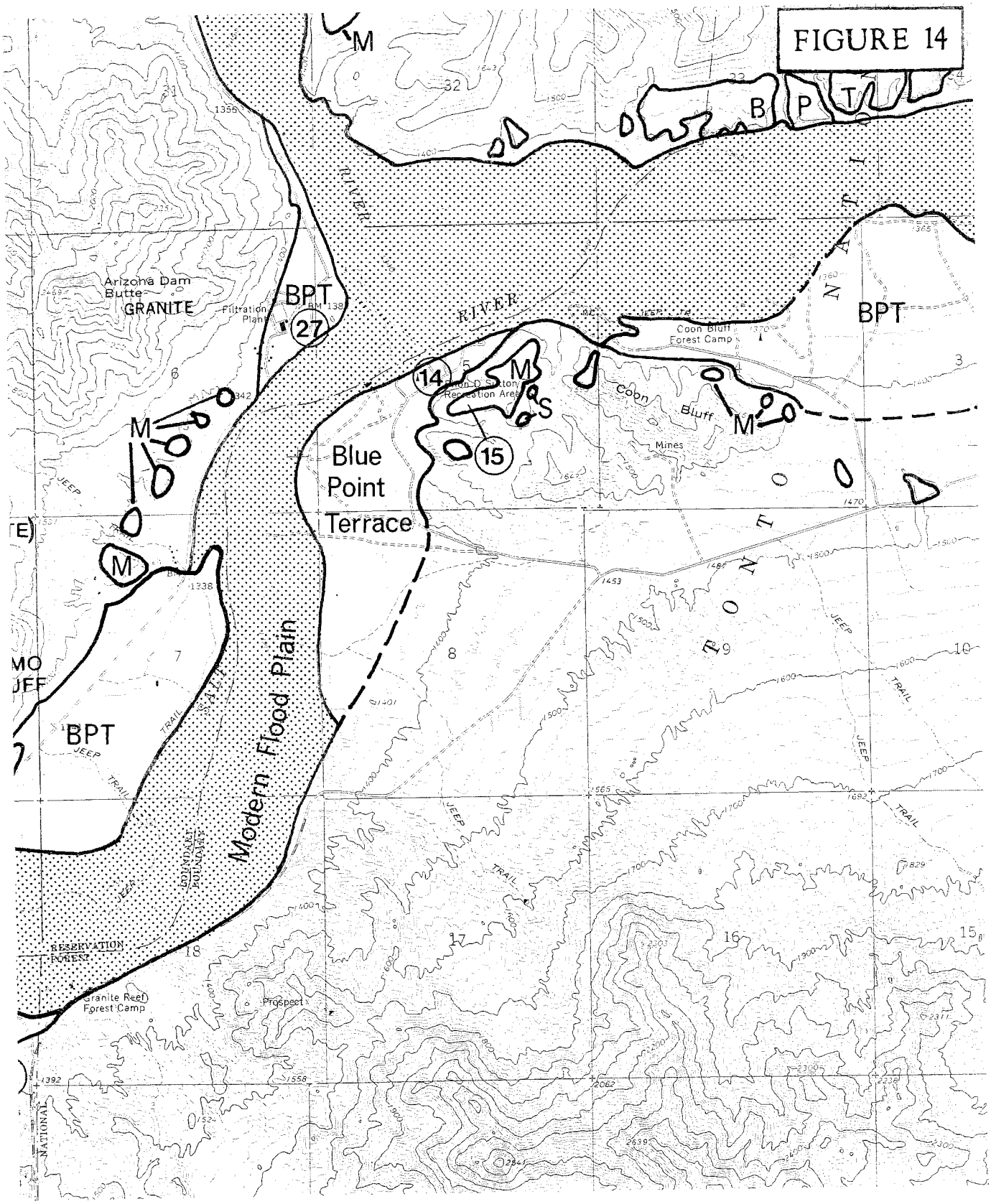
FIGURE 14
M
B
P
T
BPT
Arizona Dam Butte
GRANITE
Filtration Plant
27
RIVER
Coon Bluff Forest Camp
14
Coon
Bluff
Mines
15
Blue Point Terrace
Modern Flood Plain
JEEP
TRAIL
BOUNDARY
RESERVATION FOREST
Granite Reef Forest Camp
Prospect

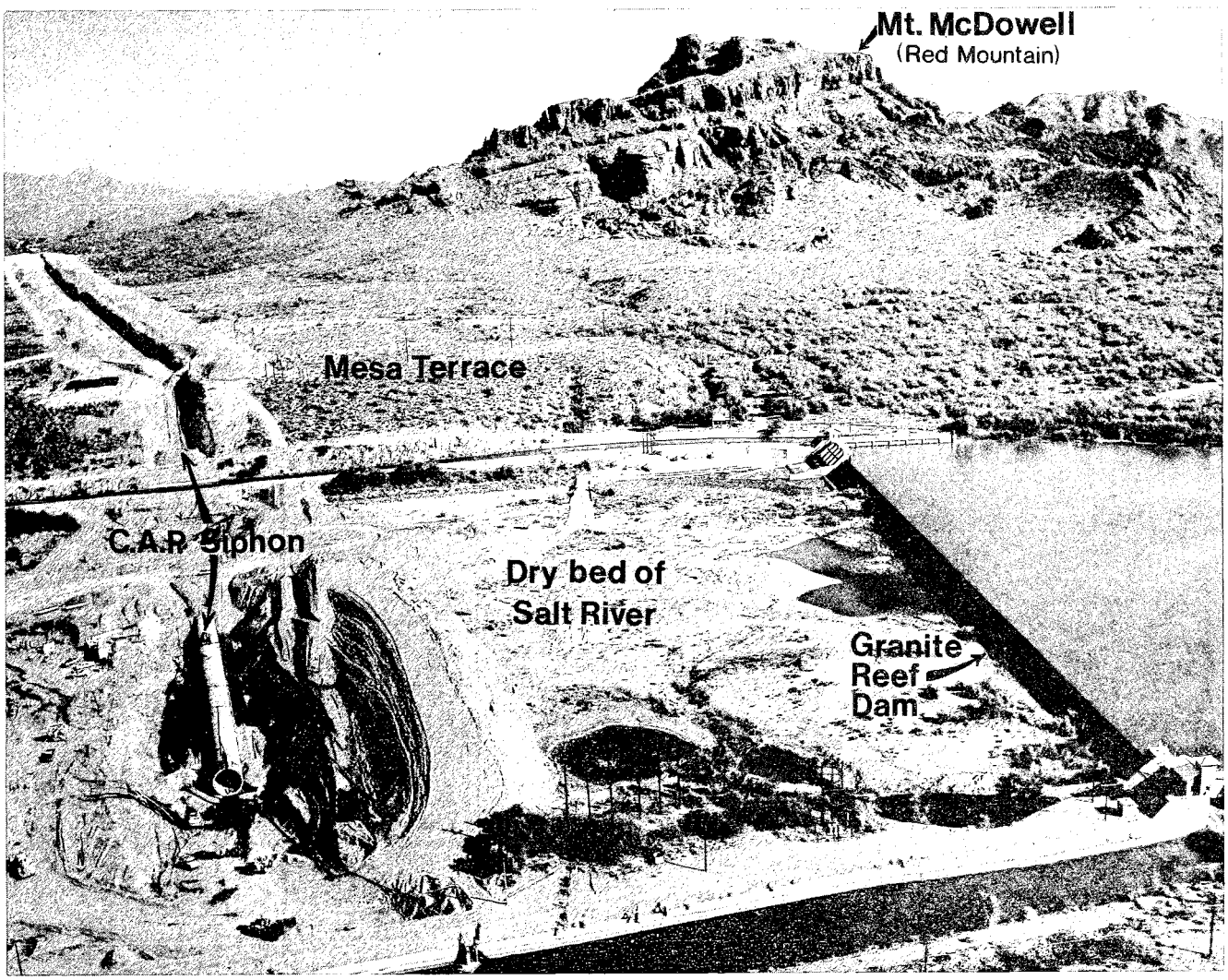

Figure 15. Granite Reef Diversion Dam on the Salt River. Aerial view to north. CAP siphon is being constructed in the open trench at left. (Photograph by Nyle Leatham, The Arizona Republic, September, 1977.)

supplying water and power to the arid Phoenix and central Arizona region in 1911, and today provides water from the Salt and Verde Rivers and from 255 deep wells through a 138-mile canal network. The Salt River Project was the first multi-purpose project authorized under the Federal Reclamation Act of 1902 and today it is comprised of the Salt River Valley Users Association and the Salt River Project Agricultural Improvement and Power District. The Salt River Project was organized February 9, 1903 by some 4,000 land owners to secure from the U.S. Government a loan for the construction of Theodore Roosevelt Dam.

Granite Reef Diversion Dam was completed in 1908. It is only 29 feet high but 1,000 feet long. Its purpose is to divert water, released from the reservoirs upstream, to the canals north and south of the river for delivery to water users in the Salt River Project. No power is generated at Granite Reef Dam. The Arizona Canal and the Southern Canal are the most upstream canals on the lower Salt River and were built many years ago: the Arizona Canal in 1883–1884 and the Southern Canal in 1908. Actually, there was a small diversion dam called the Arizona Dam at this site many years ago. It was built in the early Eighties to divert water into the canals (Davis, 1897).

A few hundred yards downstream from Granite Reef Dam the Central Arizona Project Canal carrying Colorado River water passes under the Salt River by means of a giant siphon.

From **STOP 13** proceed along the modern floodplain of the Salt River; on part of the pediment; and then to **STOP 14**, Phon D. Sutton Recreation Area.

STOP 14. PHON D. SUTTON RECREATION AREA. This picnic area is on a low terrace of the Salt River about 40 feet above the river (fig. 14). It is part of the Blue

Point Terrace. Note that the Blue Point Terrace, as well as the Mesa and Sawik Terraces, are increasingly higher above the modern floodplain as one goes upstream.

STOP 15. COON BLUFF. A remnant of Mesa Terrace overlies bedrock at an elevation of 1,480–1,550 feet at this locality. The surface is 160–180 feet above the modern river. A great many of the large boulders have been fractured in place with displacement of 2 to 6 inches. Such fracturing appears to be present only of clasts on the Mesa and Sawik Terraces. The fracturing and displacement is by caliche formation while in the caliche level. Subsequent erosion and carbonate solution has exposed fractured boulders and cobbles.

It can be here noted that many of the boulders, especially the quartzite boulders, have well-developed impact scars or percussion marks, the results of large boulders saltating along the river bottom under high velocity flows of the stream. Such marks are well developed on the boulders of the Mesa and Sawik Terraces but poorly developed or absent on the lower terraces, although large boulders are present in all terraces. This may suggest a stronger stream regimen during the time of deposition of the upper terrace gravels.

The rock types represented by the cobbles and boulders of the Mesa Terrace are typical both of the deposits of the terraces and those of the active floodplain of the lower Salt River Valley. Kokalis (1971) examined 5,900 samples and determined that 15% of the clasts were from the Precambrian basement complex of igneous rocks; 36% were of the volcanic rocks of Tertiary age; and 48% were sedimentary rocks of Precambrian age. The rock composition of two typical Salt River gravel samples are illustrated in Table 2. The two most common rock types in the terrace deposits are orthoquartzite and rhyolite (metarhyolite). The larger the boulder the more likely it is to be one or another of these two types of rock.

As mentioned earlier, while it is not possible to distinguish the terrace sediments and the alluvium of the active floodplain of the Salt River on the basis of lithologic characteristics, Salt River deposits may be easily distinguished from other unconsolidated sediments in the valley.

Coon Bluff is in part made up of the Tertiary Camels Head Formation (arkose conglomerate). The cobbles weathering out of this conglomerate give rise to a lag gravel on top of Coon Bluff that could be mistaken for a terrace deposit. Examination of the rock types in this lag gravel quickly shows that the percentage of sedimentary rocks of Precambrian age is very low and the percentage of granitic rocks very high; the rock types present a distribution of an over-all composition (Table 2) much different from the Salt River sediments (Kokalis, 1971).

The gravel of the Mesa Terrace on top of Coon Bluff is heavily cemented with caliche and the cobbles are entirely surrounded by calcium carbonate. Qualitatively, as mentioned earlier, it is evident that the gravel of the upper terrace, the Sawik Terrace, is most firmly cemented and has the thickest development of caliche. Thicknesses of 30 feet of caliche cap rock occur in the deposits of the Sawik Terrace and are almost that thick in deposits of the Mesa Terrace. Caliche development in Blue Point Terrace gravel is moderate to poor, relatively speaking, and is very weak to absent in gravel of the Lehi Terrace.

From this stop it is possible to look downstream at the north end of the Granite Reef Diversion Dam and see a continuation of the Mesa Terrace level.

At this stop gravels are lying 50 or 60 feet above the Mesa Terrace surface on areas of bedrock which are thought to be remnants of the higher Sawik Terrace (fig. 14).

Proceed from **STOP 15** to **STOP 16** on the Bush Highway across the lower edge of the pediment (fig. 14). The well-developed pediment extending north from the Usery Mountains to the Salt River in this area is termed the Bush Pediment (Péwé, 1971) from the new and old Bush Highways which traverse the pediment from north to south and east to west. The pediment today is, for the most part, graded to the Blue Point Terrace, although it is now being cut below this level in an attempt to be graded to the modern Salt River floodplain.

STOP 16. MESA TERRACE REMNANT (Stewart Mountain Quadrangle, 1964; fig. 16). A bedrock remnant about 200 feet above the Salt River is capped with weathered, caliche-cemented gravel which is part of the Mesa Terrace. Characteristics of the gravel here are similar to those described on Coon Bluff. A higher level gravel which is part of the Sawik Terrace lies 40 or 50 feet above this surface on bedrock. On the map (fig. 16) and the aerial photograph (fig. 17) it can be seen that there are several bedrock knobs extending 2 or 3 miles upstream, to the east, on the south side of the Salt River. The knobs bear remnants of the upper two terrace gravel deposits. This fact apparently was first pointed out by Tilford (1966, p. 19).

Looking south from this remnant up the Bush Pediment one can realize that at one time the Bush Pediment was graded to the Sawik Terrace level and

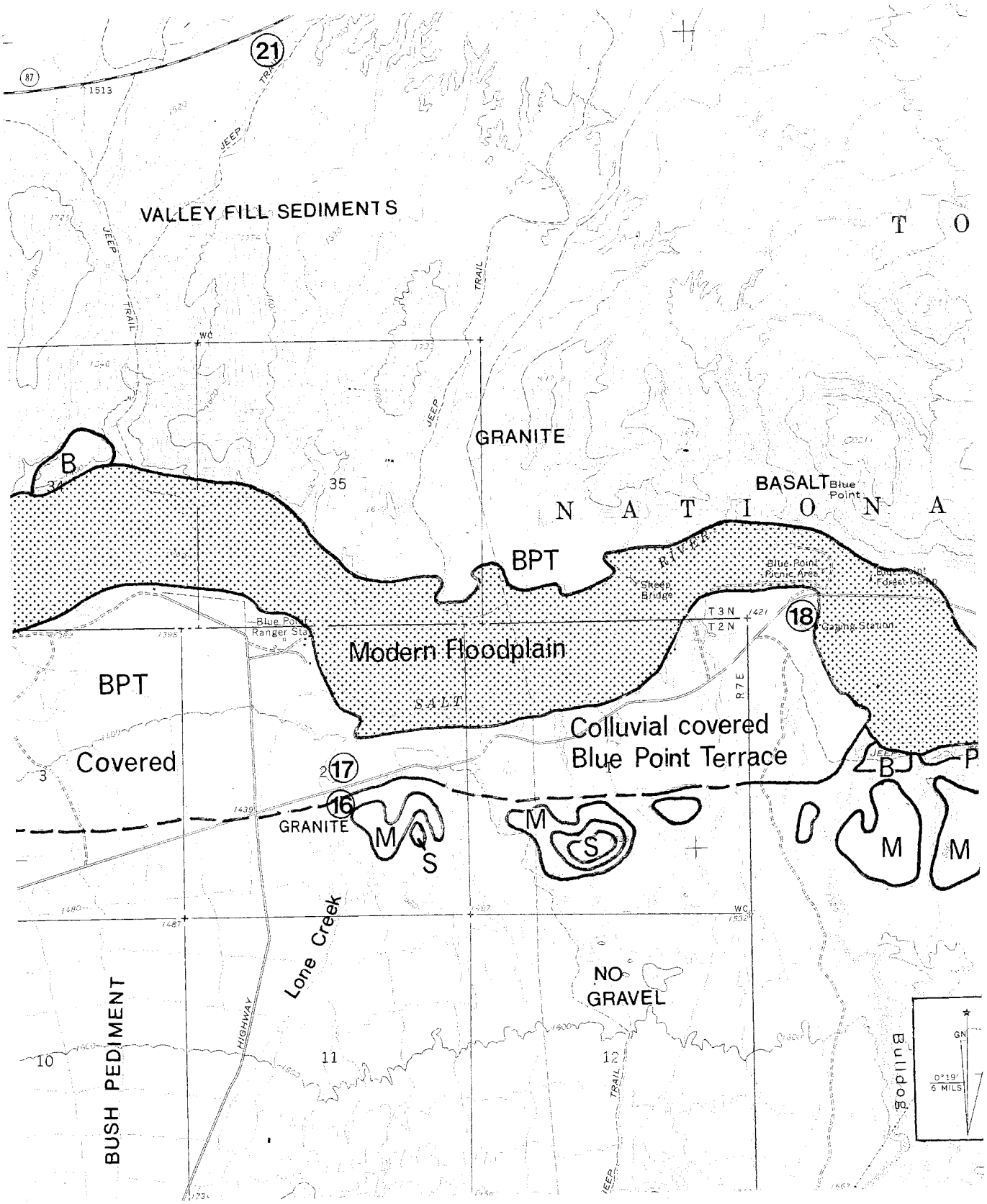

Figure 16. Field trip log map showing locations of STOPS 16–21.

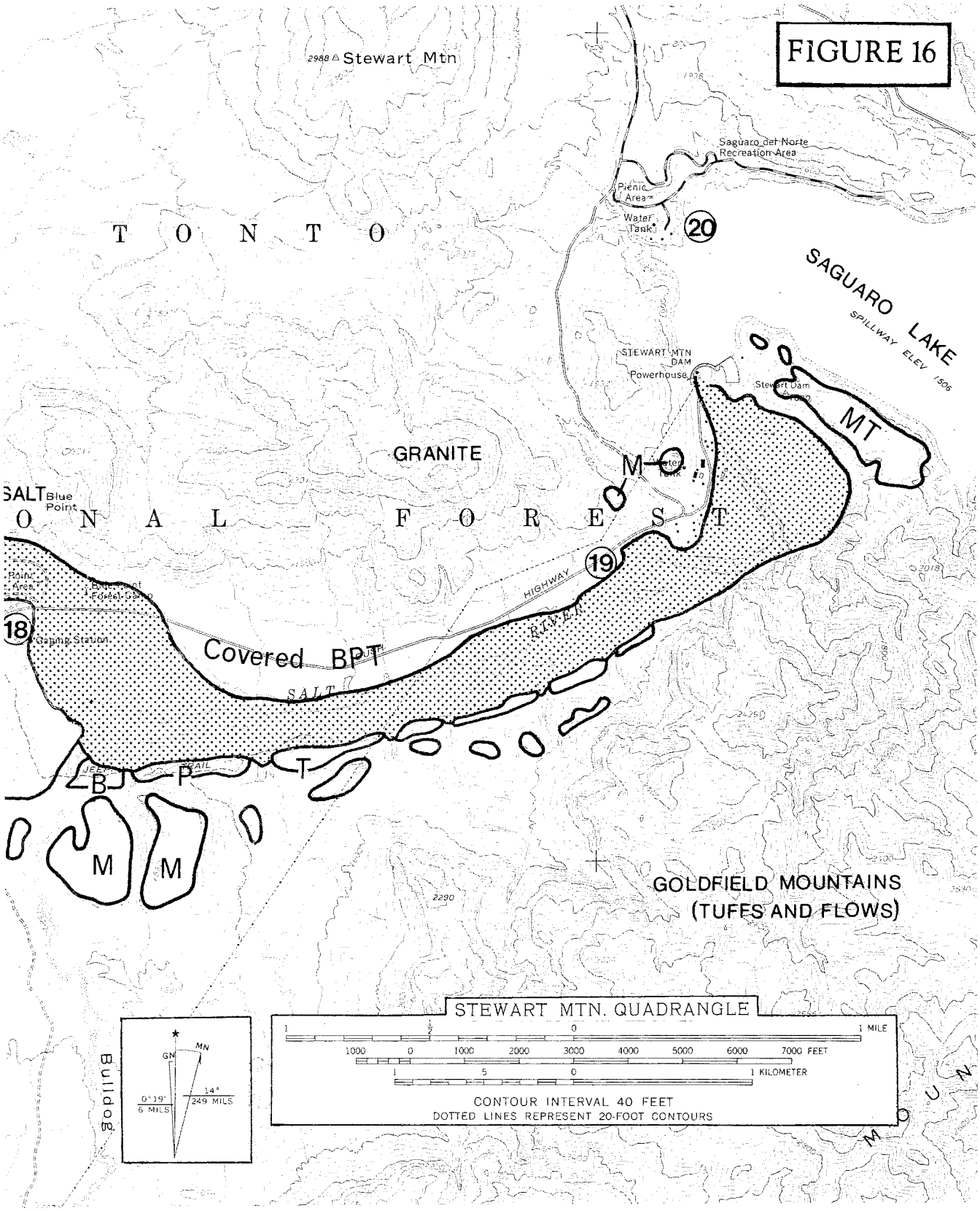
FIGURE 16
Stewart Mtn
Saguaro del Norte Recreation Area
Picnic Area
Water Tank
20
T O N T O
SAGUARO LAKE
SPILLWAY ELEV 1506
STEWART MTN DAM
Powerhouse
Stewart Dam
MT
GRANITE
M
SALT
Blue Point
O N A L F O R E S T
19
HIGHWAY
RIVER
18
Gaging Station
Covered BPT
SALT
B
P
T
M
M
GOLDFIELD MOUNTAINS
(TUFFS AND FLOWS)
STEWART MTN. QUADRANGLE
1 MILE
1000 0 1000 2000 3000 4000 5000 6000 7000 FEET
1 KILOMETER
CONTOUR INTERVAL 40 FEET
DOTTED LINES REPRESENT 20-FOOT CONTOURS
GN
MN
0°19'
6 MILS
14°
249 MILS
Bulldog
M O U N

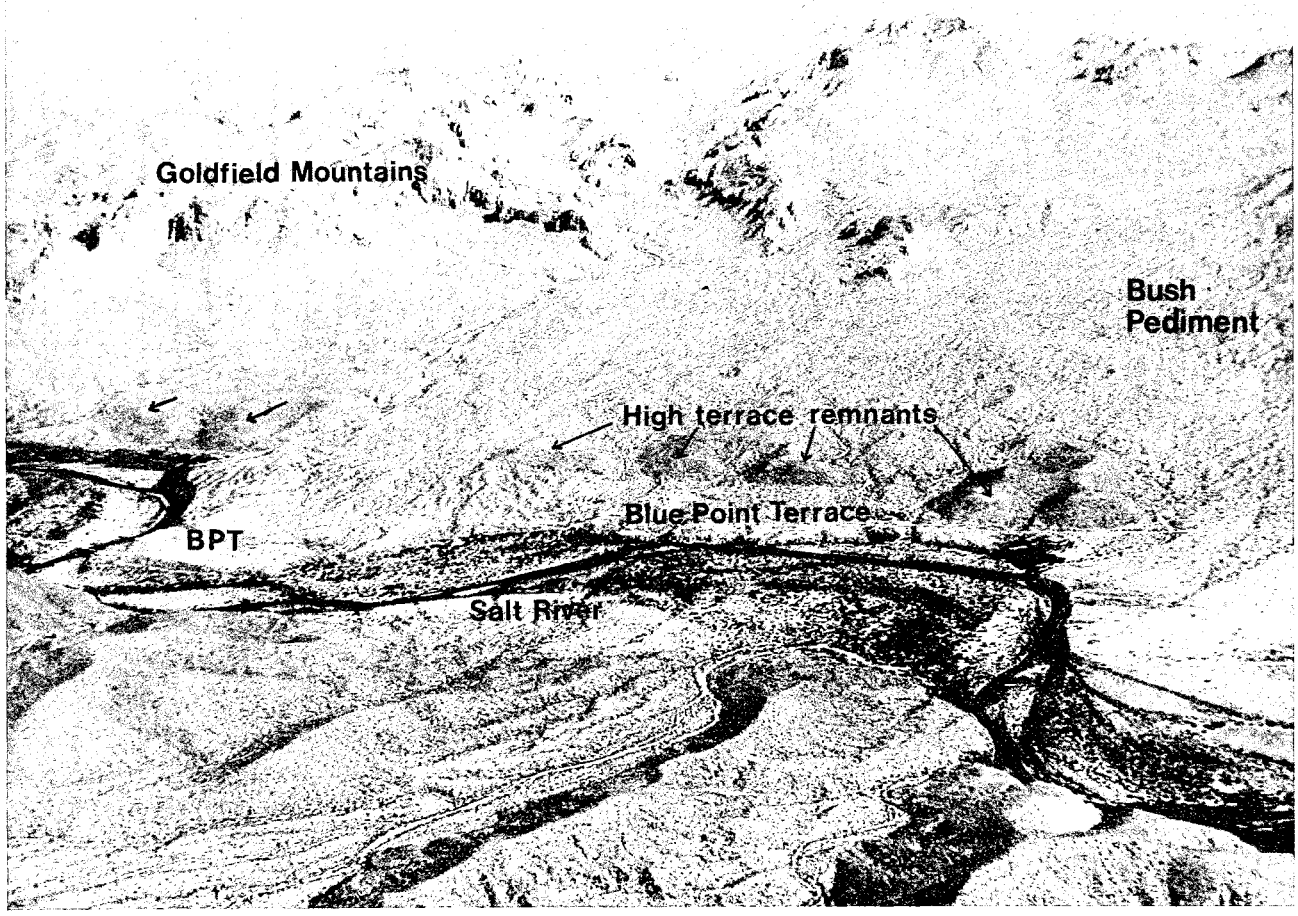

Figure 17. Aerial view of the lower Salt River Valley looking south from Lone Creek to Blue Point. Remnants of Sawik and Mesa Terraces on bedrock knobs in middle ground on southside of river (see figure 16). (Photograph No. PK 21,325 by Troy L. Péwé, June 11, 1977.)

then later to the Mesa Terrace level. Subsequently, with the lowering of local base level (the downcutting of the Salt River) the pediment has been regraded from the Mesa Terrace level to the Blue Point Terrace level, and is now being worn down even lower (fig. 17). Undoubtedly, the removal of such a large amount of granite has taken a considerable amount of time and supports the suggestion of considerable antiquity for the ages of the upper terraces.

It is evident from the STOPS so far, that the surface of Mesa Terrace rises higher and higher above the modern floodplain as one goes upstream. In the Tempe Quadrangle it was only 10 or 20 feet above the modern floodplain and cut on alluvium; it became a strath terrace near Granite Reef Dam and at this STOP it is 200 feet above the river. The surface continues to rise to about 220 feet above the river at Saguaro Lake and rises to more than 300 feet above the river upstream toward Lake Roosevelt. Figure 4 illustrates a generalized profile of the modern river and the Mesa Terrace surface between Tempe and Lake Roosevelt. It can be compared with the diverging terrace surfaces on other major streams as well as minor streams entering the Phoenix Basin.

STOP 17. LONE CREEK CROSS SECTION. An exposure on the left limit of Lone Creek from the Bush Highway north to the Salt River exhibits a thick deposit of pediment wash coming off the Bush Pediment. About 200 feet north of the Bush Highway the pediment wash deposit can be seen overlying a more or less horizontal gravel surface of the Blue Point Terrace gravel. Further downstream the gravel is exposed overlying bedrock on the left limit of the Salt River at the junction of the stream and the river. A climb to the top of the terrace surface across the

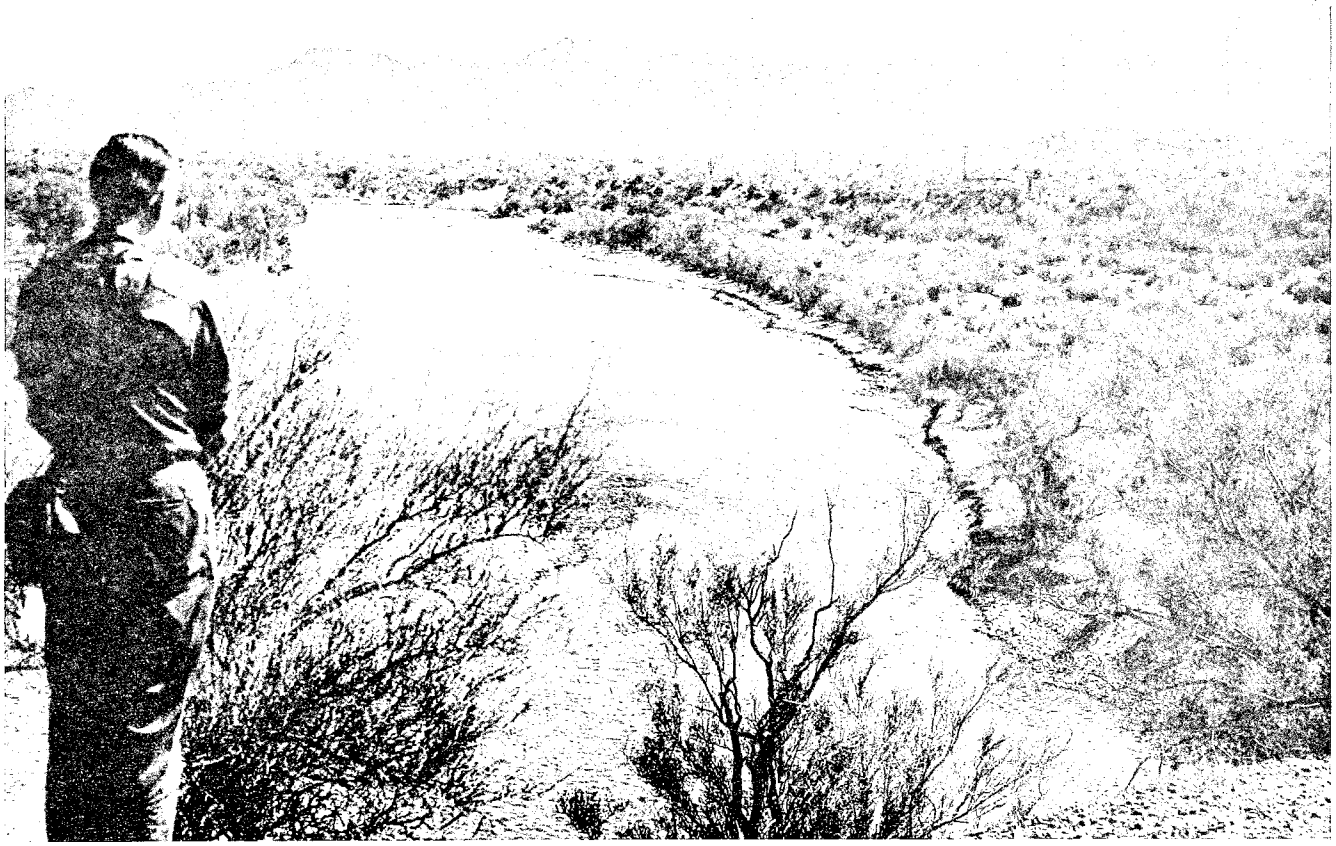

Figure 18. View upstream (east) of lower Salt River, NE Sec. 2, T. 2 N., R. 7 E. Scarp of Blue Point Terrace on right in middle ground near river; remnants of Mesa Terrace on bedrock knob on far right. Goldfield Mountains in background. (Photograph No. PK 14,203 by Troy L. Péwé, March, 1970.)

exposed gravel indicates that there is very little caliche in the coarse gravel. A view upstream (fig. 18) from this vantage point (the junction of Lone Creek and the Salt River) shows the scarp of the Blue Point Terrace on the south side of Salt River; one-half mile southeast are bedrock knobs capped with gravel patches of Mesa and Sawik ages (fig. 16). Far to the southeast lies the front of the Goldfield Mountains of volcanic flows and ejecta (Fodor, 1969; Sheridan, Stuckless, and Fodor, 1970).

Between **STOPS 17** and **18** the terrace is covered with a colluvial apron of grus (granitic weathering debris) coming from the south (fig. 17), an apron which has been dissected by downcutting streams as local base level has been lowered since Blue Point Terrace time. These streams have not only cut through the grus cover, but through the gravel and into the underlying bedrock which is exposed on the terrace scarp and also in the small drainageways traversing the terrace between **STOPS 17** and **18.**

STOP 18. BLUE POINT GAGING STATION. At the bridge over the Salt River at this locality, gravel poorly cemented by caliche overlies bedrock. The Blue Point Terrace is here about 40 feet above the Salt River. South from the bridge can be seen a cross section of the terrace showing the grus cover which thickens to the south toward the Usery Mountains. The Blue Point picnic area receives its name from Blue Point, a large mass of basalt cropping out prominently on the north side of the river at this locality (fig. 16).

From **STOP 18** cross to the north side of the river. The highway from here to **STOP 19** is on the Blue Point Terrace which is completely covered by a sloping colluvial blanket of grus.

STOP 19. BEDROCK CLIFF OVER RIVER. Here the grus cover is thin or absent, and gravels of the Blue Point Terrace crop out over bedrock cliffs 40 to 50 feet high above the river.

Upstream from **STOP 19** a large alluvial fan (fig. 16) from a small stream to the north deflects the Salt River to the south to cut into rocks of the Goldfield Mountains. A guest ranch which lies immediately

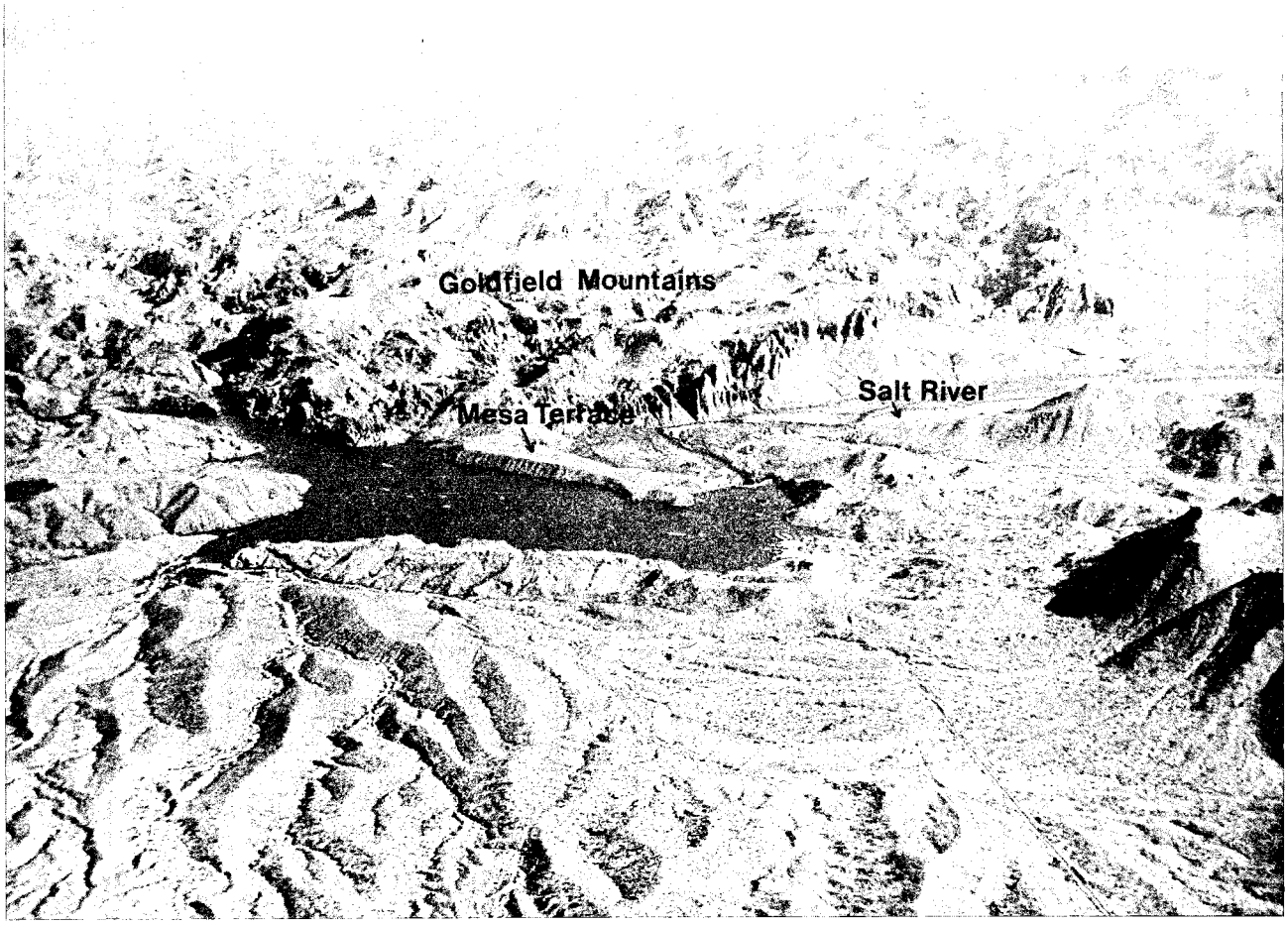

Figure 19. Aerial view of Saguaro Lake and Stewart Mountain Dam, looking south. Long finger of land extending toward dam is capped with gravel of the Mesa Terrace and is 220 feet above the river. Goldfield Mountains in middle ground behind lake. (Photograph No. PK 21,323 by Troy L. Péwé, June 11, 1977.)

upstream from this fan in the right limit of the river is on a Blue Point Terrace surface.

STOP 20. SAGUARO LAKE RECREATION FACILITY. From the restaurant an excellent view can be obtained to the north, south, and east. To the north one can see a colorful volcanic tuff layer from the Superstition Mountain area overlying the granite. To the south is Stewart Mountain Dam holding in Saguaro Lake. A long finger of land (figs. 16, 19) stretching from the Goldfield Mountains to the dam has a relatively flat-topped area which is the surface of the Mesa Terrace at an elevation of 1,620 feet or about 220 feet above river level. When the lake is drained a well-developed surface of the Blue Point Terrace present under most of the lake adjacent to this facility is visible.

Stewart Mountain Dam is one of the six dams which regulates water flow for the Salt River Project. The first dam constructed by money lent by the Federal Government (Salt River Valley Water Users' Assoc.) was the Theodore Roosevelt Dam (fig. 20). Construction of the dam began in 1905. The construction of the dam itself was a technique called cyclopian rubble. The faces of the dam were constructed from hand-hewn stones to give a finished appearance. In between the faces, the dam was filled with large boulders and mortar. Actual construction of the dam required cutting of about 350,000 cubic yards of stone from the side of the mountain.

Roosevelt Dam, the world's highest masonry dam, is 184 feet thick at the base, 16 feet wide at the crest and rises 280 feet. Its reservoir, Roosevelt Lake, has a capacity today of 1.28 million acre-feet. When filled, Roosevelt Lake has a shoreline of more than 88 miles. The dam also has a generating capacity of 36,000 kw.

To aid in water supply for irrigation as well as for power supply, additional dams were built on the lower Salt River. The first of these dams, Mormon Flat, was built between 1923 and 1925 and is located downstream from Roosevelt Dam. It has a water storage capacity of 50,852 acre-feet and

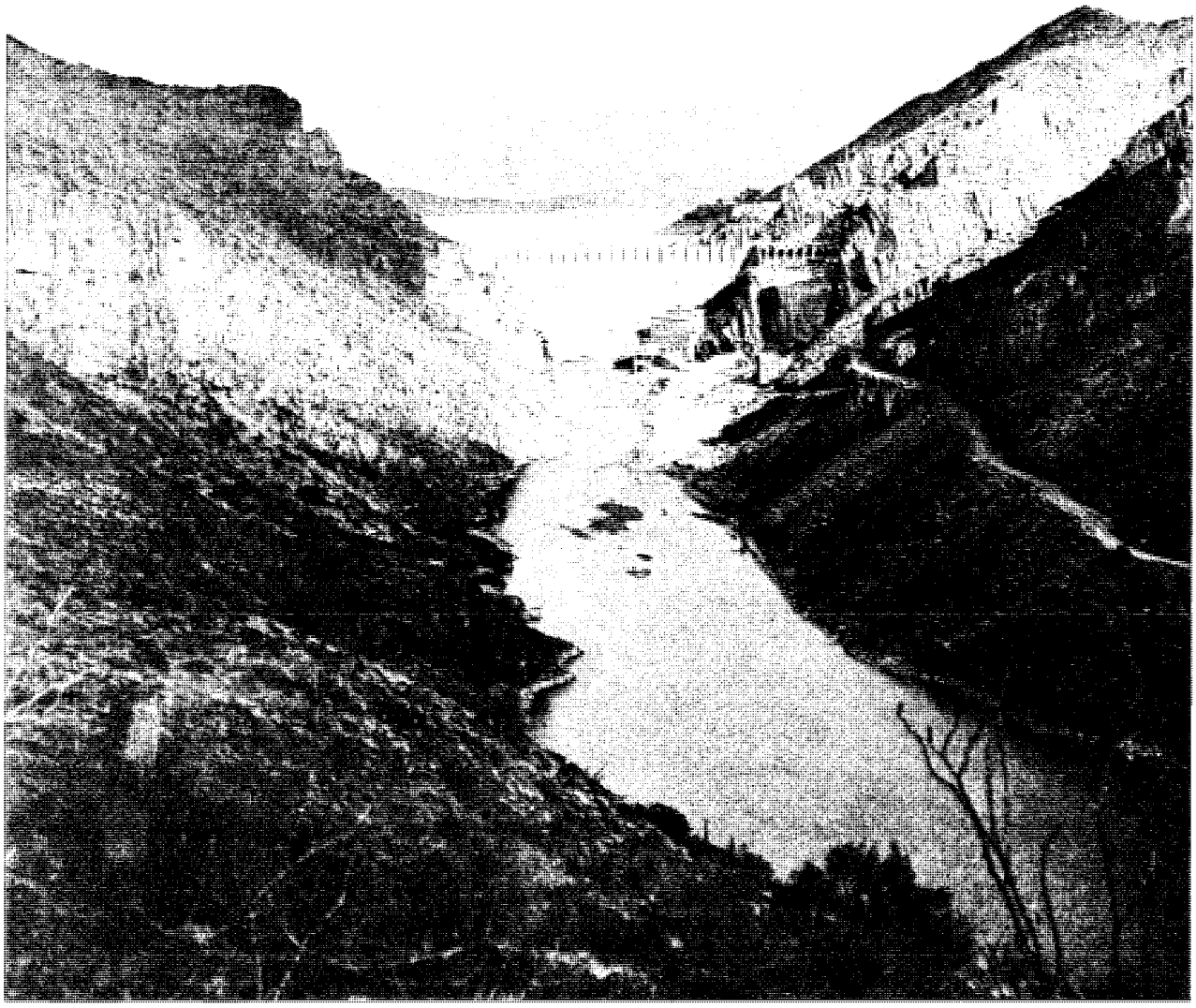

Figure 20. Theodore Roosevelt Dam and Roosevelt Lake on the lower Salt River, Arizona. Italian stone masons constructed the dam from local limestone. (Photograph through the courtesy of the Salt River Project.)

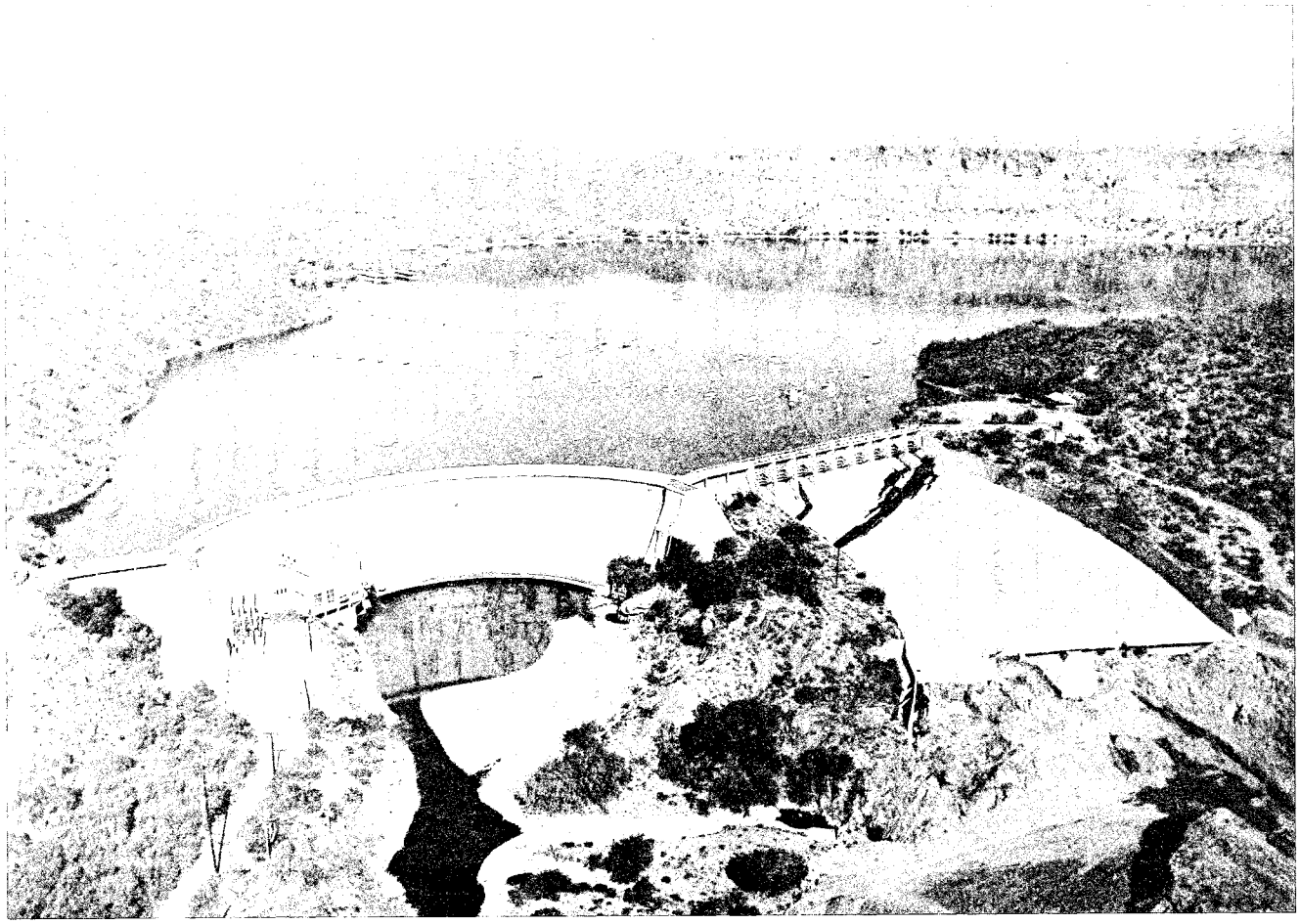

Figure 21. Stewart Mountain Dam and Saguaro Lake on the lower Salt River, Arizona. Volcanic tuff forms the light-colored cliff on the far side of the lake. Fault gouge zone extending under spillway apron is at far lower right. (Photograph through the courtesy of the Salt River Project.)

today has a generating capability of 60,000 kw.

In 1924, shortly after the Project began building Mormon Flat Dam, construction started on a third dam. This dam was named Horse Mesa Dam because it was built near a mesa allegedly used for hiding stolen horses. This dam is half way between Roosevelt and Mormon Flat Dams and forms Apache Lake with a storage capacity of 245,138 acre-feet. The generating capacity is 129,000 kw.

Stewart Mountain Dam was built during 1928–30 to provide more water storage facilities and more sophisticated regulation of water use in the generation of power in the three dams already constructed. The dam, which cost $2.8 million, was named for its proximity to Stewart Mountain, landmark of the old Stewart Ranch. The reservoir created by this dam, Saguaro Lake, has a capacity of 69,765 acre-feet and the generating capacity is 10,500 kw.*

When Stewart Mountain Dam was constructed, investigations revealed that the depth to bedrock below present stream-bed elevation at the site was 91 feet (Tilford, 1966, page 19). Stewart Mountain Dam has been an interesting structure for study by both engineers and geologists because as early as 1937 it was noted that separation of the arch section of the dam from the power house was taking place (fig. 21). The dam is sometimes referred to as "the walking dam." In 1939, survey measurements to detect the rate and direction of movement of the dam were initiated. General upstream deflection of the crest of the arch section of the dam was observed for some 10 years to occur at the rate of approximately ½ inch per year. After 1950, the rate of upstream deflection declined to approximately ⅛ of an inch per year and has remained relatively constant since (Tilford, 1966).

As a result of inspections of the structure in 1942 and 1943 by the Bureau of Reclamation, it was recognized that the structural deterioration of the concrete in the dam was due to expansion caused by an alkali-aggregate reaction. Many concrete study cores were taken from various parts of the dam and considerable concrete was added to parts of the

*Nongeologic information on the dams and reservoirs has been provided by the Salt River Project.

dam. It has been reported (Tilford, 1966) that the spillway was built in 1936 using the same aggregate but no concrete reaction has taken place. Also, no reaction occurred in the concrete in the Horse Mesa Dam upstream which was constructed using similar aggregate.

In 1965 Tilford began a geologic study of the dam site and he states (1966) that no geologic report on the foundation was completed before or after construction, or even during the period between 1937 and 1944 when the constructional deterioration of the concrete was studied. There was general acceptance of the hypothesis that the expansion by the alkali-aggregate reaction was sufficient and of suitable nature to have caused all observed net movement and cracking of the dam.

Tilford (1966) indicates two faults under the dam foundation. One fault containing soft gouge exists under the spillway and the present writer has observed this particular phenomenon. The material is so soft that in the flood of December 1965 water over the spillway undercut the spillway causing part of the apron to collapse (see fig. 21). It is along the same fault gouge zone near the spillway edge that a worker was killed while excavating the gouge for grout backfill in November, 1976. Tilford postulates a fault directly under the dam arch because the rocks on each side of the dam are different and the fault probably controls the location of the gorge. Such a fault has not been seen in the bedrock to the north or south of the dam.

Tilford (1966) suggests that the net movement could be due solely to the alkali-aggregate reaction or in part, perhaps, to some movement along the fault zones under the dam. Subsequent to 1966 more detailed geologic work was done by the U.S. Bureau of Reclamation and no detrimental geologic conditions were reported.

Proceed north to granitic terrain and then onto the poorly consolidated terrestrial detrital material called "Tertiary Valley Fill." Junction with Beeline Highway (Highway 87); proceed south to **STOP 21.**

STOP 21. TERTIARY VALLEY FILL. Exposed in road cuts along the highway is poorly consolidated, poorly rounded material of fairly local origin; however, when a weathered lag gravel appears on the interfluves, it can be confused with terrace gravel of the Salt or Verde Rivers. Kokalis (1971), as well as Pope (1974), have demonstrated that there is a distinct difference in rock types between the Salt River gravel, Verde River gravel, and the Tertiary Valley Fill deposits (Table 2).

The Tertiary Valley Fill material is a term given to a widespread deposit of fine to coarse material shed from the fault block mountains and collected in the intervening basins. It includes a variety of fine to coarse-grained alluvial sediments with interbedded siltstones and sandstones. In this particular area, and into the Verde River valley, the material consists of a variety of bedded rock types ranging from nearly pure orthoquartzites to subgraywackes. Various granitic rock types serve as the main detrital source followed by volcanic and metamorphic detritals (Table 2). The Valley Fill deposits are typical of the inter-basinal sediments in an arid to semi-arid region and are probably representative of late to middle Tertiary deposits. All terrace gravel of the Salt and Verde Rivers are younger than the Valley Fill deposits.

STOP 22. HIGH TERRACE REMNANT ALONG VERDE RIVER. Adjacent to the Beeline highway, both to the north and south on the east side of the Verde River, are well-preserved remnants of the high Mesa Terrace (fig. 22). The rounded river gravel of the Verde river overlies Tertiary Valley Fill deposits. The 20 or 30 feet of thickness of river gravel is exceedingly well cemented by caliche and forms a resistant caprock. The upper surface of the terrace has well developed laminar caliche several inches thick. The surface of the terrace lies approximately 150–160 feet above the Verde River and additional terrace remnants occur on the east side of the Verde river downstream to near the junction of the Salt River (fig. 22). In addition, remnants of the Mesa Terrace occur on both sides of the river to the north as far as Bartlett Dam. These terraces are the continuation of the Mesa Terrace surface of the Salt River.

SUMMARY OF GENERAL GEOLOGY OF LOWER VERDE VALLEY

A view upstream from **STOP 22** (fig. 23) illustrates the highlights of the late Cenozoic history of the lower Verde Valley. As part of an overall study of both age and origin of alluvial terraces, pediments, and a general understanding of erosional and depositional features, as well as Quaternary tectonic development in the Phoenix area (Péwé, 1966, 1970; Kokalis, 1970, 1971; Pope and Péwé, 1973; Pope, 1974; Shank, 1973; Shank and Péwé, 1973; Péwé and Shank, 1973; and Christenson, Welsch and Péwé, 1975), Pope and Péwé undertook a study of the general geology of the lower Verde Valley from Bartlett Dam to its confluence with Salt River with the main objective of studying the distribution, characteristics, and origin of the terrace remnants. As with the terrace study along the lower Salt River, many 200-pound samples were taken for detailed mechanical analyses and geologic studies.

Prior to the entrance of the Verde River into the present lower Verde Valley, the deposits were mostly local and from the adjacent metamorphic and volcanic mountains (Table 2). In addition to this coarse valley fill there are thick silt and clay deposits.

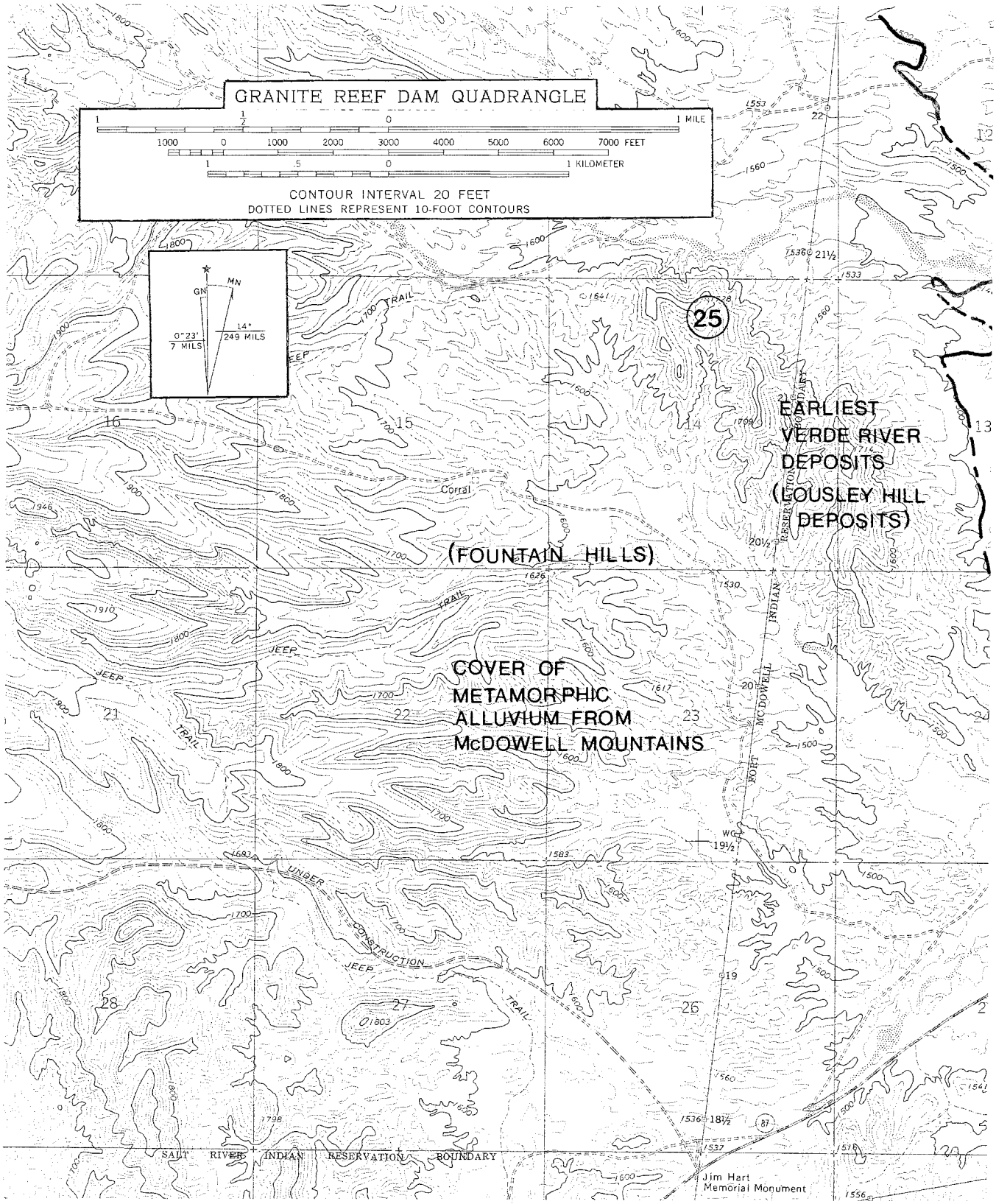

Figure 22. Field trip log map showing locations of STOPS 22–26.

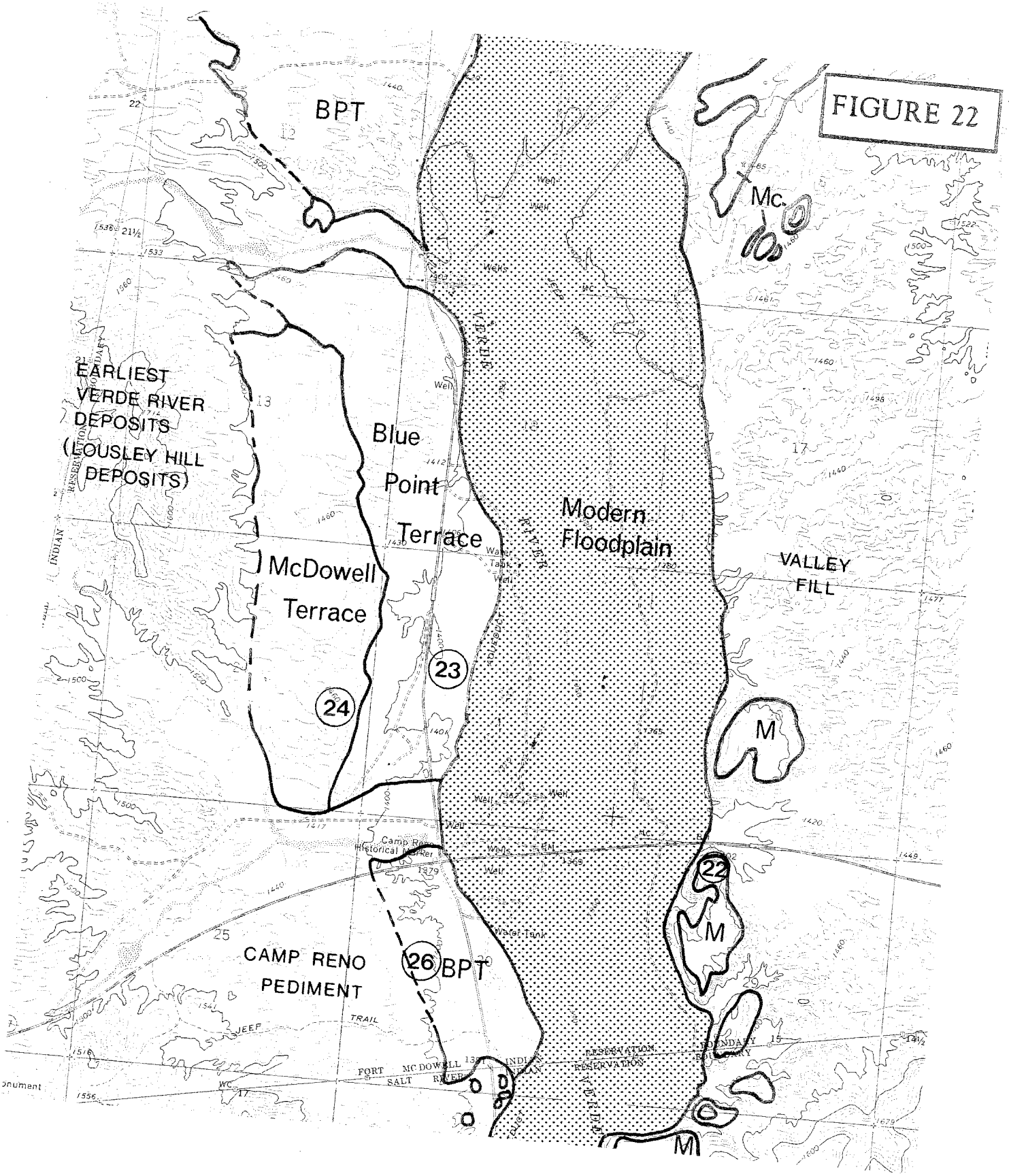
FIGURE 22
BPT
Mc.
EARLIEST
VERDE RIVER
DEPOSITS
(LOUSLEY HILL
DEPOSITS)
Blue
Point
Terrace
Modern
Floodplain
McDowell
Terrace
VALLEY
FILL
23
24
M
22
M
CAMP RENO
PEDIMENT
26
BPT
M
JEEP
TRAIL
FORT
MC DOWELL
SALT
RIVER
INDIAN
RESERVATION
Water Tank
Camp Reno
Historical Marker

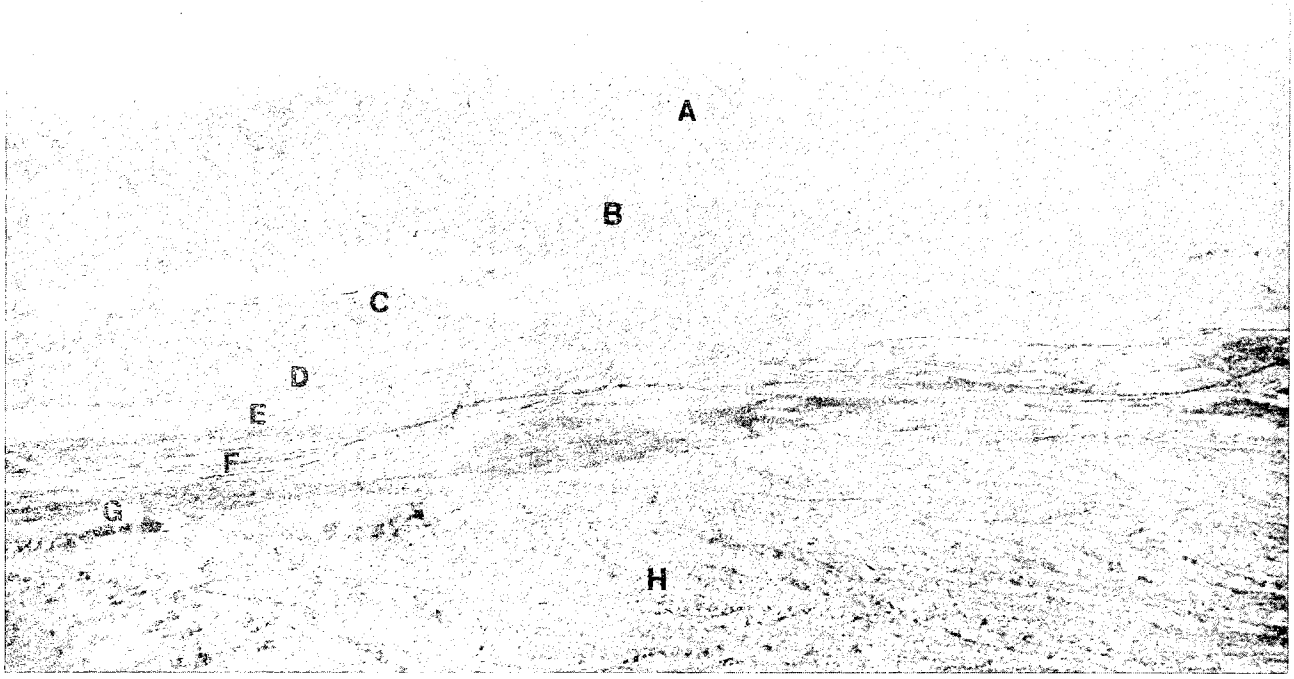

Figure 23. Aerial view of lower Verde River Valley looking west-northwest. A—McDowell Mountains; B—"finger"-like projections of metamorphic colluvium; C—Lousley Hill deposits; D—McDowell Terraces; E—Blue Point Terrace; F—modern floodplain of Verde River; G—Mesa Terrace; and H—valley fill deposits. White cleared area is Fountain Hill Development (see fig. 22). (Photograph No. PK 15,836 by Troy L. Péwé, December 30, 1972.)

From earlier investigations in the surrounding regions, several observations can be made which are perhaps related to the geologic history of the lower Verde River Valley area. McKee and McKee (1972), Melton (1960) and Merrill (1974) suggest that central Arizona stood higher than the present Grand Canyon region and that the drainage was to the north until late Tertiary time. This highland provided gravels of the Precambrian, early Paleozoic, and middle Tertiary volcanic rocks to the northern region. More than 10 million years ago, either uplift began in the north or basin collapse began to the south, apparently causing drainage reversal to the south. This reversal was suggested to occur no later than 5 million years ago, subsequently forming the ancestral drainage of the Verde River (McKee and McKee, 1972). The earliest known sediments within the lower Verde Valley that might represent this initial reversal are the Lousley Hill Deposits. These deposits are of rounded river gravel containing rock types derived from outside of the basin, such as limestones and other rocks not present in the surrounding hills of the lower Verde Valley. Therefore, one can suggest that the drainage forming the Verde River was initiated no earlier than 10 million years ago and no later than 5 million years ago. Perhaps the river did not directly enter the present valley but may have flowed into the Payson Basin (Pederson and Royse, 1970). Later diversion occurred causing the ancestral Verde River to flow into the present valley. The various gravels are highly calichified, greatly weathered and split by caliche formation, and occur above any of the lower terraces in the valley. Although no direct connection has been made, there is a possibility that these may represent gravel of Sawik age on the lower Salt River.

Following the formation of the Lousley Hill Deposits, the lower Verde River area was rejuvenated at least four separate times. The stages of rejuvenation are readily illustrated by three alluvial terraces and the modern Verde River floodplain (figs. 23, 24).

The Mesa Terrace remnants are well displayed and both the Lousley Hill Deposits and the Mesa Terrace gravels are well calichified. However, the gravels of all of the terraces and the Lousley Hill Deposits have similar rock types, and are distributed in the same size distribution. All are classed as a sandy gravel (fig. 25).

The two lower terraces, the McDowell and the Blue Point, have longitudinal profiles which are essentially parallel to the modern stream profile. However, the Mesa Terrace rises more than 93 m above the modern floodplain in

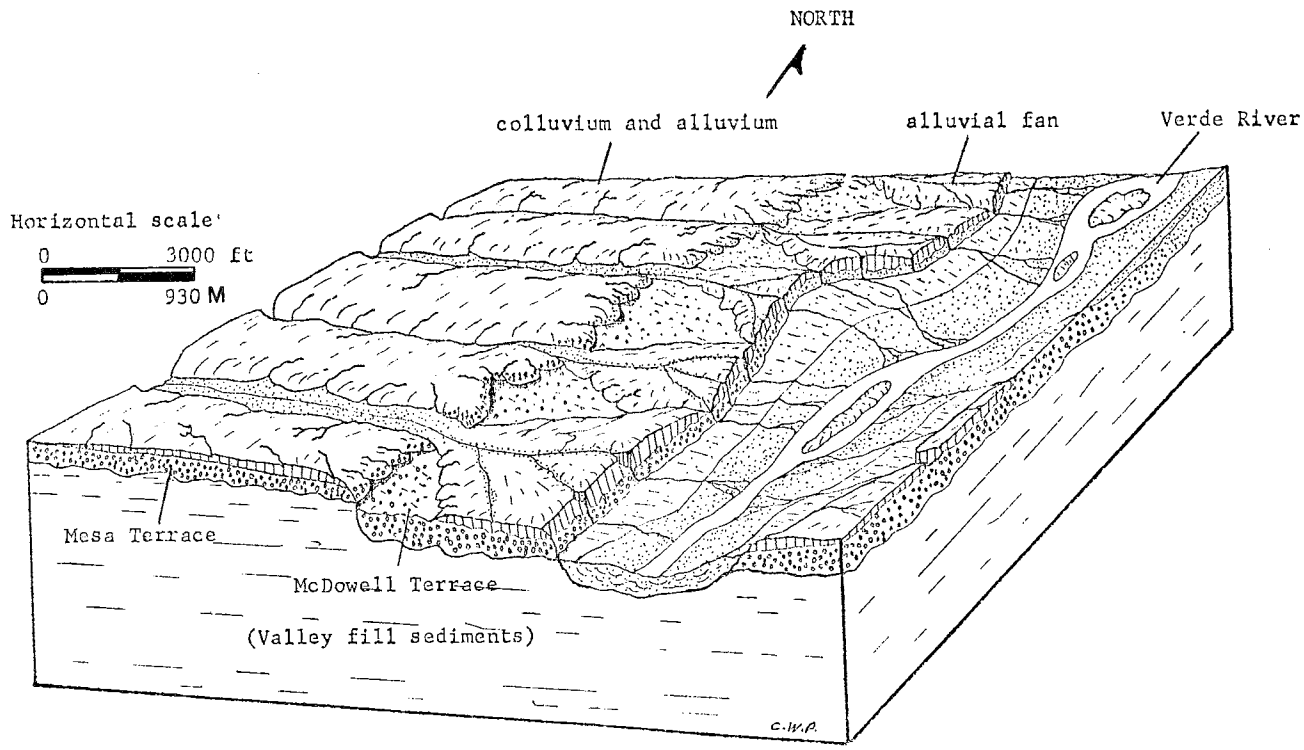

Figure 24. Block diagram showing alluvial and colluvial deposits shed from the McDowell Mountains overlying terrace deposits on the west side of the lower Verde River. Diagram portrays conditions during Blue Point time. (From Pope, 1974, fig. 17.)

the northern part of the study area from only 43 m above the modern floodplain in the south (fig. 4).

Work by Pope and Péwé illustrate that the ancient and modern Verde River alluvia are essentially the same. Throughout the development of the Verde River there has been no significant change in the rock types constituting the alluvium. Basaltic rocks remain the most dominant rock type (19–56 percent) followed by granitic rock types (10–26 percent), purple orthoquartzite (12 percent), metamorphic rocks (15 percent), volcanic rocks (18 percent), and minor amounts of a variety of other rock types.

The ancestrial Verde River may have had a slightly higher regimen however, because the clasts are slightly larger (frequently 3 feet in diameter).

STOP 23. BLUE POINT TERRACE. The Blue Point Terrace is well preserved and extensively covered with as much as 30 feet of metamorphic colluvium and alluvium. This cover is spread over the terrace down to the modern stream channel. The upper surface is moderately dissected with an occasional vertically exposed section. Such sections can be seen about 1 mile north of **STOP 23** along the highway as well as in the southern part of Section 12 (fig. 22). The amount of decay and splitting of cobbles is negligible compared with that in the other terraces.

The Blue Point terrace is best preserved on the west side of the Verde River (fig. 23).

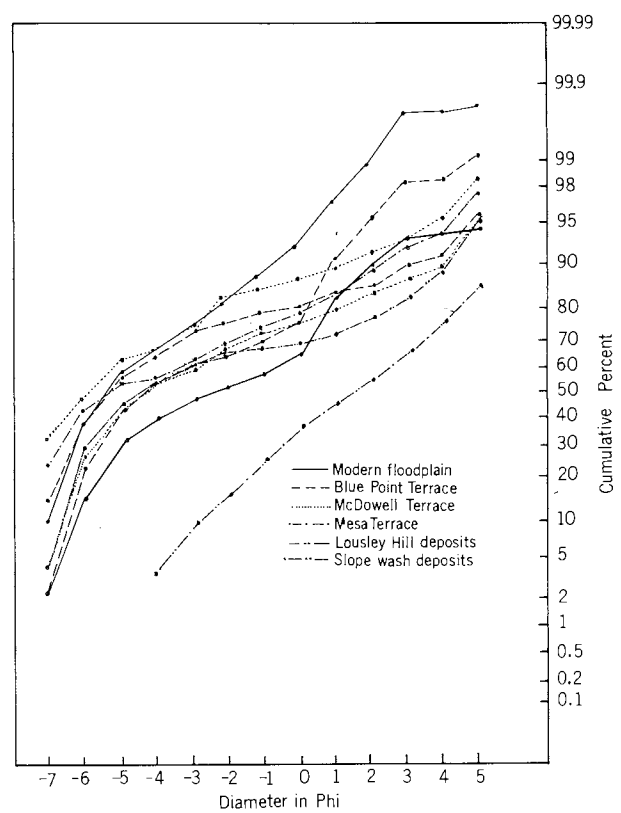

Figure 25. Cumulative-frequency distribution curves for analyses of sediments of modern floodplain and terraces of the lower Verde River Valley, Arizona. (After Pope, 1974.)

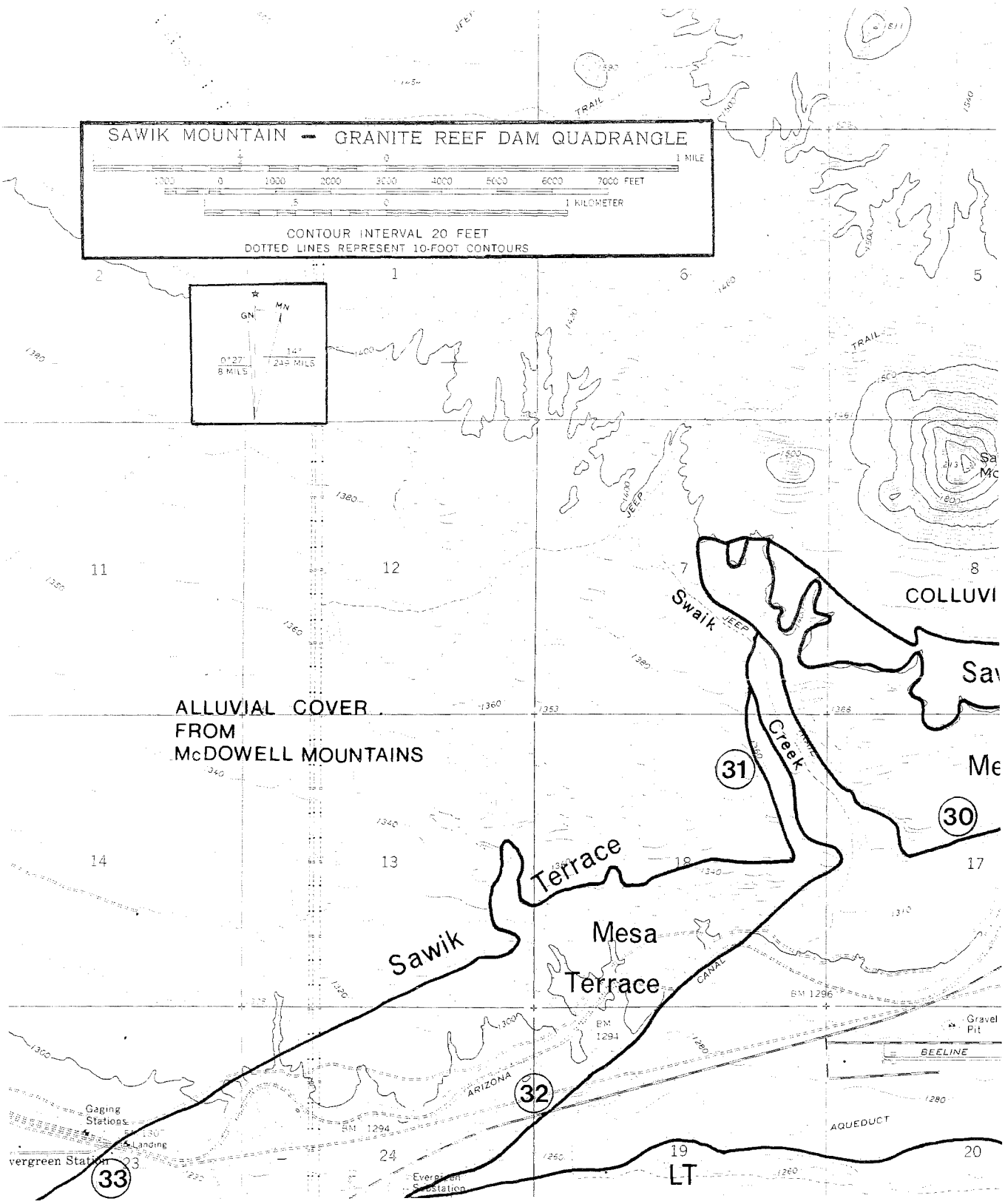

Figure 26. Field trip log map showing locations of STOPS 29—33.

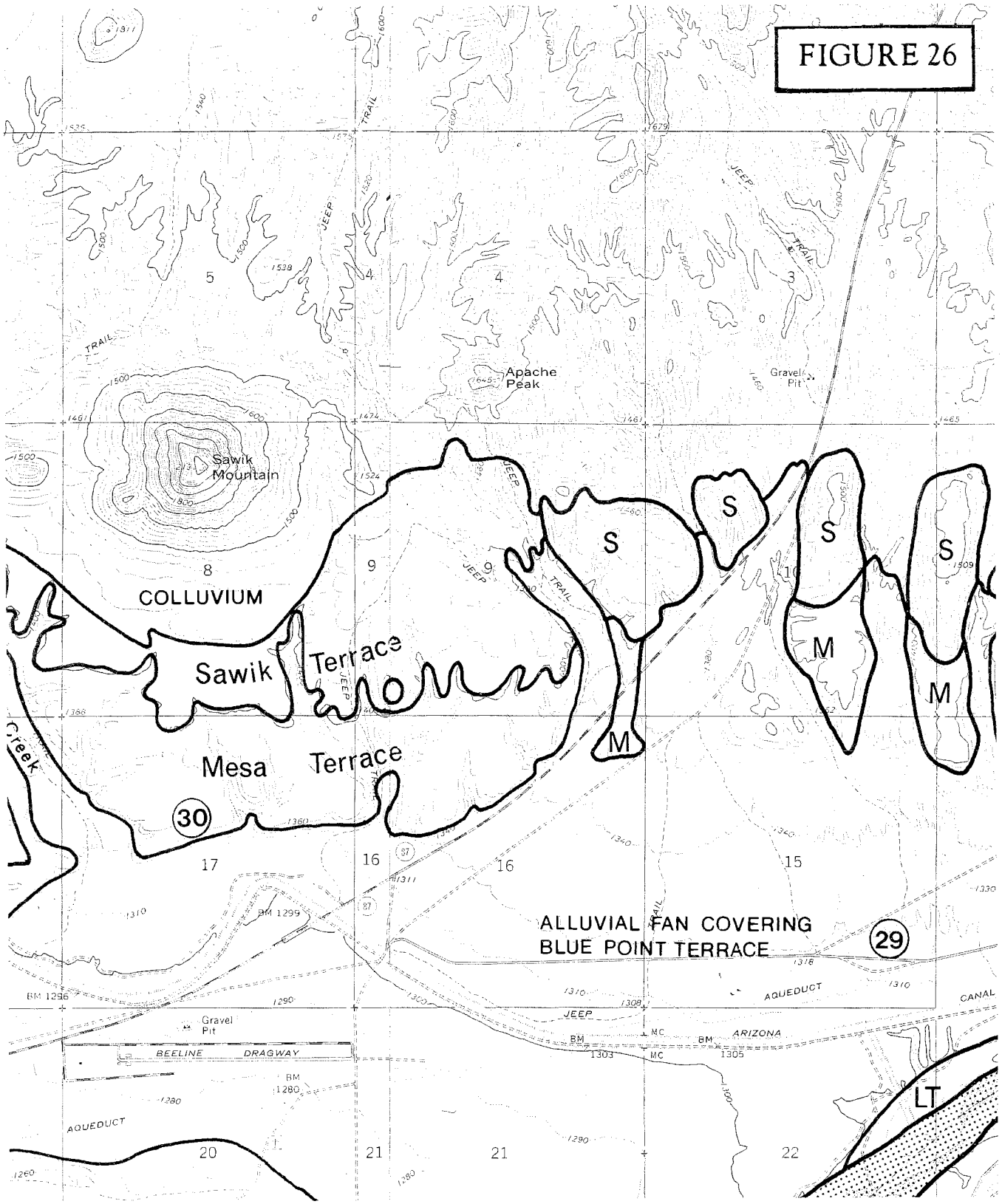
FIGURE 26
Sawik Mountain
Apache Peak
Gravel Pit
COLLUVIUM
Sawik Terrace
Mesa Terrace
Creek
S
M
LT
30
29
ALLUVIAL FAN COVERING
BLUE POINT TERRACE
BM 1299
BM 1296
BEELINE DRAGWAY
AQUEDUCT
CANAL
ARIZONA
JEEP
TRAIL

STOP 24. MCDOWELL TERRACE. The McDowell Terrace is named after the Fort McDowell Indian Reservation and its predecessor, the village of Fort McDowell. The coarse gravel crops out mainly on the upper edge of the terrace scarp. The terrace surface is covered with a sloping colluvial cover of metamorphic debris shed from the McDowell Mountains (fig. 24).

Surface boulders and cobbles, mainly quartzites and rhyolites, are characteristically fractured and split due to calichification. Many of the coarse-grained granitic rocks and other rock types are badly weathered and broken down, but to a lesser degree than equivalent rock types in the Mesa Terrace gravel. Normally, only the upper part of the rock types are heavily decayed, in contrast to the clasts in the Mesa Terrace which are nearly completely broken down. The McDowell Terrace deposits are noticeably less calichified than the Mesa Terrace deposits.

STOP 25. TOP OF HILL IN FOUNTAIN HILLS SETTLEMENT—DEPOSIT OF LOUSLEY HILL GRAVEL. The cobbles and the boulders of the Lousley Hill deposits are more weathered than those of the younger Verde River terrace gravels. For example, the degree of "boulder splitting" is pronounced in Mesa Terrace gravel; however, the clasts in the Lousley Hill deposits are not only split but many have been completely destroyed, leaving only decayed debris. From the top of the hill the Verde River can be seen coming from the north. The river is 210 miles long and originates at an elevation of 6,000 feet. It joins the Salt River at Mt. McDowell at an elevation of 1,250 feet. The Verde River drains an area of 6,600 miles^2.

STOP 26. GRAVEL REMNANTS. Just south of the Salt River Indian Reservation boundary, in Section 30 (fig. 22) 1 mile south of Beeline Highway, are scattered remnants of Verde River gravel of the Blue Point Terrace at an elevation of 40–50 feet above the river. The granite pediment adjacent to this area on the west is here named the Camp Reno Pediment after the Camp Reno historical monument on the highway. This pediment was graded to the Blue Point Terrace but now is being dissected.

Proceed south to the Filtration Plant at the junction of the Verde and Salt Rivers. The highway at the base of the steep granite cliffs is near the flood-plain level. The "granite" is really granodiorite and has been dated as 1,395 ± 45 million years (Stuckless and Naeser, 1972).

STOP 27. FILTRATION PLANT. Across the road (fig. 15) from the filtration plant, a small knob of Camels Head Formation (arkose conglomerate) crops out. The gravels of the Blue Point Terrace lap around this bedrock knob except on the river side where the river has steepened the slope exposing the bedrock.

The discussion point here involves taffoni. Taffoni are purse-shaped pockets or cavities 10 cm to 20 m in diameter weathered in granite or granite-like rocks in arid regions. They are common in all the major deserts of the world and are extremely well developed in the lower Sonoran desert of Arizona. Although debates still occur concerning the origin of taffoni, the writer believes they are due to differential weathering caused by the decay of feldspars and associated minerals. It is thought that the development of these erosional cavities takes an extremely long time and work is currently in progress by the writer and associates to obtain information along this line. The question at this locality is whether the taffoni developed before or after the formation of the Blue Point Terrace. If the taffoni formed after the Blue Point Terrace was dissected, it would appear that the terrace is of considerable antiquity because taffoni 3 m across have formed in this arkose conglomerate.

STOP 28. MESA TERRACE AT GRANITE REEF DAM. This stop is at the edge of the mountains; downstream from here the Salt River spreads out into the broad valley. At the time of the formation of the Mesa Terrace, the river spread very widely north and south, from the edge of the McDowell Mountains to the edge of the Usery Mountains. The gravel here on the Mesa Terrace surface is on granitic bedrock (fig. 15). To the west, the surface has been cut on alluvial fill. The surface of the terrace is 80 to 100 feet above the river at this spot. A well-developed Mesa Terrace scarp can be seen in the distance several miles to the southwest.

In 1977 a deep cut was made across the terrace north to south at this locality to accommodate the Central Arizona Project siphon that goes under the Salt River (see **STOP 13**). The cut was 50 feet deep, mostly in granite. On the south edge of the terrace at this locality there is about 8 or 9 feet of calichified terrace gravel over granite. This is a buried granite hill because as one proceeds 100 yards to the north the hill disappears and the cut, to depths of at least 40 feet, is entirely in Mesa Terrace gravel. The cut exposed about 3 or 4 feet of a reddish soil, 11 feet of highly calichified gravel, and

beneath was typical coarse Salt River gravel with crossbedded sands and gravel with clasts up to 2 feet in diameter.

From here proceed to the west over a large, gently sloping alluvial fan of silt.

STOP 29. ALLUVIAL FAN OVER BLUE POINT TERRACE (Sawik Mountain Quadrangle, 1964; fig. 26). This locality is in the center of a large alluvial fan about 10 miles square which emanates from a dissected pediment to the north and covers the widespread Blue Point Terrace here with silt and colluvium from 1 to 30 feet thick. Toward the distal end of the fan, remnants of the Blue Point gravel surface are exposed. The size of this fan indicates that a long period of time must have elapsed since the cutting of the Blue Point Terrace.

The Beeline Dragway (fig. 26) is built on this alluvial fan. To the north can be seen the scarps of the Sawik and Mesa Terraces. Proceed west on Beeline Highway.

STOP 30. MESA TERRACE. The Arizona Canal makes a very sharp southward bend near this stop to accommodate a small fan coming from Sawik Creek; the small fan is part of the overall fan described at **STOP 29**. The Mesa Terrace is well developed at this locale and is about 100 feet above the modern floodplain. The terrace is entirely cut in alluvium and stands above the alluvial fan described earlier. The gravel is highly calichified and a great number of split boulders are exposed on the edge of the terrace.

STOP 31. SAWIK TERRACE. The Sawik Terrace is excellently displayed in this area and is named from Sawik Mountain (Péwé, 1971). Sawik Mountain is composed of basalt and dacite, and rubble from the mountain overrides the terrace surface. The Sawik Terrace at this locality stands 20 to 40 feet above the Mesa Terrace, and extends westward into Scottsdale (fig. 26).

A fine exposure of the terrace gravel, highly cemented by caliche, occurs in the middle reaches of Sawik Creek, a few hundred yards to one-half mile up from STOP 31. The cemented gravel forms vertical walls 20 to 40 feet high. To the north, colluvium from the McDowell Mountains have spread over the terrace. Where fine colluvium and alluvium have spread over the terrace immediately to the west, agriculture has been successful; but where the terrace gravel is at the surface, or close to the surface, the crops do not do well.

STOP 32. MESA TERRACE SCARP. Adjacent to the Beeline Highway (fig. 26) the scarp of the Mesa Terrace is dissected by transverse streams and caliche-cemented gravel is well exposed. Here also may be seen the river-truncated edge of the alluvial fan of silt that covers the Blue Point Terrace.

STOP 33. EVERGREEN STATION. The Evergreen station is at the junction of Camelback Road and the Arizona Canal (fig. 26). There is an overflow channel from the canal south to the Salt River. This channel gives an excellent cross section of the amount and type of colluvium overlying the Mesa Terrace. The colluvium is poorly cemented and about 10 feet thick near Evergreen Station; it thins rapidly to the south and is absent at the scarp of the Mesa Terrace. The underlying Mesa Terrace gravel is strongly cemented by caliche.

From STOP 33 proceed south on Beeline Highway toward Mesa.

STOP 34. HOHOKAM CANAL (Mesa Quadrangle). Near the edge of the Mesa Terrace are remnants of ancient canals built by the Hohokam Indians about 800–1,000 years ago (fig. 9). Parts of the old Indian canals have been destroyed by the shifting of the Salt River in the last 1,000 years. The terraces were evidently hacked out of the caliche-cemented gravel by hand using crude stone implements. An extensive array of these canals existed in the valley many years ago.

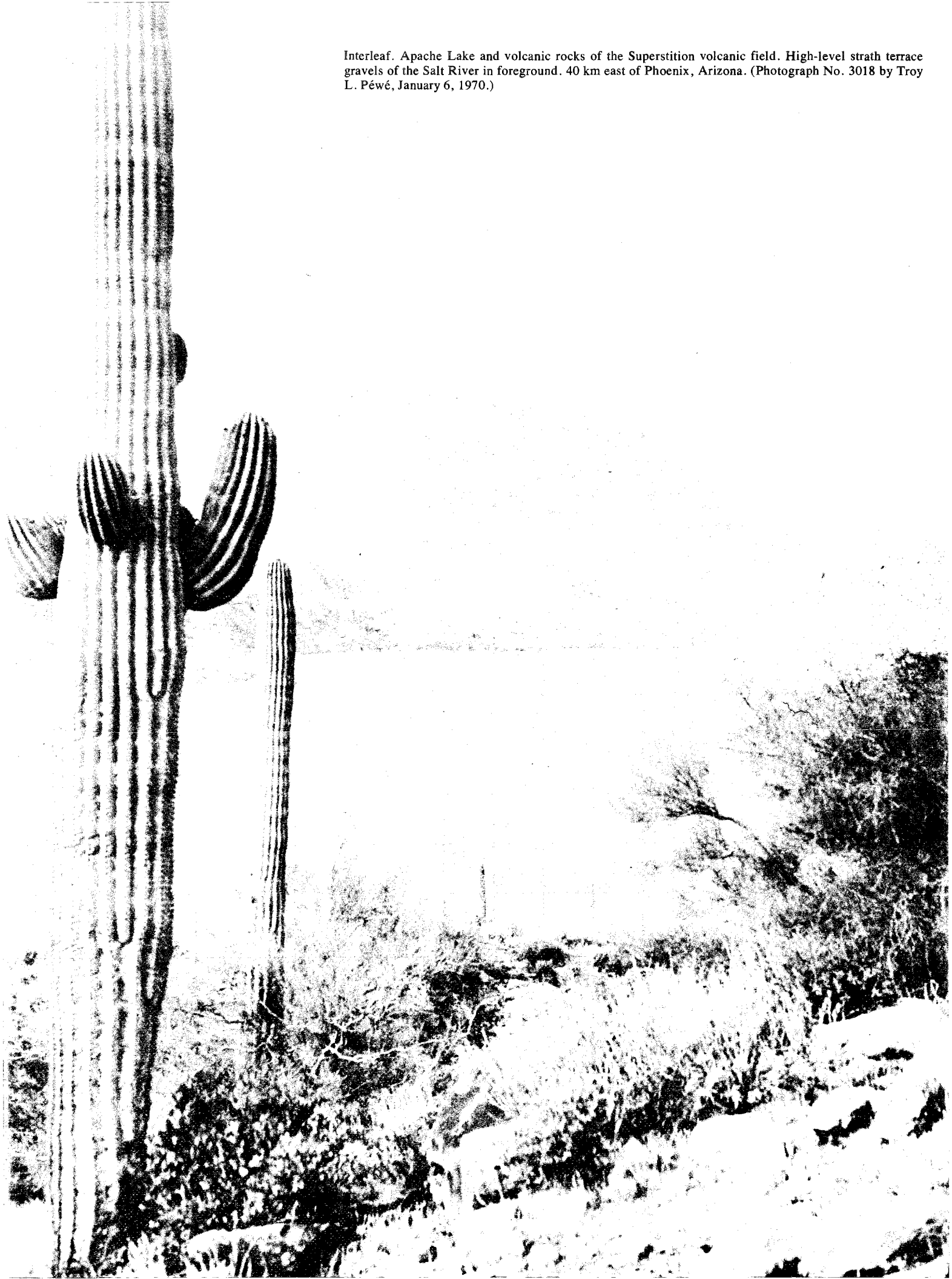

Interleaf. Apache Lake and volcanic rocks of the Superstition volcanic field. High-level strath terrace gravels of the Salt River in foreground. 40 km east of Phoenix, Arizona. (Photograph No. 3018 by Troy L. Péwé, January 6, 1970.)

GEOLOGY OF THE PINACATE VOLCANIC FIELD

by
James T. Gutmann
Department of Earth & Environmental Sciences
Wesleyan University, Middletown, Conn.
and
Michael F. Sheridan
Department of Geology
Arizona State University,
Tempe, Arizona

This 2½ day trip will cross the international border into Mexico to examine basaltic rocks in the northeastern part of the Pinacate field, including cinder cones, a large collapse depression, and a tuff cone. Participants should bring proof of U. S. citizenship, sleeping bags, ponchos, canteens, and sturdy boots. We will camp out in the Sonoran desert for two nights. The trip is moderately strenuous owing to locally precipitous terrain.

INTRODUCTION

The Pinacate volcanic field is located in northwestern Sonora, Mexico, near the northern end of the Gulf of California. The field comprises 2,000 km^2 of basaltic volcanic rocks. It is dominated topographically by the Sierra Pinacate, a broad, composite volcanic pile in the southern half of the field with a maximum elevation of 1,206 m. Many of these volcanic rocks evidently are of late Pleistocene age, although others are deeply dissected by erosion and may be considerably older. The field is characterized by an abundance of cinder cones. Many of the flows can be traced sourceward to a vent complex marked by a cinder cone and recording a multi-stage eruptive history involving alternating effusive and pyroclastic activity. In addition, the field contains eight circular collapse depressions and a partially collapsed tuff cone (Cerro Colorado). The collapse depressions, which range up to 1.7 km in diameter, are flat floored and have steep walls exposing various sequences of flows, shallow intrusions, and pyroclastic rocks. Many of these rocks represent volcanic units pierced by the crater but otherwise unrelated to it, whereas others were derived from vents located within the area now occupied by the crater and some clearly are part of the sequence of eruptions which culminated in collapse and crater formation. All of the collapse depressions are surrounded by units of tuff breccia which form crater rim deposits. These pyroclastic rocks are rich in vesicular, juvenile lapilli and ash. Some contain abundant accidental ejecta derived from unconsolidated sediment beneath the volcanic section. All contain accessory blocks and smaller fragments of holocrystalline basaltic rocks torn from vent walls during culminating phreatomagmatic eruptions.

Primary depositional structures and textures of pyroclastic-surge deposits are well displayed at Crater Elegante and Cerro Colorado. The three principal bed forms (sandwave, massive, and planar of Sheridan and Updike, 1975) show a concentric distribution consistent with the deflation model of emplacement described by Wohletz and Sheridan (in press). These features contrast with the avalanche-type bedding typical of cinder cones.

Cerro Colorado and six of the eight collapse depressions are disposed along an arcuate path trending westward across the northern part of the volcanic field (fig. 1). Ives (1936) suggested that, prior to diversion by the lavas, the Sonoita River flowed westward across what is now the northern part of the field and discharged into the Gulf of California at Pozo Caballo on Adair Bay. Jahns (1959) noted the general correspondence between the arc of collapse depressions and the ancient course of the Sonoita River and suggested that the availability of groundwater was an important element in the genesis of the tuff-breccia-forming eruptions. In providing the first general geologic description of the large, flat-floored depressions, Jahns (1959) pointed out that the volumes of accessory ejecta in their associated tuff-breccia units are much smaller than the volumes of the depressions themselves and emphasized the importance of collapse in their formation.

The majority of Pinacate lavas are relatively mafic hawaiites with about 48 wt percent SiO_2, 17 wt percent Al_2O_3, 2.7 wt percent TiO_2, 5 wt percent MgO, 12 wt percent total iron (as Fe_2O_3), 9 wt percent CaO, 4 wt percent Na_2O, and 1.3 wt percent K_2O. Small amounts of normative nepheline are indicated in a few analyses. The normative plagioclase generally is andesine although some of the lavas contain normative labradorite and are alkali

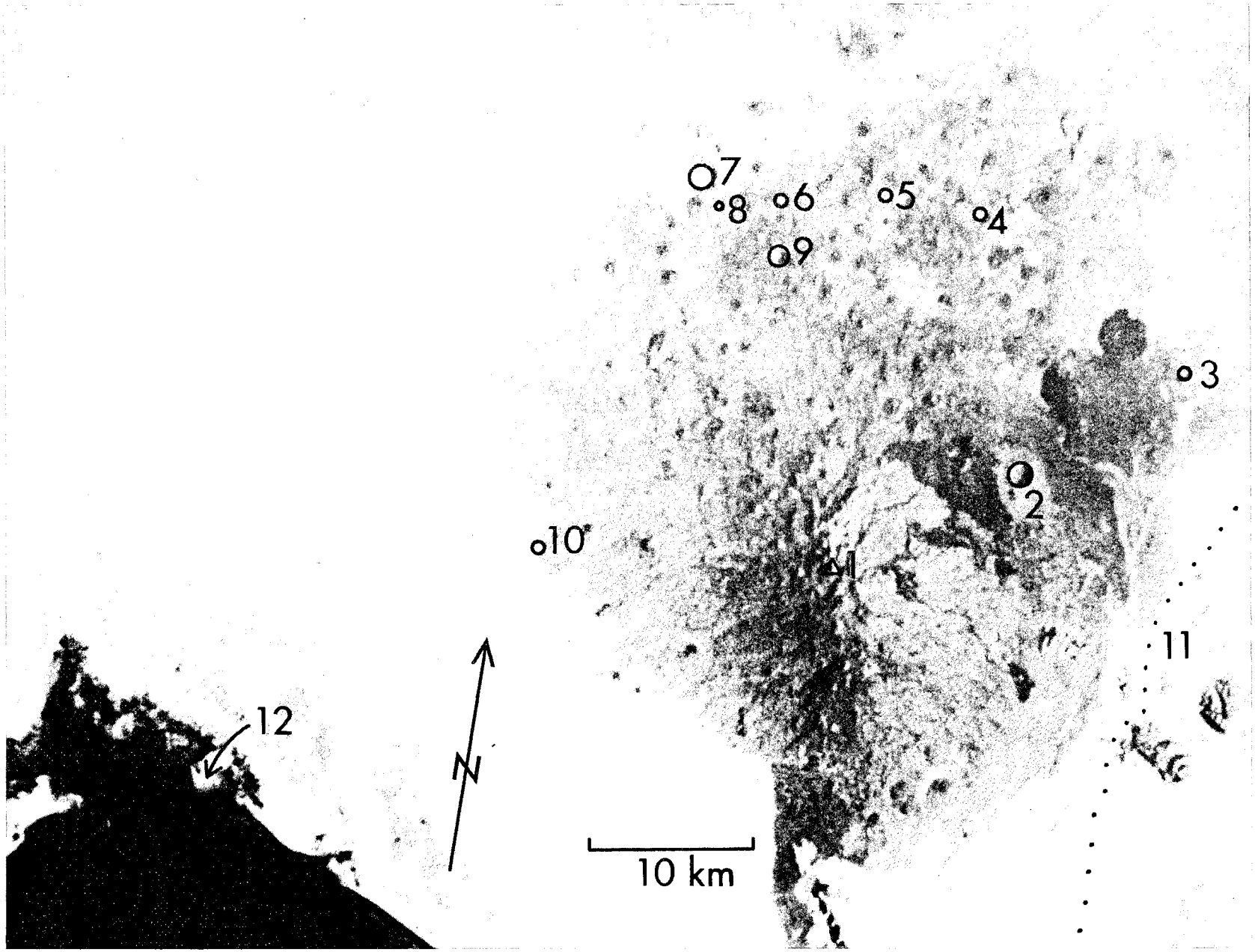

Figure 1. Pinacate volcanic field. This is a portion of a NASA photograph taken from Apollo 6. 1, summit of Sierra Pinacate; 2, Crater Elegante; 3, Cerro Colorado; 4, Celaya Crater; 5, Kino Crater; 6, Badillo Crater; 7, MacDougal Crater; 8, Molina Crater; 9, Crater Grande (Sykes Crater); 10, Moon Crater; 11, present course of Sonoita River; 12, Adair Bay on Gulf of California.

basalts. The rocks are typified petrographically by unusually large crystals of labradorite, olivine, augite, and magnetite. The labradorite crystals are as much as 10 cm in maximum dimension. The crystals of all four phases can range continuously downward in size to small phenocrysts and microphenocrysts. In thin section, many of the phenocrysts exhibit skeletal morphologies typical of rapid growth, including individuals as much as 1 cm long. Many other coarse crystals evidently have been resorbed.

Published studies in the Pinacate field include Jahns' (1959) description of the collapse depressions and Ives' (1964) summary paper on geographic aspects of the Pinacate region. The volcanic field was mapped at a scale of 1:62,500 by Donnelly (1974). Gutmann (1974) described tubular fluid inclusion textures in the coarse labradorite crystals and Gutmann and Martin (1976) described the crystal chemistry, unit cell parameters, and Al-Si ordering of these materials. Arvidson and Mutch (1974) discussed sedimentary patterns in and around five of the collapse depressions and Bull (1974) described playa processes within two of them. Wood (1974) reported the results of geophysical surveys across four of them and Gutmann (1976) described the geology of Crater Elegante. Gutmann (1977) discussed the textures and genesis of the phenocrysts and megacrysts in Pinacate lavas. Gutmann (in prep.) describes the cyclic eruptive behavior at Pinacate cinder cones and discusses controls of their activity. Wohletz and Sheridan (in press) develop a model for emplacement of pyroclastic-surge deposits using as an example the tuff breccia at Crater Elegante.

REFERENCES CITED

Arvidson, R. E., and Mutch, T. A., 1974, Sedimentary patterns in and around craters from the Pinacate volcanic field, Sonora, Mexico: some comparisons with Mars: Geol. Soc. America Bull., v. 85, p. 99–104.

Bull, W. B., 1974, Playa processes in the volcanic craters of the Sierra Pinacate, Sonora, Mexico: Zeit. F. Geomorph., Suppl. v. 20, p. 117–129.

Donnelly, M. F., 1974, Geology of the Sierra del Pinacate volcanic field, northern Sonora, Mexico, and southern Arizona, U.S.A. (Ph.D. dissert.): Stanford, Calif., Stanford Univ., 722 p.

Gutmann, J. T., 1974, Tubular voids within labradorite phenocrysts from Sonora, Mexico: Am. Mineralogist, v. 59, p. 666–672.

——1976, Geology of Crater Elegante, Sonora, Mexico: Geol. Soc. America Bull., v. 87, p. 1718–1729.

——1977, Textures and genesis of phenocrysts and megacrysts in basaltic lavas from the Pinacate volcanic field: Am. Jour. Sci., v. 277, 29 p.

Gutmann, J. T., and Martin, R. F., 1976, Crystal chemistry, unit cell dimensions, and structural state of labradorite megacrysts from Sonora, Mexico: Schweiz. Mineral. Petrogr. Mitt., v. 56, p. 55–64.

Ives, R. L., 1936, Desert floods in the Sonoyta valley: Am. Jour. Sci., v. 232, p. 349–360.

——1964, The Pinacate region, Sonora, Mexico: Occ. Papers Calif. Acad. Sci., no. 47, 43 p.

Jahns, R. H., 1959, Collapse depressions of the Pinacate volcanic field, Sonora, Mexico: Ariz. Geol. Soc., Southern Arizona Guidebook 2, p. 165–184.

Shakel, D. W., and Harris, K. M., 1972, Potsherd evidence for minimum age of Cerro Colorado crater, Pinacate volcanic field, northwestern Sonora, Mexico: Geol. Soc. America, Abs. with Programs for 1972, v. 4, p. 408.

Sheridan, M. F., and Updike, R. G., 1975, Sugarloaf Mountain tephra—A Pleistocene rhyolite deposit of base-surge origin in northern Arizona: Geol. Soc. America Bull., v. 86, p. 571–581.

Wohletz, K. H., and Sheridan, M. F., in press, A model of pyroclastic surge: Geol. Soc. America Memoir.

Wood, C. A., 1974, Reconnaissance geophysics and geology of the Pinacate craters, Sonora, Mexico: Bull. Volcanol., v. 38, p. 149–172.

ROAD LOG AND STOP GUIDE

MILES Interval	Total	
		1st DAY (Leave Tempe, Ariz., at noon).
0.0	0.0	Corner of Rural Road and Apache Boulevard, Tempe. Head south on Rural Road to the Superstition Freeway on-ramp. Take the Superstition Freeway west to Interstate 10.
4.9	4.9	Junction Interstate 10. Take Interstate 10 south toward Tucson.
8.0	12.9	Maricopa exit. Take the interstate off-ramp south to Maricopa.
16.8	29.7	Town of Maricopa.
13.0	42.7	Junction Arizona 84. Turn west toward Gila Bend.
6.1	48.8	Junction Interstate 8. Keep west toward Gila Bend.
40.4	89.2	Gila Bend. Take the Interstate 8 off-ramp for Arizona 85 south toward Ajo.
40.6	129.8	Ajo.
13.5	143.3	Why. Bear south on Arizona 85.
28.2	171.5	International border at Lukeville. Be prepared to obtain Mexican tourist permit to visit Parque Natural del Pinacate. Valid proof of U.S. citizenship is needed (birth certificate, passport, or voter registration card).
2.0	173.5	Town of Sonoita. Bear right (west) on Mexico Rte. 2 toward San Luis.
31.6	205.1	Bear left on dirt road at sign marking entrance to Parque Natural del Pinacate (a unit of the Mexican counterpart of the U.S. National Park system).
3.8	208.9	Bear right (west) on dirt road.
6.0	214.9	Road junction. Continue straight ahead (stay right).
0.4	215.3	**STOP 1.** Steep front of an aa flow. Most Pinacate flows are aa flows with extremely rough surfaces. This flow emerged from a breach in the large (150 m high), young cone to the west. It overlies ejecta from that cone;

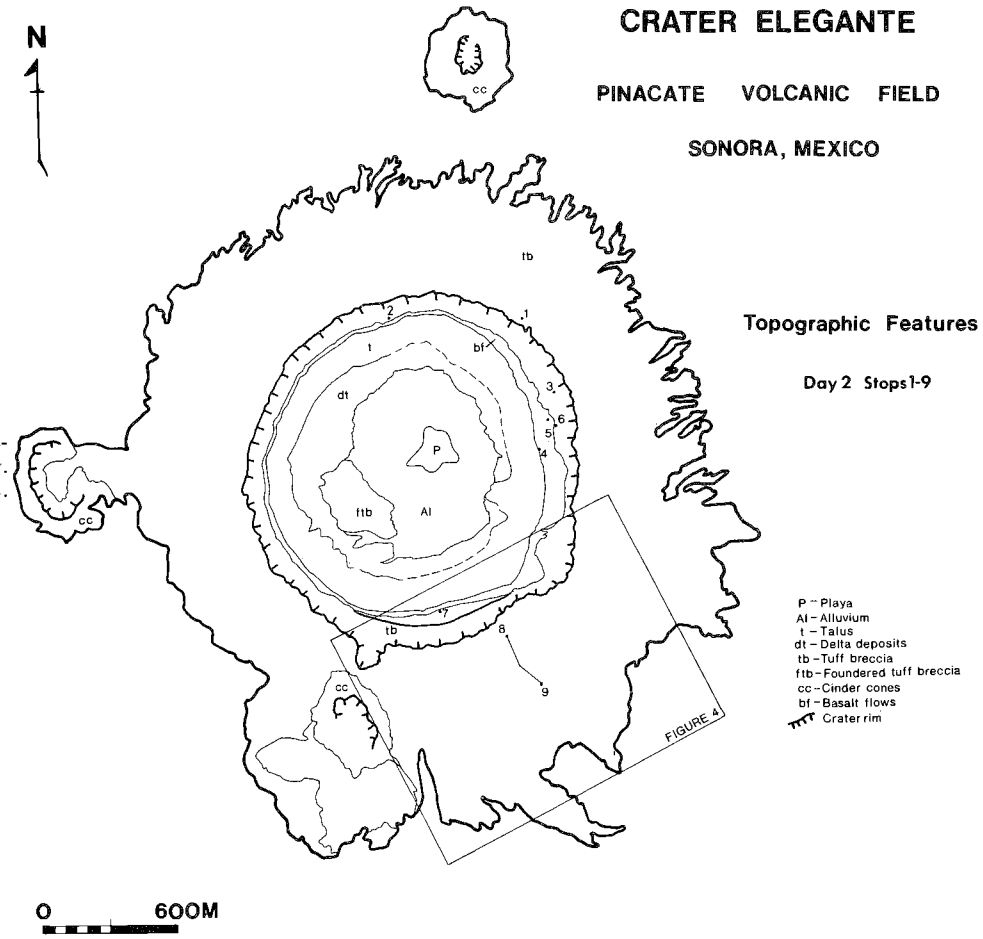

Figure 2. Sketch map of Crater Elegante. Major units indicated by key. Stops for DAY 2 given by numerals. (Modified from Gutmann, 1976.)

these ejecta also occur resting on the flow as scattered masses of cinder derived and rafted from the breach in the wall of the cone. Pale yellow, gem-quality labradorite megaphenocrysts up to 5 cm long occur sparingly in this flow and in cinders near the vent.

2.8 218.1 Road junction. Continue straight ahead.

0.9 219.0 Road junction. Camp here.

2nd DAY

Walk the road 1 km up to the rim of Crater Elegante. Figure 2 shows stops for today and a general plan view of the crater and environs.

STOP 1. Crater Elegante is 1.6 km in diameter and 244 m deep. The stratigraphic record revealed in its walls includes four major parts (see Gutmann (1976) for details). The oldest exposed rocks are flows of mafic hawaiite, many of which evidently originated at the cinder cone immediately south of the crater, both preceding and accompanying pyroclastic eruptions there. Erosional dissection of this cone prior to deposition on it of Elegante tuff breccia suggests that it is considerably older than Crater Elegante.

Resting on these old flows is a cinder cone, the vent for which lay in the southeastern part of what is now the crater. This "gray cinder" cone is displayed in cross section in the crater walls (fig. 3); it was breached to the southeast following emplacement of sills within the cone structure and along its base south of the vent. Renewed eruptions from essentially the same vent then produced cinder units ("brown cinders"), flows, and dikes, all of which are especially rich in phenocrysts.

Cinder eruptions occurred next from a vent in the southern part of what is now the crater; these were immediately preceded by a flow that baked the base of the overlying cinder section locally.

Finally, a flow was erupted from a vent probably located near or somewhat northeast of the center of the crater. Minor cinder eruptions may have followed this flow but the nature of eruptions changed quickly as groundwater gained access to the vent and magma column. The ensuing phreatomagmatic eruptions gave rise to the unit of tuff breccia that forms the crater's rim beds. This unit is as much as 70 m thick in the northeastern parts of the rim. Its chief constituents, listed in order of decreasing abundance at the rim, are vesicular pellets of glassy, juvenile ash rich in tiny crystals, accessory blocks and smaller fragments of holocrystalline basalt torn from vent walls, and quartzofeldspathic sand, silt, and clay of accidental origin.

Accessory ejecta decrease rapidly in abundance with distance from the crater rim, while the abundance of accidental ejecta increases in the same direction. An upper limit on the amount of accessory debris deposited outside the crater indicates that the diameter of the vent piercing the volcanic section was not greater than 672 m and may have been considerably less. A vent of this size implies the former existence of a tuff breccia cone over much of the site of the present crater. The large hill apparent on the crater floor consists of tuff breccia and probably represents the upper parts of this vanished cone. Crater Elegante formed chiefly by wholesale collapse when the volcanic edifice subsided into a phreatomagmatic explosion chamber developed within fine-grained sediment beneath the section of volcanic rocks.

Proceed counterclockwise around the crater rim to a point due north from the center of the crater.

Descend to the base of the rim bed section. WATCH YOUR FOOTING AT BRINK OF CLIFFS.

STOP 2. Contact of tuff breccia with underlying flow. This flow was mobile when the tuff breccia was deposited on it and flowed in response to differential loading with tuff. Flow-top breccia is largely absent here but present nearby to east and west. Note the wavelike bulge of the flow top with crest subparallel to the crater rim, the curious "sharktooth" texture of the upper surface of the flow here, the dike originating within the flow and cutting the overlying tuff, the contact effects on the tuff adjacent to this dike, and the folds and faults within the lower 10 m of the tuff breccia section. Note also scattered small xenoliths and xenocrysts of quartzofeldspathic debris in the flow. Such accidental inclusions are rare in Pinacate flows. Their presence here indicates admixture of sediment within the magma column somewhat prior to the onset of phreatomagmatic eruptions.

Return to the crater rim. Proceed clockwise around the rim to a point on bearing 63° from the center of the crater. Descend toward the base of the rim bed section.

STOP 3. The descent route traverses a well-exposed section of the tuff breccia. Note the gray unit of lapilli tuff about half way down through the section; this unit is relatively poor in ash and accidental ejecta but unusually rich in frothy juvenile lapilli, as if the supply of meteoric water and sediment temporarily diminished during the culminating eruptions. Excellent exposures of tuff breccia occur further down the slope. Note the lens of coarse breccia at the base of the section here. This breccia is rich in accessory blocks and juvenile lapilli but poor in ash; it evidently represents early, vent-clearing explosions consequent upon initial access of abundant meteoric water to the magma column.

Descend through the underlying cinder section to the edge of the cliffs. The massive buttress to the north is an intrusion petrographically related to the brown cinders and probably emplaced laterally through the cinder section from a source to the south.

Traverse left (south) about 200 m along the base of the gray cinder section to a prominent vertical dike.

STOP 4. Lowermost parts of a composite dike of porphyritic basalt cutting the gray cinders. Both the keel and the crest of this dike are exposed. Its crest is grossly horizontal and extends northward more than 100 meters to the top of the section of gray and brown cinders. There the dike fed a small flow upon which the tuff breccia was deposited. Presence of the keel and attitude of the crest indicate that the dike was emplaced horizontally through the cinder section from a source to the south near or coinciding with the vent of the gray and brown cinders.

The dike here comprises several pairs of narrow, vertical zones symmetrically disposed about its core and recording the passage and chilling of successive pulses of magma. The core of the dike is occupied by an intrusion of chilled, porphyritic basalt which widens upward in the dike. Note the increase in size and abundance of the coarse labradorite megaphenocrysts inward to a zone especially rich in these as well as in small xenoliths and pea-sized crystals of olivine. This inward increase suggests flowage differentiation. At the same time, the groundmass of the dike is depleted in plagioclase relative to that of nearly aphyric Pinacate lavas such that the entire intrusion is not significantly enriched in plagioclase. The numerous giant labradorite crystals evidently formed from the liquid whose other solid products now enclose them and are truly phenocrysts. Please refrain from sampling the dike at this locality.

Also well exposed here are the lower parts of the gray cinder section. The tan layers within this section contain quartzofeldspathic sand and silt of accidental origin together with abundant juvenile ash and lapilli. The juvenile constituents are highly vesicular glass with numerous tiny crystals and some are slightly palagonitized. These tuffaceous layers evidently represent phreatomagmatic interaction between wet sediment and briskly vesiculating magma in the conduit. Implied breaches, periodically reopened in the conduit walls during the early phases of cinder eruption, must have been sealed or failed to provide copious amounts of meteoric water, however, for ash and accidental ejecta are largely absent from the bulk of the gray cinder section.

LUNCH STOP. Some may wish to traverse south along the base of the gray cinder section toward the vent region. Descent to the talus slope rising from the floor of the crater is easy near the vent and affords access to a thick dike that fed a laterally extensive, shallow intrusion emplaced within the lowermost parts of the gray cinder pile (Devil's

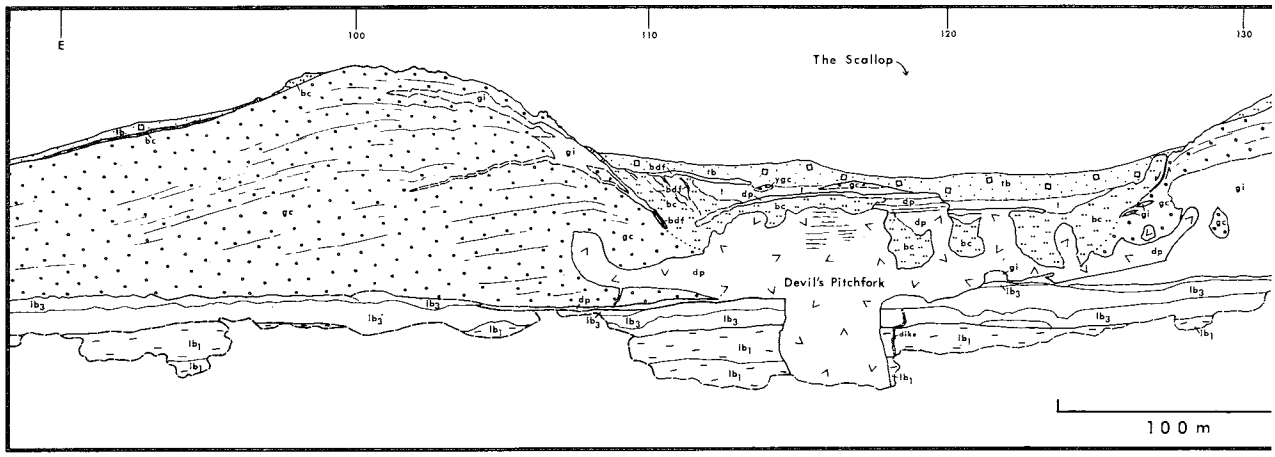

Figure 3. Geologic relationships exposed in southeastern walls of Crater Elegante as seen from the center of the crater floor. Numbers along the top of the figure give azimuths from center of crater. No vertical exaggeration. lb_1 and lb_3—lower basalt flows; gc—gray cinders; gi—gray intrusions; bc—brown cinders; bdf—dikes and flows associated with brown cinders; rdc—ribbon dike cinders; rds—ribbon dike and sill; dp—Devil's Pitchfork intrusion and associated flows; ygc—younger gray cinders; tb—tuff breccia; t—talus.

Pitchfork of fig. 3). Others may wish to traverse about 100 meters southward and descend over the flows and down over talus to the crater floor. Noteworthy features of the crater floor include the foundered mass of tuff breccia, topset and foreset deposits in a lake that formerly occupied the crater to a maximum depth of about 60 m, and large oval subsidence pits and linear depressions within the playa.

Return northward 50 m from the keel of the dike and ascend the gully to the upper parts of the dike.

STOP 5. The thin crestal parts of this dike contain sheetlike gas cavities at the core. These megavesicles are a few cm wide but can be a few meters in vertical dimension or parallel to strike of the dike. They probably represent accumulation of gas in the upper parts of the intrusion. Note the "drips" of magma on exposed walls of the gas cavities. These drips consist of porphyritic basalt that was too viscous to flow to the bottoms of the sheetlike voids.

Ascend southward to the crest of the dike. Note bifurcations of the dike.

STOP 6. The crest of the dike here lies just below the top of the gray cinder section. The overlying section of brown cinders contains scattered, subhedral to euhedral, single crystals of labradorite as much as 5 cm long. Euhedral phenocrysts of olivine and magnetite a few mm across also occur in this unit, as do augite crystals up to 3 cm in maximum dimension.

Ascend to the crater rim and proceed clockwise around the rim. The scallop-shaped depression in the southeastern rim of the crater reflects breachment of the gray cinder cone through its eastern flank as well as several subsequent events. Tumuli of the breaching flow are apparent on the flats to the east. Continue around the rim to a point on bearing 168° from the center of the crater. Descend through the tuff breccia section and younger gray cinders to the top of the highest flow.

STOP 7. Contact of younger gray cinders on a flow. The younger gray cinders attain maximum thickness in this region. The cinder layers dip gently southward and dips increase upward in the section to as much as 13° near the top. The vent evidently was located in the southern part of the area now occupied by the crater. The phenocryst assemblage in the cinders is identical to that of the underlying flow, which rests on gray and traces of brown cinders with very different phenocryst assemblages. Where flow-top breccia separates the flow from the overlying younger gray cinders, the lowermost few meters of these cinders are faintly pinkish. Where flow-top breccia is absent, as at this locality, the basal cinders are oxidized and indurated to form a resistant, red cinder ledge a few tens of cm thick. These cinders were baked by the underlying flow, which must have immediately preceded them, presumably from the same vent. This represents the third instance at Crater Elegante wherein a flow *preceded initiation* of pyroclastic eruptions.

Return to crater rim and walk eastward back along the rim to a point on bearing about 145° from the center of the crater.

STOPS 8 and 9. Outcrops of tuff breccia surrounding Elegante Crater extend slightly less than one crater diameter from the present rim, where they range from 40 to 70 m in thickness. Their dips range from nil to 2° for distal beds to about 15° outward at the crest of the rim. These beds are characteristic of pyroclastic-surge deposits, features that are becoming much more widely recognized and better understood.

Radial dissection of the rim beds provides excellent exposures of pyroclastic surge deposits south of the crater.

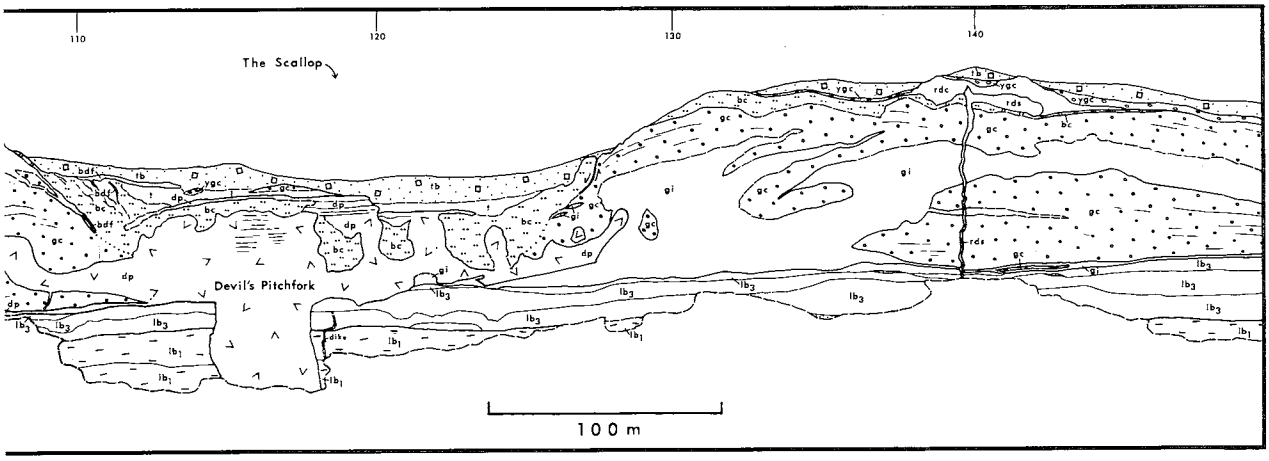

Figure 4 shows a plane table topographic map of the southern portion of the tuff deposits with the location of 30 measured sections. We will proceed down one of the south-trending gullies to observe the primary structures as well as the lateral and vertical variation of the deposits.

There are three principal bed forms in pyroclastic surge deposits (Sheridan and Updike, 1975): 1) sandwave, 2) massive, and 3) planar. Particles deposited in a sandwave bed were transported by saltation or dilute suspension in a surge blast. Massive beds were emplaced as a relatively dense suspension of particles with a bulk void fraction of 0.6 to 0.9. Planar beds represent yet more dense, only slightly dilated, traction carpets with a void fraction of less than 0.6. Complete transition occurs between bedding types, and outcrops may show one bedform that grades into another.

Three measured sections illustrate the variation of structure with distance from the rim (fig. 5). Sections 1B, 1E, and 1H are located 100 m, 225 m, and 525 m respectively from the present crater rim. The proximal section (1B) is dominated by sandwave beds, the medial section (1E) by all three bed-form types, and the distal section (1H) by planar beds. Using a Markov technique, Wohletz and Sheridan (in press) defined surge facies for every measured section. The boundaries of these three facies (sandwave, massive, and planar) are shown on figure 4. The pattern of facies distribution is similar for all pyroclastic-surge deposits studied: the sandwave facies is proximal, the massive facies medial, and the planar facies distal.

The data from three groups of spatially related, measured sections were used to reconstruct the generalized surge cloud as a function of distance from the present rim. Figure 6 shows the reconstructed cloud for Elegante surges at the southern part of the crater. This construction requires an assumption of void space during flow for each bed-form type in order to expand the measured section to flow heights. Obviously the surge clouds collapse or deflate with distance, giving rise to a deflation model of surge transport (Wohletz and Sheridan, in press).

Field and experimental evidence support the assumed flow densities. A good example of the type of exposure that allows flow density calculation is near station 5F (fig. 7). Here an accessory block in a massive bed occurs with relationship to bedding such that the bed around it must have deflated after coming to rest. The thickness of the flowing bed (h_t) was somewhat more than 31 cm and the present thickness (h_p) is 24 cm. The density of the flowing bed relative to the present bed, given by h_p/h_t, is 0.77. The void fraction (Φ) is given by the equation below:

$$\Phi = \frac{\rho_p - \rho_b}{\rho_p} = 1.0 - \frac{\rho_b}{\rho_p}$$

where ρ_p is the particle density and ρ_b is the bulk density. Assuming a particle density of 3.0 gr/cc and a rest bulk density of 1.2 gr/cc, the bulk density of the flow was 0.92 gr/cc and the void fraction (Φ) is then 0.69. Other values from outcrop data as well as experimental data from fluidized systems yield void fractions for massive beds from 0.6 to 0.9.

The planar beds are analogous to the grain dispersion flows that commonly produce inverse grading. Their void fraction of 0.6 is that which will just allow the dilation of beds so that they flow down slope. A sandwave void fraction of greater than 0.9 is taken from the results of wind tunnel experiments in which grains saltate or travel in a dilute suspension.

In making the radial traverse you should see lateral and vertical transition from sandwave to massive and from massive to planar types. Planar to sandwave or sandwave to planar transitions are rare.

Other structures also occur here. Because the massive beds are deposited in a near-fluidized, inflated condition,

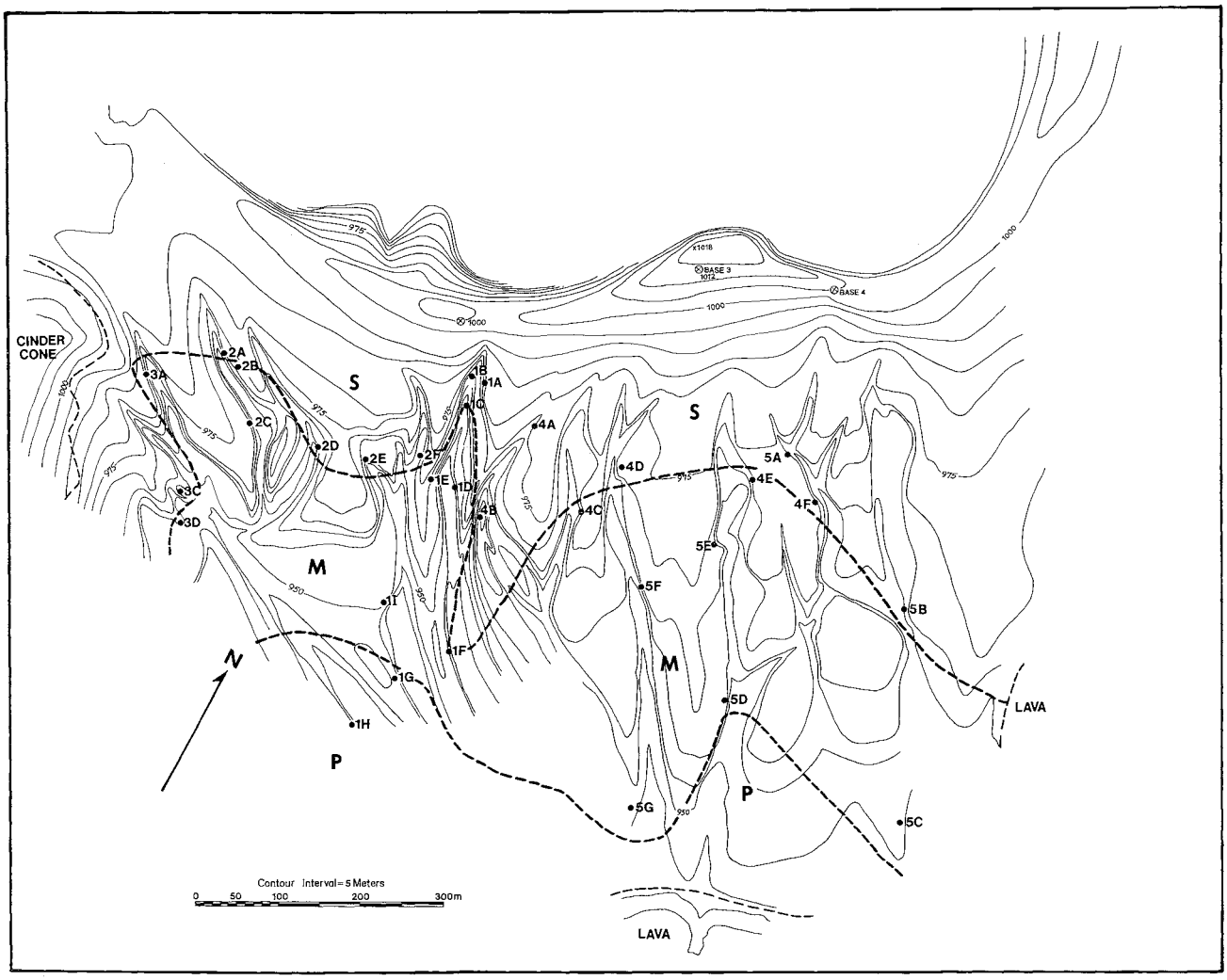

Figure 4. Facies map of Elegante surge deposits. Locations of 30 measured sections given by bold alphanumeric characters. Sandwave (S), Massive (M), and Planar (P) facies indicated by bold capital letters. Contours give relative elevation. Location of this figure given in Fig. 2.

they show many soft-sediment types of structural features, such as slump and flame structures, and bedding sags due to ballistic impact of blocks.

3rd DAY

MILES Interval	Total	
		Return eastward, retracing route of 1st day.
0.9	0.9	Road junction. Continue straight ahead.
3.0	3.9	Road junction. Continue straight ahead (stay left).
6.0	9.9	Junction with major road connecting Rte. 2 with quarry at cinder cone. Bear right (south).
0.2	10.1	Gate (normally locked) at entrance to quarry workings in young cinder cone. Cinders are mined here for construction and decorative purposes. Drive through the gate and around to the quarry.

STOP 1. This is one of the youngest cones in the Pinacate field. An unusual and particularly noteworthy feature of the eruptive history of Pinacate cinder cones is the eruption of flows from the vent *prior to* building of the cone. Although it cannot be demonstrated at this locality, exposures of the volcanic stratigraphy in the steep walls of several of the collapse depressions show that lava flows were the initial eruptive products at many Pinacate cinder cone vents. Exposures at this particular locality provide evidence that cinder eruptions ensued while the basal flow still was both hot and mobile. This flow, mantled with cinder, is exposed south of the cone. The lapilli are welded to the top of the flow locally and the lowermost parts of the cinder section are reddened and oxidized where they rest on the basal flow.

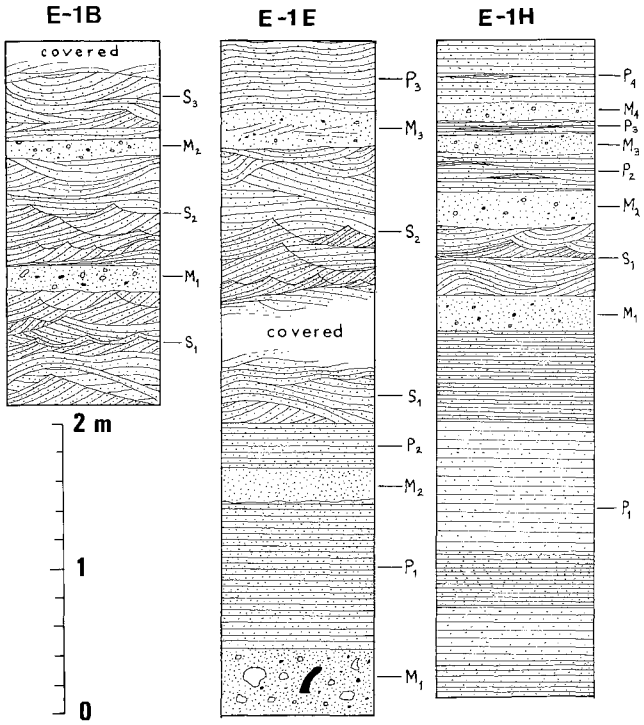

Figure 5. Measured sections of typical sandwave (E–1B), massive (E–1E) and planar facies (E–1H). Section locations shown in Fig. 4.

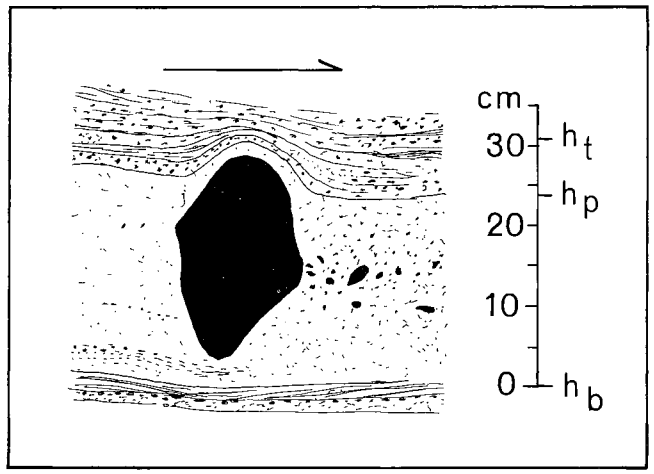

Figure 7. Compaction of massive bed due to degassing. The void fraction during flow for this bed is 0.77.

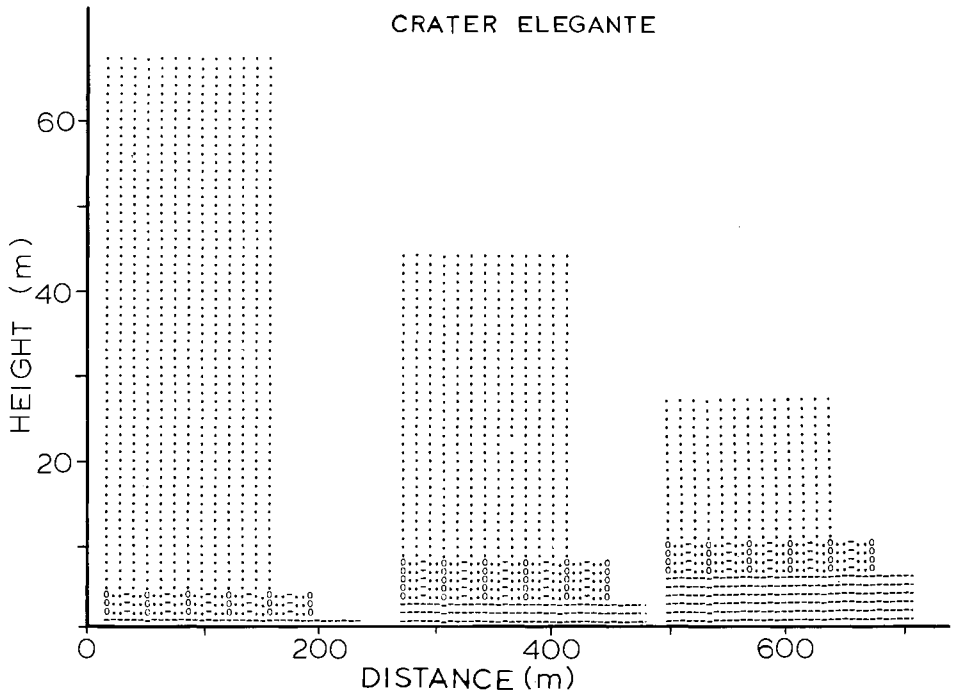

Figure 6. Deflation model of cumulative Elegante surge cloud. Data compiled from sections averaged over intervals of 0–300 m, 300–600 m and greater than 600 m. Cloud height calculated from assumed voidage ratios of 0.95 for sandwave beds, 0.75 for massive beds and 0.60 for planar beds. Distance measured from present rim. From Wohletz and Sheridan (in press).

The exposed parts of a small, dome-like hummock a few meters high immediately south of the cone comprise oxidized and indurated lapilli, probably very near the base of the cinder section, which were baked by the underlying flow. Dips of the cindery layers in the sides of this anticlinal hillock attain at least 65° and reflect folding of the cinders during development of a tumulus on the moving flow beneath. Exposures in the walls of the cinder quarry in April, 1976, revealed that normal faults cut the layering of at least 12 m of the lower parts of the cinder section in the flank of the cone (fig. 8). The strike of these faults appeared roughly perpendicular to the flow direction of the underlying basal flow and the faults dipped steeply away from the vent region. Thus, the side away from the vent was the downthrown side. The throw of the faults was as much as 1 m. These structural features indicate that the flow still was mobile after a substantial portion of the pyroclastic section had been deposited upon it. Continued motion of the basal flow away from the vent probably reflects differential loading of the molten layer by the cinder pile. Mobility of the flow is reasonable in light of the rapidity with which cinder cones can be built and the efficacy of insulation of the flow by the overlying cinders.

The summit of this small cone, which is about 80 m high, affords a good view of the tuff cone of Cerro Colorado to the east-southeast and of the northeastern marginal parts of the volcanic field. The cinder cone is breached to the north. A breaching flow, which moved southward around the cone, rafted numerous, very large masses of cinder from the breach. Nearly all Pinacate cinder

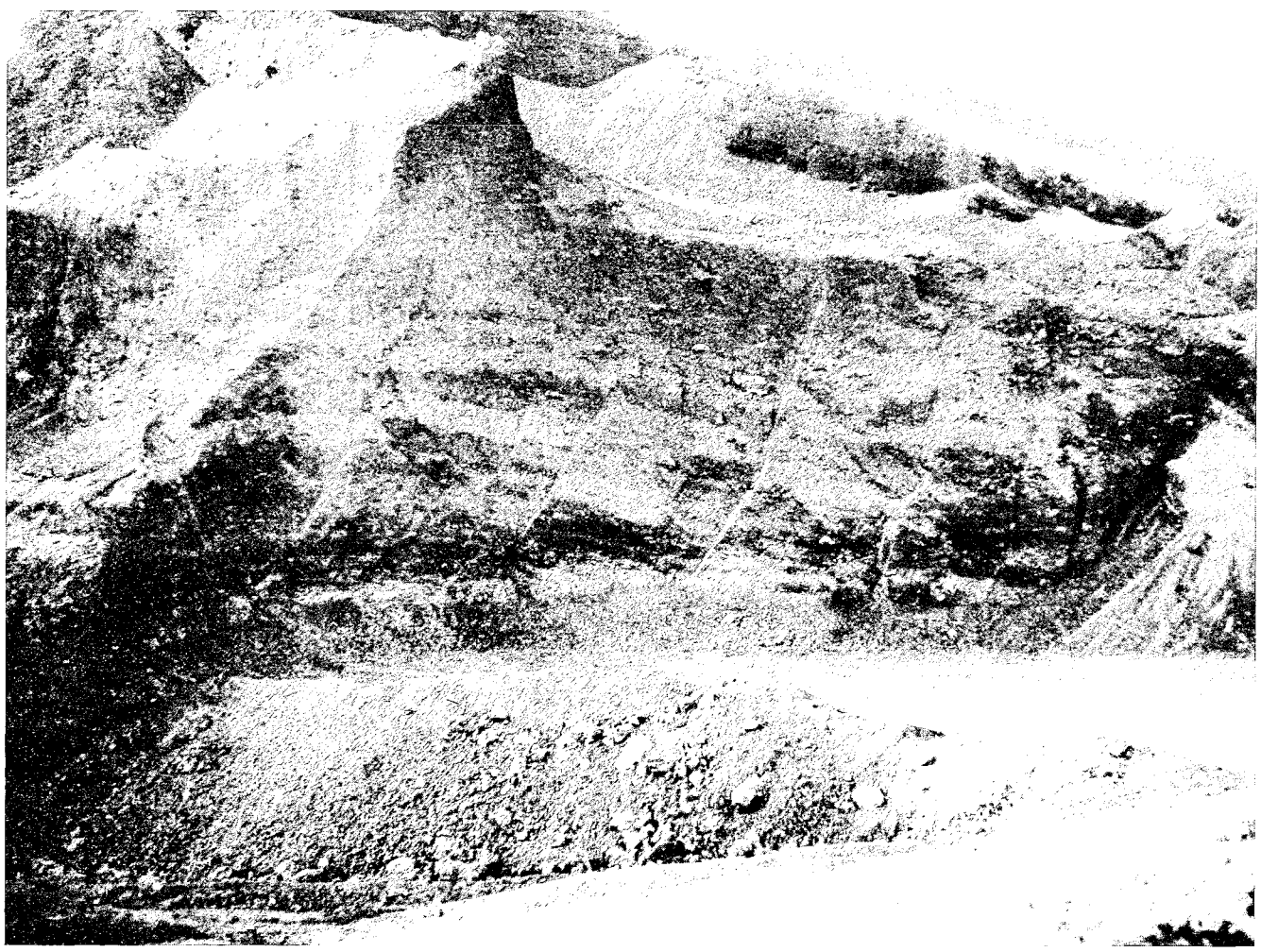

Figure 8. Normal faults cutting lower parts of the cinder section in the flank of the cone at STOP 1, 3rd day. The level crest of the vertical wall of the quarry here is about 9 m above the adjacent quarry floor.

cones are breached in similar fashion. At several localities, vertical dikes extending radially outward from the vent cut the lower half to three quarters of the cinder section and suggest that magma welled up to high elevations within the cinder cone structure prior to breachment. Abrupt truncation of the cinder layers in the walls of the breach commonly indicates removal of rafted masses of cinder when the wall of the cone finally failed owing to outward pressure from the contained lava lake. At some localities, cinder layers wrap down into the breach, as if this opening was maintained by continued or periodic flowage from the vent during pyroclastic eruptions. However, in many instances upwelling of magma occurred following the close of pyroclastic eruptions which had built an unbreached cone. Breachment may have attended development of fluid pressure in the contained lava lake sufficient to lift the surrounding cinder walls and give rise to sills at the base of the cone structure.

Return to cars. Cars return to gate. Resume road log mileage at gate.

0.2	10.3	Bear right (east) on dirt road.
3.1	13.4	Road junction. Bear right (south).
0.3	13.7	Road junction. Fork left.
0.4	14.1	Cerro Colorado. Park cars and walk east to the highest point on the north rim of the crater for lunch.

STOP 2. The crater of Cerro Colorado is about 1,000 m in mean diameter and its floor is more than 110 m below the highest point on the rim of the tuff cone. In the western wall of the crater, the tuff rests on a flow from an unknown source to the west; at the foot of the northern and eastern walls, exposures of the basal contact show that the tuff rests here on pinkish tan mudstone that probably represents playa deposits. The eruptive history of Cerro Colorado involved several episodes of phreatomagmatic eruption and deposition of tuff punctuated by at least two episodes of collapse wherein the inner walls of the tuff cone slumped into a vent. The multilobate form of the crater in plan view suggests the existence of three and perhaps four centers of eruption and subsequent collapse (fig. 9). Although the age of the crater is not known, the presence of Hohokam potsherds on erosion surfaces bevelling the tuff deposits indicates that Cerro Colorado is at least 1,000 years old and supports an age more on the order of 10,000 years (Shakel and Harris, 1972).

Cerro Colorado is different from Crater Elegante in many respects. The tuff beds near the high point of the crater rim dip much more steeply (20-25°) than those of Elegante. These beds are much thicker and in many places the original crater rim is preserved. Indeed, individual beds can be traced from the crater floor up and over the rim to the distal outer flanks where they are buried by alluvium.

The tuff of Cerro Colorado is rich in vesicular, slightly palagonitized, juvenile lapilli and ash together with very abundant accidental ejecta consisting of quartzofeldspathic sand and gravel. Accretionary lapilli are common, especially within the youngest unit of tuff, which underlies the rim of the crater here on its northern side. Note the remarkable lateral continuity of these tuff layers. Many of the uppermost beds are normally graded suggesting an airfall origin for these layers.

Return toward cars and thence to outer slopes of the tuff cone south of the cars.

STOP 3. Surface features of the proximal pyroclastic surge beds. Ejecta in surge beds at this location were blasted up over a collapsed crater rim from the small vent to the southeast. Near the rim, the beds are even and flat, but within about 15 m from the present rim, longitudinal wave forms appear (fig. 10). The longitudinal dunes continue for about 30 m down slope where they give way to a broad, arching transverse dune. Small-scale features, such as ripple marks on the longitudinal dunes, are remarkably well-preserved. These longitudinal dunes have a wave length of about 6 m and a wave height of 50 cm, yielding a height-to-length ratio of 1:12. Such features have not been previously described at any other volcano, although radial gullies are common.

Blanketing the dune horizon are normally-graded, pyroclastic-fall beds. This good marker horizon is locally stripped away.

If time permits we will proceed to the crater floor.

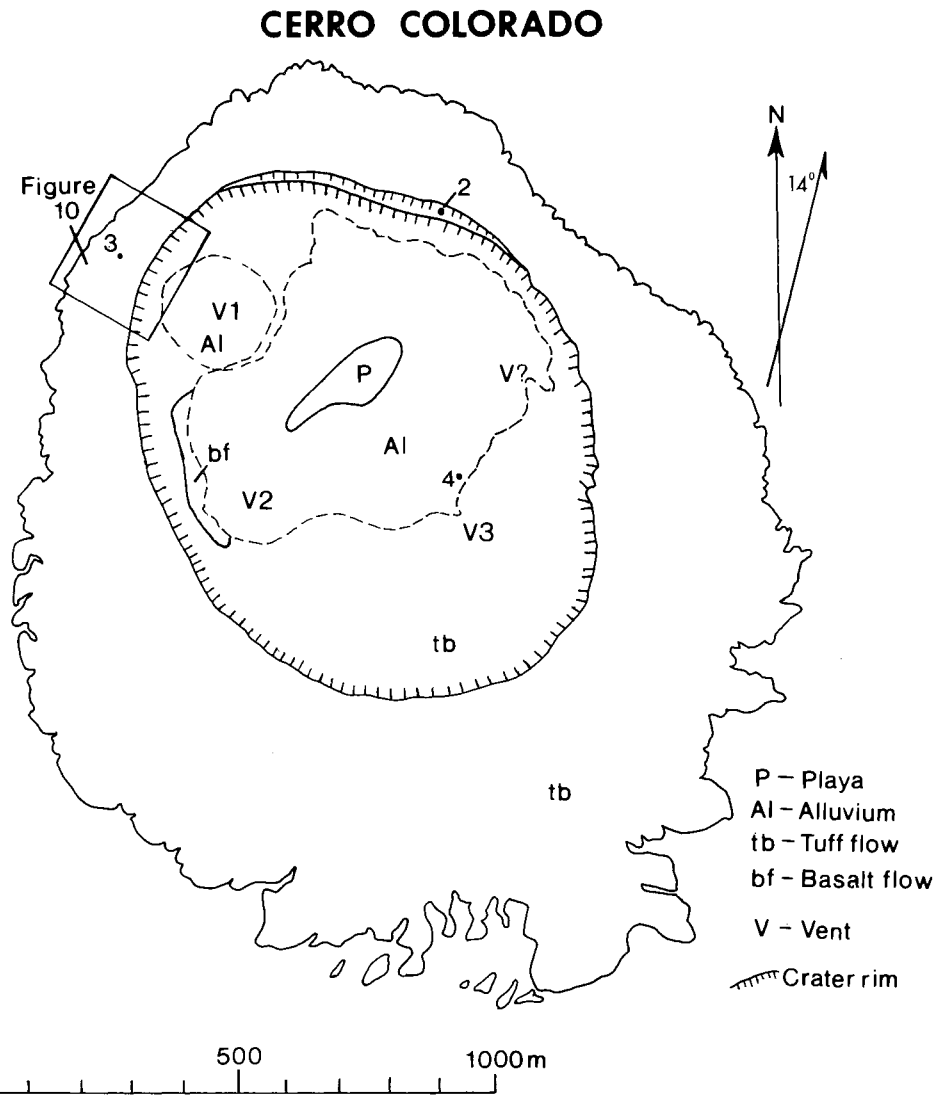

Figure 9. Sketch map of Cerro Colorado. Major units indicated by key. Stops for day 3 given by numerals. (Simplified from Jahns, 1959.)

STOP 4. Inward dipping beds. Associated with the several vents are inward-dipping beds whose bedding planes define portions of downward-pointing funnels. The funnel-like structures converge toward an apex that marks the vent location. These beds apparently represent an explosive phase of eruption following collapse. Vertical crater walls are unconformably overlain by these inward-dipping beds. In a few places, collapse cut the inward dipping beds.

One of the most remarkable features of these beds are the giant sandwave bedforms that make colossal climbing ripples. These forms are best seen in the vincinity of **STOP 4** in figure 9.

Return to cars and to Tempe.

0.4	14.5	Road junction. Bear right.
0.3	14.8	Road junction. Fork left.
3.1	17.9	Road junction. Bear right.
3.8	21.7	Junction with Mexico Rte. 2. Turn right (east).
31.6	53.3	Town of Sonoyta. Turn left toward international border.
2.0	55.3	International border at Lukeville, Arizona. Return to Tempe.

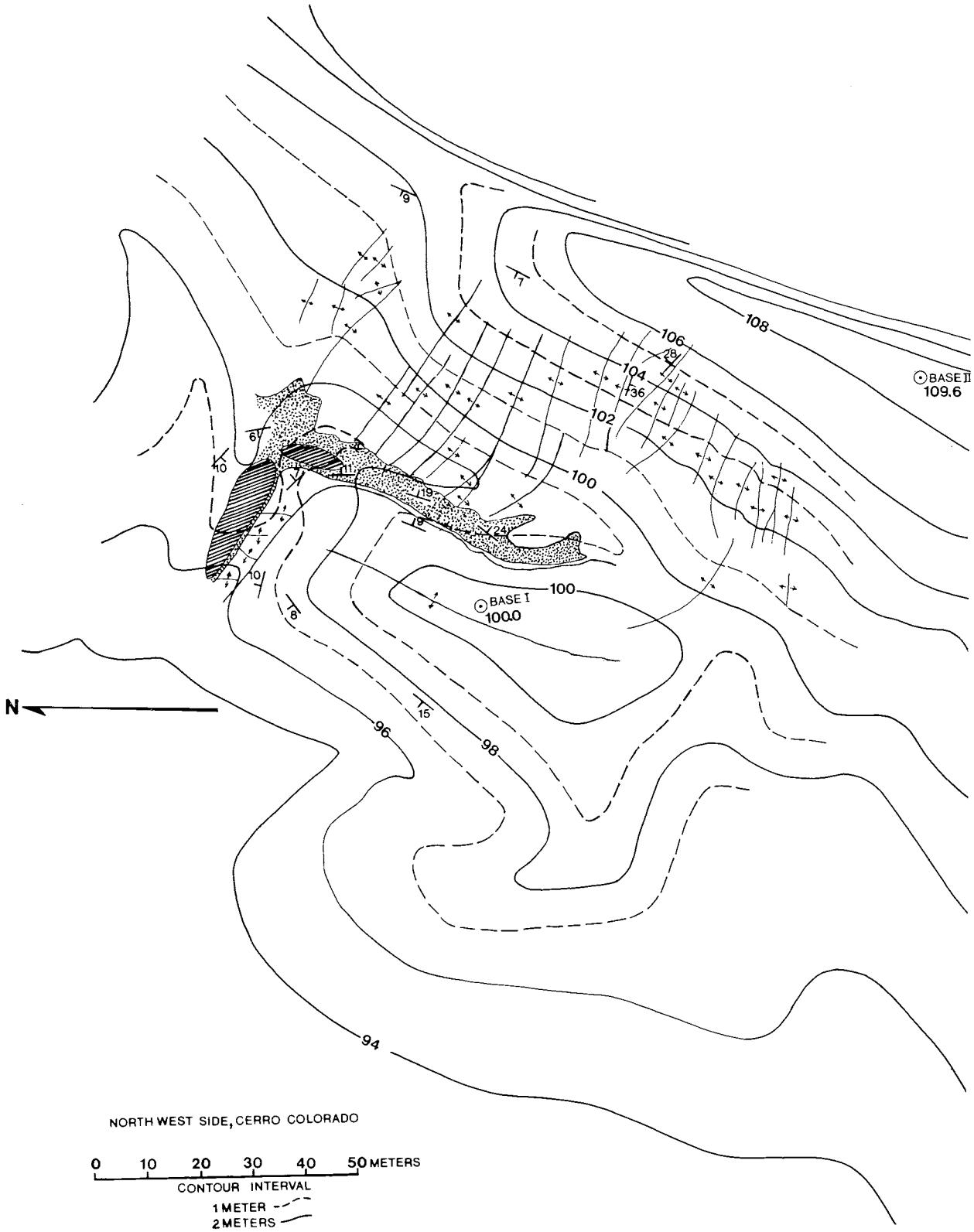

Figure 10. Map of radial dunes at Cerro Colorado. Location of diagram shown in Fig. 9. Contour elevations are relative. Lined and stippled patterns both show air-fall deposits that rest on surge beds. Dune crests indicated by lines with small arrows.

Interleaf. Landscapes of rounded boulders produced by spheroidal weathering of granite in an arid environment. Beeline Highway, 40 miles northwest of Phoenix. Long. 111° 30′—Lat. 33° 45′. (Photograph No. 3806 taken by Troy L. Péwé, February 16, 1976.)

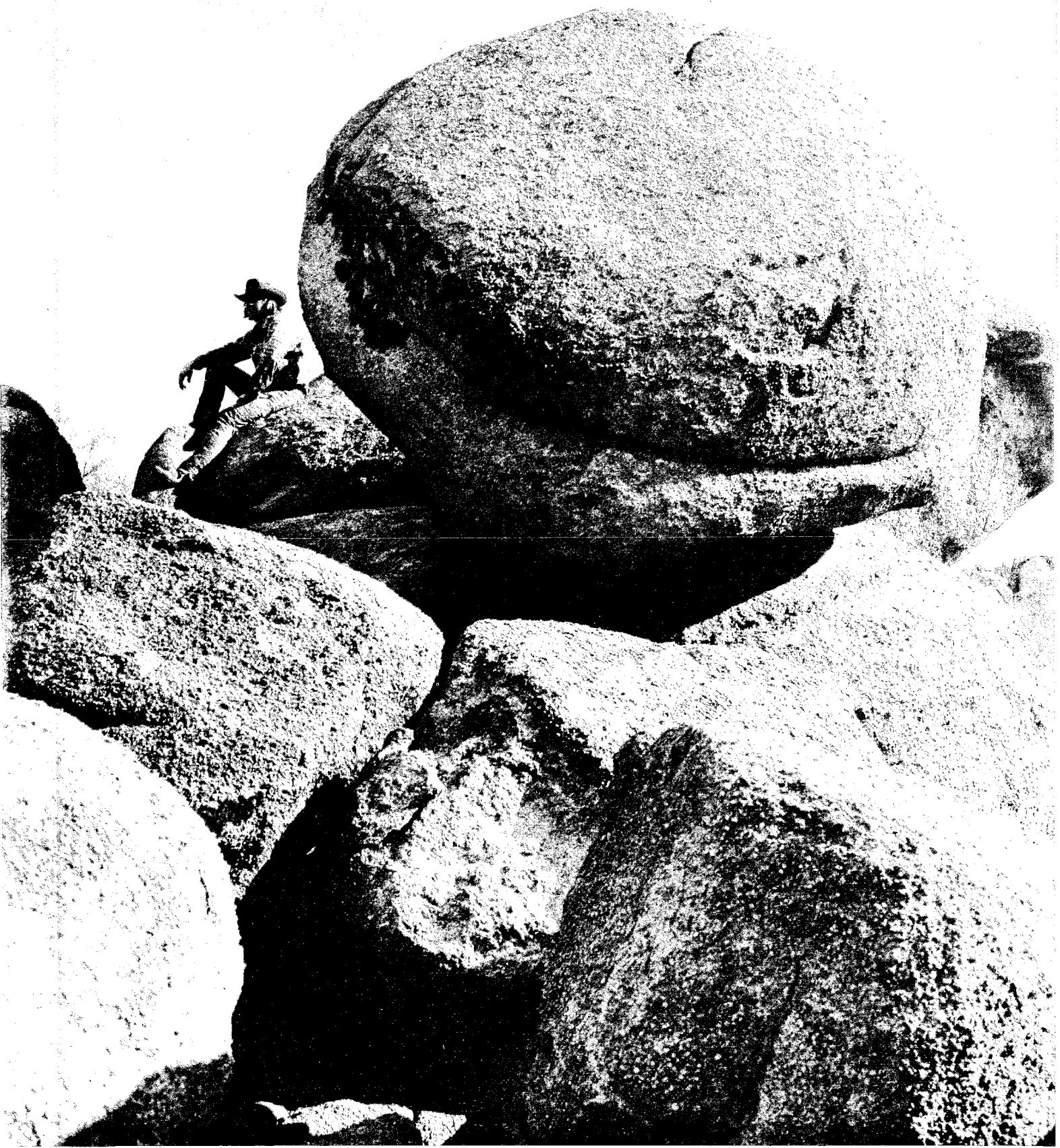

LITHIUM PEGMATITES OF THE WHITE PICACHO DISTRICT, MARICOPA AND YAVAPAI COUNTIES, ARIZONA

by
David London
and
Donald M. Burt

Department of Geology
Arizona State University

This one-day field trip visits several small lithium pegmatites on private property in typical desert terrain, and normal desert field equipment (boots, hat, canteen, etc.) is recommended. Two short hikes will be made totaling about 2 km. The road to the pegmatites has too many sharp curves for buses, but can be negotiated by ordinary sedans if drivers are careful not to become stuck in the loose sand of San Domingo Wash.

Figure 1. View of the Red and White Picachos from the west.

INTRODUCTION

The Arizona pegmatite belt is a broad region that extends from central to northwestern Arizona (Jahns, 1952). The White Picacho pegmatite district is located near the SE end of this belt. The Arizona Bureau of Mines bulletin by Jahns (1952) remains the best general reference on the district, and the reader is referred to it for a more complete description of the pegmatites. Jahns' detailed maps of the geology of the pegmatite workings are still usable, inasmuch as only minor mining and development work has been carried out in the district over the past 25 years.

Later geologic studies in the district include the county maps by Wilson et al. (1957) and the Arizona Bureau of Mines (1958), a study of tungsten deposits by Dale (1959), an age-dating study of pegmatite minerals by Laughlin (1969), a study of placer gold by Johnson (1972), and a thesis study of the volcanic rocks to the east by Ward (1977). This guide incorporates, in addition, preliminary results of thesis research by London (in progress, 1978). The discovery of eucryptite in the district (Burt et al., 1977) has been confirmed by Jahns (personal communication, 1977).

The pegmatites of the White Picacho district are mainly indicated on the Red Picacho 7.5′ topographic quadrangle map of the U.S. Geol. Survey (1964), although several workings on this map are misnamed. The district derives its name from White Picacho, a prominent peak about 1 km northeast of Red Picacho (fig. 1). The field trip area spans the Maricopa/Yavapai county line and lies mainly in sections 10 and 16, T7N, R3W. This is about 80 km northwest of Phoenix and 10 km east of Wickenburg, in the southwest foothills of the Wickenburg Mountains, at an elevation of 800–900 m (2,600–3,000 ft.). The main drainages are San Domingo Wash, which also provides

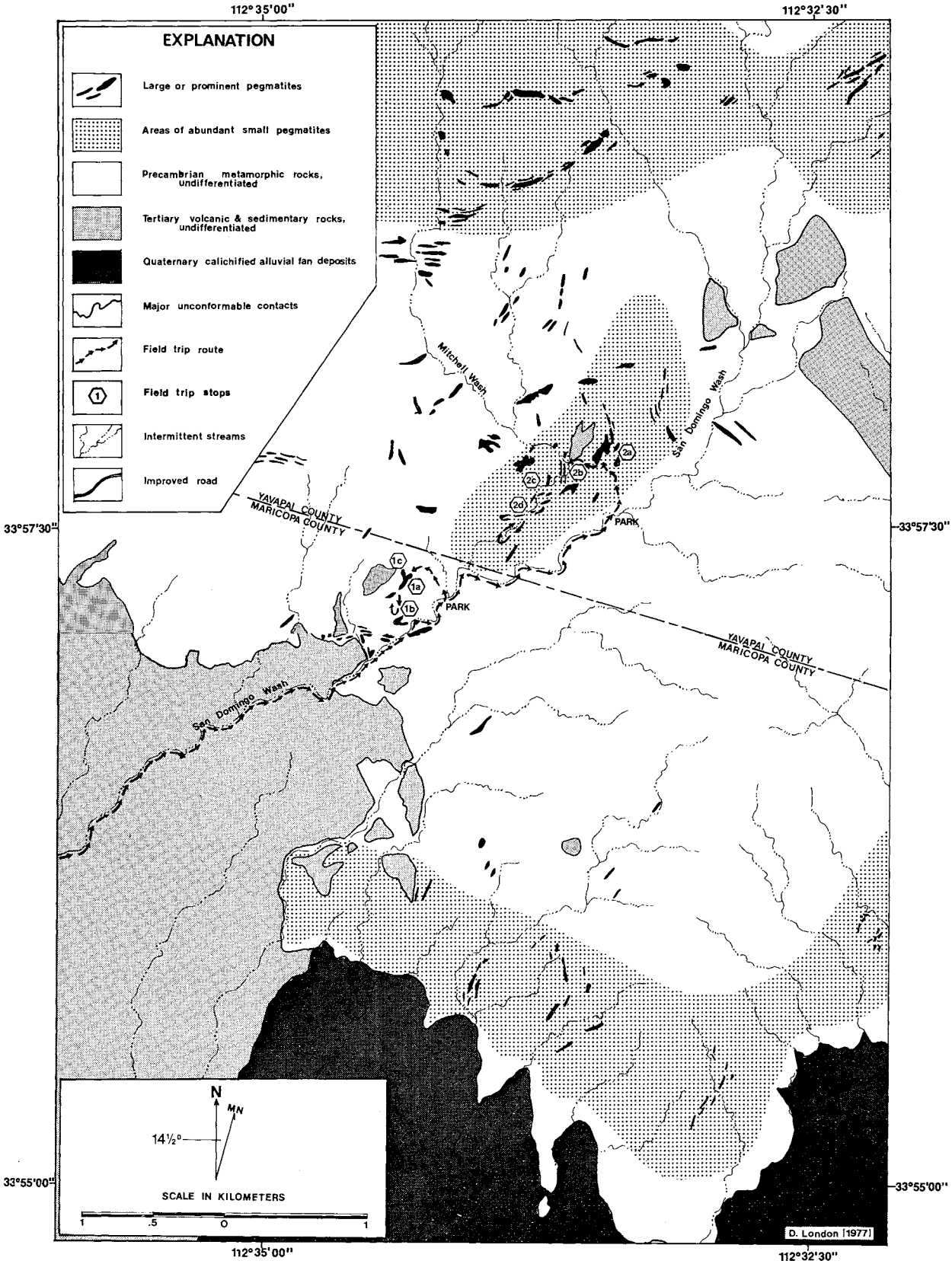

Figure 2. Map showing the distribution of major rock types in the district.

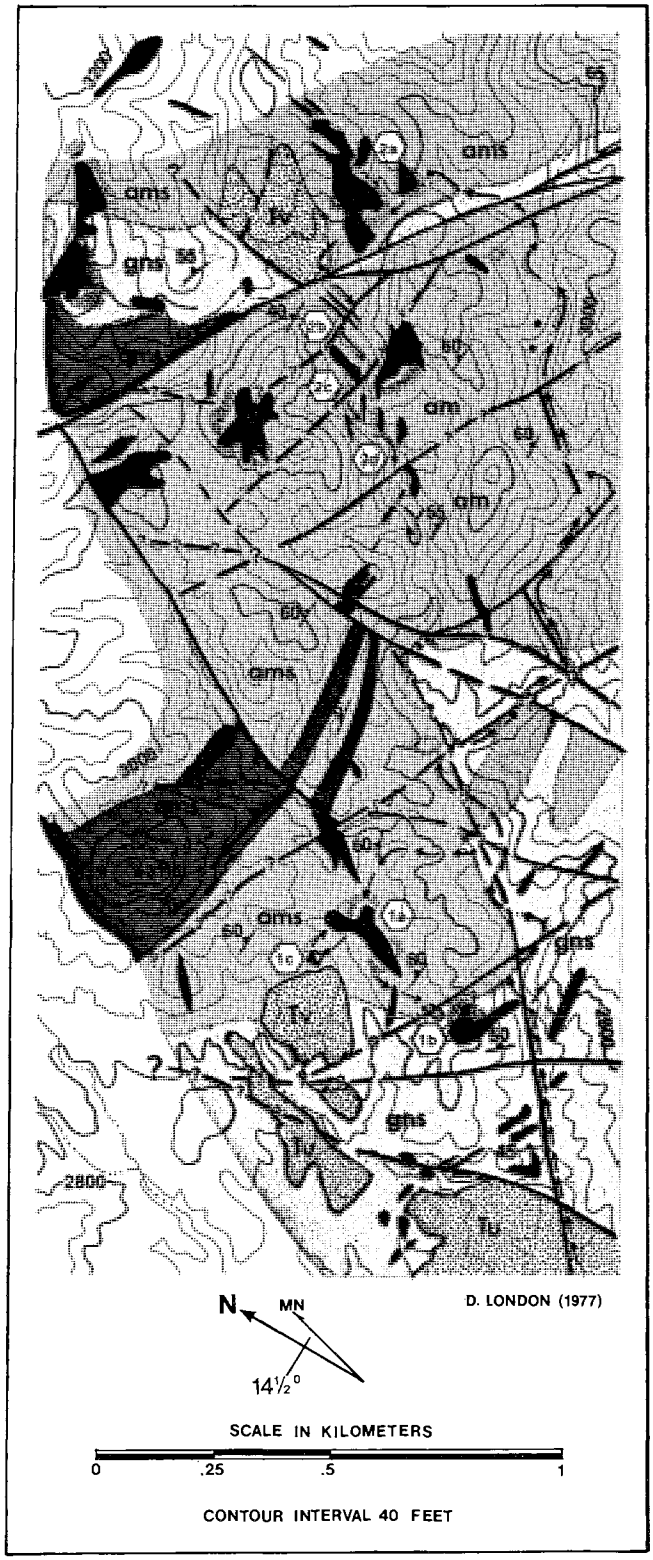

Field trip route. Field trip stops. Vertical mine shaft.

EXPLANATION

Large or prominent pegmatites.

Dump material.

ams

Northern part of map area: predominantly fine to medium grained, well foliated hornblende amphibolite, containing significant amounts of sulfides (pyrite and chalcopyrite) as disseminated grains and discontinuous patches parallel to foliation; heavily rust stained on weathered surfaces; black on fresh surfaces.

Southern part of map area: sulfidic biotite-hornblende amphibolite and biotite schist.

am

Predominantly hornblende-epidote amphibolite and hornblende-plagioclase amphibolite. Hornblende-epidote amphibolite is fine to medium grained, well foliated, with irregular, discontinuous epidote-rich layers; hornblende-plagioclase amphibolite is medium grained, well foliated, and homogeneous. Weathers dark gray to black, locally rust stained; unit contains minor fine grained, gray, massive quartz-muscovite impure quartzites. Well exposed in Mitchell Wash.

qms

Medium grained, well foliated muscovite-quartz schist; locally contains small, euhedral, pink garnets; foliation surfaces are multiply crenulated; silvery on fresh and weathered surfaces, locally rust stained.

gns

Predominantly very fine to fine grained, well foliated quartz-chlorite-epidote (?) schists, quartz-feldspar-biotite or chlorite gneisses, and biotite schists; heavy brown-black varnish on weathered surfaces, green or black on fresh surfaces. Similar rocks occurring in some shear zones and around most pegmatites appear to be products of retrograde hydrothermal alteration.

Tv

Tertiary volcanic rocks: predominantly porphyritic gray intermediate volcanics; phenocrysts are plagioclase and biotite in fine grained gray groundmass.

Tu

Tertiary volcanic and sedimentary rocks, undifferentiated.

Mostly subvertical fault zones of sheared or brecciated rock; some breccia zones are welded with very fine grained chlorite/epidote matrix; others are welded with very coarsely crystalline buff-colored calcite. Nature of offset in the various types of fault zones is not known at this time. Faults verified by ground truth.

Extention of fault zone based on air photo linears and topography. Faults may be verified by further ground mapping.

Extension of fault zone based solely on topography. Fault zones may be buried by unconsolidated materials and thus are not directly observable on the ground.

Sharply gradational lithologic contact, dashed where approximately located.

Broadly gradational lithologic contact, approximately located.

60

Strike and dip of layering and foliation in metamorphic rocks.

Figure 3. Reconnaissance geologic map of the field trip area.

vehicle access, and its tributary, Mitchell Wash, which will be visited on foot. Flora and fauna are typical of the upper Sonoran desert region; visitors are especially warned to watch out for rattlesnakes and wasps, which abound in the old pegmatite workings.

STRUCTURAL SETTING

Figure 2 shows the distribution of major age/lithologic rock types in the district. The pegmatite minerals have been dated by Laughlin (1969); K-Ar dates on different minerals yield apparent ages ranging from 750–1580 m.y., with muscovite giving a minimum age of 1270 m.y.

The northern part of the area depicted in figure 2 is dominated by Precambrian igneous and metamorphic rocks; the eastern and southwestern parts by Tertiary volcanics and sediments. A stratigraphy of Tertiary rocks exposed to the east of the map area has been developed by Ward (1977). Poorly consolidated alluvial deposits cover much of the area to the south; these deposits are presumably Quaternary in age.

The pegmatites exposed in the White Picacho district lie in a broad zone that generally trends northeast. Pegmatites in the south part of the district are grossly discordant; to the north, however, the pegmatites conform to the regional strike (but not necessarily dip) of the host rocks. The significance of host rock petrochemistry and regional structure as influences on pegmatite mineralogy, shape, and trend is currently under investigation. A study of various types of remote sensing imagery of the area (E. B. H. London, unpublished report, 1977) revealed that San Domingo Wash is a major lineament that appears on all types of imagery (LANDSAT, ERTS, high-level color infrared, and black and white photography). Preliminary imagery interpretation and reconnaissance mapping indicate that generally east-west trending metamorphic rocks and pegmatite zones bend abruptly into parallelism with the San Domingo lineament, most prominently in the upper reaches of San Domingo Wash.

Pegmatites are abundant in a zone along San Domingo Wash, although this is not the only belt in which they are concentrated (see fig. 2). Ground reconnaissance and imagery interpretation suggest that other features, such as rock types and lithologic contacts, may be important in determining zones of pegmatite concentration.

The San Domingo lineament can be traced northeast into the Spud Fault zone of Blacet (1966) (Anderson and Blacet, 1972); the observation of shear textures and major discontinuities across San Domingo Wash suggests that the Spud Fault system may extend into this area.

Figure 3 is a reconnaissance geologic map of the field trip area. The region consists of greenschists (probably chlorite-(muscovite)-quartz), biotite-rich schists and gneisses, hornblende-epidote and hornblende-plagioclase amphibolites, muscovite-quartz schists, and minor impure quartzites. Mineralogy and grain size suggest a general increase in metamorphic grade from southeast to northwest across the area; as of this writing, however, no petrographic work has been performed to verify mineral assemblages.

The rocks are extensively sheared by a set or sets of complex fault systems; most fault zones are subvertical and consist of sheared, mylonitized, or brecciated rock fragments. Rocks in and around most fault zones cutting metamorphic rocks are highly altered to chlorite and/or epidote.

Small-scale folds have been observed in numerous outcrops. Pre- or synmetamorphic isoclinal folds occur in the thinly layered amphibolites; postmetamorphic open and ptygmatic folds occur in all types of metamorphic rocks. Drag folds in fault zones and folds (probably) related to pegmatite emplacement are prevalent throughout the region.

As regards the structures of the pegmatites themselves, the reader is referred to Jahns (1952) as well as to later general reviews (Jahns, 1953; 1955). Details on the several pegmatites to be visited are given in the road log and stop guide.

MINERALOGY

For reference, table 1 is a partial list of minerals reported from the pegmatites of the district; underlined species are those regarded as likely to be encountered by participants in the field trip. For a more complete list, consult Jahns (1952, p. 33–34).

The only mineral on this list not described by Jahns is eucryptite, which, together with albite, forms an inconspicuous alteration product of spodumene. It was recognized by its red fluorescence under short wave ultraviolet light. The reaction by which it formed (Brush and Dana, 1880) involves sodium metasomatism of spodumene to yield intimately intergrown eucryptite and albite:

$$\underset{\text{spodumene}}{2\ LiAlSi_2O_6} + Na^+ \rightarrow \underset{\text{eucryptite}}{LiAlSiO_4} + \underset{\text{albite}}{NaAlSi_3O_8} + Li^+$$

The fact that the silica-deficient mineral eucryptite commonly occurs with quartz implies that end member spodumene must be unstable at low pressures and temperatures (Burt et al., 1977). Spodumene is indeed heavily altered in most pegmatites of the district, most commonly to muscovite or various clay minerals. Studies of spodumene alteration and eucryptite genesis are in progress.

TABLE 1. SOME MINERALS FROM THE WHITE PICACHO PEGMATITES

NAME	COMPOSITION
Quartz (milky)	SiO_2
Perthitic Microcline	$(K,Na)AlSi_3O_8$
Albite (Cleavelandite)	$NaAlSi_3O_8$
Eucryptite	$LiAlSiO_4$
Muscovite (incl. pink muscovite)	$KAl_2AlSi_3O_{10}(OH)_2$
Lepidolite	$K(Li,Al)_3(Si,Al)_4O_{10}(F,OH)_2$
Zinnwaldite	$KLiFe^{2+}Al(AlSi_3)O_{10}(F,OH)_2$
Biotite	$K(Mg,Fe)_3AlSi_3O_{10}(OH)_2$
Cookeite	$LiAl_4(AlSi_3)O_{10}(OH)_8$
Tourmaline	$(Na,Ca)\ (Fe^{2+}, Fe^{3+}, Al,Li)_3Al_6(BO_3)_3Si_6O_{18}(OH,F)_4$
Schorl	
Elbaite	
Beryl	$Be_3Al_2Si_6O_{18}$
Spessartine	$Mn_3Al_2S_{13}O_{12}$
Spodumene	$LiAlSi_2O_6$
Lithiophilite - Triphylite	$Li(Mn,Fe)PO_4$
Amblygonite	$LiAlPO_4(F,OH)$
Triplite	$(Mn,Fe)_2PO_4(F,OH)$
Apatite	$(Ca,Mn)_5(PO_4)_3F$
Monazite	$(Ce,La)PO_4$
Fluorite	CaF_2
Scheelite	$CaWO_4$
Columbite - Tantalite	$(Mn,Fe)\ (Nb, Ta)_2O_6$
Microlite - Pyrochlore	$(Na,Ca)_2\ (Ta,Nb)_2O_6(O,OH,F)$
Cassiterite	SnO_2
Magnetite	Fe_3O_4
Gahnite	$ZnAl_2O_4$
Sulfides (pyrite, pyrrhotite, loellingite, etc.)	

ECONOMIC IMPORTANCE

Economic mineral production from the White Picacho pregmatites has been small. Mining has included the lithium ore minerals spodumene, lepidolite, and amblygonite, and the nonlithium ores of feldspar, mica, beryl, columbite-tantalite, and bismuth minerals. Most mining and development work appears to have been done between 1947, when lithium minerals were first discovered, and 1952, when Jahn's report appeared. Later small-scale mining has been performed by the long-time owners, Earl F. and Sidney B. Anderson of Mesa, who maintain a caretaker on their property.

For carrent data relating to lithium uses and resources, consult, *e.g.*, Vine (1976). The implication is that the pegmatites exposed in the district do not at present represent a large enough resource to justify a large-scale mining operation.

Elsewhere in the district there has been minor production of gold and tungsten (scheelite) from quartz veins and placers, and of copper from meta-volcanics.

REFERENCES CITED

Anderson, C. A., and Blacet, P. M. (1972), Geologic map of the Mount Union quadrangle, Yavapai County, Arizona: U.S. Geol. Survey Geol. Quad. Map GQ-997.

Arizona Bureau of Mines, University of Arizona (1958), Geologic map of Yavapai County, Arizona (scale 1:375,000).

Blacet, P. M. (1966), Unconformity between gneissic granodiorite and overlying Yavapai Series (older Precambrian), central Arizona: U.S. Geol. Survey Prof. Paper 550-B, pp. B-1–B-5.

Brush, G. J., and Dana, E. S. (1880), Mineral locality at Branchville, Connecticut: Fourth Paper. Spodumene and the results of its alteration: Am. Jour. Sci., v. 20, no. 118, pp. 257–285.

Burt, Donald M., London, David, and Smith, Michael R. (1977), Eucryptite from Arizona and the lithium aluminosilicate phase diagram (abst.): Geol. Soc. Am. Program, v. 9, no. 7, p. 917.

Dale, Vernon B. (1959), Tungsten deposits of Yuma, Maricopa, Pinal, and Graham Counties, Arizona: U.S. Bur. Mines, RI 5516, 68 p.

Jahns, R. H. (1952), Pegmatite deposits of the White Picacho District, Maricopa and Yavapai Counties, Arizona: Ariz. Bur. Mines Bull. 162, 105 p.

———(1953), The genesis of pegmatites, I: Occurrence and origin of giant crystals: Am. Min., v. 38, pp. 563–598.

———(1955), The study of pegmatites, *in* Bateman, Alan M., ed., Soc. Econ. Geol., 50th anniv. vol., part II, pp. 1025–1130.

Johnson, Maureen G. (1972), Placer gold deposits of Arizona: U.S. Geol. Survey Bull. 1355, 103 p.

Laughlin, A. William (1969), Excess radiogenic argon in pegmatite minerals: Univ. Ariz., PhD Thesis, 187 p.

Vine, James D., ed. (1976), Lithium resources and requirements by the year 2000: U.S. Geol. Survey Prof. Paper 1005, 162 p.

Ward, Michael B. (1977), The volcanic geology of the Castle Hot Springs area, Yavapai County, Arizona: Ariz. State Univ., MS Thesis, 74 p.

Wilson, Eldred D., Moore, R. T., and Pierce, H. W. (1957), Geologic map of Maricopa County, Arizona (scale 1:375,000): Univ. Ariz., Ariz. Bur. Mines.

ROAD LOG AND STOP GUIDE

MILES Interval	Total	
0.0	0.0	Leave the loading dock behind the F-wing, Physical Sciences Center (Geology-Physics) at A.S.U.; turn left (west) onto University Dr., and proceed through the next 6 traffic lights.
2.6	2.6	Turn left (south) onto 48th St.
0.4	3.0	Turn right onto I-10 westbound (Phoenix); stay on I-10/I-17 for the next 22.6 miles.
0.3	3.3	Phoenix South Mountain Park, largest municipal park in the U.S., lies to the south; the mountains are composed of Precambrian gneisses, schists, and greenstones and Tertiary granodiorite.
2.1	5.4	To the right (northeast) is Camelback Mountain. The camel's head, to the west, is composed of Tertiary arkosic sandstones and conglomerates; it sits unconformably on a body of Precambrian granite. The sharp peak to the northwest of Camelback is Squaw Peak, composed of Precambrian metarhyolites, metatuffs, quartzites, and greenstones. It is the site of Field Trip No. 8.
4.1	9.5	The Sierra Estrella (Precambrian) lie to the left (southwest), downtown Phoenix is to the right.
10.5	20.0	The Phoenix Mountains to the right (east) are composed chiefly of Precambrian phyllites and schists. The hills to the north and west of the Phoenix Mountains are mostly intermediate to mafic volcanics of probable Tertiary age.
5.6	25.6	Exit right onto Bell Rd. westbound; stay on Bell Rd. for the next 13.8 mi.
12.7	38.3	The White Tank Mountains are straight ahead (west), the Wickenburg Mts. are northwest, and the Hieroglyphic Mts. are north. All three ranges are composed of Precambrian igneous and metamorphic rocks overlain by Tertiary igneous and sedimentary rocks.
1.1	39.4	Turn right (northwest) onto Grand Ave. (U.S. 60 and 89; State 93) to Wickenburg; stay on it for the next 20.6 mi., to Morristown.
20.3	59.7	Morristown railroad overpass. The famous Vulture gold mine is located in the Vulture Mts. to the northwest. Red Picacho is the knob to the north; White Picacho which gives the pegmatite district its name is hidden behind it. The pegmatites to be visited are about 5 km west of Red Picacho.
0.3	60.0	Morristown. Turn right (northeast) onto the Castle Hot Springs Rd. (just past the Morristown sign).
1.6	61.6	Cross State 70. Continue straight onto gravel road; Red Picacho is straight ahead.
2.5	64.1	Turn left at fork near top of hill; if you miss this turnoff, another is available over the hill, 200 m farther.
0.4	64.5	Continue straight ahead (northwest) on the Old Wickenburg Stage Route. Exposures for the next 6 mi. are of volcanic and sedimentary rocks of probable Tertiary age. The volcanic rocks are predominantly flows of intermediate composition (maroon to mauve colored quartz latites or rhyodacites), with minor layers of basalt and tuffaceous rhyolite. The sedimentary rocks, well exposed in San Domingo Wash, are predominantly pebbly arkosic sandstones and subangular, polymictic conglomerates. The rock fabric, long tabular beds, and absence of channel features suggest that these are alluvial fan deposits. Very coarse conglomeratic breccias (?) appear to be debris flows of unknown (sedimentary or volcanic) origin.
1.1	65.6	Bear left across the wash; a placer gold operation is visible to the right.
1.9	67.5	Make a hard right turn into San Domingo Wash; continue up the wash and avoid stopping in loose sand.
0.5	68.0	On the left (west) is a good exposure of a low angle fault (fig. 4). The fault surface dips about 25° to the east; drag folds indicate dextral motion of the upper block to the north-northeast. This fault probably represents a décollement, inasmuch as at least one other low angle fault in the area shows an opposite direction of transport. However, block rotations of nearly 90° are common in the sedimentary rocks; thus apparent thrusts or décollements may be normal faults rotated by subsequent deformation.
2.5	70.5	You are crossing the buried contact between the Tertiary volcanics and sediments and the Precambrian metamorphics.
0.5	71.5	**STOP 1.** Park in San Domingo Wash at the foot of the trail to the North Morning Star pegmatite.

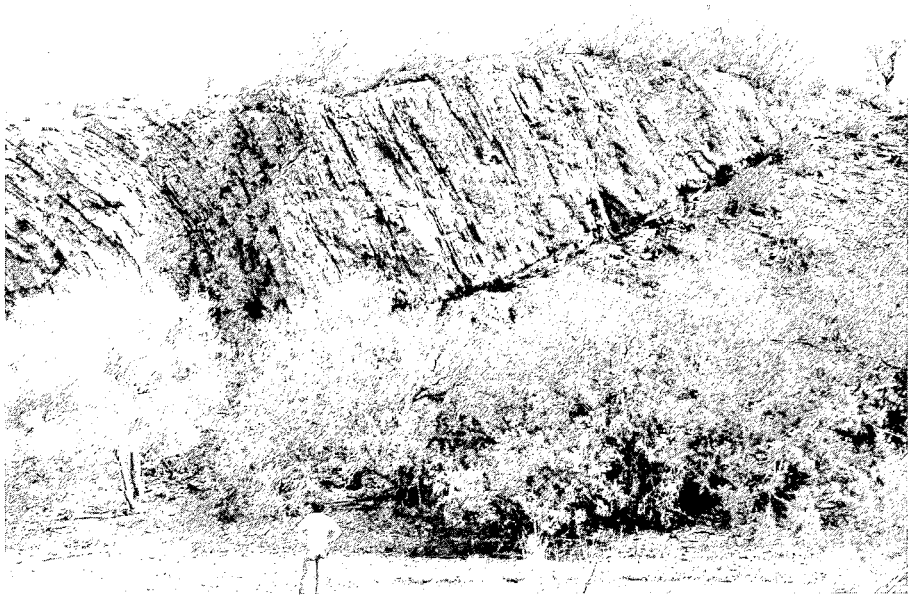

Figure 4. Low angle fault in the Tertiary sedimentary rocks exposed in San Domingo Wash.

STOP 1a: Hike up the path to the North Morning Star pegmatite. WATCH OUT FOR RATTLESNAKES. The North Morning Star (fig. 5) is one of the best-exposed lithium pegmatites in the district. Like other relatively large pegmatites, it shows a textural gradation from a medium grained border zone to a giant textured core. Mineral assemblage zones are particularly well developed, although this may not be immediately apparent. The pegmatite core consists of giant-textured, anhedral quartz; lithium minerals, mostly amblygonite and spodumene, are concentrated in the inner intermediate zones; predominantly quartz-perthite pegmatite constitutes the outer intermediate and border/wall zones. The North Morning Star's zones are unusually uniform in thickness and regular in extent (see figs. 6 and 7); the pegmatite is more sheet-like than most other lithium pegmatites of the district (for example, the South Morning Star pegmatite, **STOP 1b.** Jahns (1952) concluded that most of the pegmatites were emplaced along pre-existing fractures, along foliation, or along other planar features in the host rocks; the relations of the North Morning Star to its confining rocks appear to support this interpretation. Although some pegmatites show signs of forceful injection, the North Morning Star may have undergone relatively passive emplacement. Foliation and layering in the country rocks are consistent up to the pegmatite's border zone; there are no forcefully intruded dikelets nor drag-folded metamorphics at the borders. No offset of the host rocks has been observed across the pegmatite, and no shear or breccia

Figure 5. The North Morning Star pegmatite, viewed from the east.

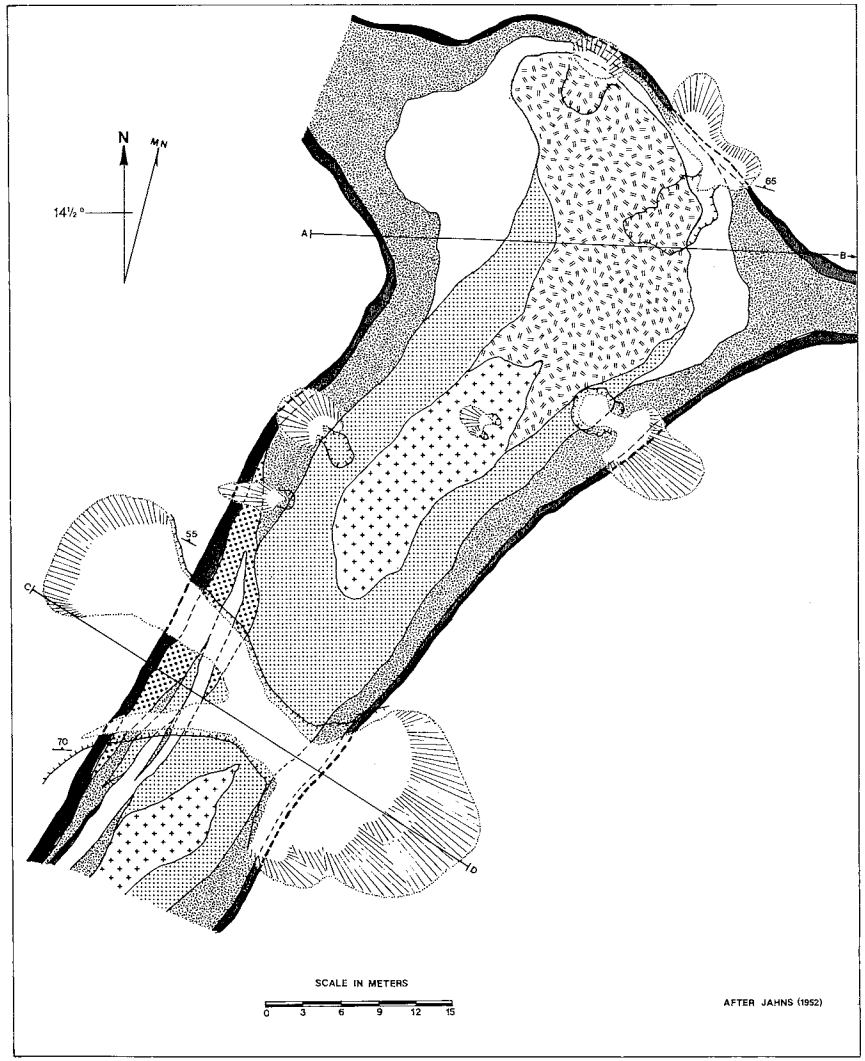

Figure 6. Geologic map of the North Morning Star pegmatite.

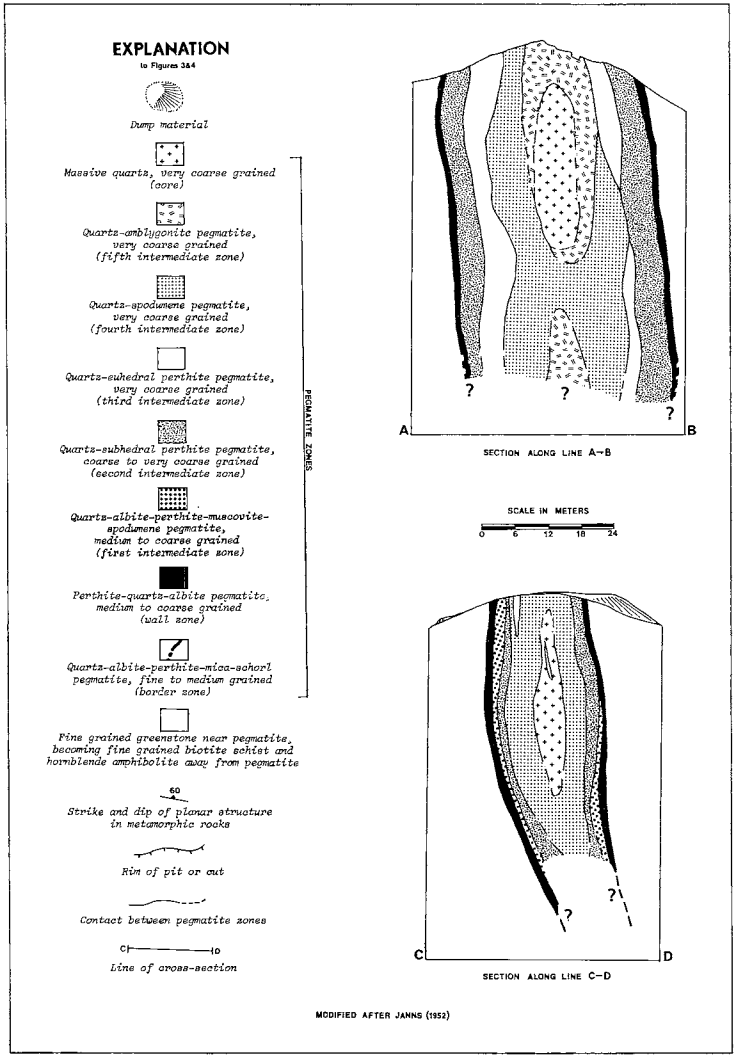

Figure 7. Cross sections through the North Morning Star pegmatite.

Figure 8. The White Ridge pegmatite, viewed from the south.

zone can be traced into the metamorphic rocks in either direction off the pegmatite's long axis. The absence of deformation or brecciation localized at the pegmatite borders suggests that the North Morning Star was emplaced in a tensional structural environment.

STOP 1b. Follow the path from the North Morning Star pegmatite south to the South Morning Star pegmatite. The South Morning Star is mineralogically similar to the North Morning Star but differs from it in shape. The bulbous, irregular shape of the South Morning Star is characteristic of pegmatites in the district that intrude well-foliated muscovite or chlorite schists. Muscovite schists exposed to the north and west of the South Morning Star are highly folded and crenulated; foliation in these rocks appears to wrap around the pegmatite. Jahns (1952) reports that potassium metasomatism has impregnated the border host rocks with K-feldspar and books of yellowish-green muscovite. Within the district, diffusion and metasomatism of pegmatite materials into country rocks is generally most pronounced in schistose metamorphic rocks; whether or not appreciable amounts of materials from the host rocks have diffused into the pegmatites is not known at this time.

Return to the north end of the North Morning Star; cross the ravine to the west.

STOP 1c. Copper and gold prospect in amphibolite. This hill displays some of the salient geologic features of the region. The unconformable contact of Tertiary volcanics on Precambrian metamorphics can be seen half way up the ridge. Fresh pieces of volcanics and sulfide-rich amphibolite are visible on the main (eastern) dump. Also in the dump are chunks of altered amphibolite breccia, indicating the presence of a fault zone (in or near the ravine). Brecciation probably facilitated the formation of enriched copper minerals, such as bornite and malachite; malachite-stained breccia and amphibolite occur on the small stockpile to the north of the main prospect. BE CAREFUL AROUND PROSPECT PITS AND SHAFTS. There are numerous copper prospects and mines throughout the region; the Abe Lincoln and Constellation Mines are among the largest. Pyrite, however, is by far the most abundant sulfide; its uniform, widespread distribution through the amphibolite suggests that it has a primary volcanic origin.

Return to the North Morning Star, and take the path back to the cars. Proceed up San Domingo Wash 1.3 mi. to **STOP 2.** You will pass the old mica mill and homestead of the Anderson brothers on the left.

STOP 2. Park in the wash, and proceed up the path to the left (northwest) to **STOP 2a.** Along the path are rather poor exposures of breccia zones, altered diabase dikes, and sheared greenstones and schists. This is part of a major fault zone that extends from the upper reaches of Mitchell Wash southeast across most of the Red Picacho quadrangle. The fault is easily traced on air photos for about 8 km; apparent sinistral offset of almost a kilometer can be observed in steeply-dipping metamorphic rocks in the southeast portion of the fault zone.

STOP 2a. White Ridge lithium pegmatite (fig. 8). WATCH FOR WASPS IN THE ADIT! The White Ridge consists of several large, irregular pegmatite dikes and pods. Jahns (1952) does not report lithium minerals from the White

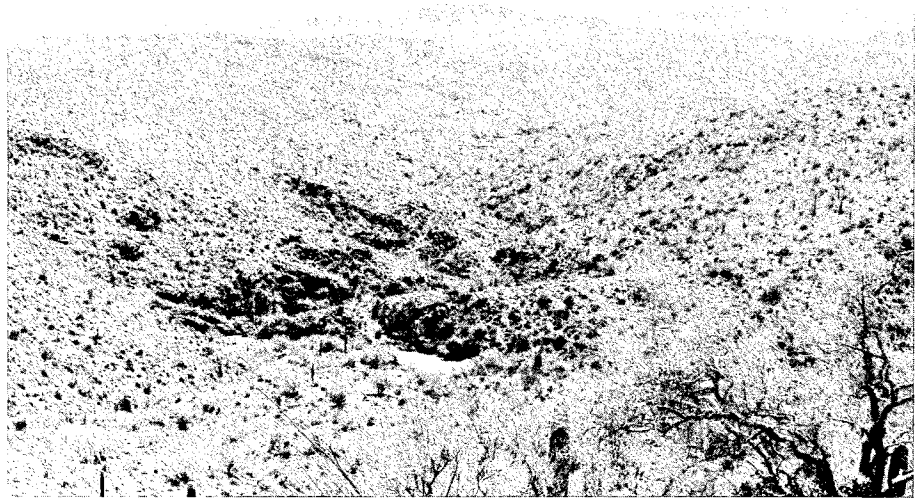

Figure 9. View looking southwest down Mitchell Wash Canyon.

Ridge, but subsequent development work revealed a zone of fresh, very coarse to giant-textured spodumene-quartz-albite pegmatite. Traces of lithium phosphates have also been seen in the dumps and in the eastern pegmatite cuts. Note the pink weathering of the otherwise fresh white spodumene. The White Ridge was not mapped by Jahns (1952), and a detailed description of its zoning is not yet available.

Return to the path leading into Mitchell Wash. Once in the wash, head southwest into Mitchell Wash Canyon (fig 9).

STOP 2b. A prominent shear zone is well-exposed where the wash first jogs from southwest to west. The wash is clearly controlled by lithology, attitude of layering and foliation, and sheared fault zones throughout its length. Small, irregular pegmatite pods and stringers are ubiquitous in the wash exposures. Most pegmatites are composed of perthite-quartz-(spodumene)-schorl; the schorl is noticeably concentrated along pegmatite borders and occasionally permeates the host rock up to about 10 cm from the contact.

STOP 2c. Lower Jumbo lithium pegmatite. The Lower Jumbo (figs. 10 and 11) consists of two large pegmatite bulges; the large bulge exposed in Mitchell Wash contains a core zone of giant spodumene crystals up to about 2 m in

Figure 10. The Lower Jumbo pegmatite viewed from above.

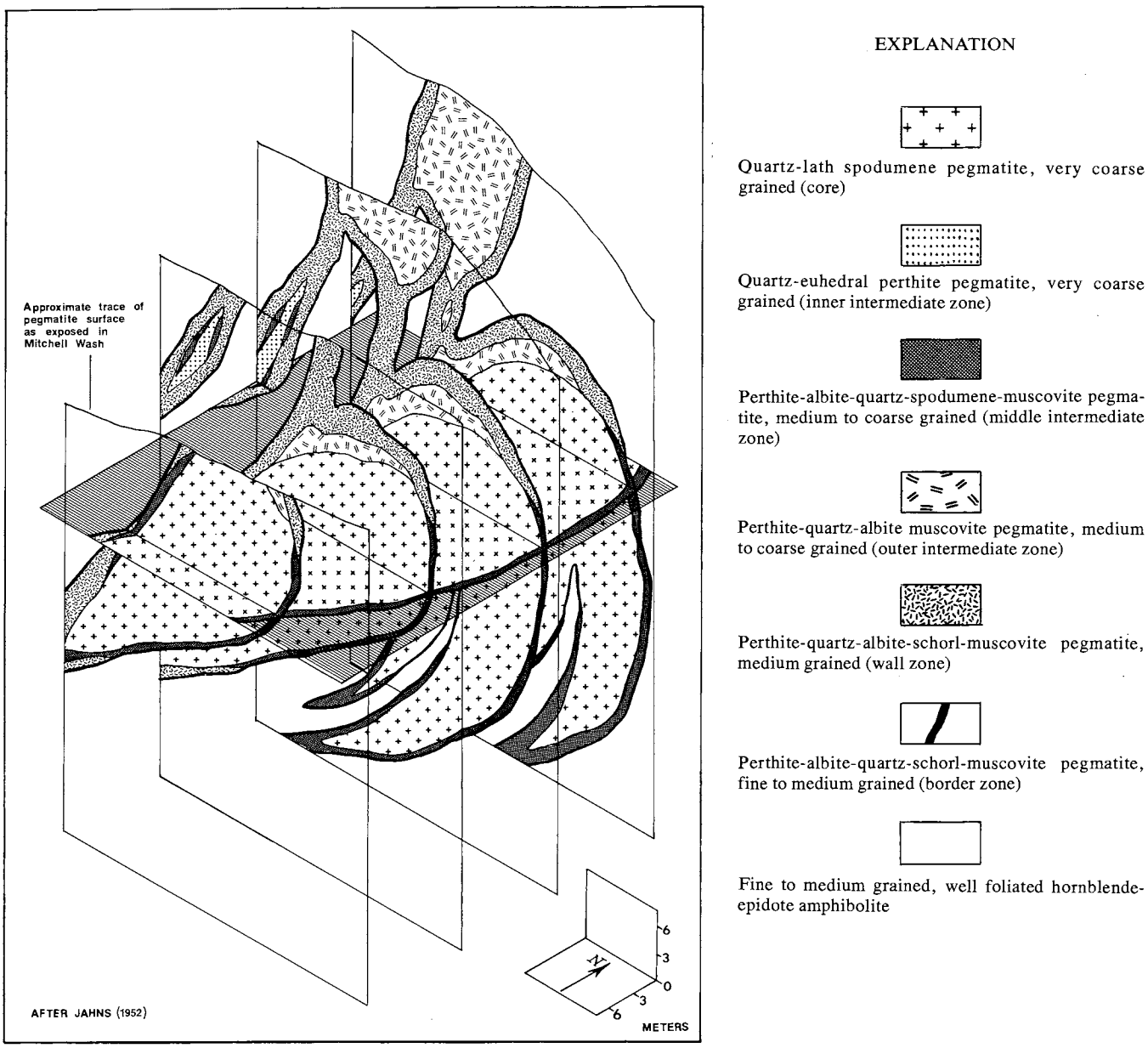

Figure 11. Isometric plate diagram of the Lower Jumbo pegmatite.

length enclosed in anhedral quartz. Note the diverse "jackstraw" orientation of the spodumene lathes.

Continue down the wash to **STOP 2d.**

STOP 2d. A portion of the wash in which tourmaline metasomatism of the host rocks is particularly well-developed. Even thin pegmatites have relatively thick border zones of almost pure schorl (fig. 12); tourmalinization of host rocks can also be observed in many outcrops. Pegmatite stringers anastomose through the host rocks and appear as stockworks following pre-existing joint patterns in the metamorphic rocks (Jahns, 1952).

Retrace the path to the north end of Mitchell Wash Canyon.

OPTIONAL STOPS

OPTION 1. Hike up Mitchell Wash and up a trail to the left to the Sunrise pegmatite (a zoned lithium pegmatite similiar to the North Morning Star, and mislabelled "Picacho View" on the Red Picacho 7.5′ topographic map). The Picacho View pegmatite (a large zoned non-lithium pegmatite) is not shown on the topographic map, but is visible from the Sunrise about 1 km to the northeast, across Mitchell Wash. It can also be visited.

Figure 12. Tourmalinization of host rocks along pegmatite contact, Mitchell Wash Canyon.

OPTION 2. Return to Phoenix via State Highway 74 to see the Pike's Peak Precambrian iron formations (Field Trip 4, this guidebook).

In either case, return to the Castle Hot Springs Road by retracing the trip route. Turn around in San Domingo Wash and proceed down the wash for 4.8 miles; take the improved dirt road to the left (the Old Stage Road).

ACKNOWLEDGEMENTS

We are grateful to R. H. Jahns for much useful information, to M. R. Smith for laboratory and field assistance, and especially to E. F. and S. B. Anderson for permission to visit and study their pegmatites.

PRECAMBRIAN PIKE'S PEAK IRON-FORMATION, CENTRAL ARIZONA

by
Roger M. Slatt, Greta M. Heintz,
Patrick H. Lowry, and Patrick F. O'Hara

Department of Geology
Arizona State University
Tempe, Arizona

INTRODUCTION

The Pike's Peak iron-formation is the largest of a discontinuous series of iron deposits, about 120 km long by 60 km wide, within the Precambrian Yavapai Series of central Arizona (fig. 1). The Pike's Peak deposit consists of a series of lenticular bodies of interlaminated chert and iron oxide which form an outcrop belt about 6 km long by 700 m wide within more areally extensive phyllites and associated meta-volcanic rocks.

Precambrian iron-formations occur worldwide (James and Sims, 1973). Although it is generally agreed that they are the products of chemical sedimentation, the many published accounts have emphasized their regional extent, economic potential, and petrology rather than their sedimentology and stratigraphy. The Pike's Peak iron-formation is no exception. Farnham and Havens (1957) and Harrer (1964) provided generalized information on the economic potential and geology of the deposit. Sharp (1963) investigated its magnetic properties.

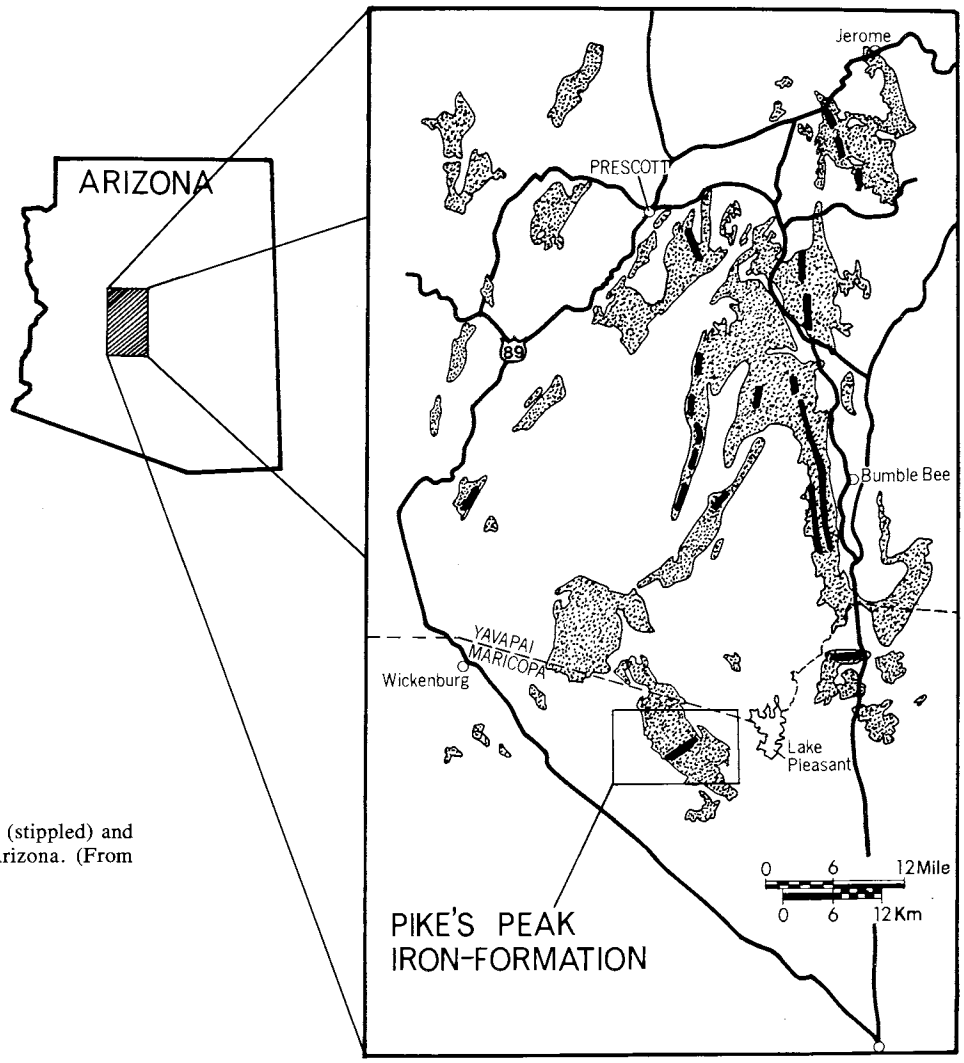

Figure 1. Distribution of Yavapai Series (stippled) and iron-formation (solid lines) in central Arizona. (From Harrer, 1964.)

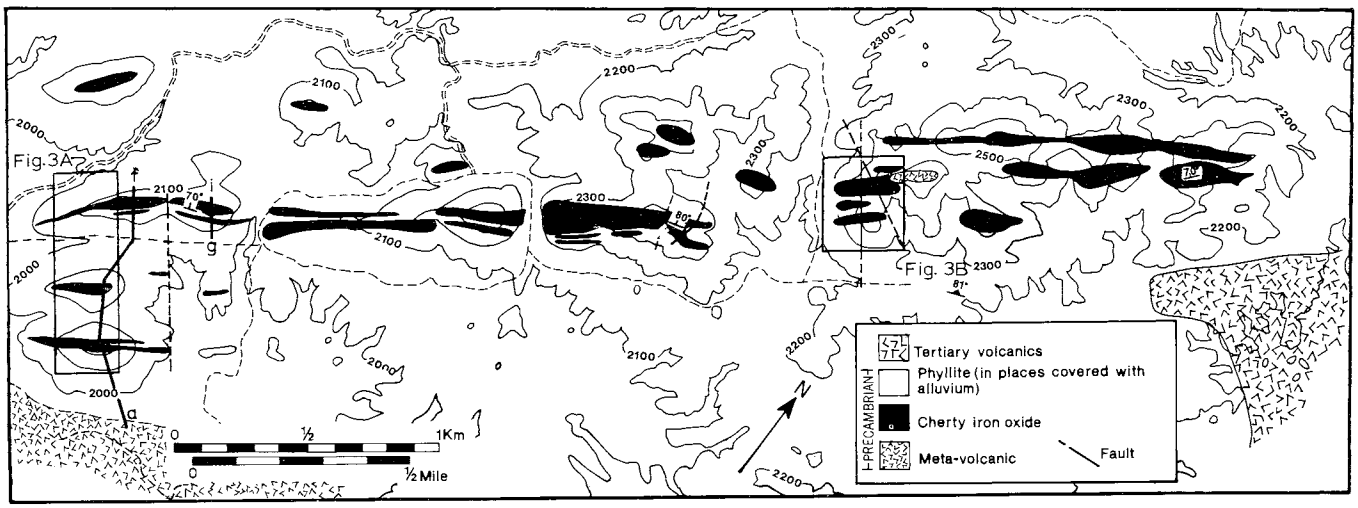

Figure 2. Geologic map of the Pike's Peak iron-formation and associated lithologies. Contour intervals are in feet.

Bayley and James (1973) included a brief description in their review of iron-formations of the United States.

The intent of this field guide and the field trip is to summarize current knowledge of the Pike's Peak iron-formation, especially its sedimentology and stratigraphy. The field trip will leave Tempe and proceed north on highway I-17, then west on the Carefree Highway (74), to about 7 miles west of the Lake Pleasant turnoff. Here, an unmarked dirt road leads to the iron-formation.

The field trip will consist of examining outcrops of the iron-formation and associated lithologies in the two areas shown in figures 3A and 3B (see fig. 2 for locations). These areas are reached by dirt roads (fig. 2). The features to be examined are described below. This information is preliminary in nature and is the result of mapping, measuring stratigraphic sections, and cursorily examining about 35 thin sections, supplemented by X-ray diffraction analysis. A general summary of the iron-formation is also presented along with a hypothesis of the depositional environment. Detailed interpretation of the origin and geologic history of the deposit awaits further work.

GENERAL GEOLOGY

The Pike's Peak iron-formation comprises part of the Yavapai Series, a complex of metamorphosed volcanic and associated rocks more than 6 km thick, which include rhyolite, diorite, greenstone, phyllite, schist, amphibolite, quartzite, argillite, and graywacke (Harrer, 1964). Based upon radiometric age determinations, the Yavapai Series has been formally defined as a time-stratigraphic unit encompassing the period 1770 ± 10 m.y. to 1820 ± 1 m.y. (Anderson and others, 1971).

The areal distribution of the Pike's Peak iron-formation is shown in figure 2. It occurs as lenticular bodies of laminated chert and iron oxide beds, hereafter called cherty iron oxide, which range in width from 15 to 100 m, which are rarely continuous for more than 350 m along strike, and which form resistant ridges more than 200 m higher than adjacent valleys (figs. 3A and B). Beds strike approximately N.60°E. and dip steeply toward the northwest.

Phyllite underlies valleys between cherty iron oxide ridges, and occupies lower ridge slopes (figs. 3A and B); occasionally phyllite forms a small hill. The phyllite generally is silver-gray in color with a prominent, steeply-dipping, axial plane cleavage (fig. 3F). A whitish-gray phyllite containing coarser clasts, hereafter called sandy phyllite, occurs locally. Phyllites weather to a variety of colors.

Along mid- and upper-slopes of ridges, the cherty iron oxide and phyllite are interbedded (figs. 3D and E). Here, the cherty iron-oxide occurs as small lenses, giving rise to a pinch-and-swell character (fig. 3E). Some lenses are folded (fig. 4F).

Other lithologies are not common in the area. Thin beds of gray calcite, interlaminated with chert and iron oxide (fig. 4C), occur locally. Meta-volcanic rocks are found south of the iron-formation and are interbedded with cherty iron oxide along one ridge-top (fig. 2). Gray bedded chert occurs near the meta-volcanics in one area. Dikes of Tertiary andesite porphyry (?) and coarse quartz veins cross-cut the iron-formation at several locales.

The iron-formation is dissected by many small faults which trend obliquely to the regional strike and which often form small saddles or terraces within resistant ridges. The faults are recognizable by small breccia zones (fig. 4E), occasional slickensides, and displacement of individual beds. Offset appears to be minor. Owing to the difficulty in recognizing small fault breccias and minor offsets, more faults probably occur than are shown in figure 2.

No evidence was found to suggest the cherty iron

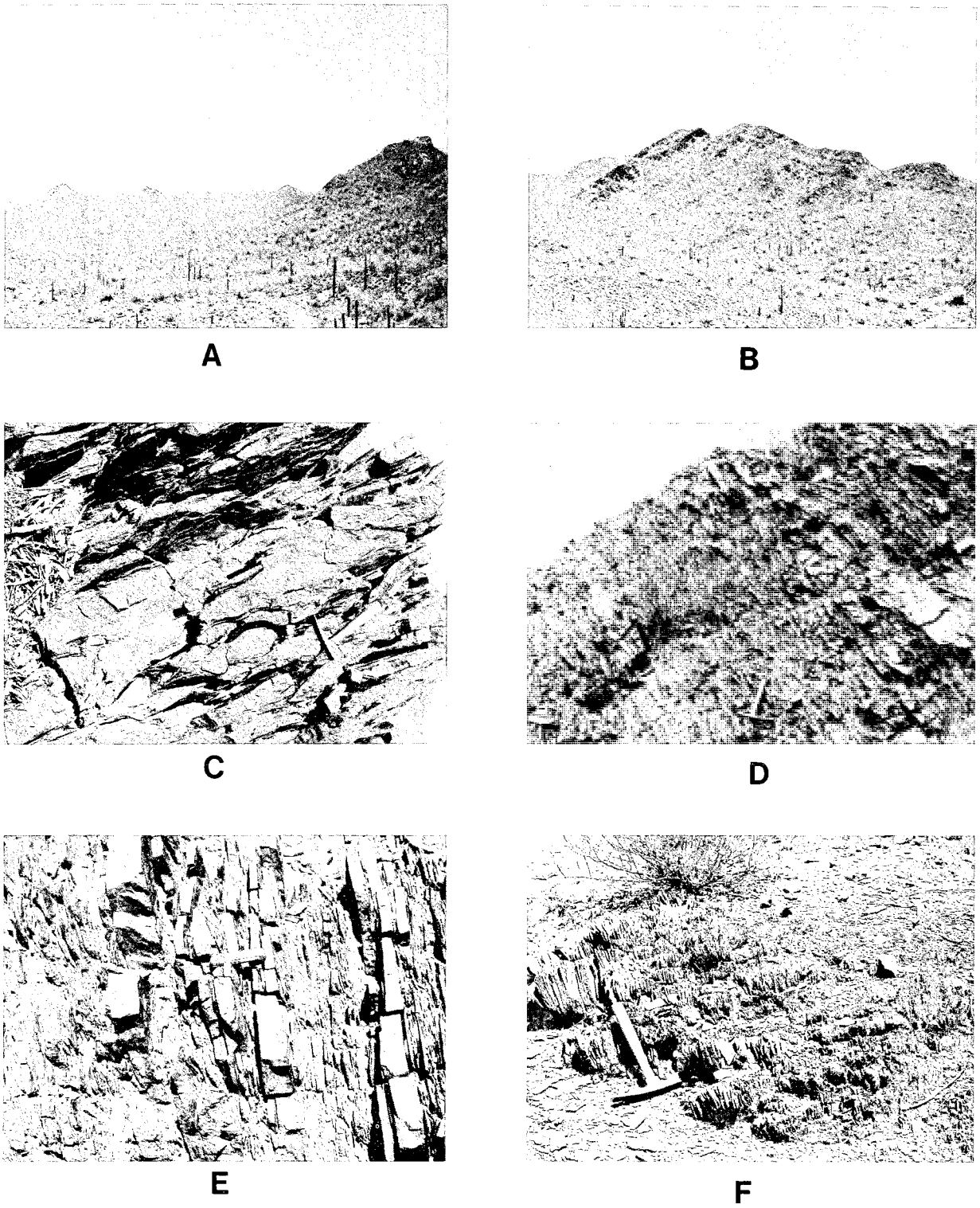

Figure 3. (A) View looking southwest at ridges of iron-formation. See fig. 2 for location. (B) View looking northeast at ridges of iron-formation. See fig. 2 for location. (C) Side, or internal view of bed of massive cherty iron oxide. Note pod structure below hammer. Top of the ridge is toward the upper right. (E) Close-up view of interbedded cherty iron oxide (resistant lenticular beds) and phyllite. Knife is about 8 cm in length. Top of the photo is toward the right. (F) View of phyllite outcrop showing axial plane cleavage.

A

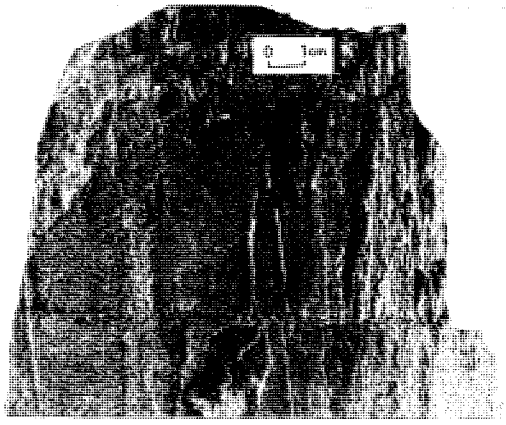

B

C

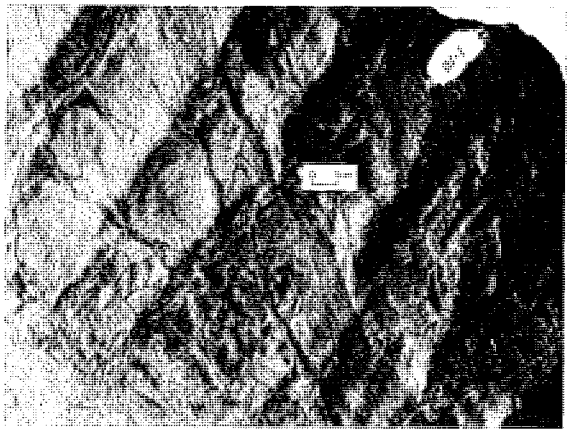

D

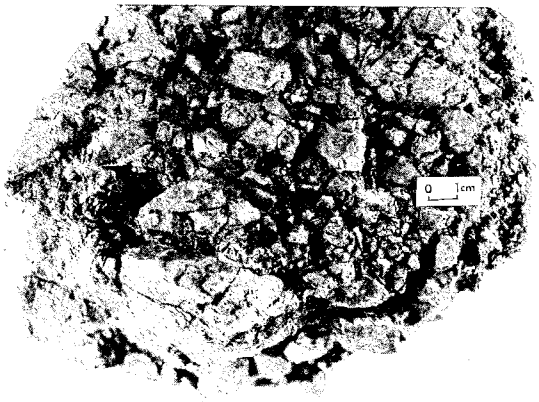

E

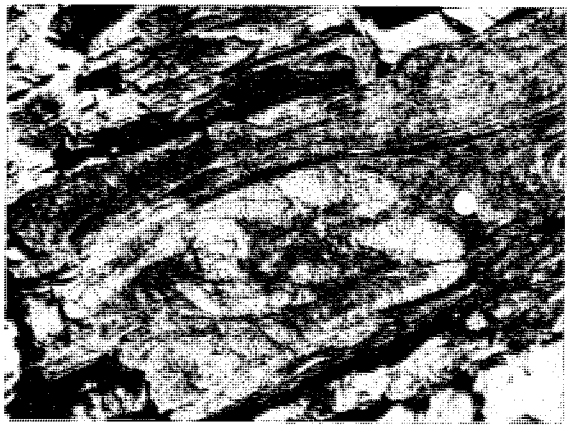

F

Figure 4. (A) Polished slab showing two thin hematite laminae between chert laminae. (B) Slaty cherty iron oxide with two linear grooves oriented about 350°. (C) Laminated carbonate lithology containing a small lense of hematite. (D) Ripple-like features on a bedding plane. (E) Fault breccia. (F) Side, or internal view of folded cherty iron oxide.

oxide ridges are repeated by folding within the outcrop area of the iron-formation, even though beds of cherty iron oxide are sometimes folded (fig. 4F).

STRATIGRAPHY

Because of a lack of evidence for repetition of beds by folding or faulting, the ridges of cherty iron oxide and intervening valleys underlain by phyllite are assumed to form a continuous stratigraphic sequence. Two stratigraphic sections were measured. (See fig. 2 for locations.) Section a-f (fig. 5) extends from the meta-volcanics northwestward across three cherty iron oxide ridges (fig. 3A). The measured thickness of 930 m represents a maximum thickness due to some folding of beds (figs. 3C and 4F). Section g-i (fig. 6) crosses one major cherty iron oxide ridge. The measured thickness of 270 m also represents a maximum possible value. The total thickness of the iron-formation and associated lithologies was not measured, so it presently is unknown.

At Section a-f, cherty iron oxide occurs in three separate horizons within thicker sections of phyllite (fig. 5). The highest horizon at Section a-f is correlative with the one cherty iron oxide horizon measured at Section g-i (fig. 6). Silver-gray phyllite is most common throughout the sections; sandy phyllite is restricted to the lower third of Section a-f.

Zones of interbedded cherty iron oxide and phyllite are most frequent near beds of massive cherty iron oxide (without interbedded phyllite). Visual estimates of the proportions of the two lithologies, taken at intervals ranging from 3 to 10 m along Section g-i (fig. 6), indicate there is a systematic increase in the proportion of cherty iron oxide interbeds, at the expense of phyllite, as beds of massive cherty iron oxide are approached. Although similar measurements were not made at Section a-f, the same systematic variation was noted.

The three horizons of iron-formation (fig. 5) appear to record three major cycles of sedimentation.

PETROLOGY

CHERTY IRON OXIDE

In outcrop, most of the cherty iron oxide has a blocky or massive appearance. It consists of planar to lenticular laminae of alternating quartz (occasionally jasper) and hematite which range from less than 1 to greater than 35 mm in thickness (fig. 4A); quartz laminae normally are thickest.

In thin section, the cherty laminae comprise a mosaic of polygonal, equidimensional to elongate, interlocking quartz crystals which range in size from about 0.03 to 0.20 mm (fig. 7A). Thin bands of differing crystal size often are adjacent to one another. Fine hematite crystals

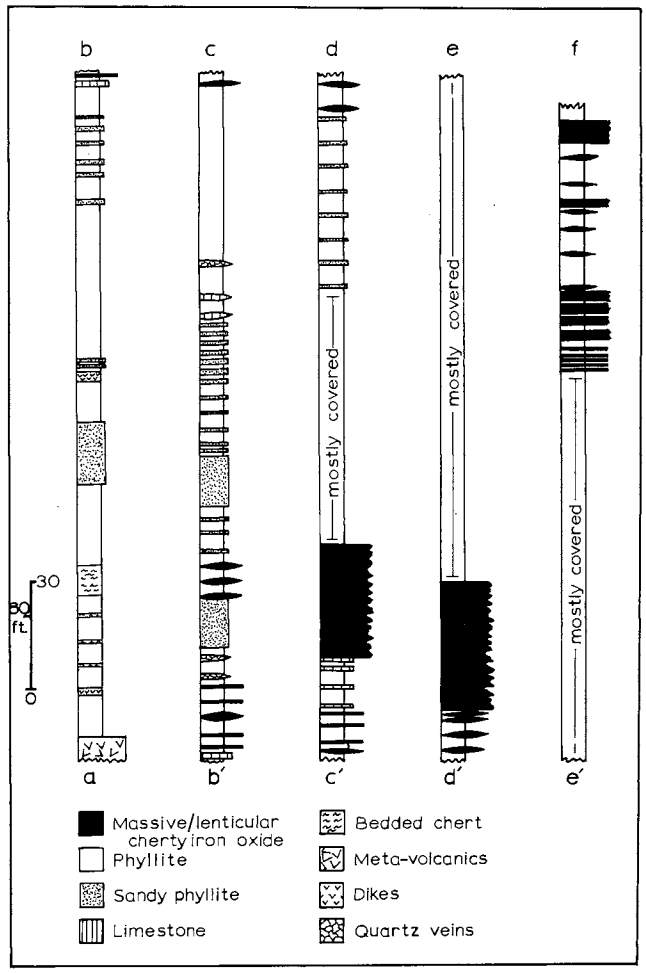

Figure 5. Measured stratigraphic section a–f. See fig. 2 for location.

are aligned within chert laminae; red jasper laminae contain the greatest proportion of hematite. Feldspar, calcite, muscovite, and biotite are also minor constituents; the latter two normally are oriented parallel to laminae.

Boundaries between chert and hematite laminae are sharp (fig. 7B). The hematite laminae are composed principally of fine granular hematite, in places weathering to limonite and goethite, with minor dispersed quartz, muscovite, and biotite. Magnetite, reported by Harrer (1964), generally is not present in sufficient quantities to be detected by X-ray diffraction analysis.

Some of the cherty iron oxide has a slaty (rather than blocky or massive) appearance (fig. 4B). In thin section, the slaty-oxide lithology tends to be more micaceous, to exhibit good schistosity, and to contain larger quartz crystals (> 0.30 mm); small quantities of magnetite are detectable by X-ray diffraction.

PHYLLITE

The phyllite is composed of chlorite, calcite, muscovite, albite, quartz, opaques, and stilpnomelane (?) (fig. 7D).

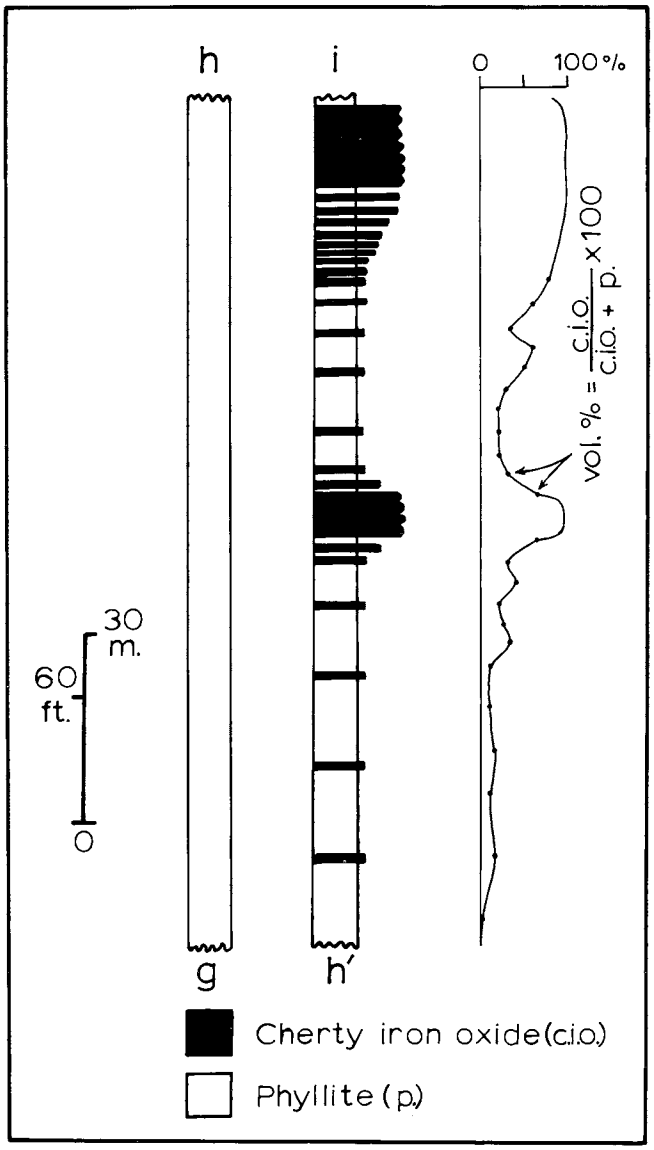

Figure 6. Measured stratigraphic section g–i. See fig. 2 for location. Volume % = proportion of cherty iron oxide in cherty iron oxide/phyllite interbeds. Data points mark intervals and stratigraphic locations of visual estimates.

The micaceous minerals define a schistose foliation. The sandy phyllite is similar, but it also contains scattered, larger grains of quartz (fig. 7E) which are clearly visible in hand specimen.

CARBONATE

The carbonate rock is composed of thin laminae of gray calcite, rust-gray chert, and steel gray-black, lenticular hematite (fig. 4C). In thin section, the calcite is finely-crystalline (fig. 7C) and contains elongate aggregates of hematite which either are oriented parallel to laminations or define micro-folds. Quartz grains and muscovite needles are minor constituents. Both chert and hematite laminae are similar to those of cherty iron oxide.

META-VOLCANICS

The meta-volcanic rocks are dark green with flattened, white streaks parallel to foliation. They are of intermediate (?) composition, having been altered to an assemblage of chlorite, muscovite, calcite, quartz, and opaques (fig. 7F). Some relict clinopyroxene (?), hornblende (?), and plagioclase can be seen in thin section.

CHEMISTRY

Partial chemical analyses of cherty iron oxide samples (Farnham and Havens, 1957) are compared in table 1 with average chemical compositions of other iron-formations (James, 1966). The Pike's Peak deposit is relatively enriched in Mn and Al_2O_3, particularly when compared with other hematite-rich iron-formations. The high Mn content is present in pyrolusite, which occurs in sufficient quantities to be detected by X-ray diffraction analysis. The Al_2O_3 content probably reflects the occurrence of micas.

Harrer (1964) reports the presence of 0.01–0.1 percent Co, Ni, Ti, and Cu and 0.001–0.01 percent V in a cherty iron oxide sample.

TABLE 1. COMPARATIVE CHEMISTRY OF PIKE'S PEAK AND OTHER IRON-FORMATIONS.

	A	B	C	D	E	F	G	H
SiO_4	43.9	33.1	44.8	34.0	36.7	37.6	34.1	31.2
Al_2O_3	0.75	2.77	2.73	1.42	6.90	4.7	3.9	4.1
CaO	0.32	1.48	1.70	1.97	0.13	1.0	1.2	1.1
Fe	38.0	36.7	27.3	25.6	20.0	30.6	32.5	31.2
Mn	0.03	0.59	2.1	1.2	Tr	2.7	3.9	2.8
P	0.04	0.11	0.10	0.14	0.09	0.14	0.12	0.13
S	0.01	0.09	0.22	0.06	21.6	0.04	0.06	0.05

A. Hematite-rich iron formation (moderately metamorphosed). James (1966), Table 10, analyses A-K.
B. Magnetite-rich iron formation. James (1966), Table 12, analyses A-L.
C. Silicate-rich iron formation. James (1966), Table 14, analyses A-K.
D. Siderite-rich iron formation. James (1966), Table 17, analyses A-P.
E. Sulfide-rich iron formation, James (1966), Table 18, analysis A.
F. Surface trench samples, Pike's Peak iron formation. Farnham and Havens (1957), Table 2; several analyses.
G. Underground samples, Pike's Peak iron formation. Farnham and Havens (1957), Table 2; several analyses.
H. Overall composite of surface trench and underground samples, Pike's Peak iron formation. Farnham and Havens (1957), Table 2.

DEFORMATION AND METAMORPHISM

The Pike's Peak iron-formation has undergone at least one episode of deformation. The cherty iron oxide shows evidence of isoclinal folding (fig. 4F) while phyllites exhibit an axial plane cleavage (fig. 3F). Details of the deformation history await further investigation.

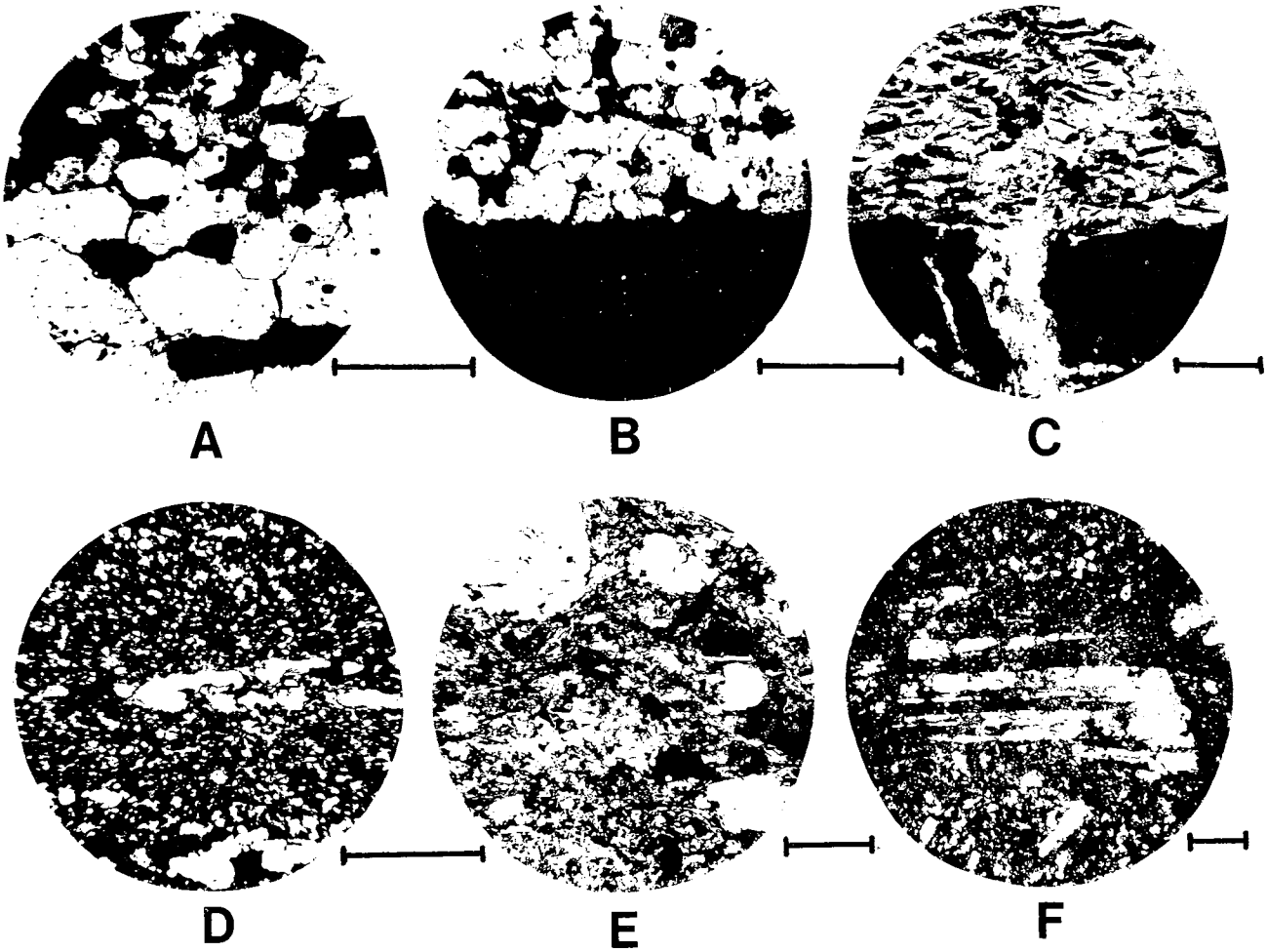

Figure 7. (A) Thin section of chert laminae showing variations in size of mosaic quartz crystals. Black mineral is hematite. Plane polarized and reflected light. (B) Thin section showing sharp contact between upper chert lamination and lower hematite lamination. Plane polarized and reflected light. (C) Thin section of upper calcite lamination and lower hematite lamination. Black elongate mineral in calcite is hematite. The vertical fracture in the hematite lamination is filled with calcite. Plane polarized and reflected light. (D) Thin section of phyllite. Note the band of quartz which appears to be folded. Plane polarized light. (E) Thin section of sandy phyllite. Plane polarized light. (F) Thin section of meta-volcanic. Note the altered plagioclase. Plane polarized light. Bar scale is 250 μm for A–F.

The mineral assemblage of the phyllite indicates the rocks have undergone regional prograde metamorphism to chlorite grade. The foliation defined by micaceous minerals (fig. 7D) is due to pre- or syn-tectonic recrystallization in the quartz-albite-muscovite-chlorite subfacies of the greenschist facies. The phyllites were probably shales, mudstones, and sandy mudstones prior to metamorphism.

The mosaic of polygonal quartz crystals which comprise chert laminae (fig. 7A) is typical of recrystallized quartz in cherty iron-formations (Mukhopadhyay and Chanda, 1972). Sizes of recrystallized quartz have been used by James (1955), Klein (1973), and others as an indicator of metamorphic grade in iron-formations. This was not possible for the Pike's Peak iron-formation because of the wide variety of crystal sizes present within single chert laminae (figs. 7A and B). Recrystallization of cherty iron oxide has obliterated any primary sedimentary textures that may have been present.

DEFORMATION AND SEDIMENTARY STRUCTURES

Gross (1972) described and illustrated a variety of primary sedimentary textures and structures common to iron-formations. These include granules and oolites, nodules, microbreccias, scour-and-fill structures, ripple marks, shrinkage cracks, and penecontemporaneous convolute folds. Listed below are similar structures found in the Pike's Peak deposit, but which we ascribe mainly to deformation.

(1) Sets of symmetrical ripples on bedding planes (fig. 4D); when viewed in cross-section, their internal structure is seen to be the result of compressional pinching of cherty iron oxide laminae.

(2) Folds which appear to be convoluted (fig. 4F); fold limbs usually are parallel, suggesting a deformation origin.

(3) What appear to be desiccation cracks in hematite laminae (fig. 7C) possibly are micro-fractures.

(4) Sets of linear grooves, similar to tool marks, on the undersides of slaty cherty iron oxide beds (fig. 4B); the sets are always parallel and perfectly straight, indicating they formed after lithification.

(5) Breccias (fig. 4E) which cut across cherty iron oxide beds, indicating they are fault breccias.

(6) Pinch-and-swell features of cherty iron oxide beds (figs. 3D and E), which resemble rippled beds; Beukes (1973) attributes similar features to diagenetic shrinkage of an original gel. More likely these are the product of deformation.

Interbedding of phyllite and cherty iron oxide (figs. 3D and E) appears to be a primary sedimentary feature. The origin of these interbeds is discussed below.

DEPOSITIONAL ENVIRONMENT

Gross (1965) classified iron-formations into the *Algoma*-type associated with volcanic and volcaniclastic rocks in eugeosynclinal belts, and the *Superior*-type associated with continental shelf sediments. Other proposed origins for iron-formation include deposition in lacustrine environments (Govett, 1966; Eugster and Chou, 1973) and penecontemporaneous replacement of shallow marine calcareous sediment (Kimberley, 1974; Dimroth, 1977b).

Based upon the stratigraphic association of iron-formation with meta-volcanics and meta-sediments, Bayley and James (1973) suggested the Pike's Peak iron-formation is of the *Algoma*-type. Dimroth (1977a) claims that *Algoma*-type iron-formations are characteristically lenticular bodies of parallel laminated beds that are associated with volcanic, turbidite and pelagic sediments. He suggests iron-formations are intercalated between turbidites, thus they were chemically precipitated on turbidite fans during periods of cessation of clastic sedimentation.

The Pike's Peak iron-formation exhibits these features, so a similar origin could be proposed. Phyllites and sandy phyllites may be metamorphosed distal and proximal turbidites. If so, then at least three major cycles of turbidite sedimentation are recorded in the measured stratigraphic Section a-f (fig. 6). Each cycle would terminate by the gradual transition from clastic to chemical sedimentation, as evidenced by the progressive development of cherty iron oxide beds at the expense of phyllite within cherty iron oxide horizons (fig. 7). The source of iron and silica could have been submarine volcanism (Goodwin, 1956 and 1973; Trendall and Blockley, 1970) or upwelling deep ocean water (Holland, 1973; Drever, 1974).

There are two obstacles to this origin. First, the typical radial growth pattern of submarine fans usually prevents superimposition of successively younger fans (Nelson and Nilson, 1974), thus contradicting the apparent cyclicity of the Pike's Peak deposit. However, not all turbidites are deposited on fans. For example, trench turbidites are transported axially, thus hindering development of prominent fans (Piper, et al., 1973). In addition, apparent sedimentary cycles could be preserved by a series of coalescing turbidite fans. Secondly, of the four sedimentary facies of iron-formation defined by James (1954)—oxide, carbonate, silicate, and sulfide—the oxide facies, which comprises the Pike's Peak deposit, is thought to precipitate in shallow water (James, 1954; Goodwin, 1973).

We propose, as an alternate hypothesis, that the Pike's Peak iron-formation is part of a tidal flat/deltaic complex. The model is illustrated in figure 8. Three features of the iron-formation are critical to this interpretation: (1) the common occurrence of interbeds of cherty iron oxide and phyllite (figs. 3D and E) and their association with beds of massive cherty iron oxide (figs. 5 and 6), (2) the systematic increase in proportion of cherty iron oxide to phyllite interbeds toward the more massive cherty iron oxide beds (fig. 6), and (3) the large-scale cyclicity of cherty iron oxide horizons between phyllite (fig. 6).

The interbeds of cherty iron oxide and phyllite bear a striking physical resemblance to tidal flat deposits (see Ginsburg, 1975 for several examples). A typical tidal flat sequence grades vertically from a shallow sub-tidal sand, into low-tide/inter-tidal sand and mud interbeds, then into high-tidal flat muds (Klein, 1975). Iron oxide oolites of shallow water origin are common in unmetamorphosed and low-grade iron-formations (Gross, 1972; Dimroth, 1977a), so it is conceivable that hematite laminae of the Pike's Peak deposit were oolitic prior to recrystallization. If so, the beds of massive cherty iron oxide may be analogous to sub-tidal oolite sand, while the cherty iron oxide/phyllite interbeds are analogous to inter-tidal deposits. Systematic variations in lithologies, as observed between cherty iron oxide and phyllite (fig. 6), also are characteristic of tidal flat sequences.

A tidal origin for the deposit requires both clastic and chemical sedimentation to occur in close proximity. Although the Precambrian depositional setting probably was not equivalent, bog iron deposits (James, 1966) may provide a partial modern analog. Slatt (1970) and Hoskin and Slatt (1972) describe an example of bog iron being precipitated on a clastic tidal flat. Also, it has been suggested that bacteria aided in the precipitation of iron-formation (Cloud, 1973), as is known to be the case in the production of bog iron (Harder, 1919; Pringsheim, 1949). Other examples of mixed clastic/chemical tidal flat deposits include limestone/sandstone (Shinn, 1973), dolomite/shale (Hoffman, 1975) and evaporite/mud (Thompson, 1975).

Our model accounts for the cyclicity of the Pike's Peak iron-formation by assuming tidal flat sedimentation occurred upon a delta surface. Deltaic sedimentation is often cyclic (Maill, 1976). One cycle consists of seaward progradation of a delta lobe followed by channel abandonment, subsidence, and marine transgression. Subsequently, a new delta lobe is deposited upon that of the earlier cycle. Each

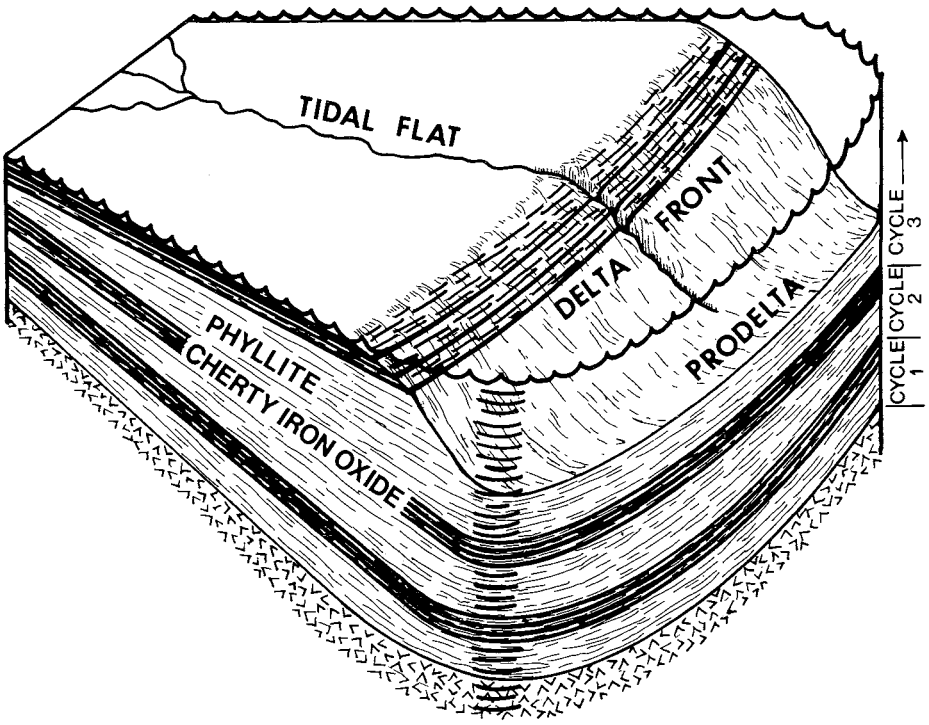

Figure 8. Model for the origin of the Pike's Peak iron-formation.

cycle may generate a stratigraphic sequence between 50 and 150 m or more in thickness, which is similar to the thickness between cherty iron oxide horizons of the Pike's Peak deposit (fig. 5).

In summary, we suggest that at least three cycles of deltaic sedimentation led to the development of the Pike's Peak deposit. Each cycle of sedimentation is represented by prodelta and delta front phyllites overlain by tidal flat cherty iron oxide. Chemical sedimentation in very shallow water might indicate the iron was derived from terrestrial chemical weathering (James, 1954; Lepp and Goldich, 1964).

ECONOMIC GEOLOGY

The Pike's Peak iron-formation is covered by 72 mining claims (Harrer, 1964). Preliminary assessment by Kaiser, Co., Inc. indicates iron resources of 100 million tons to an inferred depth of 130 m. If other occurrences of iron-formation are included (fig. 1), the low-grade iron resources within the mineralized belt of the Yavapai Series exceed this value (Harrer, 1964).

Average grade of ore is about 31 percent Fe (table 1). Because of low iron and high silica content, ore would have to be concentrated for commercial exploitation. Farnham and Havens (1957) describe several possible methods of increasing recovery and grade of the ore. The deposit could be mined by open pit methods.

ACKNOWLEDGMENTS

We express our appreciation to Kaiser Steel Corporation (Oakland, California office) for allowing us access to their property, to Michael Ward (Arizona State University) for first showing the Pike's Peak iron-formation to Slatt, and to Edmund Stump (Arizona State University) and William Jones (Kaiser Steel Corp.) for helpful suggestions and advice. Heintz and O'Hara were financially supported by Research Assistantships from Arizona State University's College of Liberal Arts.

REFERENCES CITED

Anderson, C. A., Blacet, P. M., Silver, L. T., and Stern, T. W., 1971, Revision of Precambrian stratigraphy in the Prescott-Jerome area, Yavapai County, Arizona, U.S. Geol. Surv. Bull. 1324-C, p. C1-C16.

Bayley, R. W. and James, H. L., 1973, Precambrian iron-formations of the United States, Econ. Geol. v. 68, p. 934–959.

Beukes, N. J., 1973, Precambrian iron-formations of southern Africa, Econ. Geol., v. 68, p. 960–1004.

Cloud, P., 1973, Paleoecological significances of the banded iron-formation, Econ. Geol., v. 68, p. 1135–1143.

Dimroth, E., 1977a, Facies models 5. Models of physical sedimentation of iron formations, Geosci. Canada, v. 4, p. 23–30.

——, 1977b, Facies models 6. Diagenetic facies of iron formation, Geosci. Canada, v. 4, p. 83–88.

Drever, J. I., 1974, Geochemical model for the origin of Precambrian banded iron formations, Bull. Geol. Soc. Amer., v. 85, p. 1099–1106.

Eugster, H. P., and Chou, I., 1973, The depositional environments of Precambrian banded iron-formations, Econ. Geol. v. 68, p. 1144–1168.

Farnham, L. L., and Havens, R., 1957, Pike's Peak iron deposits, Maricopa County, Arizona, U.S. Bur. Mines Rept. Inv. 5319, 31 p.

Ginsburg, R.N. (ed.), 1975, Tidal deposits, Springer-Verlag, N.Y., 428 p.

Goodwin, A.M., 1956, Facies relations in the Gunflint Iron Formation, Econ. Geol., v. 51, p. 565–595.

——, 1973, Archean iron-formations and tectonic basins of the Canadian Shield, Econ. Geol., v. 68, p. 915–933.

Govett, G. J. S., 1966, Origin of banded iron formations, Bull. Geol. Soc. Amer. v. 77, p. 1191–1212.

Gross, G. A., 1965, Geology of iron deposits in Canada, Vol. 1, General geology and evaluation of iron deposits, Canada Geol. Survey Econ. Geol. Rept. 22, 181 p.

——, 1972, Primary features in cherty iron-formations, Sediment. Geol., v. 7, p. 241–261.

Harder, E. C., 1919, Iron-depositing bacteria and their geological relations, U.S. Geol. Survey Prof. Paper 113, 89 p.

Harrer, C. M., 1964, Reconnaissance of iron resources in Arizona, U. S. Bur. Mines Inf. Circ. 8236, 204 p.

Hoffman, P., 1975, Shoaling-upward shale-to-dolomite cycles in the Rocknest Formation (Lower Proterozoic), Northwest Territories, Canada, *in* Ginsburg, R. N. (ed), Tidal Deposits, Springer-Verlag, N.Y., p. 257–265.

Holland, H. D., 1973, The oceans: a possible source of iron in iron-formations, Econ. Geol., v. 68, p. 1169–1172.

Hoskin, C. M. and Slatt, R. M., 1972, Iron in surface and subsurface waters, Grizzly Bar, southeastern Alaska, Univ. Alaska Inst. Water Resources Publ. No. IWR-29, 15 p.

James, H. L., 1954, Sedimentary facies of iron-formation, Econ. Geol., v. 49, p. 235–293.

——, 1955, Zones of regional metamorphism in the Precambrian of northern Michigan, Bull. Geol. Soc. Amer., v. 66, p. 1455–1488.

——, 1966, Chemistry of the iron-rich sedimentary rocks, U.S. Geol. Survey Prof. Paper 440-W, p. W1-W61.

James, H. L. and Sims, P. K., 1973, Precambrian iron-formations of the world, Econ. Geol., v. 68, p. 913–914.

Kimberley, M. M., 1974, Origin of iron ore by diagenetic replacement of calcareous oolite, Nature, v. 250, p. 319–320.

Klein, C., 1973, Changes in mineral assemblages with metamorphism of some banded Precambrian iron-formations, Econ. Geol., v. 68, p. 1075–1088.

Klein, G. de V., 1975, Sandstone depositional models for exploration for fossil fuels, Continuing Educ. Publ. Co., Champaign, Ill., 109 p.

Lepp, H., and Goldich, S. S., 1964, Origin of Precambrian iron formations, Econ. Geol., v. 58, p. 1025–1061.

Maill, A. D., 1976, Facies Models 4. Deltas, Geosci. Canada, v. 3, p. 215–227.

Mukhopadhyay, A. and Chanda, S. K., 1972, Silica diagenesis in the banded hematite jasper and bedded chert associated with the iron ore group of Jamda-Koira Valley, Orissa, India, Sediment. Geol., v. 8, p. 113–135.

Nelson, C. H. and Nilsen, T. H., 1974, Depositional trends of modern and ancient deep sea fans, *in* Dott, R. H. and Shaver, R. H. (eds.), Modern and ancient geosynclinal sedimentation, Soc. Econ. Paleon. Mineral. Spec. Publ. 19, p. 56–68.

Piper, D. J. W., von Huene, R., and Duncan, J. R., 1973, Late-Quaternary sedimentation in the active eastern Aleutian Trench, Geology, v. 1, p. 19–22.

Pringsheim, E. G., 1949, Iron bacteria, Biol. Rev., v. 24, p. 200–245.

Sharp, R. R., 1963, Some magnetic properties of a part of Pike's Peak iron deposit, Maricopa County, Arizona, unpubl. M.S. thesis, Univ. of Arizona, 115 p.

Shinn, E. A., 1973, Sedimentary accretion along the leeward, SE coast of Qatar Peninsula, Persian Gulf, *in* Purser, N.H. (ed), The Persian Gulf, Springer-Verlag, N.Y., 471 p.

Slatt, R. M., 1970, Sedimentological and geochemical aspects of sediment and water from ten Alaskan valley glaciers, unpubl. Ph.D. thesis, Univ. Alaska, 125 p.

Thompson, R. W., 1975, Tidal-flat sediments of the Colorado River Delta, northwestern Gulf of California, *in* Ginsburg, R. N., (ed) Tidal Deposits, Springer-Verlag, N.Y., p. 57–66.

Trendall, A. F. and Blockley, J. G., 1970, The iron formation of the Precambrian Hamersley Group, Western Australia, West. Australia Geol. Survey Bull. 119, 353 p.

THE SACATON PORPHYRY COPPER DEPOSIT

by
Robert B. Cummings
ASARCO, Incorporated
Casa Grande, Arizona

This one-day field trip visits an active open pit copper mine about 35 miles south of Tempe. Boots are recommended; hard hats and safety glasses will be supplied at the mine. Figure 1 is included in place of a road log. The geology of the deposit will be described more completely in an article being prepared for the second porphyry copper volume under the editorship of S. R. Titley (University of Arizona).

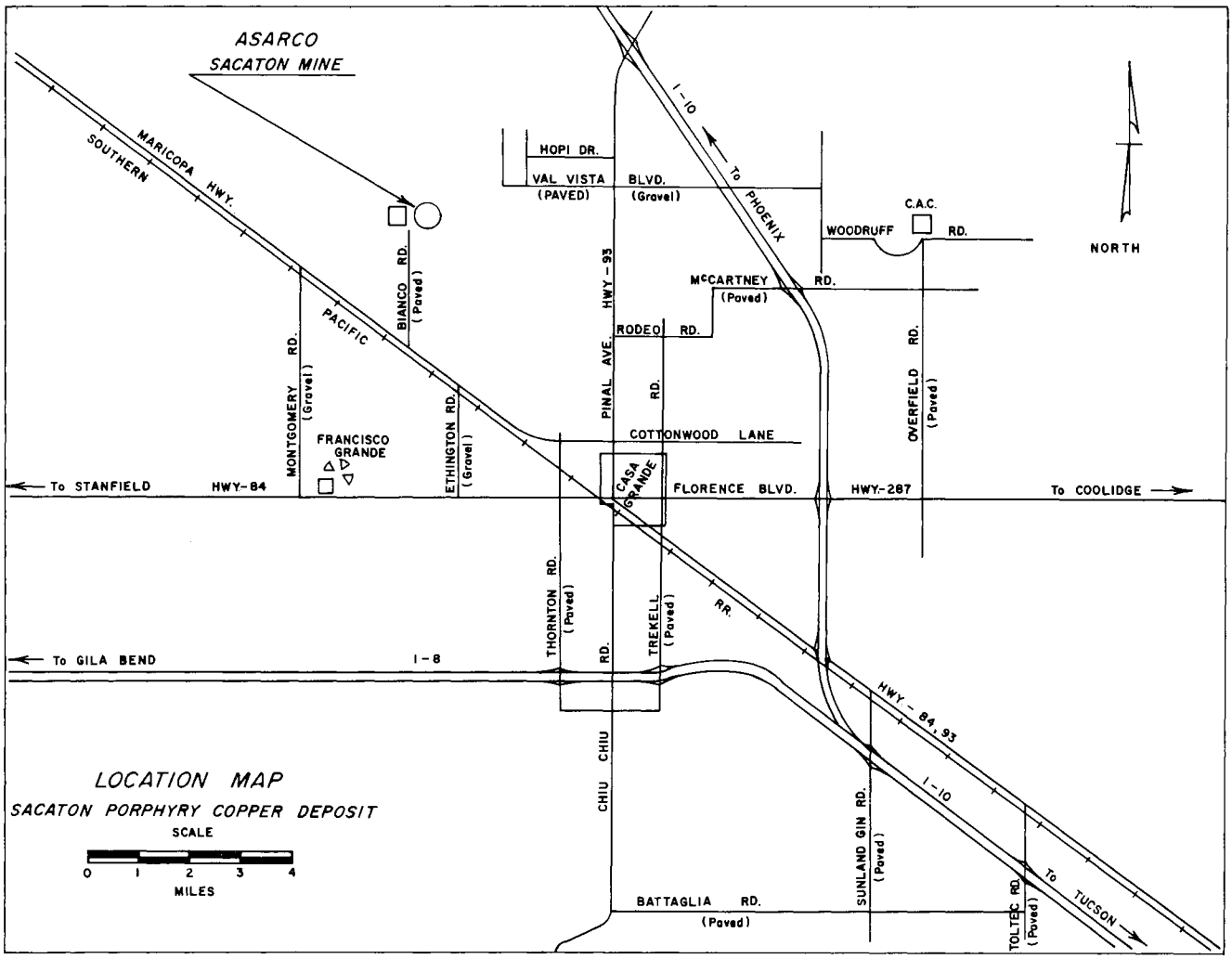

The Sacaton copper deposit is located in the west-central portion of Pinal County, Arizona, about 6 miles northwest of Casa Grande and 65 miles northwest of Tucson. The mine is on a gently dipping alluvial plain south of the Sacaton Mountains. Vegetation is sparse and the climate is semiarid. The average altitude in the mine area is 1,450 feet.

Early in 1961 Asarco geologists examined a small outcrop of leached capping south of the Sacaton Mountains. The outcrop forms a low hill, about 300 feet in diameter, which is surrounded by Quaternary alluvium. The closest pre-mineral rocks are found one and one-half miles to the north. The outcrop is composed of granite which is cut by several thin monzonite porphyry dikes. Both rocks contain pervasive phyllic and argillic alteration. The nature of the leached capping suggests the original sulfides were about 2 percent pyrite by volume with traces of chalcocite.

With the altered outcrop as a positive exploration lead a

drilling program was initiated which eventually outlined two zones of ore grade copper mineralization which are separated by a steeply dipping normal fault (the Sacaton Fault). The west ore body, on the up-thrown side of the fault, is presently being mined by open pit methods. Before commencement of mining activities the ore reserves were estimated to be 33.0 million tons at an average grade of 0.76 percent copper with a cutoff of 0.30 percent copper. The east ore body will eventually be mined by block caving methods. Full-scale production in the west ore body started in February, 1974. At the present time the mine is producing approximately 11,000 tons of ore per day.

Outcrops in the vicinity of the Sacaton deposit include Precambrian Pinal Schist and Oracle Granite and the Laramide Three Peaks Monzonite. The ore bodies are completely covered by Quaternary alluvium.

Within the ore bodies Oracle Granite is intruded by monzonite and quartz monzonite porphyries of probable Laramide age. The porphyries occur as mixed breccias, monolithic breccias, large poorly defined dike-like intrusive masses, and thin well-defined dikes. The center of the west ore body is occupied by an irregular pre-mineral breccia in which fragments of granite and the porphyries are intimately mixed.

Pre-mineral rocks occurring in and around the ore bodies exhibit pervasive hydrothermal alteration. The principal alteration minerals include sericite, quartz, undifferentiated clays, biotite, and chlorite. A well-defined zonation of alteration assemblages has not been identified, but the strongest alteration is generally coincident with the most intense sulfide mineralization.

Hypogene sulfide mineralization (as pyrite, chalcopyrite, and molybdenite) occurs in veinlets, disseminations, and breccia cavity fillings. All pre-mineral rock types are mineralized. The total sulfide content varies from 1.5 percent to 4.0 percent by volume. The best hypogene mineralization occurs in an arcuate-shaped zone which underlies ore grade supergene mineralization. Within this zone the copper content averages over 0.40 percent as chalcopyrite and the pyrite to chalcopyrite ratio varies from 1:1 to 3:1.

Supergene sulfides (chalcocite and minor covellite) occur as replacements of chalcopyrite and pyrite. Supergene mineralization in the west ore body is irregular in thickness, configuration, grade, and continuity. The supergene blanket has a gentle to moderate northerly dip and varies in thickness from less than 50 feet on the margins to over 500 feet.

The original supergene blanket was extensively modified and partly destroyed by a period of post-enrichment oxidation and leaching. During this period a significant quantity of chalcocite from the blanket was oxidized. A portion of the oxidized copper was fixed in place as various oxide copper minerals. The remainder was leached and probably flushed out of the mine area.

THE SUPERSTITION CAULDRON COMPLEX

by
Michael F. Sheridan

Department of Geology
Arizona State University

This one-day field trip examines the rock types, stratigraphy, structure and petrology of the volcanic units associated with the Superstition cauldron complex. Most stops are located along the Apache Trail, but there will be some hikes across rugged desert terrain.

INTRODUCTION

The Superstition-Superior volcanic field is one of several mid-Tertiary silicic centers in the Basin and Range province of southern Arizona. Tuffs associated with this field cover an irregular area approximately 100 km in diameter (fig. 1). The geology of the western part of this field has been investigated by students at Arizona State University (Fodor, 1968; Stuckless, 1969, 1971; Malone, 1972; Sedgeley, 1976; Suneson, 1976; and Hillier, 1977). Rocks in the eastern part of the field have been examined by U.S. Geological Survey scientists (D. W. Peterson, 1960, 1961, 1968, 1969; Creasy and others, 1975; N. P. Peterson, 1954, 1962, 1963; Peterson and others, 1951; and Ransome, 1903, 1919).

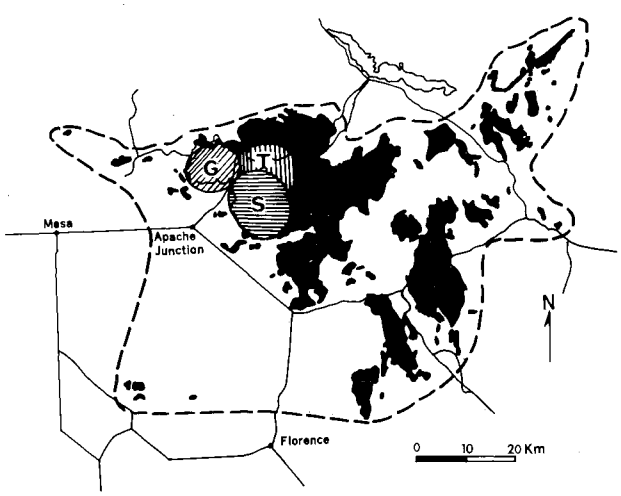

Figure 1. Distribution of volcanic rocks associated with the Superstition-Superior field. Superstition cauldron (S), Goldfield cauldron (G), and Tortilla caldera (T) are indicated by the line pattern.

Sheridan and others (1970) were the first to recognize large cauldrons in the Superstition area. Subsequent mapping has confirmed the existence of the Superstition cauldron and defined its limits. However, a revised interpretation (fig. 2) shows two new structures, the Goldfield cauldron and the Tortilla caldera. Earlier-described calderas are superceded by these structures as defined by their boundary faults on this map.

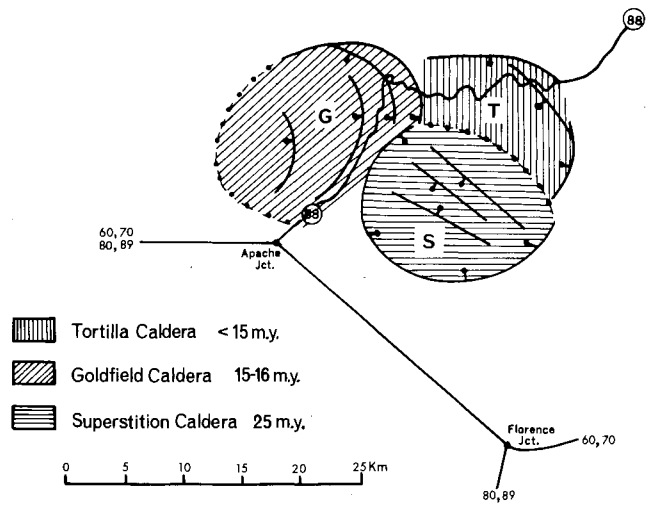

Figure 2. Detail of the three principal cauldrons. Main faults shown with the ball on the down-dropped side.

In this report *cauldron* is used to describe a large subcircular volcanic collapse structure, the topographic expression of which has been erased by erosion. *Caldera* refers to a similar collapse structure that retains some or all of its topographic rim. In this sense the Superstition and Goldfield structures are cauldrons, but the Tortilla structure is a caldera. The Superstition resurgent cauldron is filled with a thick section of welded tuff that has been arched up to produce a broad dome with a central graben. The Goldfield cauldron is composed of at least three tectonic blocks tilted to the northeast (fig. 5) so that the southwest half of the structure has little or no vertical displacement and relatively thin infill units. The Tortilla caldera is an arcuate graben filled with lahar that lies within a topographic rim capped with a rhyolite lava.

The stratigraphy of the Superstition area is now fairly well known, although several significant questions still remain unanswered. Figure 3 shows stratigraphic columns for

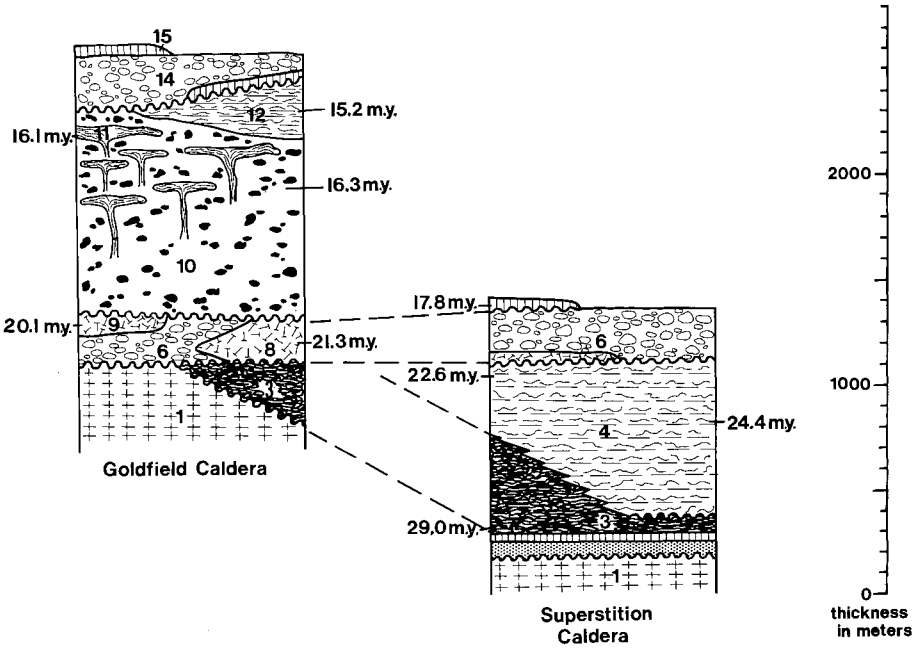

Figure 3. Stratigraphic columns: 1) Precambrian granite, 3) latite complex, 4) Siphon Draw member, Superstition Tuff, 6) breccia of First Water, 8 & 9) rhyodacite domes and lavas, 10) Geronimo Head tuffs, 11) Geronimo Head lavas, 12) Canyon Lake member, Superstition Tuff, 14) breccia of Mesquite Flat, 15) basalt of Willow Spring.

infill deposits of the Superstition and Goldfield cauldrons. Documentation of the ages was done by Damon (1969) and Stuckless and Sheridan (1971). There are two principal stratigraphic units: 1) the Superstition Tuff, a rhyodacite welded tuff composed of several members, and 2) the Geronimo Head Formation, a rhyolitic non-welded tuff and lava sequence.

The oldest volcanic rocks of the Superstition cauldron are alkali basalts that are interbedded with or overlie arkosic conglomerates. The major volcanic episode began with the extrusion of a ring of latite domes during a period from 29 to 25 m.y. ago. This phase ended with the eruption of the Siphon Draw member of the Superstition Tuff and collapse of the Superstition caldera at 25 m.y. ago. A period of resurgence marked by rhyodacite lavas dated at 20 to 21 m.y. was followed by caldera infill by the breccia of First Water and the post-caldera basanite of Black Mesa.

The Goldfield caldera sequence began at a slightly later time with the extrusion of rhyodacite domes, lavas, and breccias at 20 to 21 m.y., coincident with similar lavas in the Superstition caldera. A period of quiet was followed by the eruption of the Geronimo Head tuffs and lavas resulting in major caldera collapse at 16 m.y. A final phase of activity from this caldera produced the Canyon Lake member of the Superstition tuff, a 15 m.y. old welded tuff sheet that extends at least 20 km northeast of the caldera rim.

The stratigraphy of the Tortilla caldera is not yet well documented by radiometric dates. Basalt and latite similar to that of the Superstition cauldron occur northeast of the structure in Horse Mesa. Rhyodacite lava similar to that of the Goldfield cauldron is located along the northern caldera rim beneath a thick sequence of tuffs and lavas similar to those of the Geronimo Head Formation. The most distinctive units in this caldera are the rim rhyolite lava and its

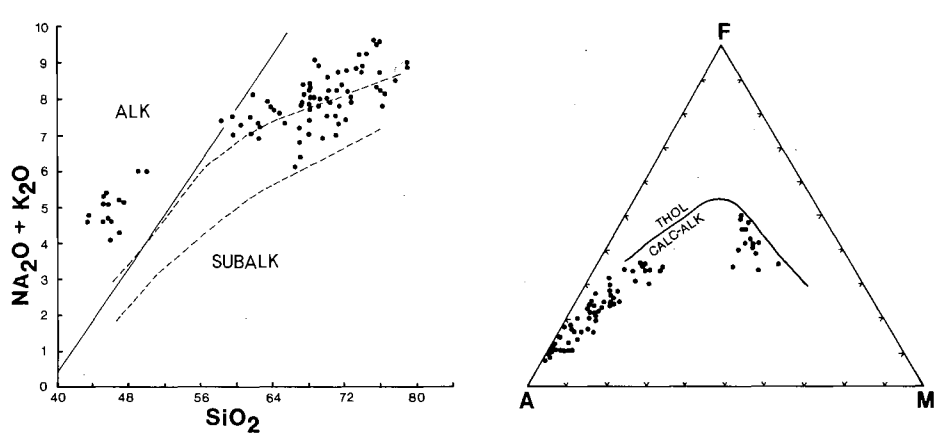

Figure 4. Chemical variation diagrams for volcanic rocks from the Superstition cauldron complex. (From Suneson, 1976.)

associated graben-filling lahar. Above and below the lahar are thin alkali basalt flows.

The rocks of this complex fall into two petrographic suites (fig. 4). The dominant series is composed of calc-alkali silicic rocks ranging from latites through rhyolites. However, a minor series of alkali basalts occurs below and above the major silicic sequence. Data from isotopic studies (Stuckless and O'Neil, 1973) and petrologic models (Malone, 1972; Stuckless, 1971) suggest an independent origin for alkalic and calc-alkalic suites. The transition from calc-alkali to basalt volcanism in this area at 15 to 18 m.y. (Suneson and Sheridan, 1975) is consistent with similar changes throughout the Basin and Range province (Lipman and others, 1972).

TABLE 1—SYMBOLS FOR MAP UNITS

B3	basalt of Willow Springs
BRm	breccia of Mesquite Flat
RH	rhyolite of Horse Mesa
B2	basalt of Canyon Lake
Sc	Canyon Lake member, Superstition Tuff
Gt	tuffs of Geronimo Head Formation
Gl	lavas of Geronimo Head Formation
Bl	basalt of Black Mesa
BRo	breccia of First Water
RD	rhyodacite lavas
Ss	Siphon Draw member, Superstition Tuff
LT	latite lavas, breccias, and domes
Bo	older basalts
AK	arkosic conglomerate
GR	Precambrian granite

REFERENCES CITED

Creasey, S. C., Peterson, D. W., and Gambell, N. A., 1975, Preliminary geologic map of the Teapot Mountain quadrangle, Pinal County, Arizona: U.S. Geol. Survey open-file rept. no. 75–314.

Damon, P. E., 1969, Correlation and chronology of ore deposits and volcanic rocks: U.S. Atomic Energy Comm., Ann. Prog. Rept. no. C00-689-120, 90 p.

Fodor, R. V., 1969, Petrology and petrography of the volcanic rocks in the Goldfield Mountains, Arizona (M.S. thesis): Tempe, Arizona, Arizona State University, 66 p.

Hillier, Mark, 1978, A geochemical study of the older dacite complex, Superstition Mountains, Arizona: Tempe, Arizona, Arizona State University, M.S. thesis.

Lipman, P. W., Prostka, H. J., and Christiansen, R. L., 1972, Cenozoic volcanism and plate-tectonic evolution of the western United States. I. Early and Middle Cenozoic: Phil. Trans. R. Soc. Lond., ser. A, v. 271, p. 217–248.

Malone, G. B., 1972, The geology of the volcanic sequence in the Horse Mesa area, Arizona (M.S. thesis): Tempe, Arizona, Arizona State University, 68 p.

Peterson, D. W., 1960, Geology of the Haunted Canyon quadrangle, Arizona: U.S. Geol. Survey Map GQ–128.

Peterson, D. W., 1961, Dacite ash-flow sheet near Superior and Globe, Arizona (Ph. D. thesis): Stanford, California, Stanford University, 130 p.

Peterson, D. W., 1966, Geology of Picket Post Mountain, northeast Pinal County, Arizona: Ariz. Geol. Soc. Dig., v. 8, p. 159–176.

Peterson, D. W., 1968, Zoned ash-flow sheet in the region around Superior, Arizona: Ariz. Geol. Soc. Southern Arizona Guidebook III, p. 215–222.

Peterson, D. W., 1969, Geologic map of the Superior quadrangle, Arizona: U.S. Geol. Survey Map GQ–818.

Peterson, N. P., 1954, Globe, Arizona-Geology: U.S. Geol. Survey Map GQ-41.

Peterson, N. P., 1962, Geology and ore deposits of the Globe-Miami district, Arizona: U.S. Geol. Survey Prof. Paper 342, 151 p.

Peterson, N. P., 1963, Geology of the Pinal Ranch quadrangle, Arizona: U.S. Geol. Survey Bull, 1141-H, 18 p.

Peterson, N. P., Gilbert, C. M., and Quick, G. L., 1951, Geology and ore deposits of the Castle Dome area, Gila County, Arizona: U.S. Geol. Survey Bull. 971, 134 p.

Ransome, F. L., 1903, Geology of the Globe copper district, Arizona: U.S. Geol. Survey Prof. Paper 12, 168 p.

Ransome, F. L. 1919, The copper deposits of Ray and Miami, Arizona: U.S. Geol. Survey Prof. Paper 115, 192 p.

Schmincke, H. U., 1967, Graded lahars in the type section of the Ellensburg Formation, south central Washington: Jour. Sed. Pet., v. 37, p. 438–448.

Sedgeley, D. R., 1976, A paleomagnetic study of some welded tuffs in central Arizona: Tempe, Arizona, Arizona State University, M.S. Thesis, 110 p.

Sheridan, M. F., Stuckless, J. S., and Fodor, R. V., 1970, A Tertiary silicic cauldron complex at the northern margin of the Basin and Range province, central Arizona, U.S.A.: Bull. Volcanol., v. 34, p. 649–662.

Stuckless, J. S., 1969, The geology of the volcanic sequence associated with the Black Mesa caldera, Arizona (M.S. thesis): Tempe, Arizona, Arizona State University, 79 p.

Stuckless, J. S., 1971, The petrology and petrography of the volcanic sequence associated with the Superstition caldera, Superstition Mountains, Arizona (Ph. D. thesis): Stanford, California, Stanford University, 112 p.

Stuckless, J. S., and O'Neil, J. R., 1973, Petrogenesis of the Superstition-Superior volcanic area as inferred from strontium- and oxygen-isotope studies: Geol. Soc. America Bull., v. 84, p. 1987–1998.

Stuckless, J. S., and Sheridan, M. F., 1971, Tertiary volcanic stratigraphy in the Goldfield and Superstition Mountains, Arizona: Geol. Soc. America Bull., v. 82, p. 3235–3240.

Suneson, N. H., 1976, The geology of the northern portion of the Superstition-Superior volcanic field, Arizona: Tempe, Arizona, Arizona State University, M.S. thesis, 114 p.

Suneson, N. H., and Sheridan, M. F., 1975,, Geology of the northern portion of the Superstition-Superior volcanic field, Maricopa and Pinal Counties, Arizona (abs.): Geol. Soc. America, abs. with prog., v. 7, no. 7, p. 1287–1288.

Wohletz, K. H., 1977, A model of pyroclastic surge: Tempe, Arizona, Arizona State University, M.S. Thesis, 174 p.

Wohletz, K H., and Sheridan, M. F., 1978, A model of pyroclastic surge: Geol. Soc. America Mem. (in press).

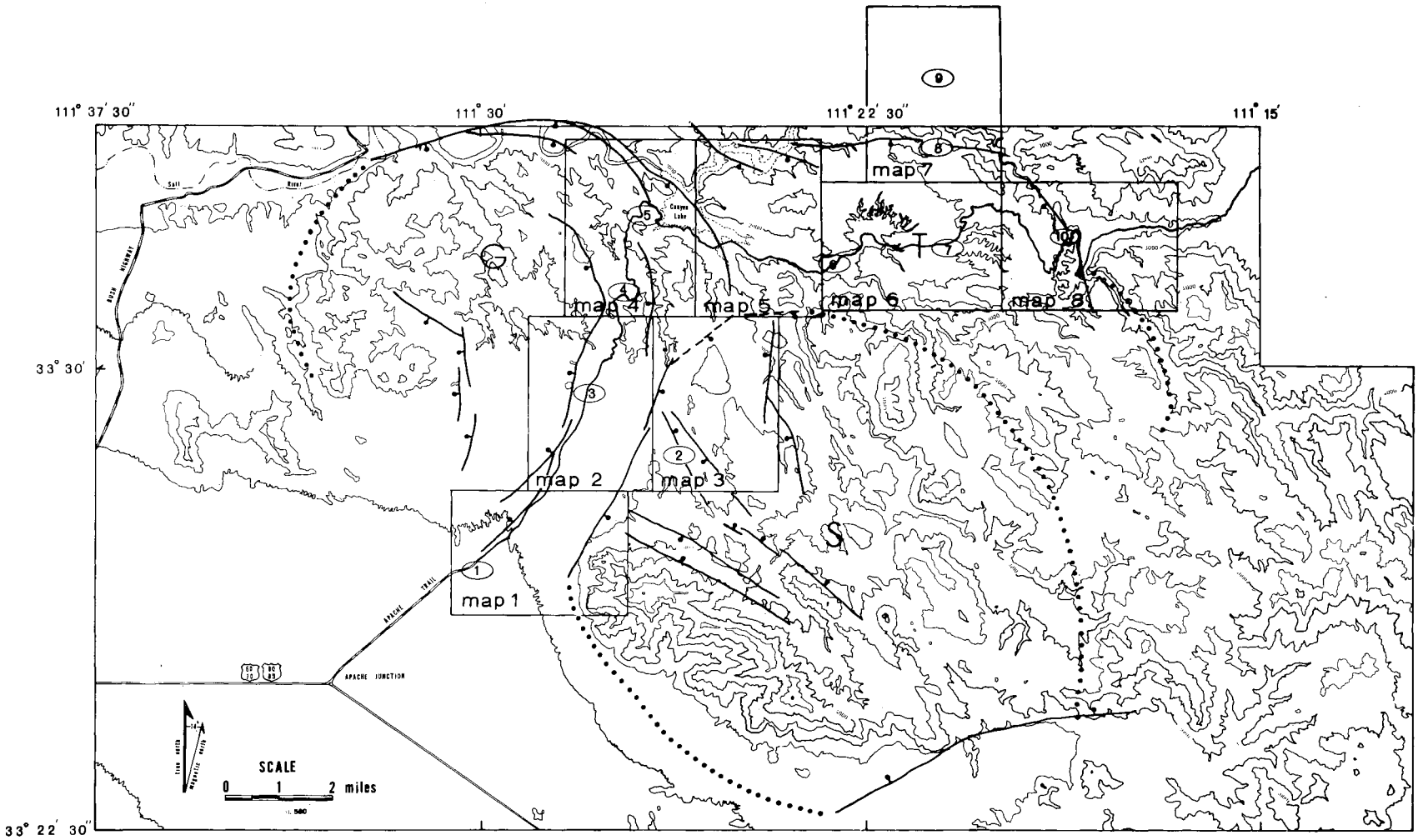

Figure 5. Location map for field trip stops.

ROAD LOG AND STOP GUIDE

The location map for the road log and stop guide (fig. 5) shows the Apache Trail, the three cauldrons with major faults, the eight topographic maps, and the ten geologic stops. The topographic maps, reproduced at a scale of 1:30,000, appear adjacent to the appropriate text without further description. Stops are indicated by bold numerals enclosed in ovals. Faults are shown with the ball on the down-dropped side. Map units are indicated by the symbols shown in table 1.

MILES Interval	Total	
0	0	Start of trip, 8:00 a.m. Corner of Rural Road and University, Tempe. Take University Drive east to the Apache Trail. Driving through Tempe, the Precambrian McDowell mountains are seen to the north. Near Falcon Field in Mesa the tilted Tertiary red-beds of Red Mountain occur to the north. Further east are the Precambrian granites of Usury Mountain. Granitic pediments in Apache Junction lead north to the tuff- and lava-capped fault blocks of the Goldfield Mountains.
20.2	20.2	Apache Trail. Turn north onto the Apache trail and proceed along the boundary zone between the Goldfield and Superstition cauldrons.
5.8	26.0	**STOP 1.** To the east is a view of the Superstition resurgent dome at Siphon Draw (MAP 1). To the west is the boundary fault of the Goldfield cauldron. The lowland area between the mountain ranges is composed of tilted fault blocks of granite (GR), arkose (AK), older basalt (Bo), and latite (LT), typical of the ring fracture zone surrounding the Superstition cauldron. A ring of latite domes and composite volcanoes surrounds the Superstition cauldron. Looking to the east, at least 5 of these small volcanoes can be seen. The oldest date obtained from the

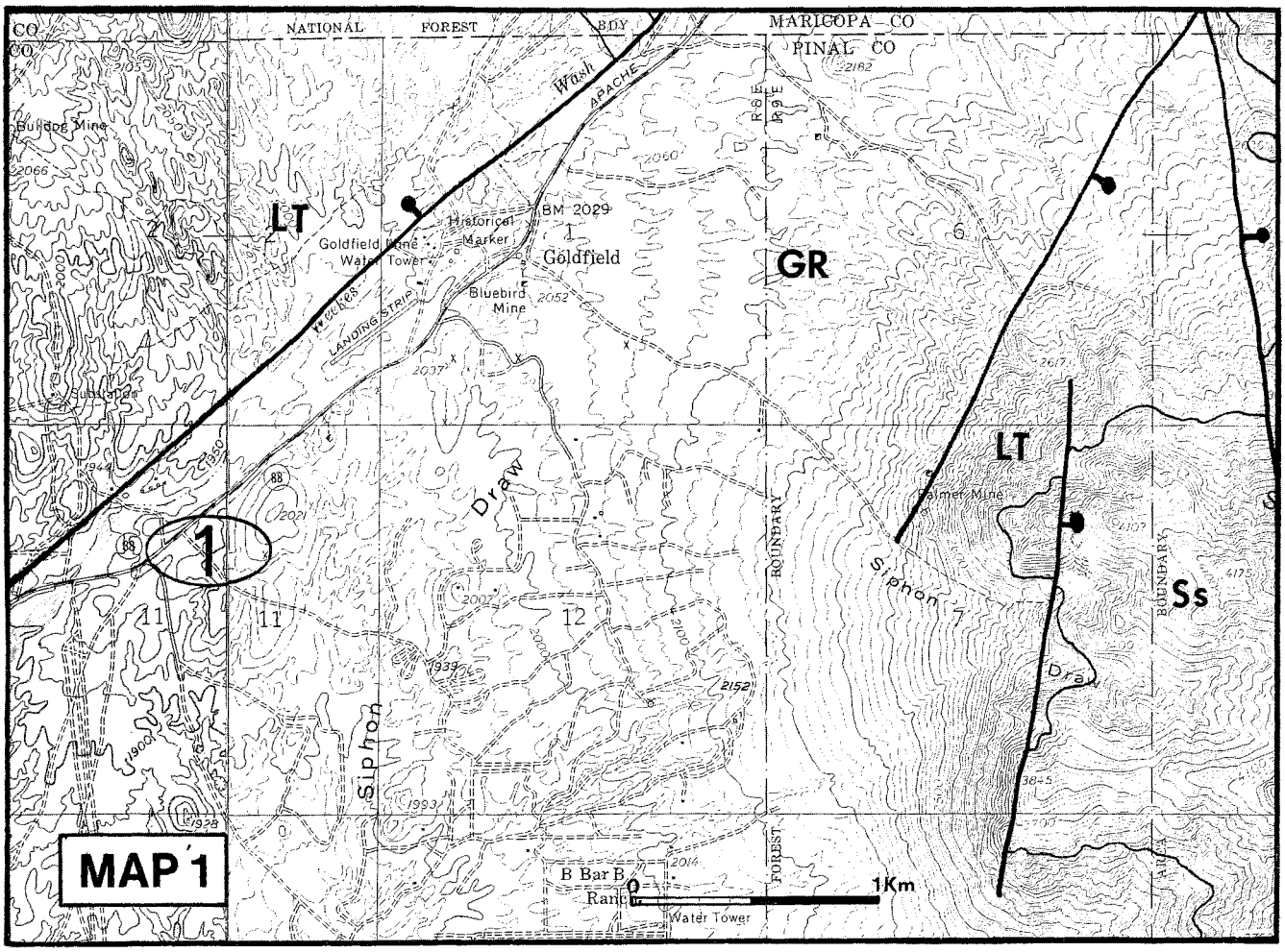

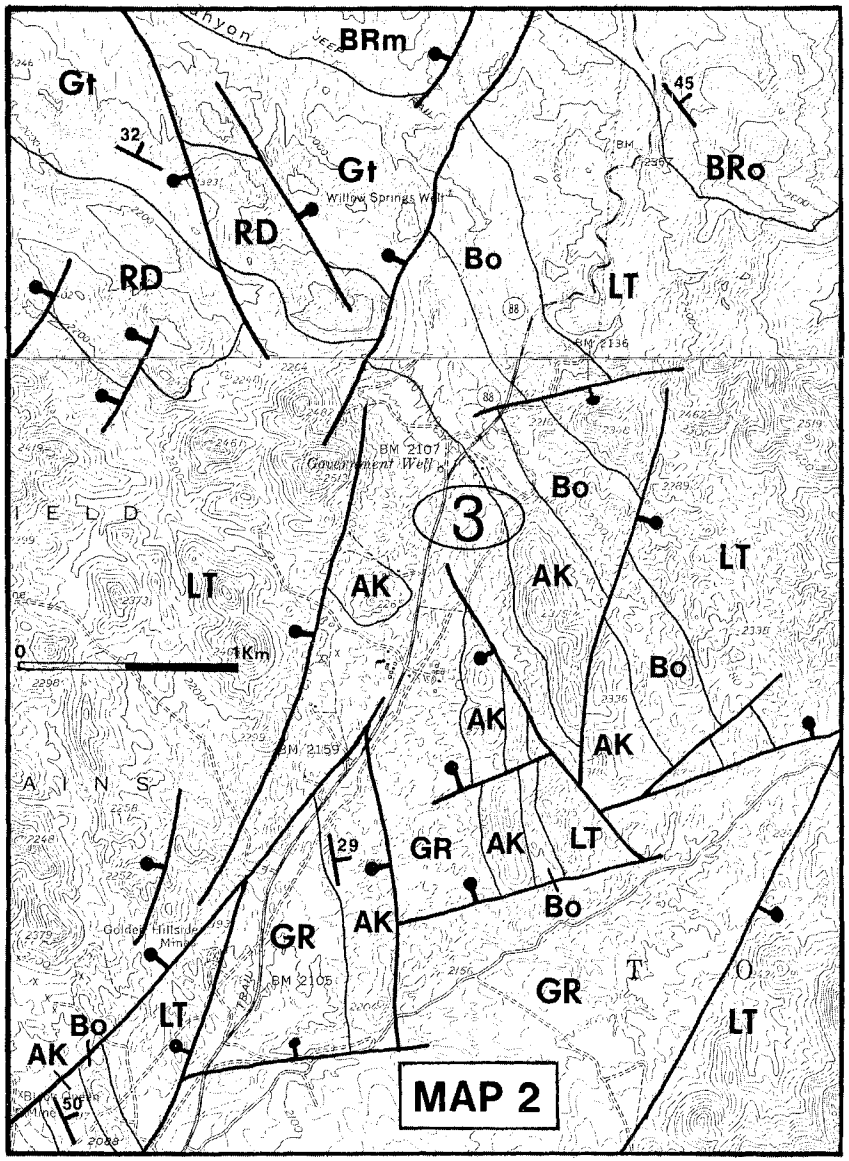
BRm
Gt
32
Gt
Willow Springs Well
RD
RD
Bo
LT
45
BRo
BM 2136
BM 2107
Government Well
3
Bo
LT
AK
AK
LT
0
1Km
Bo
AK
AK
AK
BM 2159
29
GR
AK
LT
Bo
GR
AK
BM 2105
GR
LT
Bo
AK
LT
50
MAP 2

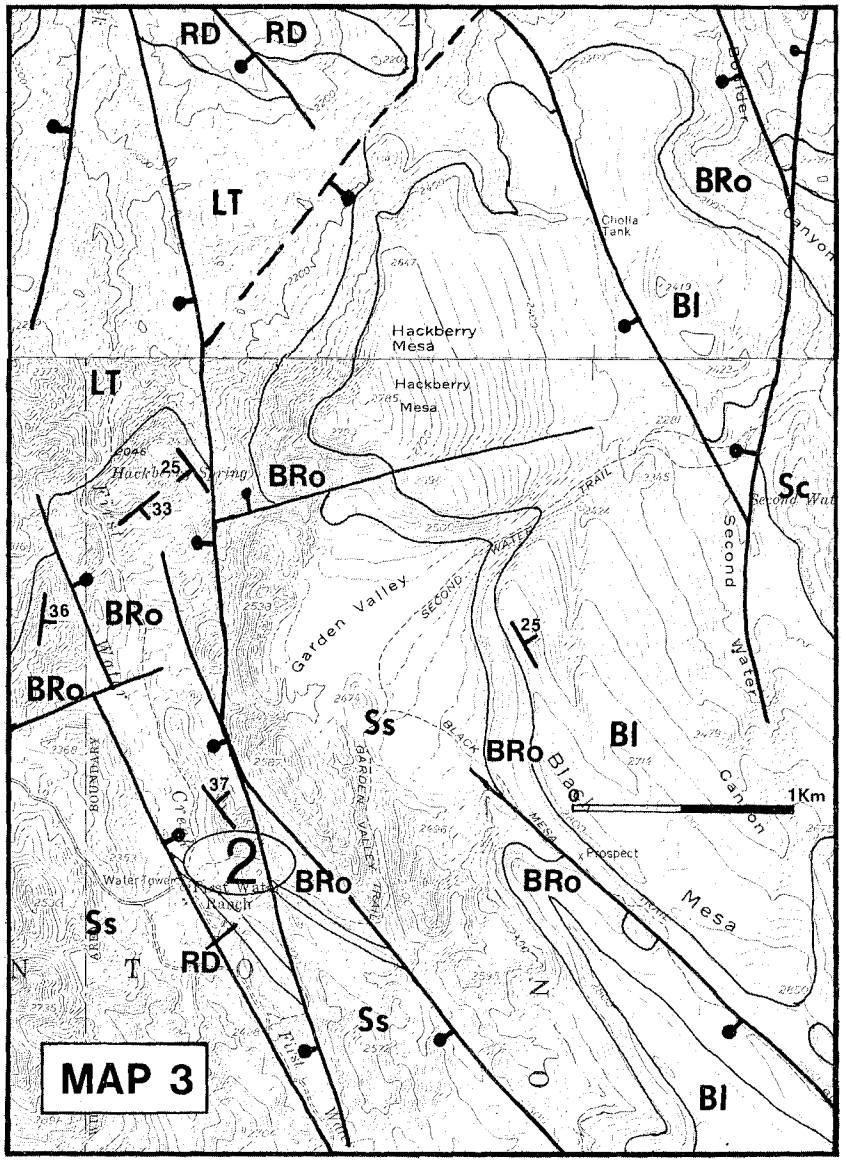
RD
RD
LT
BRo
Cholla Tank
Hackberry Mesa
Hackberry Mesa
Bl
LT
25
33
BRo
Sc
Second Water
36
BRo
Garden Valley
25
BRo
Ss
BRo
Bl
37
1Km
2
BRo
BRo
Prospect
Mesa
Ss
RD
Ss
Bl

MAP 3

base of the latite is 29.0 ± 0.5 m.y. (Stuckless and Sheridan, 1971). At about 25 m.y. ago faulting coincident with the eruption of the Siphon Draw member of the Superstition Tuff took place along the ring of latite volcanoes. The foundered caldera block was filled with rhyodacite welded tuff: outflow units spread to the San Tan Mountains, 50 km to the south. Resurgence shortly followed producing a structural dome with a broad central graben. The mountain mass directly east is the south flank of this structure.

2.3 28.3 Road to First Water. Follow this road eastward for about 2.5 miles and park. This turnoff, shown at the bottom of MAP 3, follows a dirt road across the ring fracture zone of the Superstition caldron into the resurgent dome. Road log mileage is not recorded for this leg of the trip.

STOP 2. Take a short hike along the Garden Valley Trail toward Second Water after entering the Superstition Wilderness (MAP 2). This trail successively crosses the Siphon Draw member of the Superstition Tuff (Ss), rhyodacite lava (RD), and the breccia of First Water (BRo). Resting on this breccia about 1.5 km to the east is the basanite of Black Mesa dated at 17.8 ± 3.1 m.y. (Damon, 1969). The Superstition tuff, 1 km to the east, was dated at 22.6 ± 1.0 m.y. (Damon, 1969).

Follow the Garden Valley trail eastward for about 600 m to a small hill where the breccia of First Water is well exposed. This breccia is composed of lahars that filled the central graben of the Superstition cauldron. Bedding thickness ranges from 30 cm to 1 m for individual flows. The beds are commonly composed of a massive lower portion and a cross-bedded upper part (fig. 6) similar to the lahars of the Ellensburg Formation of Washington (Schmincke, 1967). A fissile silty layer marks the sharp parting between beds. Mudcracks and rain imprints are common along these partings.

Return to the bus and take the dirt road back to the Apache Trail where the road log resumes.

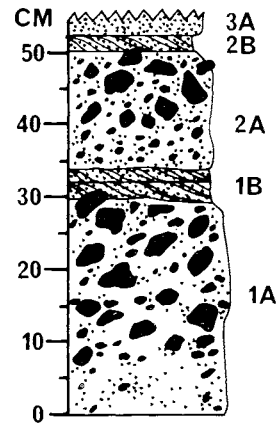

Figure 6. Typical textures in the breccia of First Water.

2.1 30.4 **STOP 3.** Weavers Needle Vista. This is the northern end of a horst block between the Superstition and Goldfield cauldrons. Bedrock at this location is the Precambrian granite that has decomposed into a gruss soil. Hogback ridges to the east are successively arkosic conglomerate (AK), older basalt (Bo), and latite (LT). Good exposures of this section may be seen in road cuts between **STOP 3** and **STOP 4.**

To the west is the fault line scarp of the Goldfield cauldron. Latite (LT), rhyodacite (RD), and Geronimo Head tuff (Gt) are down-dropped into contact with granite, arkose, and older basalt. The vertical displacement on this fault locally exceeds 1.5 km. Visible on the skyline to the north are the younger laharic breccias of Mesquite Flat that are overlain by the youngest basalt flow (B3 of MAP 4).

2.5 32.4 **STOP 4.** Apache Gap. A rhyodacite dome (RD) is intrusive into older tuffs and breccias (MAP 4). The dome has a glassy selvage and well-developed flow banding roughly conformable with its outline. A notable large-scale fold occurs just north of this point.

A number of en echelon curving faults mark the edge of the Goldfield cauldron throughout the area of MAP 4. One major segment passes southwest of the dome at Apache Gap: another cuts south of Mormon Flat Dam. North of Apache Gap is a section of more than 1,000 m of tilted Geronimo Head tuff (Gt) and lava (Gl). Beyond the cauldron boundary fault north of Canyon Lake the Geronimo Head Formation is composed of only 200 m of flat-lying tuffs.

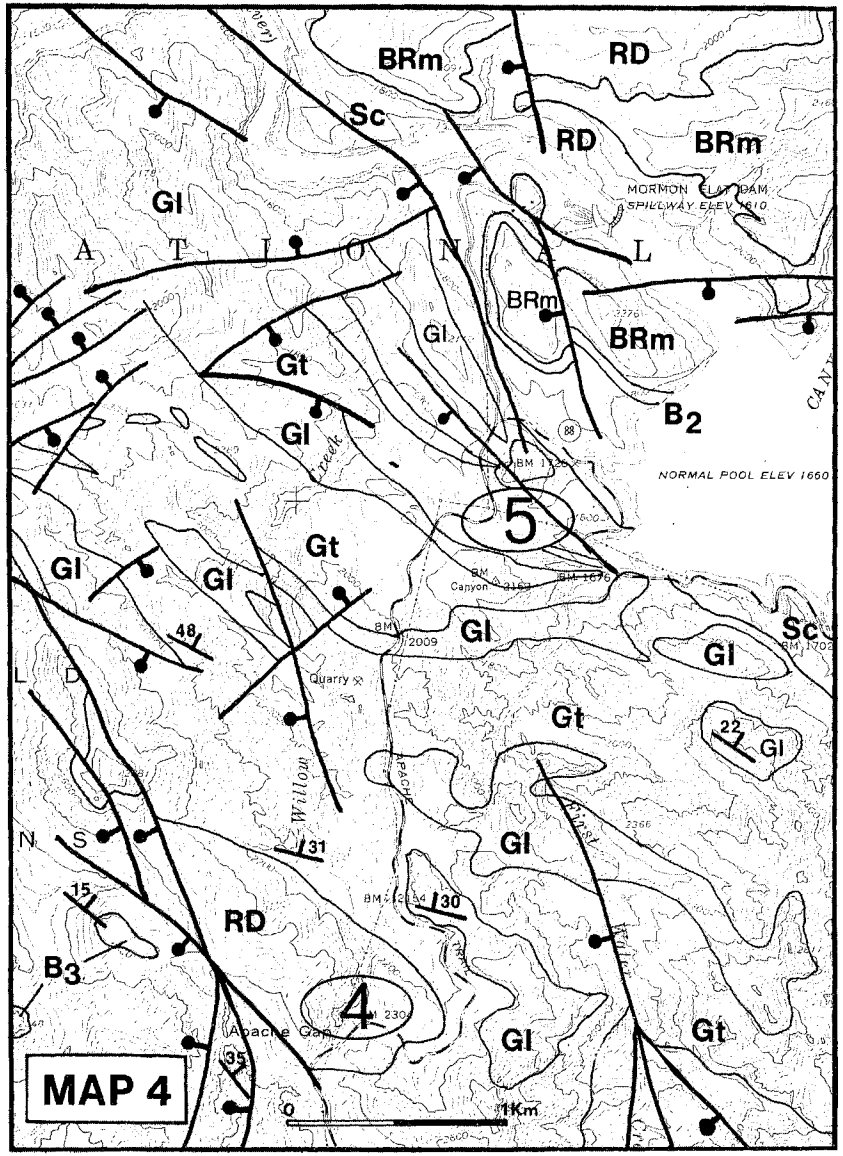
BRm
RD
Sc
RD
BRm
MORMON FLAT DAM
SPILLWAY ELEV 1610
Gl
A T I O N A L
BRm
BRm
Gl
Gt
Gl
B2
NORMAL POOL ELEV 1660
5
Gt
Gl
Gl
Gl
Sc
Gl
48
Quarry
Willow Creek
Gt
22
Gl
31
Gl
30
15
RD
B3
4
Apache Gap
Gl
Gt
35
MAP 4
0
1Km

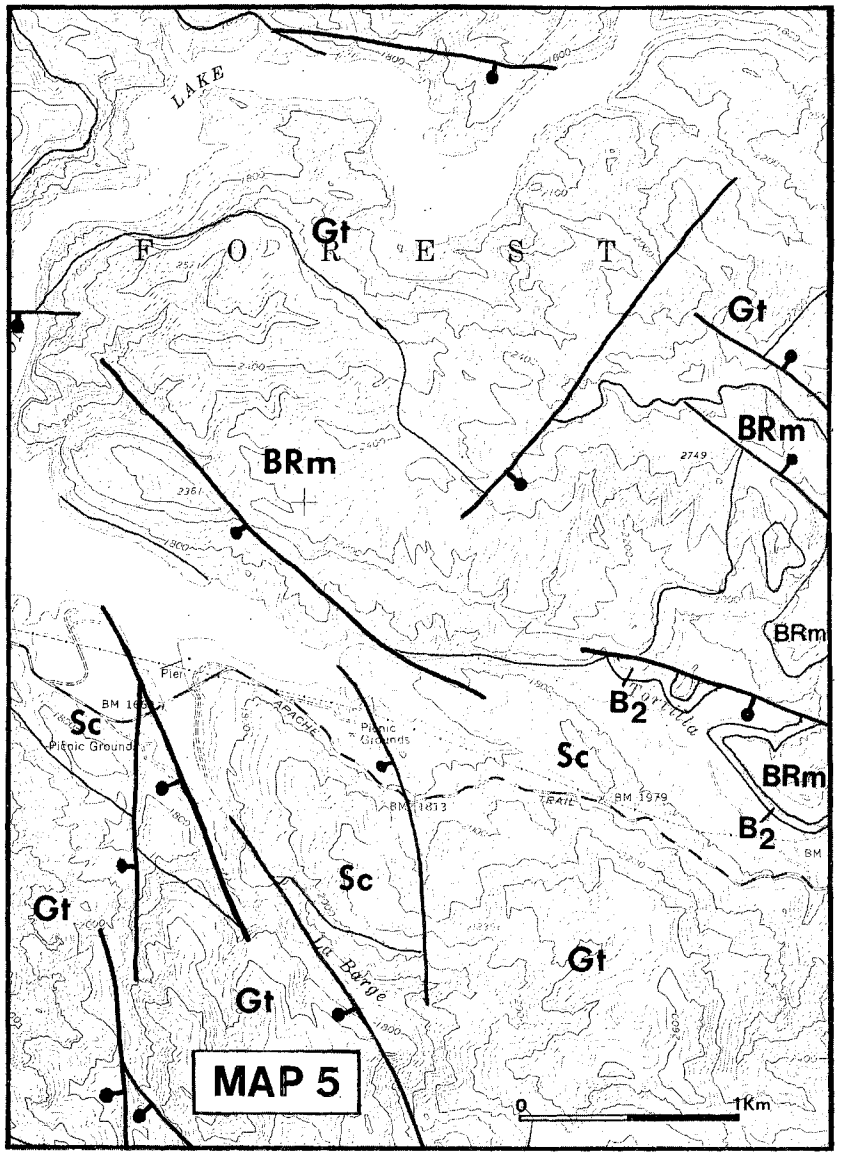
LAKE
F O R E S T
Gt
Gt
BRm
BRm
BRm
B2
Sc
Sc
BRm
B2
Sc
Gt
Gt
Gt
MAP 5
0
1Km

Between **STOP 4** and **STOP 5** are the best exposures of Geronimo Head tuffs and lavas. A few rhyolite dikes with prominent flow-banding are also cut by the road.

2.3 32.5 **STOP 5.** Canyon Lake Overlook. Here is the northeastern margin of the Goldfield cauldron. This glassy rhyolite lava with red spherulites has been dated at 16.0 ± 1.3 m.y. (Stuckless and Sheridan, 1971). At about 200 m to the northeast the Canyon Lake member of the Superstition Tuff (Sc) rests conformably on the Geronimo Head tuff (Gt). A basalt flow (B2) and the breccia of Mesquite Flat (BRm) successively overlie the welded tuff. Inside the Goldfield cauldron these units are in northeast-tilted fault blocks, but outside the cauldron they are flat-lying.

5.6 40.8 **STOP 6.** Tortilla Flat. We have passed through MAP 5 to MAP 6 while remaining essentially within the Canyon Lake member. Good exposures of this unit occur in the bed of Mesquite Creek north of Tortilla Flat where dates of 14.9 ± .08 and 15.4 ± 0.8 m.y. were obtained (Stuckless and Sheridan, 1971). Here the welded tuff overlies a lava dome of the Geronimo Head Formation (G1) and is overlain by a basalt lava (B2) and the breccia of Mesquite Flat (BRm).

This rhyolitic welded tuff was a late-stage product of the Goldfield cauldron. It ponded in depressions along the northeastern section of the caldera wall at Canyon Lake (**STOP 5**) and formed thin outflow sheets in basins as at Tortilla Flat (**STOP 6**) and Goat Mountain, 16 km to the east.

For the most part this tuff is densely welded, but at Tortilla Flat considerable variation in compaction textures is noted.

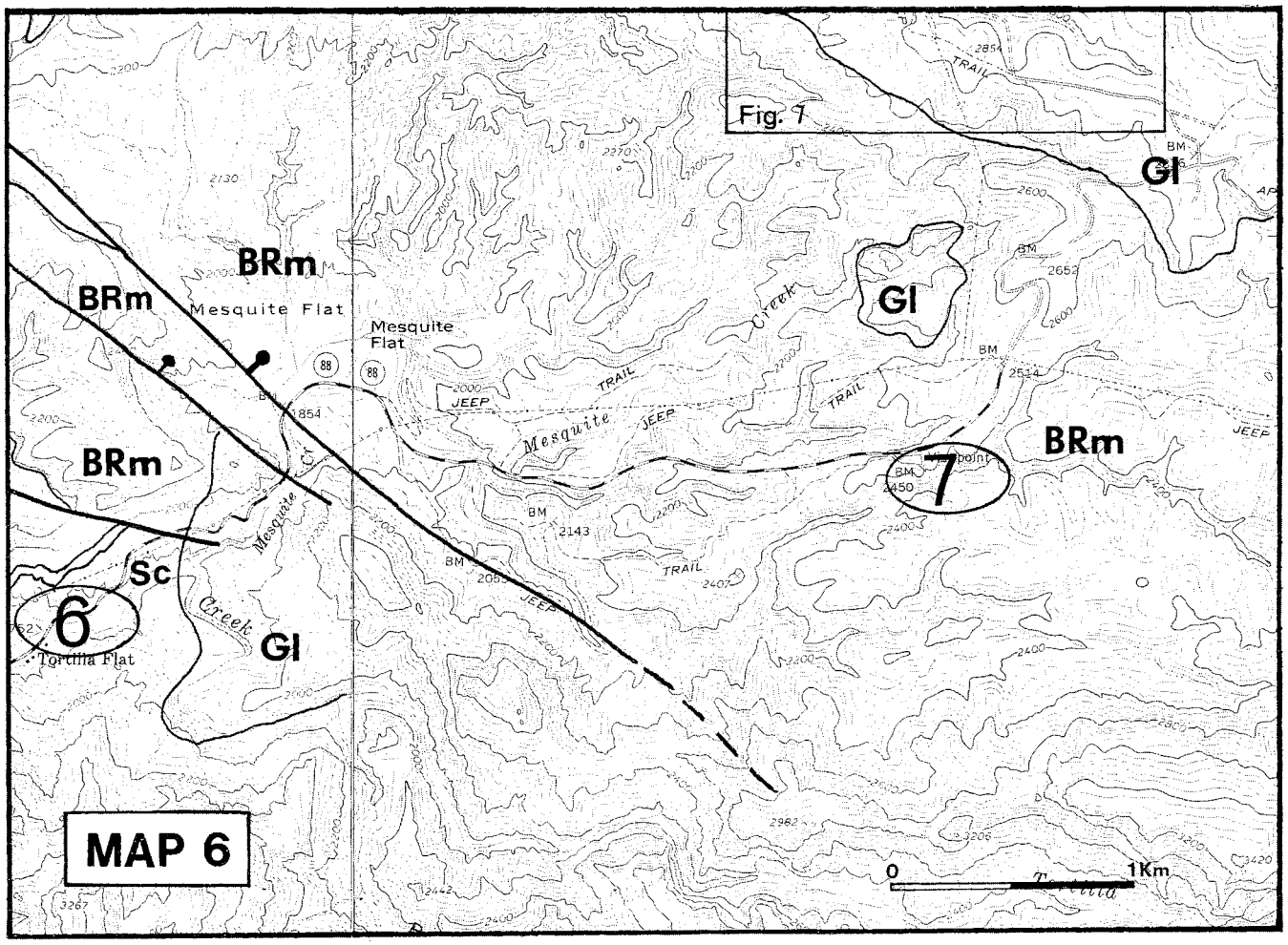

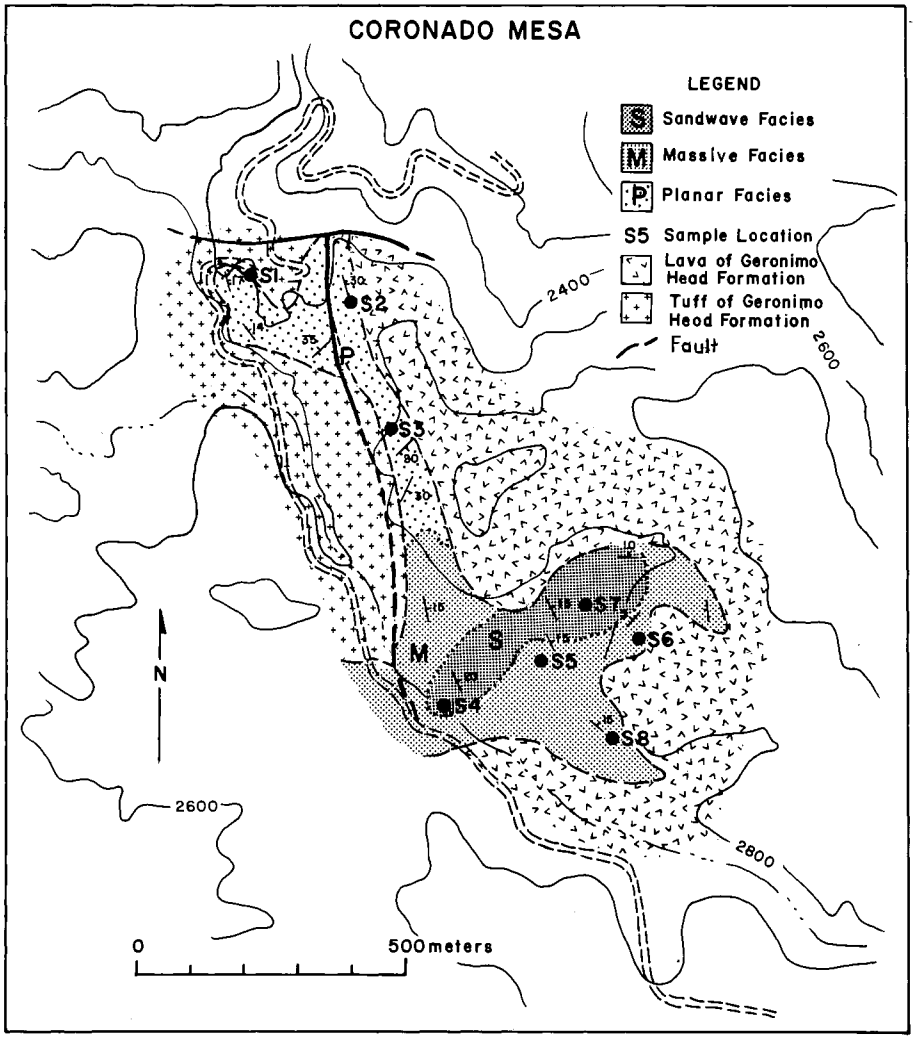

Figure 7. Map of the pyroclastic surge facies of the Coronado Mesa vent. (From Wohletz, 1977.)

Paleomagnetic work of Sedgeley (1976) as well as variations in compaction suggest that there are at least two cooling units in this sheet.

2.8 43.6 **STOP 7.** Mesquite Flat View Point. The past two kilometers of Apache Trail have passed through outcrops of the breccia of Mesquite Flat (BRm). This lahar has filled a broad arcuate graben that extends for 14 km along the down-dropped side of the Tortilla caldera boundary faults (fig. 5). The rhyolite of Horse Mesa (RH) that extends for 8 km along the caldera rim is the host for the lithic inclusions of the lahar, suggesting a genetic relationship between units. Perhaps this basin was subsiding as the rim rhyolites were erupting. Lahars, generated from the rhyolites, poured into the basin forming the Mesquite Flat breccia.

From this vantage point the rim rhyolites can be seen along the near skyline to the north. To the west is a graben fault that has displaced the laharic breccia. At the west end of this fault an intrusive rhyolite dome has turned up the lahar beds to a near-vertical position.

1.2 44.8 Horse Mesa Dam Road. Bear left onto the dirt road leading to Horse Mesa Dam. This road traverses Geronimo Head lava (G1) that projects above the former surface of the breccia of Mesquite Flat (MAP 7). The detailed geology along this part of the trip is shown on figure 7. Coronado Mesa, the broad ridge to the northeast of the road, is a rhyolitic vent complex that developed during Geronimo Head time. A series of pyroclastic surge deposits that issued from a vent near the center of the mesa was subsequently covered by cogenetic lavas (Wohletz and

Sheridan, 1978). Sandwave facies of pyroclastic surge deposits crop out to the north of the road as we travel towards **STOP 8.**

1.8 46.6 **STOP 8.** Coronado Mesa. Pyroclastic surge deposits typically show a three-fold concentric facies distribution surrounding the vent (Wohletz and Sheridan, 1978): 1) a proximal sandwave facies dominated by sandwave-type beds, 2) a medial massive facies characterized by a sub-equal abundance of sandwave, massive and planar beds, and 3) a distal planar facies dominated by planar-type beds. The distribution of surge facies for Coronado Mesa is given in figure 7. Stratigraphic columns for a sandwave facies location (S-7) and a planar facies location (S-1) are shown in figure 8. **STOP 8** at location S-1 allows close examination of the planar facies of this deposit.

About 100 m to the north is the boundary fault for the Tortilla caldera. Flat-lying tuffs and lavas of the Geronimo Head Formation (Gtl) are capped by the thick rhyolite of Horse Mesa (RH). Outcrops of this lava mark the erosional remnants of the north rim of the Tortilla caldera.

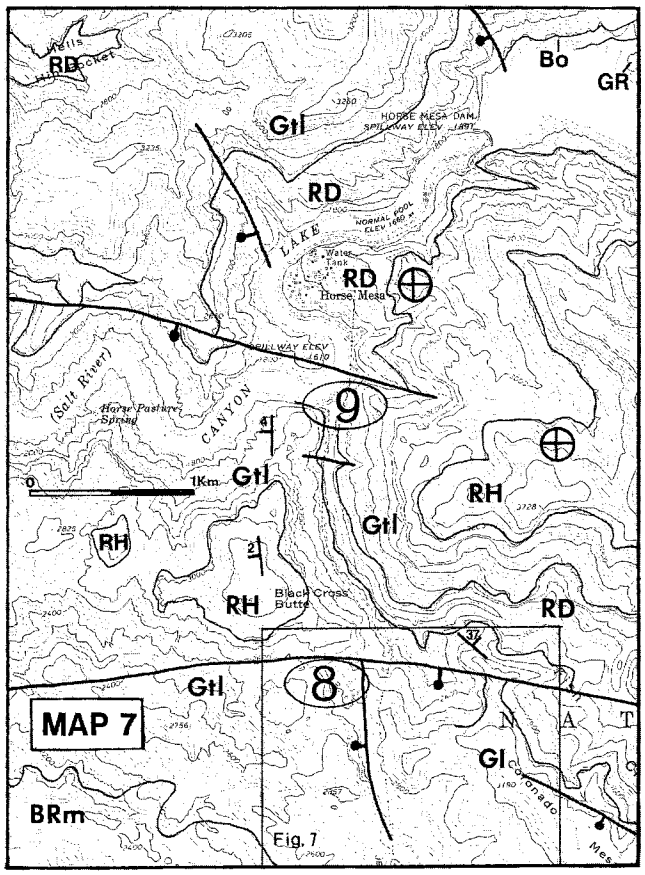

As we drive to **STOP 9** there are numerous lava domes of the Geronimo Head Formation that erupted from local vents in the vicinity of Fish Creek (MAP 7). Many of these domes have associated pyroclastic surge deposits. This concentration of vents is taken as further evidence for the proximity of the caldera ring fault.

A good exposure of the ring fault passes through the switchbacks below **STOP 8.** Silicified fault breccia stands in relief as an erosional dike with polished slickensides along the contact, to the west of the road below Black Cross Butte. To the east the near-vertical sinuous fault trace is accentuated by the contrast of dark lava displaced against light tuff. Several branching faults along the switchbacks have caused local development of low-angle faults.

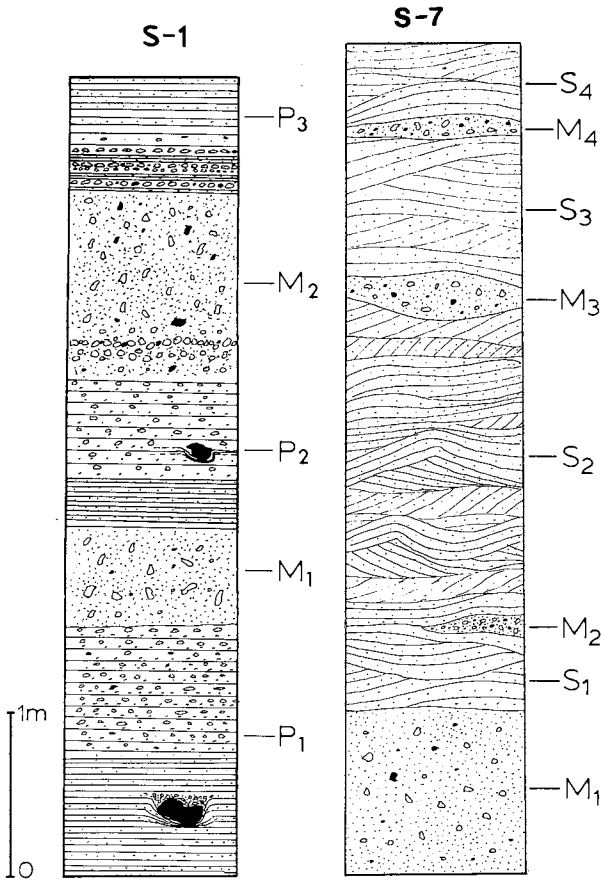

Figure 8. Sections of planar facies (S–1) and sandwave facies (S–7) of pyroclastic surge deposits at Coronado Mesa. (From Wohletz, 1977.)

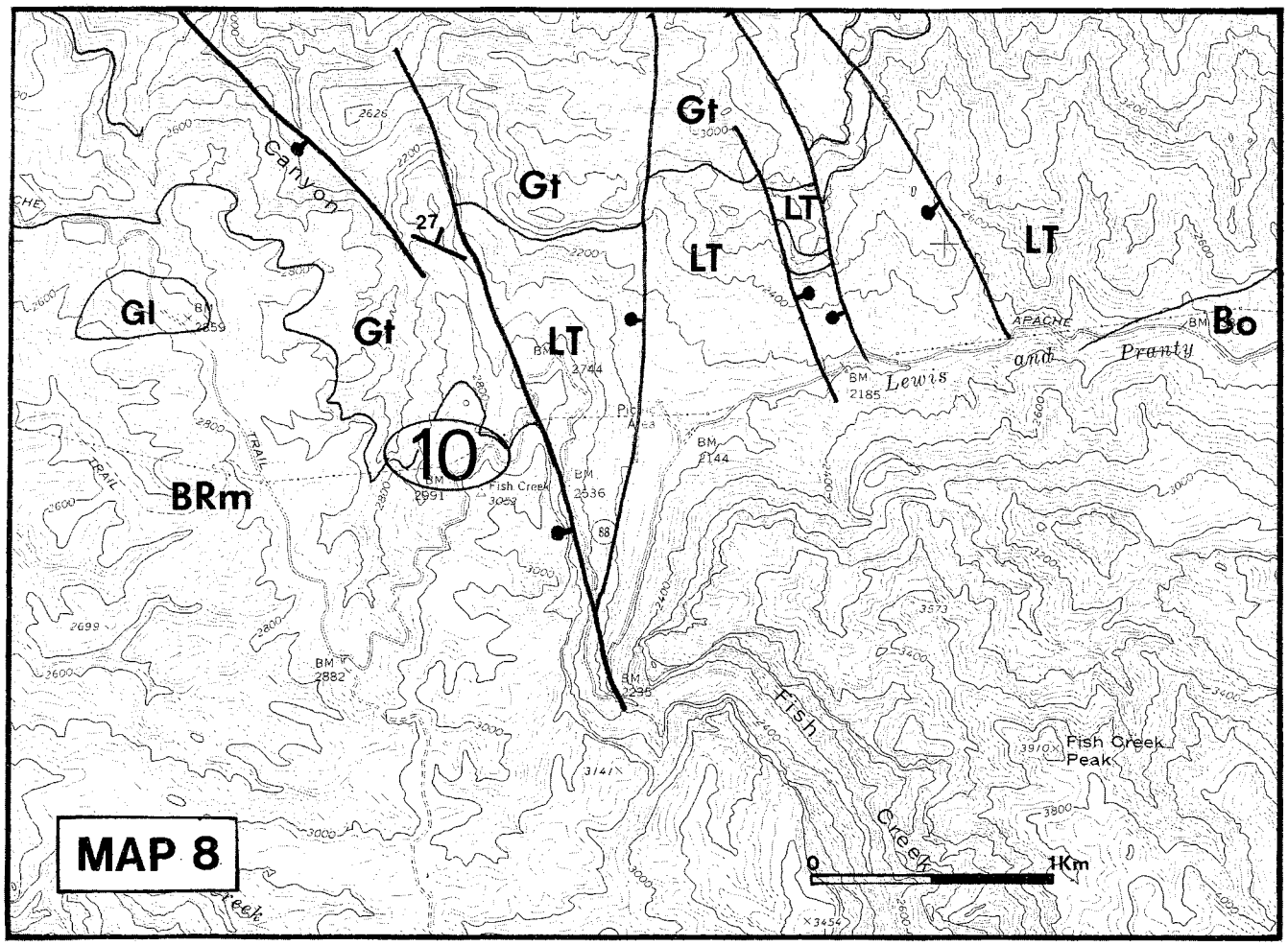

2.8 49.4 **STOP 9.** Salt River. At the base of the Fish Creek Canyon (MAP 8) is a good exposure of the rhyodacite (RD) below the Geronimo Head tuffs and lavas (Gt1). This rock is fresh and glassy with phenocrysts of plagioclase, quartz, alkali feldspar, biotite, hornblende, augite, and hypersthene. This unit typically occurs within a few kilometers of the margin of the later rhyolitic cauldrons (Goldfield and Tortilla), and probably represents a tumescent stage of eruption.

Return to the Apache Trail.

4.6 54.0 Apache Trail. Bear left on the Apache Trail and continue along the margin of the graben containing the breccia of Mesquite Flat. To the north is the erosional scarp of the Tortilla caldera marked by the flat-lying rhyolite of Horse Mesa (RH).

3.1 57.1 **STOP 10.** Fish Creek Overlook. Between **STOP 8** and **STOP 10** Fish Creek more or less follows the caldera boundary fault. We will hike a few hundred meters along the ridge to the north (MAP 8) for a better view of the geology. To the east the caldera boundary fault passes along the switchbacks in the road. The breccia of Mesquite Flat (BRm) is displaced down into contact with the latite (LT) so that the 300 to 500 m section of Geronimo Head Formation (Gt) is missing. To the east a series of faults with a similar sense of movement add to the total displacement along the caldera margin.

While standing on the breccia of Mesquite Flat, the contact with the underlying Geronimo Head formation can be traced to the east and the west. Yellow tilted Geronimo Head tuffs (Gt) are in unconformable contact with the brown flat-lying breccia of Mesquite Flat (Brm).

End of field trip. Return to Tempe.

GROUNDWATER RECHARGE WITH SEWAGE EFFLUENT

by
Herman Bouwer, Director
U. S. Water Conservation Laboratory
U.S. Dept. of Agriculture

INTRODUCTION

The Salt River Valley is in an irrigated agricultural area with a rapidly expanding urban population. Groundwater furnishes about one-third of all the water used in the area served by the Salt River Project, which is the local irrigation district. The rest comes from the Salt and Verde Rivers which are dammed in the mountains, causing the Salt River below Granite Reef Dam east of Mesa to be normally dry. This reduces groundwater recharge and, consequently, water tables have been dropping, sometimes as much as 10 ft. per year. Ironically, groundwater pumping in the Salt River Valley began in the 1920's to lower the water table, which had risen so much due to irrigation that low areas became water-logged. The urbanization of the valley produces an increase in the amount of sewage effluent (about 5 to 6 mgd each year). If this sewage could be reused for agriculture or other purposes, the overdraft on the groundwater could be reduced.

Large-scale reuse of sewage effluent for agriculture requires treatment beyond that normally applied in a conventional treatment plant. For the Salt River Valley, the additional treatment can be effectively obtained if the effluent from the treatment plant is used for groundwater recharge, letting it percolate from infiltration basins to the underlying groundwater, and using the vadose zone and aquifer as natural filters to "renovate" the sewage water. The infiltration basins should be located in relatively permeable soils, such as the loamy sand, sand, and gravel found in the Salt River bed, to obtain high infiltration rates. After the sewage effluent has percolated down to the groundwater, it can be pumped as renovated water from wells located some distance from the infiltration basins. Presently, Phoenix and surrounding cities produce about 100 mgd of sewage effluent. This is a little more than 100,000 acre-feet per year and sufficient to irrigate about 30,000 acres.

Unlike conventional sewage-treatment plants for which standard designs are available, the design and management of a groundwater recharge system for renovating sewage effluent requires local experimentation before the best design can be formulated. This is because the performance of an infiltration-recharge system for sewage effluent depends very much on local conditions of climate, soil, and groundwater hydrology. For the Salt River Valley, such an experimental system, called the Flushing Meadows Project, was installed in 1967. The system consists of six parallel infiltration basins, 20 by 700 feet each. It is located in the Salt River bed at about 103rd Avenue and uses secondary effluent from the 91st Avenue Sewage Treatment Plant. The soil consists of about 3 feet of loamy sand underlain by sand and gravel layers to a depth of 240 feet where a clay layer begins. The water table is at a depth of about 10 feet. Wells, 20 to 30 feet deep, were installed between the basins and at various distances from the basins to obtain samples of the renovated sewage water and to follow the quality improvement of the effluent water as it moves down to the groundwater and laterally through the aquifer. Almost 10 years of research with this project has shown that:

1. The largest capacity or hydraulic loading is obtained with 2- to 3-week flooding periods alternated with 2-week drying periods. At this schedule, 300 to 400 feet of effluent move into the ground per year. At these high hydraulic loading rates, however, only about 30 percent of the nitrogen is removed from the sewage water as it percolates through the soil.
2. Quantity and quality of renovated water are optimized with a hydraulic loading of about 200 feet per year, which is obtained by a schedule of 9 days flooding and 12 days drying. At this hydraulic loading rate, nitrogen removal is about 60 percent. At a loading rate of 200 feet per year, about 500 acres of basins are required to infiltrate the sewage effluent from one million people.
3. Viruses cannot be detected in renovated water sampled at a depth of 20 to 30 feet below the basins. This renovated water still contains some fecal coliform bacteria, which are completely removed after an additional lateral movement of about 200 feet in the aquifer.
4. Phosphate removal increases with increasing distance of underground movement of the renovated water and exceeds 90 percent after 200 feet.
5. The renovated water is essentially free from suspended solids and biodegradable material as expressed by the biochemical oxygen demand (BOD). Some residual organic carbon persists in the renovated water at an average concentration of 4 to 5 mg/1. Possible toxicity (carcinogenity, mutagenity, teratogenity, etc.) of these refractory organics presently is the main concern in potable use of the renovated water.

BIBLIOGRAPHY

Bouwer, Herman. Groundwater recharge design for renovating wastewater. Jour. Sanitary Engin. Div., Amer. Soc. Civil Engin. Proc., 96(SA 1):59–74. 1970.

——, Design and operation of land treatment systems for minimum contamination of groundwater. Ground Water 12(3):140–147. 1974.

——, Zoning aquifers for tertiary treatment of wastewater. Ground Water 14(6):386–395. 1976.

——, and Chaney, R. L. Land treatment of wastewater. *In* "Advances in Agronomy," Vol. 26, N. C. Brady, Editor, pp. 133–176. Academic Press, New York. 1974.

——, Lance, J. C., and Riggs, M. S. High-rate land treatment: II. Water quality and economic aspects of the Flushing Meadows Project. Jour. Water Pollut. Contr. Fed. 46(5):844–859. 1974.

——, Rice, R. C., and Escarcega, E. D. High-rate land treatment: I. Infiltration and hydraulic aspects of the Flushing Meadows Project. Jour. Water Pollut. Contr. Fed. 46(5):835–843. 1974.

Gilbert, R. G., Gerba, C. P., Rice, R. C., Bouwer, H., et al. Virus and bacteria removal from wastewater by land treatment. Appl. and Environ. Microbiol. 32(3):333–338. 1976.

——, Rice, R. C., Bouwer, H., Gerba, C. P., Wallis, C., and Melnick, J. L. Wastewater renovation and reuse: Virus removal by soil filtration. Science 192(4243): 1004–1005. 1976.

STOP NO. 1. 23RD AVENUE RECHARGE PROJECT.

The groundwater recharge project to be visited on the field trip is a larger system that was installed in the Salt River bed by the City of Phoenix in 1975 to produce renovated sewage water for unrestricted irrigation by a local irrigation district. The system consists of four 10-acre infiltration basins (fig. 1) that are intermittently flooded with secondary effluent from the 23rd Avenue Sewage Treatment Plant. The material below the basins is mostly sand and gravel, which continues to a great depth, similar to the Flushing Meadows Project. The static water table is at a depth of about 70 feet. Renovated water is to be pumped from three wells on the center dike. The first well (fig. 2), installed in 1975, is 200 feet deep, perforated from 100 to 180 feet, and delivers about 2,000 gpm. The other wells should be deeper, for example, about 300 feet and perforated from 150 to 300 feet. The renovated water has been certified by the State Health Department for unrestricted irrigation and eventually will be discharged in the Roosevelt Irrigation District canal north of the project.

Spread of renovated water in the aquifer outside the basin area is undesirable for legal and health reasons. To avoid such spread, infiltration of sewage effluent and pumping of renovated water must be managed so that groundwater levels along the project perimeter are maintained at the same height as those in the aquifer outside the system. To monitor groundwater levels at the perimeter of the system, observation wells have been installed on the north and south sides of the infiltration area (fig. 3).

Originally, the infiltration basins received effluent that had passed through an 80-acre oxidation pond. This was undesirable, however, because algae growing in the pond doubled and sometimes even quadrupled the suspended solids content of the effluent. These algae then accumulated on the bottom of the infiltration basins, causing soil

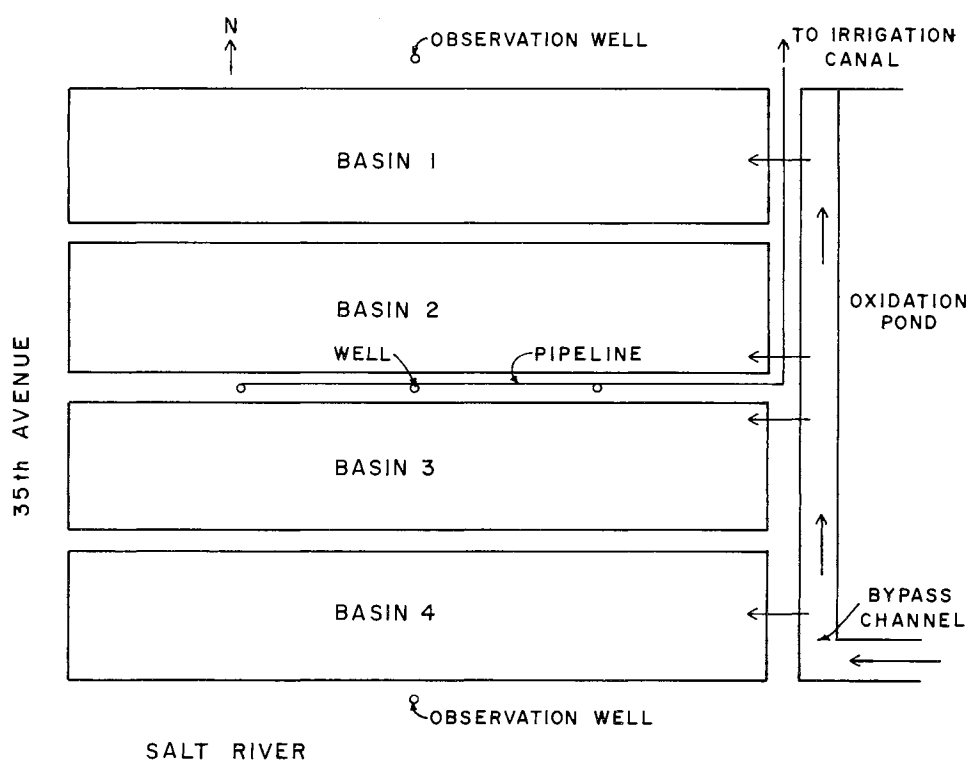

Figure 1. Schematic of rapid-infiltration project below 23rd Avenue Sewage Treatment Plant.

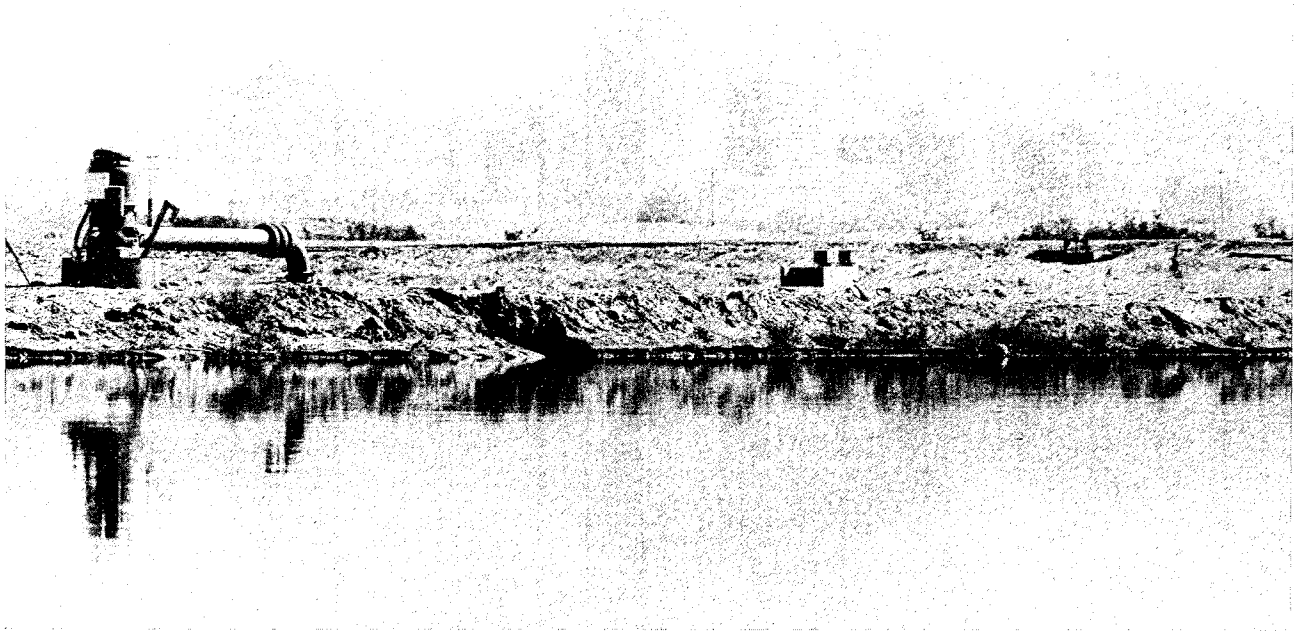

Figure 2. Infiltration basin with secondary sewage effluent and well on center dike pumping renovated sewage water from aquifer.

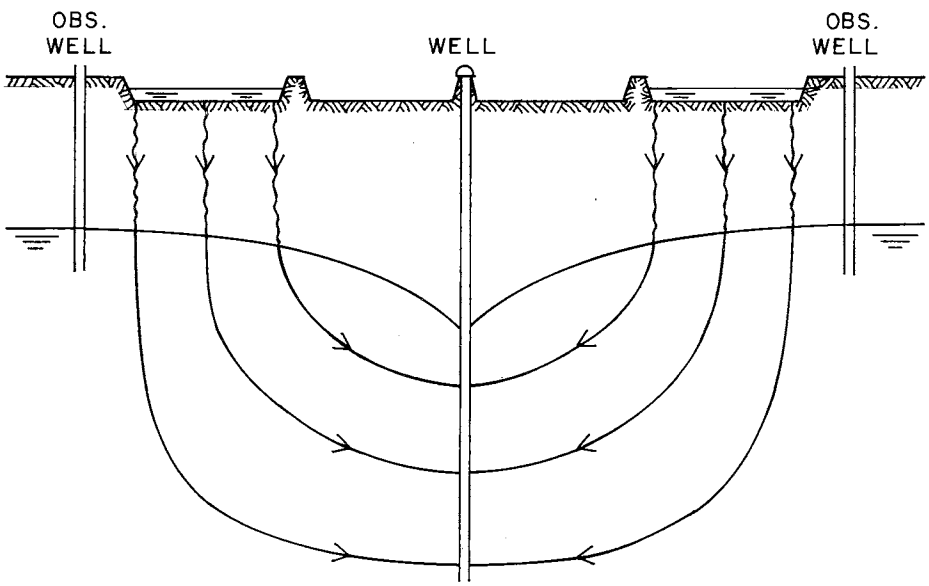

Figure 3. Schematic vertical cross section of system in Figure 1.

clogging and producing low infiltration rates. The situation will be remedied by constructing a bypass channel in the 8-acre pond to transport secondary effluent directly into the infiltration basins.

STOP NO. 2. GRAVEL PIT

Gravel excavation northeast of the infiltration basins offers an excellent opportunity for examining the local geologic profile to a depth of about 30 feet (fig. 4). The gravel-pit walls show typical "river run" sand and gravel layers, microstratification, imbrication, and layers of manganese-oxide coated gravel indicative of past water-table positions. Analysis of the response of the water table to infiltration at the Flushing Meadows Project showed that the sand and gravel layers as a whole had a hydraulic conductivity of 282 ft. per day horizontally and 17.6 ft. per day vertically. Hence, the medium was anisotropic with a horizontal to vertical hydraulic conductivity ratio of about 16.

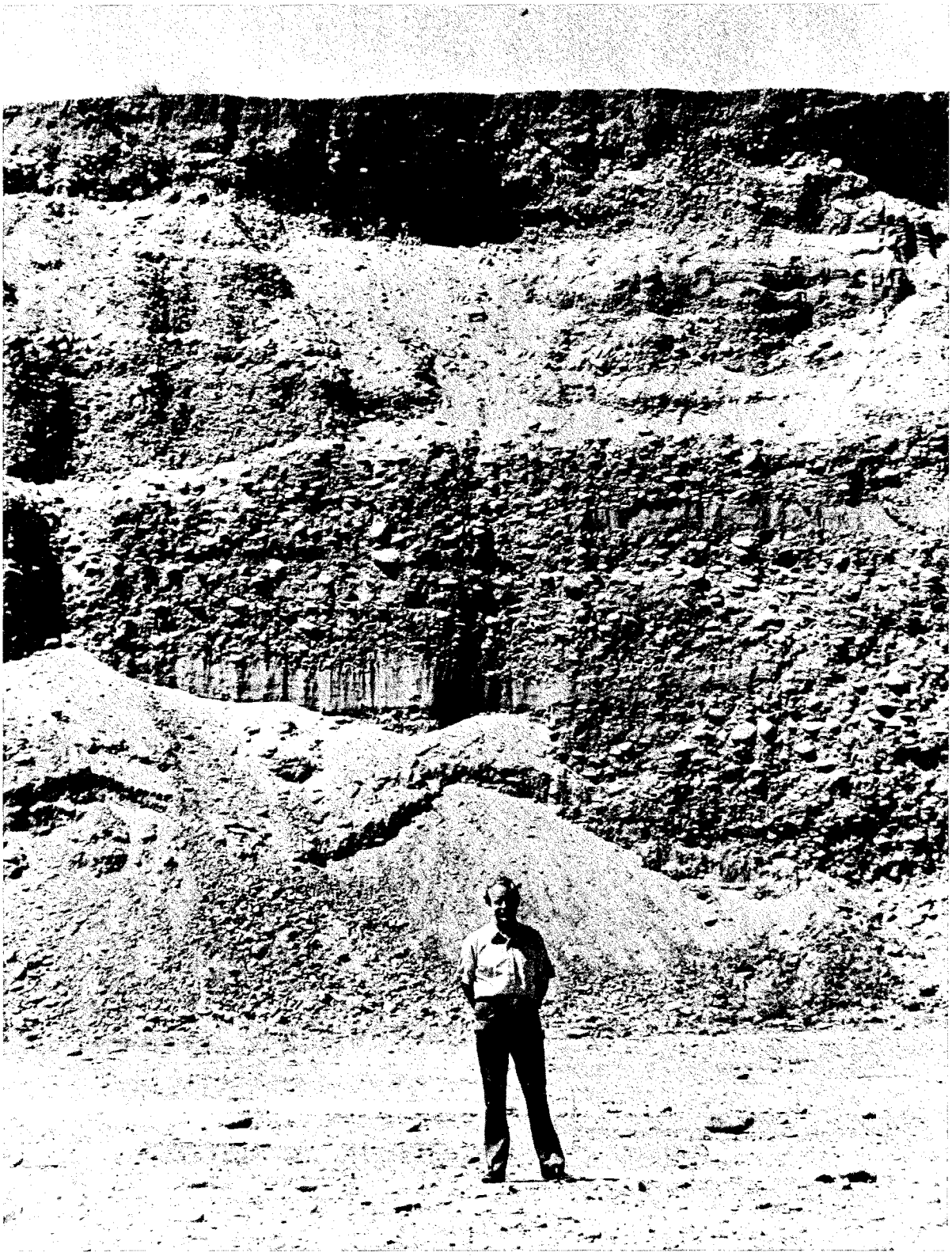

Figure 4. Wall of gravel pit northwest of infiltration basins showing sand and gravel layers.

PRECAMBRIAN METAVOLCANIC ROCKS OF THE SQUAW PEAK AREA, MARICOPA COUNTY, ARIZONA

by
Douglas G. Thorpe and
Donald M. Burt

Department of Geology
Arizona State University

This one-half-day field trip involves a 1,200 ft. (366 m) climb up a steep but well-maintained mountain trail. Sturdy shoes and a one-quart canteen are recommended; field glasses and a camera are optional for the view at the top. The trip takes place entirely within Squaw Peak Park of the City of Phoenix, in which rock and mineral collecting are prohibited.

INTRODUCTION

Squaw Peak Park of the City of Phoenix provides challenging mountain trails, parking, picnic facilities, comfort stations, and water fountains within minutes of downtown Phoenix. It is consequently a very popular park, especially the trail up Squaw Peak, maintained by a volunteer group of high school students. Squaw Peak itself (elev. 2,608 ft. or 795 m) is the highest of the Phoenix Mountains and its summit provides a striking view of the city and surrounding region. Its exact location is Sec. 2, T.2 N., R.3 W. in the Sunnyslope 7.5 min topographic quadrangle, U.S. Geol. Survey (1965–73), but its distinctly pointed profile can be recognized from almost anywhere in the Phoenix area (see fig. 1).

The northwest-trending Phoenix Mountains are typical block-faulted mountains of the Basin and Range physiographic province. They consist of steeply dipping, weakly metamorphosed Precambrian volcanics and clastic sediments that generally strike about N.30°E. Previous studies of the area include a study of mercury occurrences by Schrader (1918), the county map by Wilson, et al. (1957), and an abstract by Maisano and Malone (1973). In addition, the Phoenix Mountains were mapped as part of an environmental study by Shank (1973) and the pegmatite-bearing rocks of Mummy Mountain, east of Squaw Peak, were mapped in detail by Aylor (1973). This report incorporates the preliminary results of a thesis study by Thorpe (in progress, 1978).

Figure 1. Squaw Peak. View from 24th Street and Lincoln Drive, Phoenix.

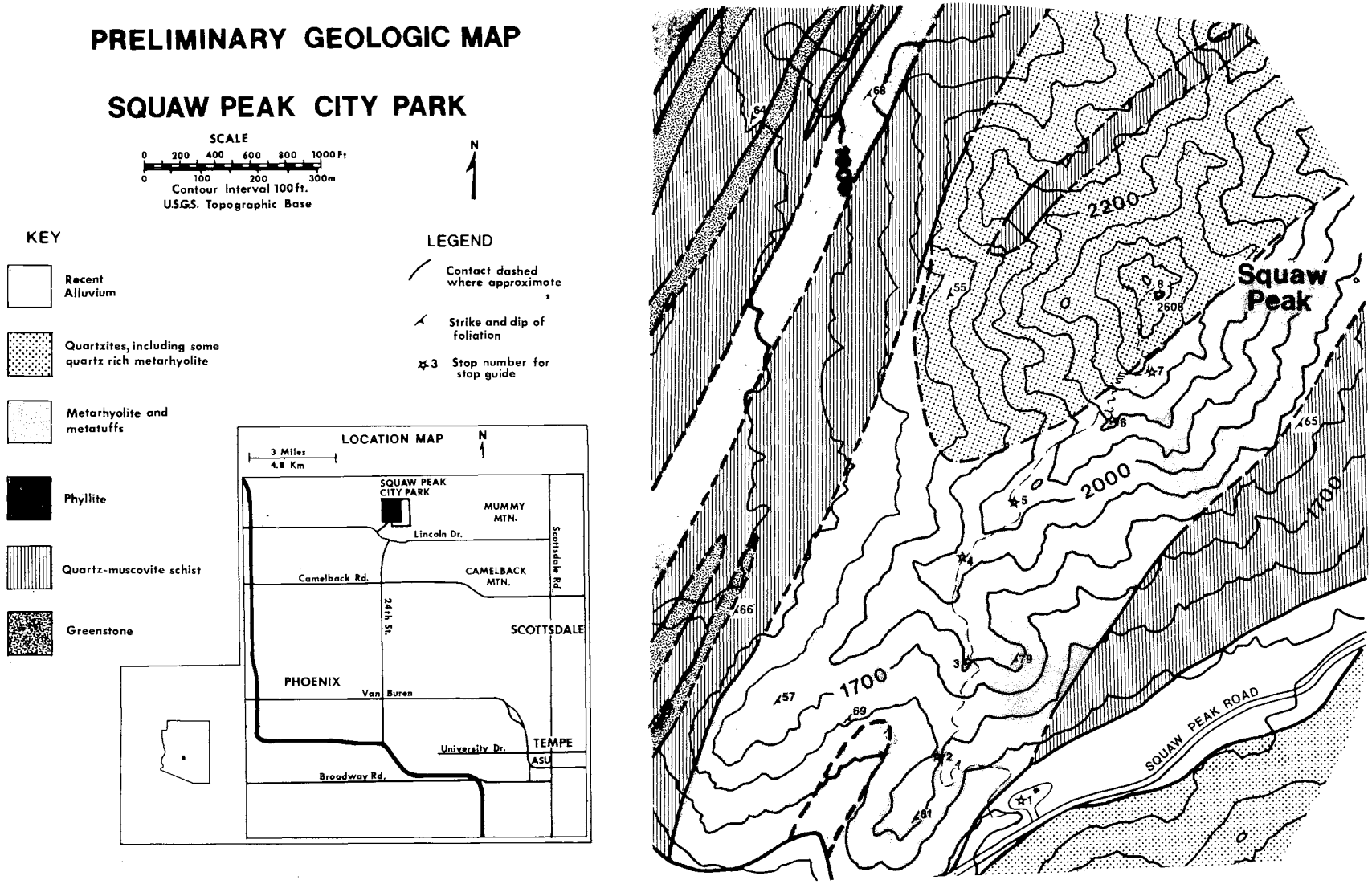

Figure 2. Preliminary geologic map of a portion of Squaw Peak Park. Inset shows location.

STRATIGRAPHY AND PETROLOGY

Stratigraphically, the lowermost units in the park are gray phyllites and micaceous brown quartzites and schists on the south side of Squaw Peak road. A thick sequence, 400–500 m across, of metarhyolites and metatuffs overlies these rocks. In the northeastern area of the park the metarhyolites and metatuffs are interbedded with massive, white, cross-bedded quartzites and thin, discontinuous pelitic zones. The metarhyolites and metatuffs are overlain by micaceous quartzites, greenstones, phyllites, and micaceous metaconglomerates. Precambrian greenstone dikes locally cut the other units. Thin dikes of Tertiary basaltic rocks also occur in the area but are not common. Many of these units are shown on the preliminary geologic map (fig. 2).

The metarhyolites and metatuffs vary considerably in their present textures and mineralogy. Quartz phenocrysts are everywhere recognizable, but feldspar phenocrysts are recognizable in only a few areas. Most of the metatuffs and metarhyolites now consist of quartz-muscovite schist, in places containing accessory viridine or piemontite, and quartz-kyanite schist. Chloritoid is rare. The accessory viridine and piemontite only occur in schists of a pale pinkish color. The pink color may be due to Mn^{3+} in the muscovite (Gresens and Stensrud, in press). Viridine and piemontite also contain Mn^{3+}, although viridine is green.

The areas of relatively fresh-appearing metarhyolite, quartz-muscovite schist, and quartz-kyanite schist are somewhat irregular in distribution and appear to grade into each other laterally as well as vertically.

The massive quartzites near the summit and to the NE of Squaw Peak are medium to fine grained and commonly contain excellently-preserved cross-bedding delineated by black magnetite-rich mineral trains in otherwise clean, white quartzite.

STRUCTURE

The cross-bedding in the quartzites indicates that bedding is overturned with tops to the west. The strike, as elsewhere in the Phoenix Mountains, is predominantly N.30°E., and the dip 60-85°E.

Metamorphic foliation is generally well-developed in all rock types except the quartzites and the Tertiary dikes. The foliation is generally parallel to the strike of the bedding and is also steeply dipping. Isoclinal folds, readily visible in dark bands rich in iron and manganese oxides, are common in the metatuffs and metarhyolites. The axial planes of these folds parallel the foliation.

Stretched quartz-rich pebbles are locally abundant in some of the metatuffs. Their intermediate and long axes lie in the plane of the foliation, and their long axes generally parallel the dip of the foliation. Elliptical zones of gray to greenish muscovite in the foliation plane have been interpreted by Maisano and Malone (1973) as stretched and flattened pumice fragments. Kink-banding of schist was also described by these authors, but it is not especially evident along the trail up Squaw Peak.

At least two generations of quartz veins are recognizable in the Squaw Peak area. The earlier quartz veins are fractured and slightly deformed and commonly contain large (1-10 cm) radial to parallel aggregates of pale blue-green to colorless kyanite crystals at their schist contacts. The orientation of the kyanite blades is perpendicular to the schist contacts. The later quartz veins do not contain kyanite, are generally unfractured, and tend to form *en echelon* sets.

MINERALOGY AND ALTERATION

The rocks of the Squaw Peak area contain a number of distinctive metamorphic minerals: viridine (greenish Mn-rich andalusite), piemontite (pinkish Mn-rich clinozoisite), and chloritoid, in addition to kyanite, pyrophyllite, muscovite, magnetite, hematite, and numerous other minerals. The Al-rich silicates andalusite, kyanite, chloritoid, and pyrophyllite suggest a metamorphic environment that was low in alkalis, because otherwise the alkalis would have reacted with these minerals to produce micas and feldspars.

The question arises, how and when did the rhyolitic volcanics locally lose their alkalis—before, during, or after regional metamorphism? Maisano and Malone (1973) suggest that kyanite and sericite formed from "late circulating hydrothermal solutions." The present authors would prefer to hypothesize that most of the leaching of alkalis was premetamorphic, due to surficial and/or hydrothermal alterations of the rhyolitic tuffs shortly after deposition.

The leaching processes involved have been characterized by Hemley and Jones (1964; *cf*. Burt, 1976) as an exchange of protons (H^+) for alkali ions (K^+ and Na^+) during neutralization of acidic solutions by country rocks. The resulting altered rocks are alkali-poor and contain clay minerals such as kaolinite and pyrophyllite in place of feldspars and muscovite. Regional metamorphism then produces rocks consisting of quartz with kyanite, andalusite, and in iron-rich areas, chloritoid as at Squaw Peak.

Gresens (1971) proposed a similar model for the formation of kyanite deposits in northern New Mexico. His model, however, implied that the alteration took place within the kyanite stability field (i.e., during metamorphism).

During Squaw Peak metamorphism abundant Mn^{3+} appears to have been available locally, as shown by the minerals viridine and piemontite. Viridine can form in coexistence with kyanite because Mn^{3+} stabilizes the andalusite structure well into the kyanite stability field (Heinrich and Corey, 1957; Strens, 1968; Abs-Wurmback and Langer, 1975).

Retrogressive mineral reactions presumably include the local sericitization of bladed kyanite in "early" quartz

veins, the growth of poikilitic andalusite around green cores of viridine, and the late formation of pyrophyllite along joints and fractures in the metatuffs.

The maximum grade of metamorphism reached is revealed by the absence of pyrophyllite (except along late fractures), the presence of andalusite with kyanite, and the presence of chloritoid instead of staurolite or almandine in iron-rich areas. Based on data summarized in Winkler (1976), Day (1976), and Anderson et al. (1977), it is relatively low (upper greenschist facies, say 350–450°C, 2.5–4.0 kb). The greenstones and greenschists of the area have not yet been studied in detail, but it is interesting that garnet of unknown composition appears in a slightly copper-stained greenstone dike about midway up the Squaw Peak trail.

ACKNOWLEDGEMENTS

D. M. Ragan and M. F. Sheridan are to be thanked for giving us access to specimens collected by them and for stimulating discussions in the field. We are also grateful to R. L. Gresens for reprints on New Mexico localities and H. L. Stensrud for samples from these localities.

REFERENCES CITED

Abs-Wurmback, I. and Langer, K. (1975) Synthetic Mn^{+3} -kyanite and viridine, $(Al_{2-x}Mn^{3+})SiO_5$ in the system Al_2O_3-MnO-MnO_2-SiO_2, Contrib. Mineral. Petrol., vol. 49, p. 21–38.

Anderson, P.A.M., Newton, R. C. and Kleppa, O. J. (1977) The enthalpy change of the andalusite-sillimanite reaction and the Al_2SiO_5 diagram., Am. Jour. Sci., vol. 277, p. 585–593.

Aylor, J. G. (1973) The geology of Mummy Mountain, Phoenix, Arizona, unpubl. M.S. thesis, Ariz. State Univ., 86 pp.

Bailey, E. H. (1969) Mercury, *In* Mineral and Water Resources of Arizona, Univ. Ariz., Ariz. Bur. Mines, Bull. 180, p. 226–230.

Burt, D. M. (1976) Hydrolysis equilibria in the system K_2O-Al_2O_3-SiO_2-H_2O-$C1_2O_{-1}$ Comments on topology, Econ. Geol., vol. 71, p. 665–671.

Cordy, Gail (1978) Environmental geology of the Paradise Valley quadrangle, Maricopa County, Arizona, Part II., unpubl. M.S. thesis, Ariz. State Univ., in prep.

Day, H. W. (1976) A working model of some equilibria in the system alumina-silica-water, Am. Jour. Sci., vol. 267, p. 1254–1284.

Gresens, R. L. (1971) Application of hydrolysis equilibria to the genesis of pegmatite and kyanite deposits in northern New Mexico, Mountain Geologist, vol. 8, p. 3–16.

——, and Stensrud, H. L. (1977) More data on red muscovite, Am. Mineralogist (in press).

Heinrich, E. W. and Cory, A. F. (1959) Manganian andalusite from New Mexico, Am. Mineralogist, vol. 44, p. 1261–1271.

Hemley, J. J. and Jones, W. R. (1964) Chemical aspects of hydrothermal alteration with emphasis on hydrogen metasomatism, Econ. Geol., vol. 59, p. 538–569.

Maisano, M. D. and Malone, G. B. (1973) Petrology and provenance: Precambrian metamorphic sequence, Squaw Peak, Phoenix, Arizona, Ariz. Acad. Sci., vol. 8, Proc. Suppl., p. 41.

Schrader, F. C. (1918) Quicksilver deposits of the Phoenix Mountains, Arizona, U. S. Geol. Survey Bull. 690-D, p. 95–107.

Shank, D. (1973) Environmental geology in the Phoenix Mountains, Maricopa County, Arizona, unpubl. M.S. thesis, Ariz. State Univ., 86 pp.

Strens, R. G. T. (1968) Stability of Al_2SiO_5 solid solutions, Mineral. Mag. vol. 36, p. 839–849.

Wilson, E. D. and Roseveare, G. H. (1949) Arizona nonmetallics, Univ. Ariz., Ariz. Bur. Mines, Bull. 155, 2nd ed., revised, 60 pp.

Wilson, E. D., Moore, R. T. and Peirce, W. (1957) Geologic map of Maricopa County, Arizona, Univ. Ariz., Ariz. Bur. Mines.

ROAD LOG

MILES Interval	Total	
0.0	0.0	Begin at parking lot behind Physical Sciences Center, F-wing (Geology-Physics), A.S.U. campus. Turn right on University Rd.
0.3	0.3	Turn north on Scottsdale Rd.
0.5	0.8	To the left is Tempe Butte with Sun Devil Stadium at its eastern end. The butte is a fault block that has been tilted to the south. The lower part consists of siltstones and sandstones containing mud cracks, ripple marks, and imprints of palm fronds. The upper third of the section is Middle to Late Tertiary porphyritic andesite flows.
0.3	1.1	Cross the Salt River
0.8	1.9	Cross the Arizona Canal
4.8	6.7	Camelback Mountain is to the left. See Mile 9.3.
1.3	8.0	Turn left (west) at the light onto Lincoln Rd.
1.2	9.2	On the right is Mummy Mountain, which marks the eastern end of the Phoenix Mts. It consists of Precambrian schists and amphibolites cut by numerous white pegmatite dikes. The pegmatites are poorly zoned and generally have a simple mineralogy, including quartz, muscovite, microcline, albite, biotite, and accessory garnet, tourmaline, magnetite, and beryl, with minor columbite-tantalite and niobian rutile. Graphic granite occurs in a few places (Aylor, 1973).
0.1	9.3	On the left is Camelback Mountain, a fault block uplifted during Basin and Range tectonism. The eastern part or "Camel's Hump" is highly fractured Precambrian granite. This is overlain at the western end of the mountain by the Camel's Head formation, a Tertiary fanglomerate. Beneath the Praying Monk, a rock promontory on the "Camel's head," can be seen the trace of the northwest-dipping fault (gravity slide?) which separates the Precambrian granite from the overlying Tertiary fanglomerate. Active boulder trains formed by spheriodal weathering of granite pose a potential hazard to residents of the area as do debris movements. In September, 1976, local heavy

rains carried tons of rock debris down the washes, depositing it in the swimming pools, carports, patios, and living rooms of the residents (Cordy, 1978).

4.7	14.00	Intersection at 24th Street. Stay on Lincoln Rd.
0.5	14.5	Turn right at traffic signal onto Squaw Peak Rd. (Follow sign to Squaw Peak Park.)
0.7	15.2	Turn left into the first paved parking lot on entering the city park. The pavilion and water fountain lie at the foot of the hiking trail up Squaw Peak.

STOP GUIDE

Innumerable stops will be made along the trail at points to be designated by the trip leaders. The numbers in the guide that follows refer to regions of the trail rather than to specific locations. Remember to fill your canteen at the water fountain and to leave your hammers in the cars or bus (no collecting allowed!).

1. FOOT OF TRAIL TO FIRST SADDLE

The blocky, light-colored outcrops in this portion of the trail are of relatively unaltered metarhyolite. In many places, 1 to 3 mm quartz and feldspar phenocrysts are clearly visible in a pale tan to reddish sericitic matrix. The ellipsoidal grayish-green areas on the foliation are sericite. Maisano and Malone (1973) suggest that these areas represent deformed and altered pumice fragments, with axial ratios 35:8:1.

2. FIRST SADDLE TO FIRST OVERLOOK

2a The pinkish altered rhyolite begins to contain viridine-rich layers in the plane of foliation.

2b Younger quartz veins occur to the west, towards the southern end of the ridge. The quartz-muscovite schist contains a few cobbles of rhyolite and quartzite. In the proper light, kink bands may be visible in the schist. Return to the saddle and continue up the main trail.

2c The large caliche-cemented kinks and folds in the schist are the result of creep (slow surface ground movement due to gravity). The large block of schist to the south has slowly rotated away from the main hillside until now the foliation dips northwest. The wedge behind the tilted block is filled with folded schist from above. Many other good examples of creep are visible higher up the trail.

2d A small outcrop of a Tertiary basalt dike occurs in the trail just above the contorted schist.

3. FIRST OVERLOOK TO SECOND SADDLE

3a Much of the fine white coating of joint surfaces in the massive blocks is fine-grained pyrophyllite. Rarely small radiating clusters are visible. Large poikiloblastic andalusite grains also occur in this area. Most have viridine cores visible in thin section.

3b A prominent ridge visible from the saddle extends to the southeast. The furthest ridge crest is of blocky unaltered metarhyolite with quartz and feldspar phenocrest (*cf.* **STOP 1**). The saddle is dark quartz-kyanite schist consisting of at least 50 percent kyanite as black radiating clusters in the plane of the foliation. The closer ridge crest is pinkish schist with viridine and occasional piemontite.

4. SECOND SADDLE TO THIRD SADDLE (Along southeast side of ridge.)

To the northwest are the Phoenix Mountains. To the northeast are Camelback, Papago Buttes, and Tempe Butte. The resistant blocky rock here is quartz-kyanite schist. Isoclinal folds are common, but kyanite in the noses of the folds is not folded. Original quartz phenocrysts are still present in the rock.

5. THIRD SADDLE TO FOURTH SADDLE (With palo verde tree and prospect pit.)

5a More isoclinally folded schist crops out in the third saddle. The quartz-muscovite schists in the valleys to the southeast also contain isoclinally folded black layers. Wherever the schist is pinkish, viridine or piemontite occur concentrated along the black layers.

5b Dikes of greenstone with small garnets and slight copper stain occur along the trail as do early quartz veins with rims of colorless kyanite. Just below the fourth saddle are good outcrops of metaconglomerate.

6. FOURTH SADDLE TO GUARD RAIL

6a Prospect pits, such as the one at the fourth saddle, are common at Squaw Peak. This one was apparently dug on traces of malachite on the outcrop, but others were dug on quartz veins in search of gold or mercury. The only economic mineral production from Squaw Peak was 38 tons of kyanite removed during World War II, before the area became a city park (Wilson and Roseveare, 1949, p. 43). Less than 100 flasks of mercury were produced in other parts of the Phoenix Mountains (Bailey, 1969, p. 228).

6b In the prospect pit is a dark metapelite containing darker spots of chloritoid. More metapelite with chloritoid occurs further up the trail.

7. GUARD RAIL TO SUMMIT

7a At the guard rail continue up the trail (to the left). Be careful here; the trail becomes very steep. Note more chloritoid spots to the left.

7b At a switchback, note the large quartz vein with pale blue bladed kyanite at the margins. The kyanite, which is normally very resistant to erosion (the backbone of Squaw

Peak is kyanite quartzite), has here been selectively attacked by hammers. This is a good example of the handiwork of inconsiderate (and illegal) collectors. Continue to the peak and enjoy the view.

8. SUMMIT OF SQUAW PEAK

In addition to the features already mentioned (Camelback, Mummy Mountain, Tempe Butte, etc.), the summit provides a clear view of Paradise Valley extending north to Cave Creek, Carefree, and New River Mesa. To the northwest are the Phoenix Mountains, with the Hieroglyphics and Bradshaws beyond. To the west are the Precambrian White Tank Mountains, to the southwest the Sierra Estrellas, and directly to the south is Phoenix South Mountain Park, where, for a small fee, you can drive your car to an overlook for a southern view of the city.

To the east are the Tertiary volcanics of the Superstitions, with the Goldfield and Usery Mts. in the foreground. To the northeast, beyond Paradise Valley and Scottsdale, are the Precambrian schists of the McDowell Mts. and beyond them the Precambrian Mazatzal Mts., marked by the distinctive profile of Four Peaks. With field glasses you can see Grady Gammage auditorium on the ASU campus, but the geology building is hidden behind Tempe Butte.

Return down the trail the same way you came up, and watch your footing. If you didn't bring a canteen, head straight for the water fountain at the foot of the trail.

The return to Tempe can be made via 24th Street and the freeway (I-10), if desired.

EARTH FISSURES AND LAND SUBSIDENCE, EASTERN MARICOPA AND NORTHERN PINAL COUNTIES, ARIZONA

by
R. H. Raymond
U.S. Bureau of Reclamation
Carl C. Winikka
Arizona Dept. of Transportation
R. L. Laney
U.S. Geological Survey

INTRODUCTION

In 1975 about 5.5 million acre-feet of ground water was pumped from the permeable alluvial deposits in the Basin and Range Physiographic Province of Arizona. About 159 million acre-feet of ground water has been withdrawn from this area since about 1900. Withdrawals of ground water greatly have exceeded the amount of natural recharge; therefore, the water came mainly from storage, and in effect was mined as a nonrenewable resource. As water levels declined the dewatered part of the alluvial deposits were subjected to stress, the land surface subsided and earth fissures developed (fig. 1). Land subsidence and earth fissures have damaged roads, streets, railroads, a reservoir, canals, irrigation-distribution systems, wells, and farmland and have caused the rerouting of a major aqueduct. These processes are continuing.

FIELD TRIP

This field trip was designed to show examples of earth fissures in known areas of water-table decline and land subsidence. Locations were selected to provide a convenient day's excursion from Tempe (fig. 2). The trip assembly point is Arizona State University in Tempe.

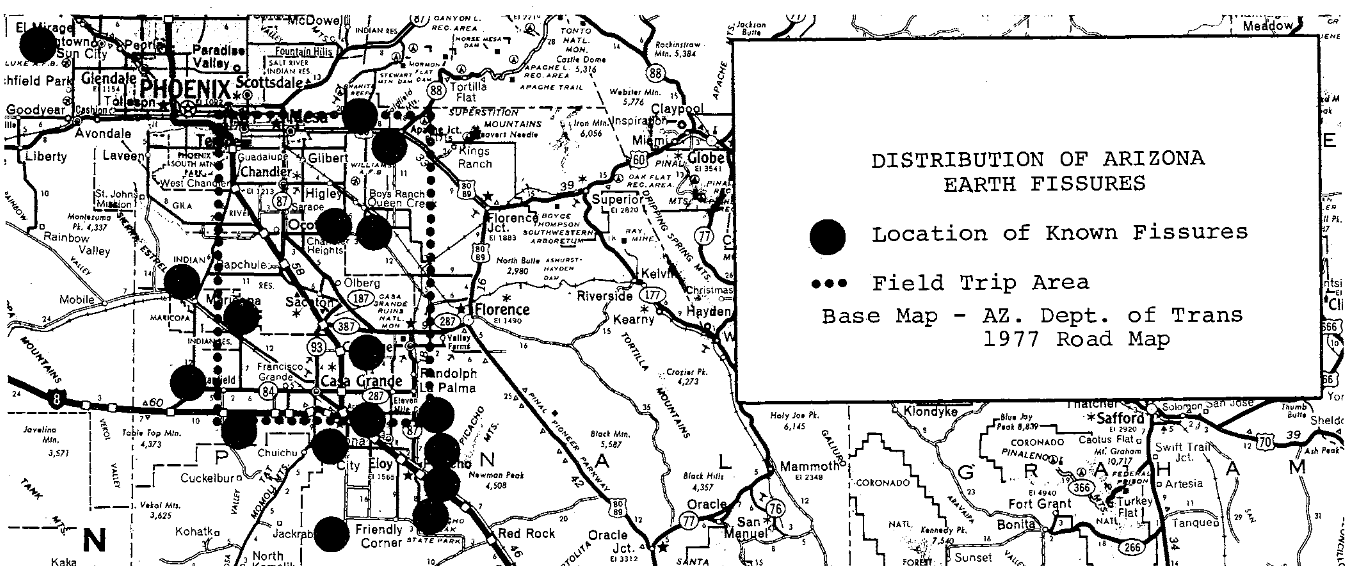

Figure 1. Map showing distribution of Arizona earth fissures.

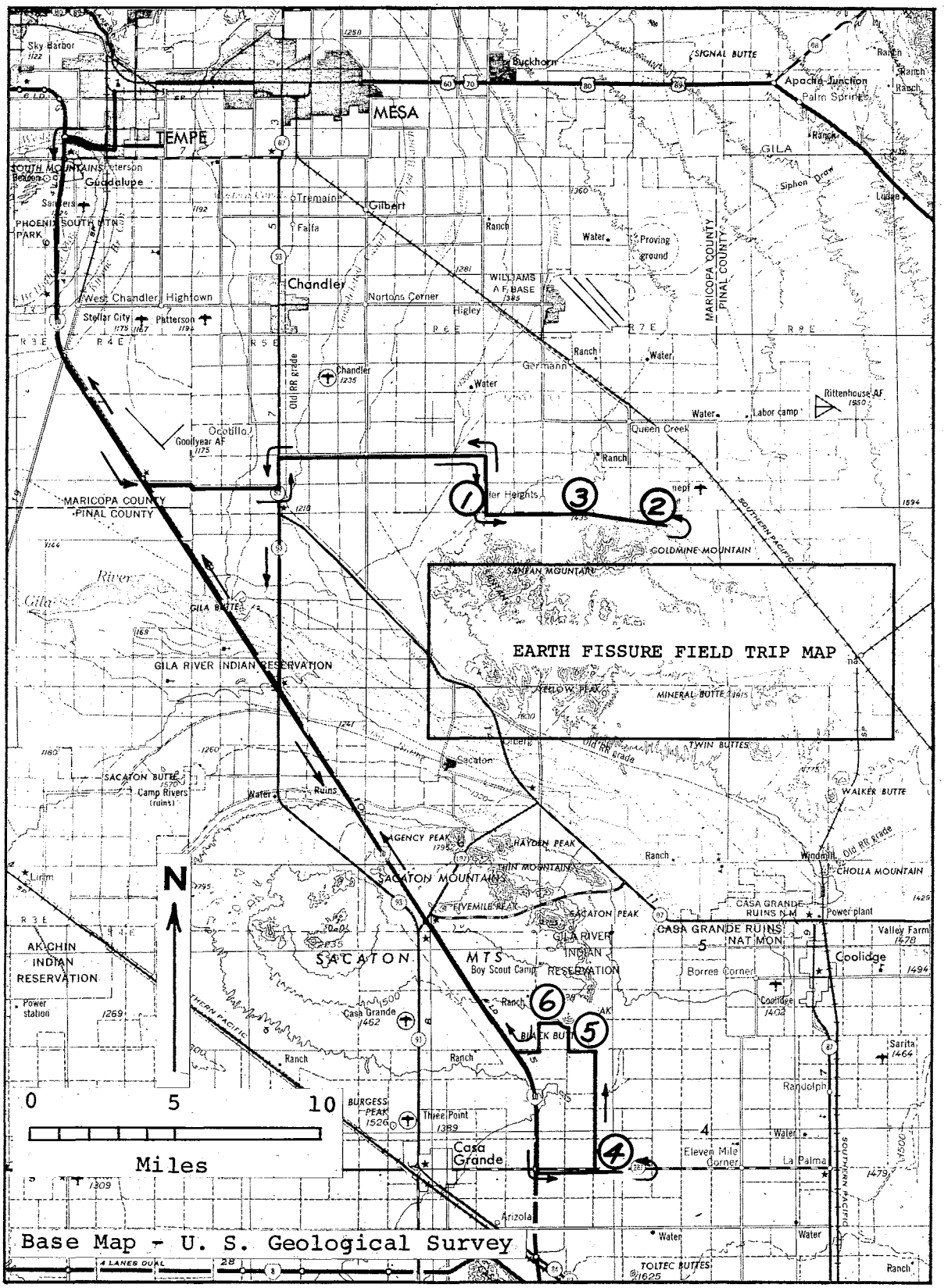

Figure 2. Map showing location of stops on field trip.

The field trip will traverse an area of broad, gently sloping plains that are partly surrounded by low, abruptly rising mountain ranges. Altitudes of the plains range from 1,100 to 1,500 feet and that of the mountains from 1,300 to 3,000 feet. The plains are underlain to a depth of a few thousand feet by alluvial deposits that consist of unconsolidated to semiconsolidated clay, silt, sand, and gravel. The upper 1,200 feet of the allvial deposits contain most of the recoverable ground water. The mountains consist of gneiss, schist, and granite, and compared to the alluvial deposits, are relatively impermeable.

The route leads south across agricultural land to the Chandler Heights area on the north side of the San Tan Mountains. In this area the water table has declined as much as 400 feet since 1923 and the land surface subsided 3 to 5 feet from 1948 to 1967 (Schumann, 1974). Stops will be made to provide an opportunity to examine and discuss numerous well-developed, erosionally-enlarged earth fissures, which we refer to as fissure-gullies (U.S. Geological Survey, unpublished manuscript). Some of the fissure-gullies have as much as 1.5 feet of vertical offset. The route continues south to an area northeast of Casa Grande and south of the Sacaton Mountains. The water in this area has declined about 150 feet since 1923, and the land surface has subsided about 2 feet since 1962. Earth fissures in a residential area and a protruding well casing will be seen. The return route to Tempe will be via the Gila River Indian Reservation and will include a stop at their art and craft shop and museum. The field trip will end at the ASU campus in Tempe.

REFERENCES

Jennings, Mark D., 1977, Geophysical investigations near subsidence fissures in northern Pinal and southern Maricopa Counties, Arizona: unpublished Masters thesis, Arizona State University, Tempe, Arizona, 103 p.

Schumann, H. H., 1974, Land subsidence and earth fissures in alluvial deposits in the Phoenix area, Arizona: U.S. Geol. Survey Map I-845-H.

ROAD LOG

Persons following this road log are advised to obtain permission of landowners prior to entering areas described in this guide book. Fissure-gullies are unstable and hazardous; and watch your step while in the vicinity.

MILES Interval	Total	
0.0	0.0	Earth fissure tour mileage begins at ASU (University and Mill Avenue) and follows Mill Avenue south to the Superstition Freeway, west on the Superstition Freeway to I-10, then south on I-10 to the Riggs Road interchange.
16.0	16.0	Turn east on Riggs Road. Note ground water pumps along Riggs Road.
2.3	18.3	Sun Lakes development south of Riggs Road
2.5	20.8	Turn north on State Highway 87 for 1 mile.
1.0	21.8	Turn east on Chandler Heights Road.
6.0	27.8	Road crosses flood control channel.
1.0	28.8	Turn south on Higley Road.
1.6	30.4	**STOP 1.** At this location a relatively short fissure-gully extends westward from the road in a direction approximately normal to the drainage. Although the fissure is about 2,000 feet from rock exposures in the mountains, recent geophysical data indicate that the alluvium here is only 150 to 200 feet thick (Jennings, 1977). In April, 1977, only a small amount of surface runoff had been captured by this fissure. As a result, only a small, discontinuous gully 1 to 3 feet deep had been eroded along the fissure interspersed with bridges of undisturbed material (fig. 3).
0.5	30.9	Turn east on Hunt Highway.

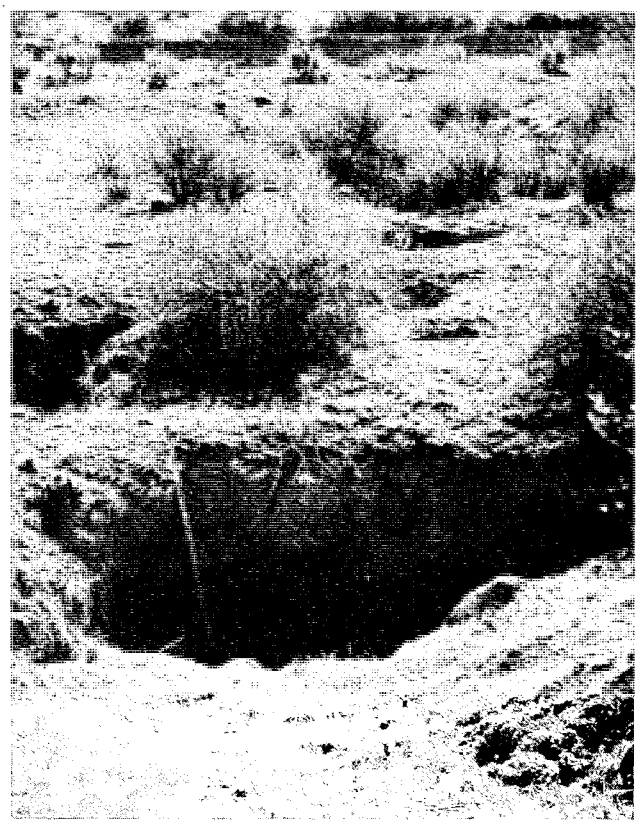

Figure 3. Line of holes along the trace of earth fissure at STOP 1. Note interconnecting tunnel by meter stick.

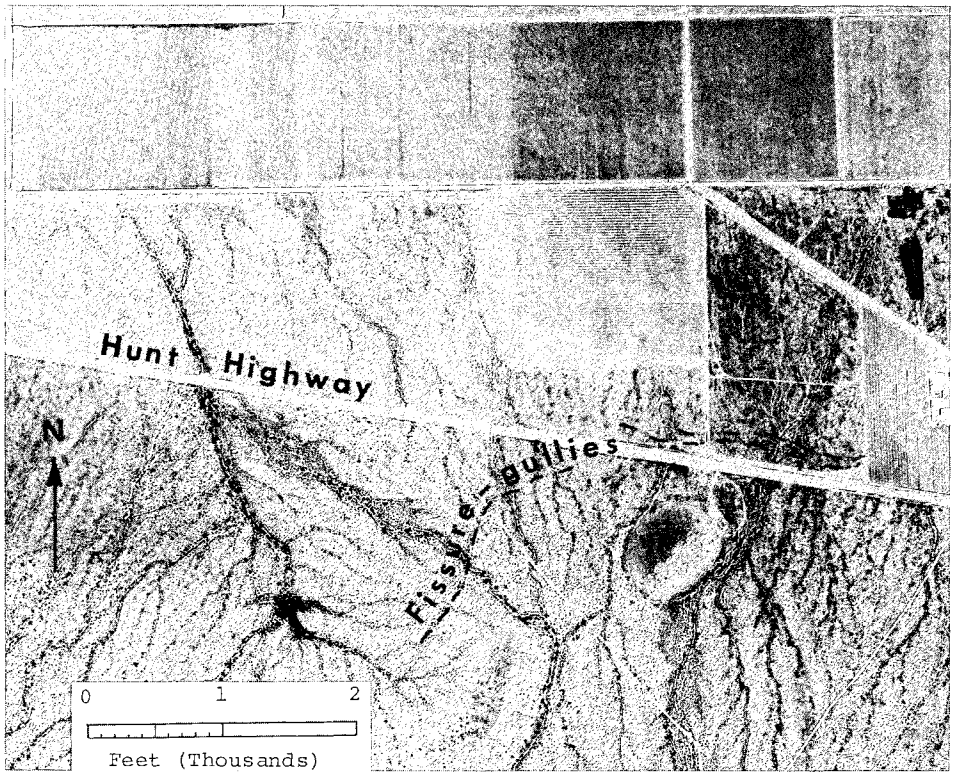

Figure 4. Aerial view of fissure gullies at STOP 2. Note influence of rock knob on the location and pattern of these gullies.

5.9 36.8 **STOP 2.** Here a complex of fissure-gullies surrounds the metamorphic rock knob on the north, east, and west sides (fig. 4). Vertical displacement is present along the two parallel fissure-gullies on the north side and has broken and tilted a concrete-lined ditch. The area between these gullies is displaced downward like a graben. Maximum displacement on the fissure-gully nearest Hunt Highway was more than 1.5 feet in April, 1977 (fig. 5). The fissure-gully on the basin side had less displacement. Near the orchard to the east, the vertical displacement and the surface evidence of the fissures was discontinuous. In places where the fissures extended to the surface, displacement of up to 6 inches was observed, but intervening areas had no apparent displacement. North-trending, nearly parallel fissure-gullies flank the bedrock knob on the east. One of these fissure-gullies had up to 0.5 foot of displacement in April, 1977. The east side was down with respect to the western side. In places the surface material had a coarser texture on the west side.

The fissure-gully on the west side of the knob is discontinuous. No displacement and little erosion was observed along this fissure-gully in April, 1977.

The orientation of these fissures close to and surrounding a bedrock knob may be related to the forming mechanism. Displacement along the fissure-gullies appears to have occurred mostly since the summer of 1976 (Mark Jennings, oral communication). At that time no displacement was evident on the fissure-gully on the east side of the knob and only a small amount was present on the fissure-gully near the Hunt Highway.

0.0 36.8 Turn around and drive west on Hunt Highway for 2.8 miles.

2.8 39.6 **STOP 3.** A fissure-gully crosses Hunt Highway here, but is not readily evident from the road. Prominent features of the fissure-gully can be seen both to the north and south of Hunt Highway. The side road to the north provides easy access to the fissure-gully.

This wide, deep fissure-gully runs parallel to the drainage which probably accounts for the extensive erosion along it (fig. 6), and is the largest in depth and width yet observed in Arizona. It was observed during a cloud burst in the early 1960's completely filled by rushing water (G. D. Ford, oral communication). Notice the parallel cracks and slump structures along the sides. Several cycles of

Interleaf. A large earthcrack located on the south side of Chandler Heights on Hunt Road, 1¼ miles east of Powers Road on the boundary between Maricopa and Pinal counties. Earthcracks are caused by land subsidence, the result of groundwater withdrawal. The Santan Mountains are in the background. The crack is open to a depth of at least 50 feet. (Photograph No. 3357 taken July 25, 1972 by Troy L. Péwé.)

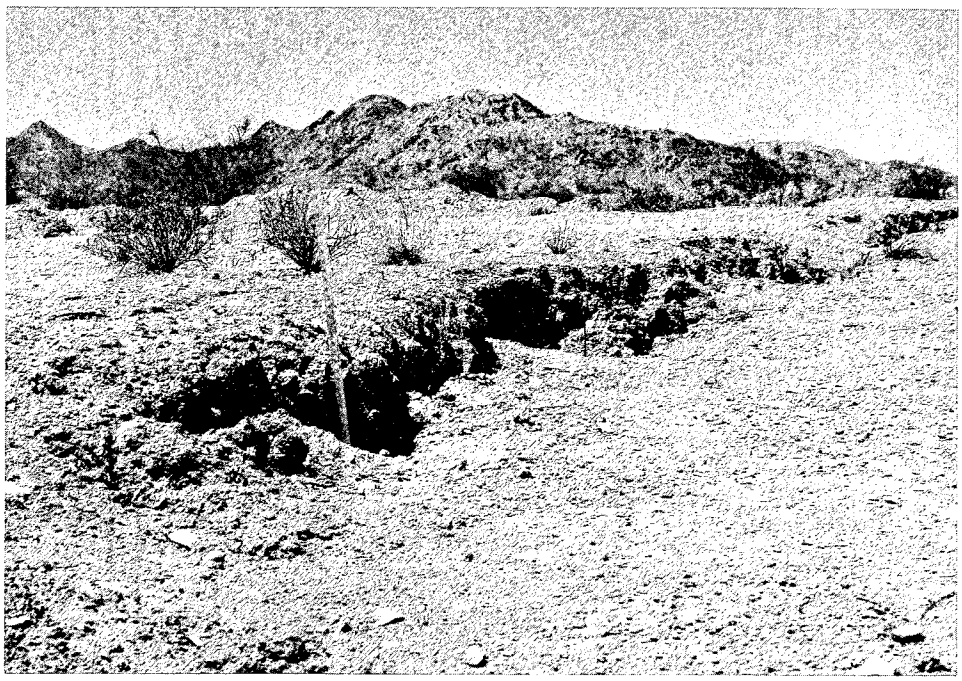

Figure 5. Offset along fissure gully at STOP 2. Stick is 1 meter long.

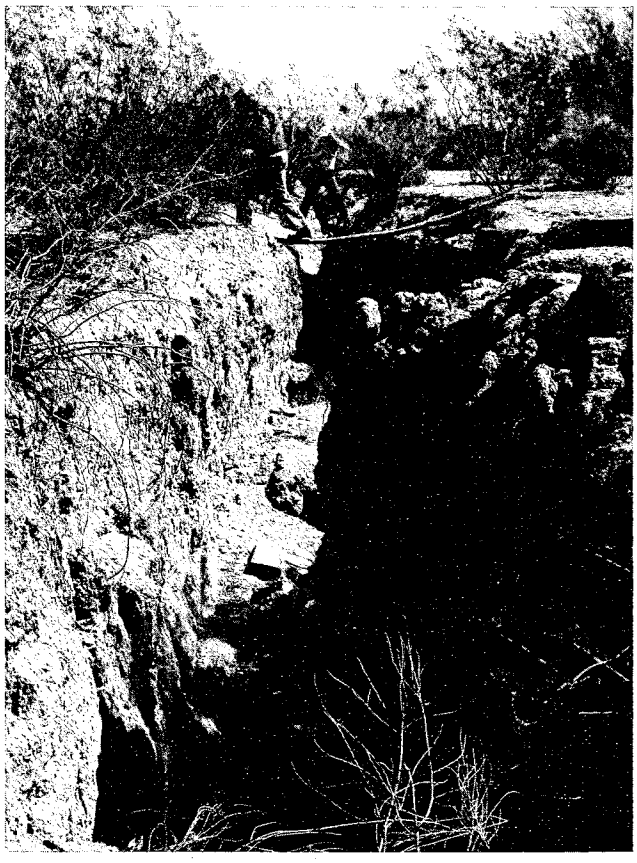

Figure 6. Deep fissure gully at STOP 3. This fissure gully is parallel to the natural drainage and has captured the runoff from a considerable area.

erosion and deposition are evident in the gully along this fissure.

3.1	42.7	Turn north on Higley Road.
2.0	44.7	Turn west on Chandler Heights Road.
7.0	51.7	Turn south on State Route 87.
7.9	59.6	Turn from State 87 southeast along Interstate 10.
19.2	78.8	Turn east on State 287 from Interstate 10 Interchange.
2.5	81.3	**STOP 4.** A well casing on the north side of the road protruding about 1 foot above the ground surface (fig. 7) is obvious evidence of land subsidence that has taken place in this basin. Since the well was about 400 feet deep when originally drilled in 1955, at least 1 foot of the consolidation took place in that interval. Two miles west of here, measured land subsidence between 1962 and 1977 was about 1.2 feet. The maximum measured subsidence in Arizona is 12.5 feet from 1952 to 1977 in the Eloy vicinity south of here. Records from a compaction recorder at Eloy indicate that consolidation of material penetrated by an 830-foot-deep well account for about 65 percent of the land subsidence.
0.0	81.3	Turn around and drive west on State 287.
0.5	81.8	Turn north on Overfield Road.
4.0	85.8	Turn west on McCartney Road.
1.0	86.8	Turn north on Sunland Gin Road.

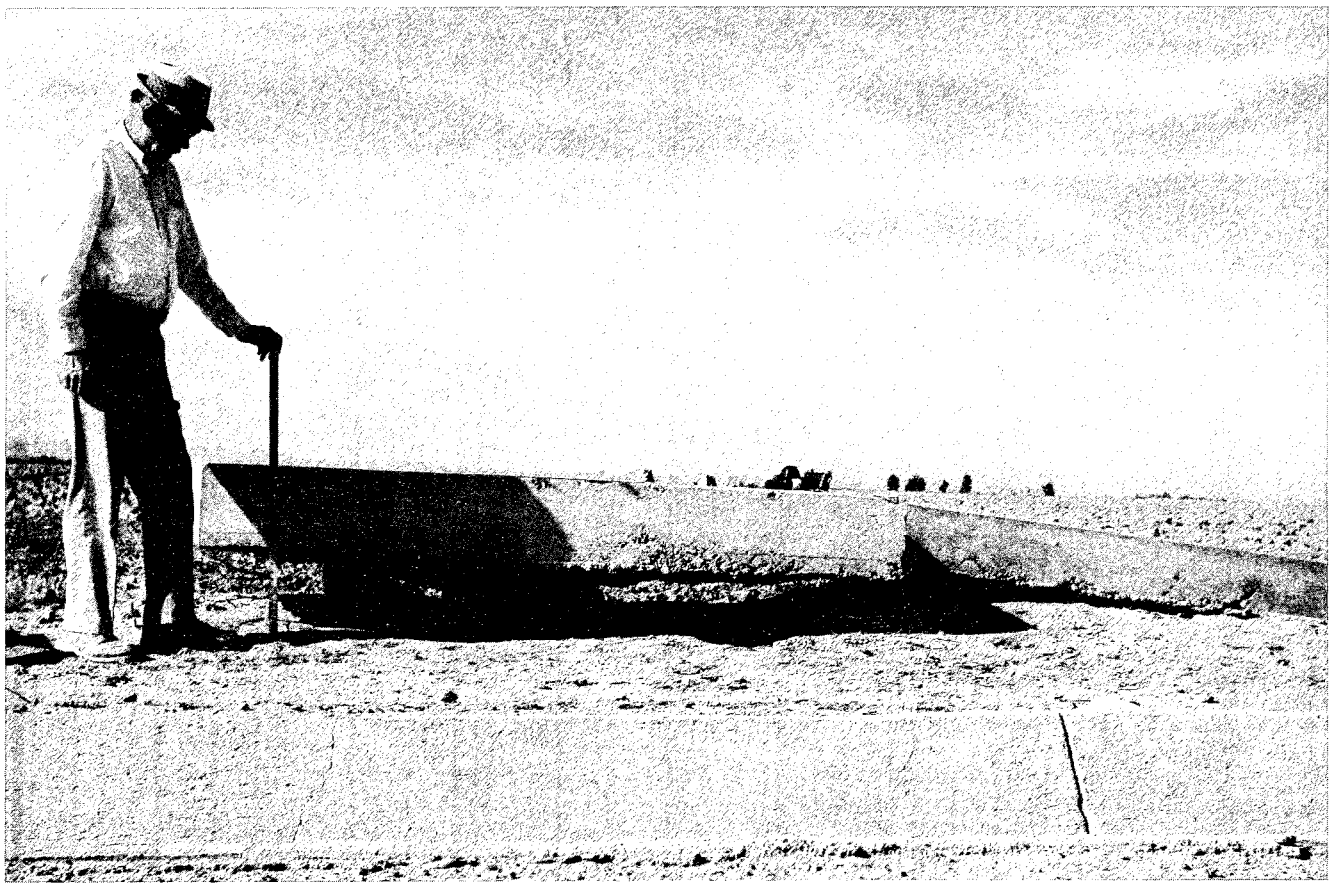

Figure 7. Extruded well casing at STOP 4. The bottom of the concrete pad is 12 inches above the ground surface.

0.3	87.1	**STOP 5.** This fissure-gully is one of several discovered in 1975 in this area. Note the luxuriant growth of the creosote bushes along both sides of the fissure-gully and note that headward erosion has developed on the upslope side. At the ends of the fissure-gully, the trace of the fissure is marked by a hairline crack or a line of holes.
0.6	87.7	Turn west from Sunland Gin Road onto Woodruff Road. Road curves gradually from a westerly direction to a northerly direction around a low rocky hill, and then turns sharply to the west. Approximately 300 feet west of this turn is the next stop.
0.3	88.0	**STOP 6.** At this stop we will not leave the bus. The fissure-gully visible on both sides of the road extends about 0.5 miles northward, nearly to the base of the mountains. In February, 1976, the fissure-gully had not reached the road but by October, 1976, it had crossed the road, heading toward the developing area.
0.7	88.7	Turn south on Cox Road.
1.0	89.7	Turn west on McCartney Road.
0.7	90.4	Turn onto Interstate 10 (west) to Phoenix.
35.8	126.2	Follow Interstate 10 to Superstition Freeway (State 360). Turn east on Superstition Freeway for 1.5 miles then north on Mill Avenue for 2.5 miles to University Drive and ASU.
4.0	130.2	ASU campus. End of trip.

Interleaf. Dr. Donal M. Ragan and Ms. Susan Anderson taking initial measurements between nails driven into asphalt at corner of 76th Street and Albany Street. Graded quarter section is in background, to west. The subsidence crack had broken the pavement on the previous day, at the same time that it had reopened in the graded area. Pavement had apparently been broken and patched along the same path before. (Photograph No. 3214 taken October 1, 1971 by Troy L. Péwé.)

GEOLOGY OF THE PALO VERDE NUCLEAR GENERATING STATION AND ADJACENT AREAS, MARICOPA COUNTY, ARIZONA

with

APPENDICES INCLUDING THE
SITE SELECTION PROCESS,
NUCLEAR REGULATORY COMMISSION
(NRC) CRITERIA,
SEISMOLOGY OF ARIZONA,
AND SUMMARY OF NEW
GEOLOGIC INFORMATION
RESULTING FROM PVNGS STUDIES

by
K. M. Euge, W. R. Lund,
and J. D. Scott
Fugro, Inc.

Because of job site rules and regulations, boots and hard hats will be required on-site. Some hard hats *may* be available at the gate. The field trip is scheduled as a one-day trip.

INTRODUCTION

This field trip guide presents the results of reconnaissance and detailed geologic studies in the vicinity of the Palo Verde Nuclear Generating Station (PVNGS), south-central Arizona. These studies were directly related to the investigation and licensing requirements for PVNGS and have provided much new geologic information on the western Phoenix Basin area. In addition to the geologic descriptions, we have provided a travel log and a series of appendices giving the background of the site selection process, synopsis of Nuclear Regulatory Commission (NRC) siting criteria, seismology of Arizona, and a summary of new geologic information resulting from the Palo Verde studies.

ACKNOWLEDGEMENTS

The authors express their thanks to the Arizona Nuclear Power Project and Arizona Public Service for permitting this field trip. Preparation for this field trip guide was supported financially by Fugro, Incorporated.

Text portions of this paper have been largely abstracted or paraphrased from two publications: The PVNGS Preliminary Safety Analysis Report (ANPP, 1974) and an article in FIELDNOTES from the Arizona Bureau of Mines (Scott and Moore, 1976). In addition, supplemental data were obtained from the files and the library of Fugro, Inc.

SUMMARY

The Palo Verde Nuclear Generating Station site is approximately 40 miles west of Phoenix and is situated within the Basin and Range physiographic and structural province of southwestern Arizona. The geology within a 25 mile radius of the site (site vicinity) is characterized by mountain ranges which are relatively short, irregular and stand sharply above broad, alluvial-filled basins. The rocks of these mountains vary from deformed crystalline rocks of Pre-cambrian age to volcanic and sedimentary rocks of middleTertiary age. Alluvium and volcanic rocks in the broad basins range from Miocene to Holocene in age, based on potassium-argon age dates of basalt interbeds.

The geology of the site area (5 mile radius) consists of 1) Precambrian metamorphic and granitic rocks, 2) Miocene volcanic and interbedded sedimentary rocks and 3) basin sedimentary deposits on the order of 400-600 feet thick and consisting of lithified fanglomerate, unlithified fan, alluvial, and lacustrine deposits with basalt interbeds. The dominant structure of the site is homoclinal folding of the volcanic bedrock dipping 15° to 23° to the southwest. The overlying basin sediments are flat-lying and undeformed. Only one northwest-trending fault, displacing the volcanic bedrock, has been observed within a 5 mile radius of the site. This fault does not displace Miocene fanglomerate.

The Palo Verde Clay, a lithologically and geophysically distinctive lacustrine member of the basin sediments, underlies and is older than the base of the Arlington basalt flow (2.0 million years—based on potassium-argon age dates supported by paleomagnetic analysis). The Palo Verde Clay can be continuously traced in borings across the site and at least 5 miles southeast of the site. Consistent correlations of the Palo Verde Clay indicate no faulting within the site for more than 2.8 million years.

Main groundwater levels at the site, based on regional water contours and actual water level measurements, range from approximately 200 to 270 feet below ground surface.

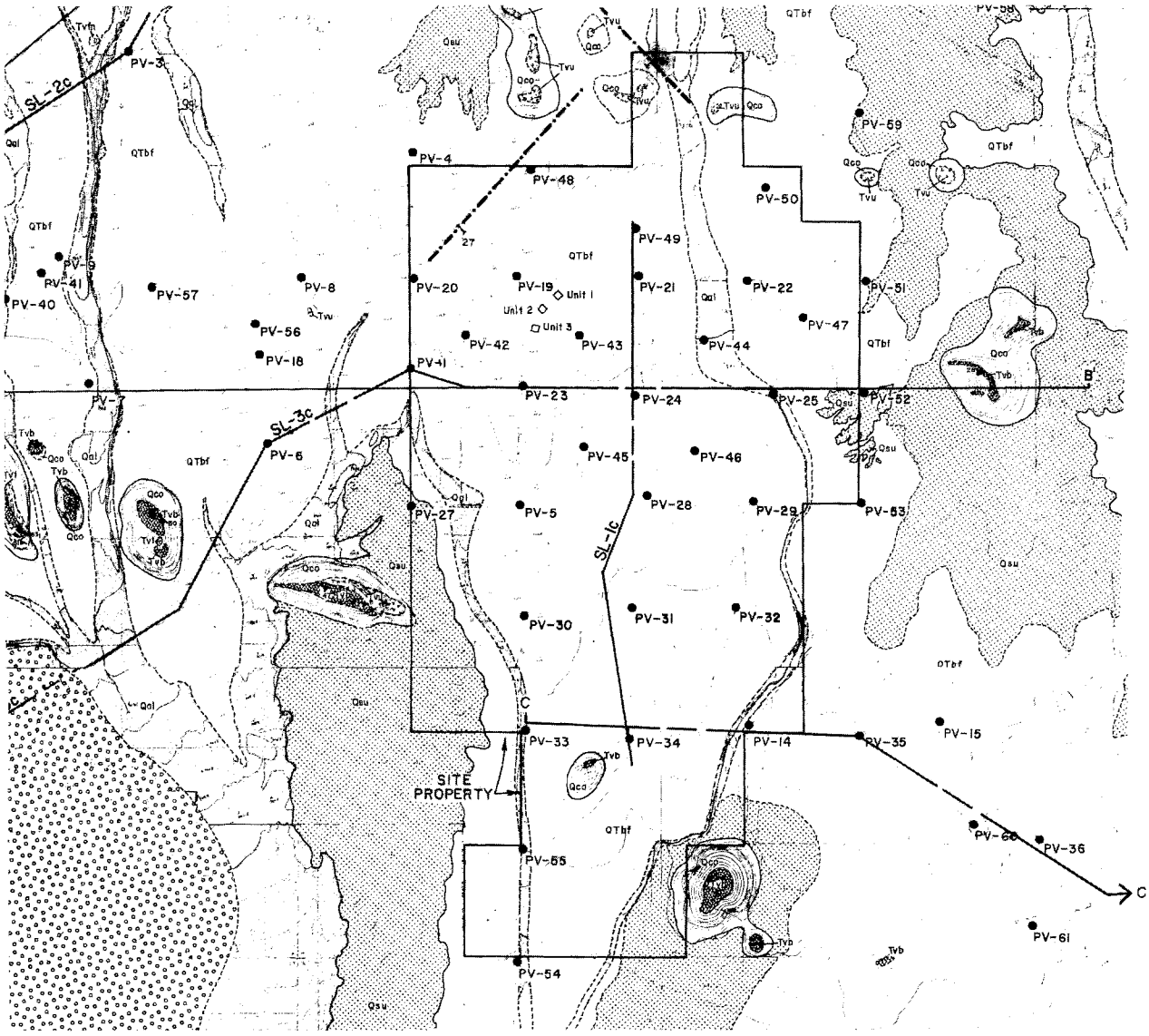

Figure 1. Geologic map of the Palo Verde site area.

A perched water zone exists in the power plant area with depth to water ranging from 15 feet to 100 feet below ground surface.

GEOTECHNICAL INVESTIGATION OF PALO VERDE

The site-specific geotechnical investigation (for the PSAR) at Palo Verde required approximately one year to complete after confirmation that the site was feasible. The activities included:

- reconnaissance and detailed geologic mapping of a 25 mile radius and 5 mile radius around the site;
- over 9 miles of seismic refraction geophysical surveys;
- reconnaissance and detailed gravity and magnetic geophysical surveys covering a 10 mile radius around the site;
- 2,000 feet of exploratory backhoe trenches;
- drilling of over 200 exploratory borings to depths ranging from 50 to 721 feet (in total about 10 miles of borings were drilled for geologic and foundation engineering analysis);
- high-resolution downhole geophysical logging of nearly all exploratory borings for stratigraphic correlation;
- potassium-argon age dating of 34 rock samples;
- analysis of approximately 550 samples of basin sediments for paleomagnetic polarity;
- static and dynamic engineering tests on core and drive samples;
- detailed groundwater analysis;
- complete research of all pertinent geologic, seismologic, and hydrologic data.

In addition, there were seven other specialists or consultants from the University of Arizona and Arizona State

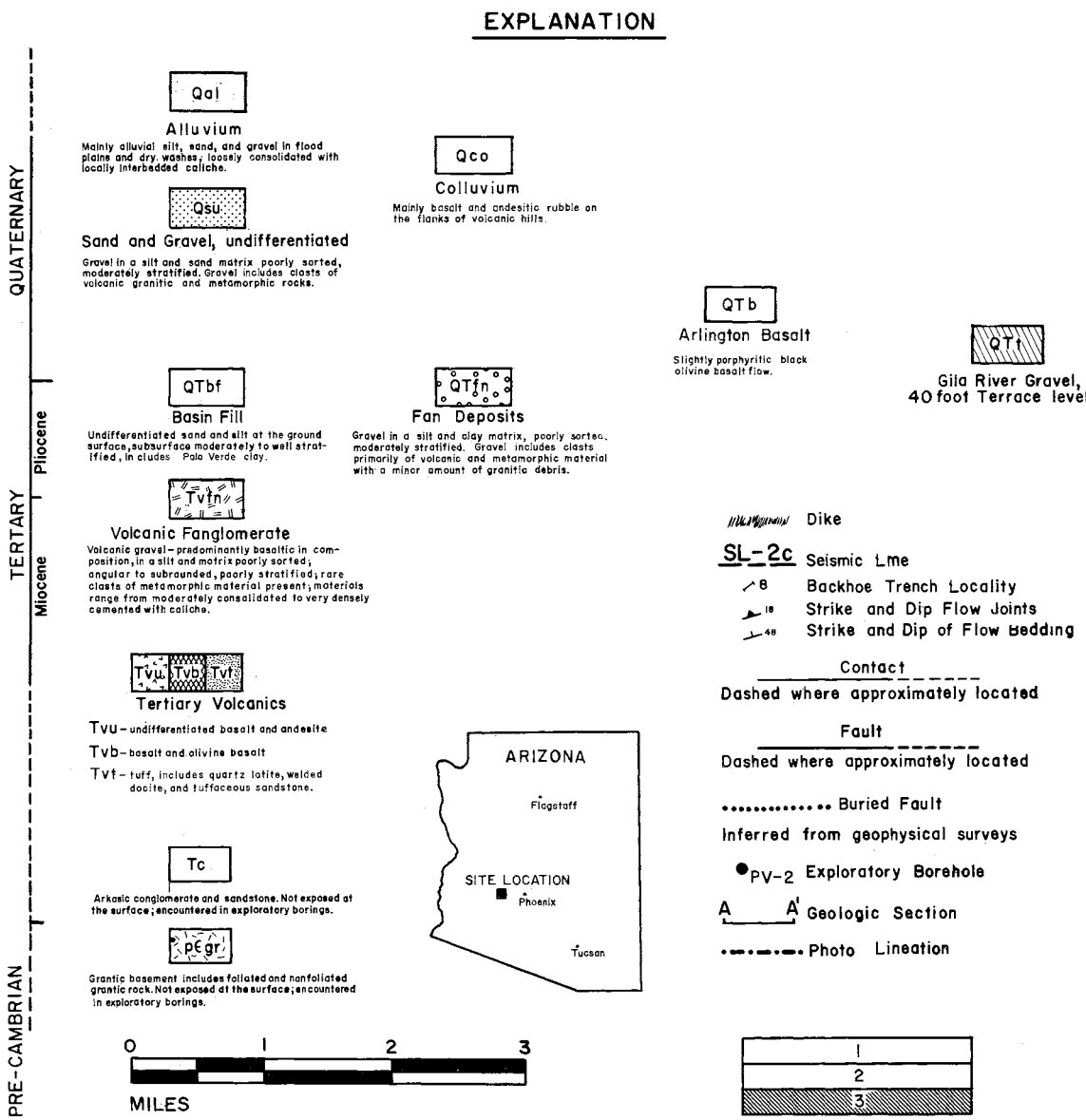

University who consulted on specific aspects of the project, such as geohydrology, stratigraphy, structural geology, petrology, clay mineralogy, palynology and geophysics.

GEOLOGY OF THE PALO VERDE SITE

The Palo Verde Nuclear Generating Station is located within a broad valley surrounded by the Palo Verde Hills, an intermittent series of low hills having a maximum relief of about 250 feet. The valley floor slopes very gently towards the Gila River about 10 miles to the south. The area studied in detail for this investigation is included within a 5 mile radius of the site. Geologic reconnaissance studies involved an even larger area (about a 25 mile radius).

The rocks of the Palo Verde Hills can be divided into three groups: 1) Precambrian metamorphic and granitic basement rocks, 2) Miocene volcanic and interbedded sedimentary rocks, and 3) Miocene to Holocene basin sediments consisting of alluvial fan, lacustrine, and basin fill deposits (**STOP 1** , fig. 8), with local interbeds of volcanic rocks (figs. 1, 2, and 3).

The crystalline basement rocks are not exposed at the ground surface in the site area but they have been encountered at a depth of several hundred feet in a number of exploratory borings. The buried granitic surface is unconformable and undulatory with a general slope toward the northeast (fig. 3).

Miocene volcanic rocks, which unconformably overlie the crystalline basement rocks, are exposed in the Palo Verde Hills. These rocks represent massive flows, plugs, dikes and flow breccia with scattered, discontinuous interbeds of tuff and tuffaceous sandstone. The rocks of flow origin range in composition from hornblende andesite,

GEOLOGIC MAP SYMBOLS (Figure 2-5-12,13,14)	LITHOLOGIC UNIT	AGE	THICKNESS	LOCATION	DESCRIPTION
Qsu	LZ-6 Young Fan Deposits	Halocene-Pleistocene	8 to 15 feet	North and east of site	Brown gravel in a loose to medium dense silt and sand matrix, poorly sorted moderately stratified. Volcanic, granitic, and metamorphic clasts.
QTb	Arlington Basalt Flow	2 m.y. (Best K-Ar date)	5 to 200 feet (estimate)	Arlington	Dark gray, hard, slightly porphyritic olivine basalt.
					UNCONFORMITY
QTbf	LZ-5 "Upper" Sand and Gravel	> 2 m.y.	Up to 50 feet	Palo Verde basin	Brown, medium dense silty sand and gravel; predominantly quartz sand with volcanic gravel; weathered mica common; locally calcareous.
					PARACONFORMITY
	LZ-4 "Upper" Silt L-10 Horizon	> 2 m.y. to 2.8 m.y.	150 to 200 feet	Palo Verde basin and south and southeast toward Arlington	Brown, medium dense to dense silt and clayey silt with generally minor interbedded fine sand; scattered fine weathered mica common; local calcareous cement; coarse sand and gravel locally at base of unit. Series of paleosols developed near upper contact.
					PARACONFORMITY
	LZ-3 Palo Verde Clay	2.8 m.y. at top	0 to 136 feet	Central part of P.V. basin and south and south-east toward Arlington	Red-brown, very stiff, calcareous, silty clay; interbedded clastic wedges near west edge of basin. Paleosols developed at upper contact.
	LZ-2 "Lower" Silt	> 3 m.y.	0 to 97 feet	Central part of P.V. basin & south and southeast toward Arlington	Brown to red-brown, stiff to very stiff, sandy and clayey silt, locally grading to sand and gravel at base of unit.
	"Lower" Sand & Gravel	> 3 m.y.	0 to 30 feet	Palo Verde basin	Brown, dense, silty and clayey sand and gravel of volcanic origin, poorly sorted.
					UNCONFORMITY
Tvfn	LZ-1 Indurated Fanglomerate	16.7 ± .3 m.y. (K-Ar date of interbedded basalt)	0 to 285 feet	Palo Verde basin	Brown, moderately to well cemented fanglomerate composed of volcanic clasts derived from underlying bedrock; local interbed of dark gray, hard basalt at boring PV-DH-33.
					MAJOR UNCONFORMITY
Tvb Tvu Tvt	Volcanic Bedrock Sequence	17.7 to 20.3 m.y. (K-Ar dates)	6,000 to 7,000 Feet	Palo Verde Hills	Miocene volcanic sequence includes interbedded basalt, andesite and tuff, Tvb differentiated basalt, Tvu undifferentiated basalt and andesite, Tvt tuff and tuffaceous sandstone.
					UNCONFORMITY
Not exposed in site area	Arkosic Conglomerate	Unknown	148 Feet	Palo Verde Hills Subsurface	Arkosic conglomerate, granite andesite and basalt clasts.
					MAJOR UNCONFORMITY
	Granitic and Metamorphic Basement	Precambrian	Unknown	Palo Verde Hills Subsurface	Granite, granitic gneiss and metamorphased volcanic and sedimentary rocks.

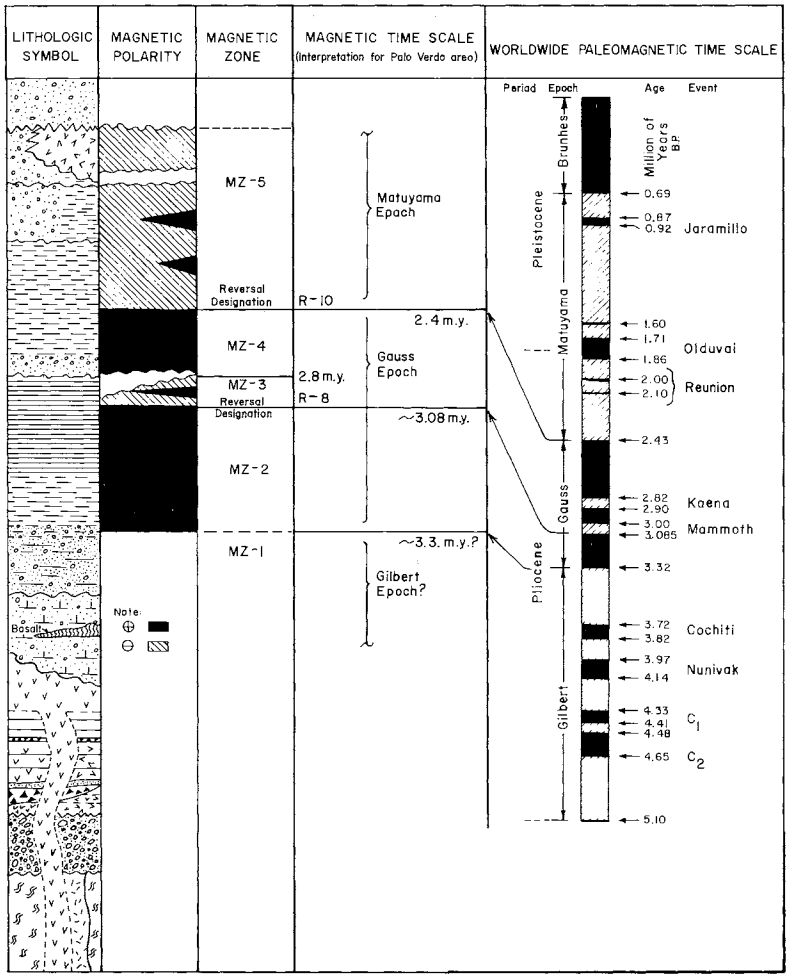

Figure 2. Stratigraphic chart of the site area.

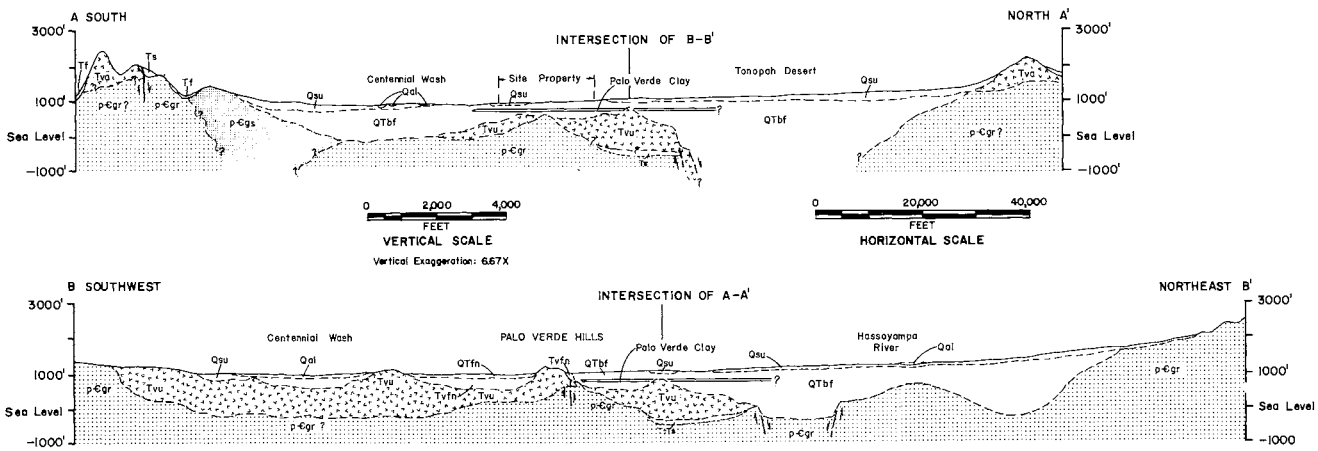

Figure 3. Geologic cross sections through the site vicinity.

which is relatively rare, to pyroxene andesite, basalt, and basanite. The pyroclastic rocks consist of welded hornblende biotite tuff. Whole-rock potassium-argon ages on basalt samples from seven localities range from 17.9 to 19.9 million years old. The many basalt dikes and plugs indicate numerous local sources for the volcanic rocks throughout the area (fig. 2).

Lithified and unlithified sediments overlying the basement and volcanic rocks cover the site and contain up to six distinctive stratigraphic units. These sediments are nearly horizontal and have an average thickness of approximately 320 feet with a variation of thickness in the site area of approximately 100 feet. The stratigraphic units within this alluvial sequence extend across the Palo Verde site and are generally continuous for at least 5 miles beyond the site boundaries towards the northeast and southeast (figs. 3 and 4).

At the base of the basin sediments is a Tertiary fanglomerate which contains rounded to angular clasts predominantly of andesite and basalt set in a well-cemented matrix of sand, silt, and occasionally, tuffaceous sand. The fanglomerate is exposed along the lower slopes of the Palo Verde Hills and unconformably overlies the volcanic bedrock. The fanglomerate has been traced into the subsurface where it commonly fills bedrock depressions and is absent on buried bedrock highs. A basalt interbed within the fanglomerate has been dated by potassium-argon techniques at 16.7 million years old, indicating a middle Miocene age.

Near the top of the basin sediment stratigraphic section another series of potassium-argon age dates was obtained from the Arlington and Gillespie basalt flows. The Arlington and Gillespie basalt flows are well exposed at the ground surface and clearly overlie basin fill sediments and Gila River terraces along old U. S. 80 (**STOPS 2** and **3**). A mean age of about 2 million years was obtained from seven samples of the Arlington basalt flow and about 3 million years for the Gillespie flow.

The stratigraphic and age correlation between the basin sediments at the site and those underlying the Arlington basalt flow 5 miles southeast was accomplished by tracing a distinctive clay stratum, named the Palo Verde Clay for this study, in relatively closely spaced borings. This clay unit is a lacustrine or lake deposit, about 200 feet below the ground surface, that averages between 80 to 100 feet thick and has a known maximum thickness of at least 136 feet. The Palo Verde Clay displays a remarkably distinctive signature in borehole geophysical logs, particularly those logs measuring natural gamma radiation. In addition, the clay was recognizable in lithologic cores because of its characteristic reddish-brown color and high clay content which contrasted to the coarser units stratigraphically above and below. Because the upper surface of the Palo Verde Clay represented a broad lake bottom, the correlations are nearly horizontal and show remarkable stratigraphic and structural continuity for the entire five miles between the site and the Arlington basalt flow. To assure that the clay was stratigraphically below the basalt, two borings were made through the Arlington flow into the Palo Verde Clay, thereby confirming that the clay was older than 2 million years. To further refine the age of the clay, a paleomagnetic analysis was made on 550 samples of the alluvial sediments from the site to the Arlington basalt. Results showed two prominent and continuous magnetic reversals which may correspond to world-wide reversals conservatively estimated to be 2.4 and 2.8 million years.

The presence, extent, and continuity of the Palo Verde Clay are of great significance to the Palo Verde site for several reasons:

1. The clay continuously underlies the site and the site area to at least 5 miles southeast and northeast (fig. 5).
2. The clay is relatively old (estimated at least 2.7 million

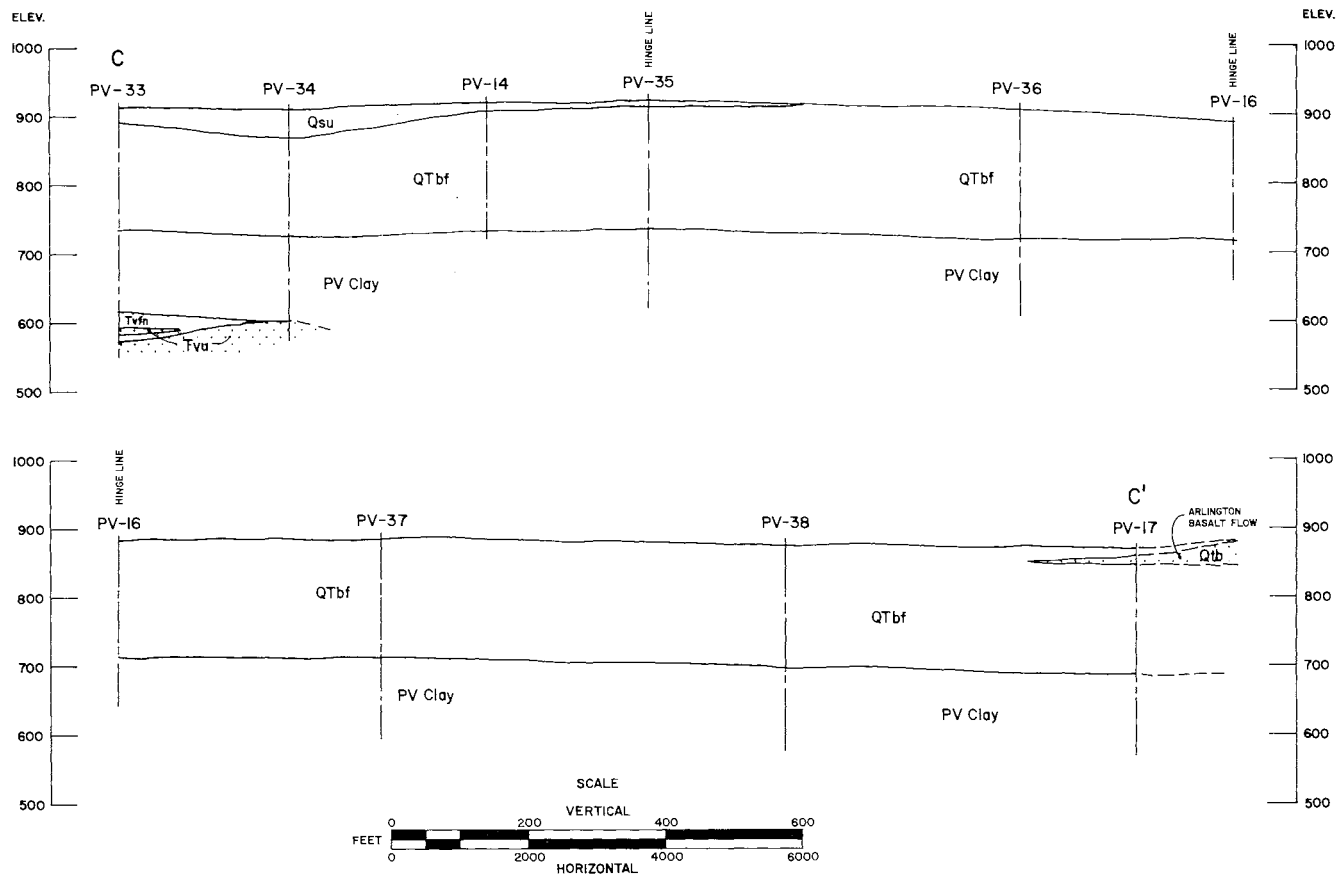

Figure 4. Geologic cross section through the southern portion of the PVNGS site to the Arlington basalt flow.

years on the upper surface) and is not deformed or faulted, indicating long term geologic stability of the area.

The only structural folding and faulting observed in the site area have been restricted to the Miocene volcanic rocks in the Palo Verde Hills. (**STOP 4**). Stratification within the Miocene volcanic bedrock sequence is indistinct but detailed geologic mapping has shown that the dominant structure of the Palo Verde Hills area is a homocline with the volcanic flow-bedding striking approximately N.40°W. and dipping 15° to 23° southwest.

Attitudes and areal extents indicate the volcanic sequence to be nearly 6,500 feet thick across the site area. Detailed mapping and trenching revealed no faulting except at one locality in the Palo Verde Hills, about 3 miles west of the site. This fault displaces Miocene volcanic rocks, trends northwest, and is approximately 2,000 feet long. The fault was traced in closely spaced backhoe trenches to a point where it is overlain by Tertiary fanglomerate. Since the fanglomerate was not displaced and was of Miocene age (16.7 million years based on a basalt interbed), the fault was pre-fanglomerate in age and not considered a safety hazard by NRC criteria.

CONTINUING GEOLOGIC ACTIVITIES

As the basin sediments are exposed by construction activities at Palo Verde, detailed geologic inspections are made of all excavations to satisfy NRC seismic safety criteria. The trenches and other excavations form an extensive network of exposures that are invaluable for subsurface geologic analysis. At least one wall of all pertinent exposures is photographed as a permanent record and geologic contacts with descriptions are logged at scales of ten feet to the inch. In Category I excavations (Category I are the most important facilities in terms of safety) detailed geologic maps are constructed at a scale of ten feet to the inch. The purpose of such detailed inspections and logging is to give site geology in as much detail as possible to:

- establish and document the actual subsurface conditions at the site;
- confirm that design considerations made during earlier investigations still are appropriate for the site conditions.
- insure that the public health and safety will not be jeopardized due to geologic processes affecting plant integrity.

Periodically, representatives of the NRC, U. S. Geological Survey and Arizona Bureau of Geology and

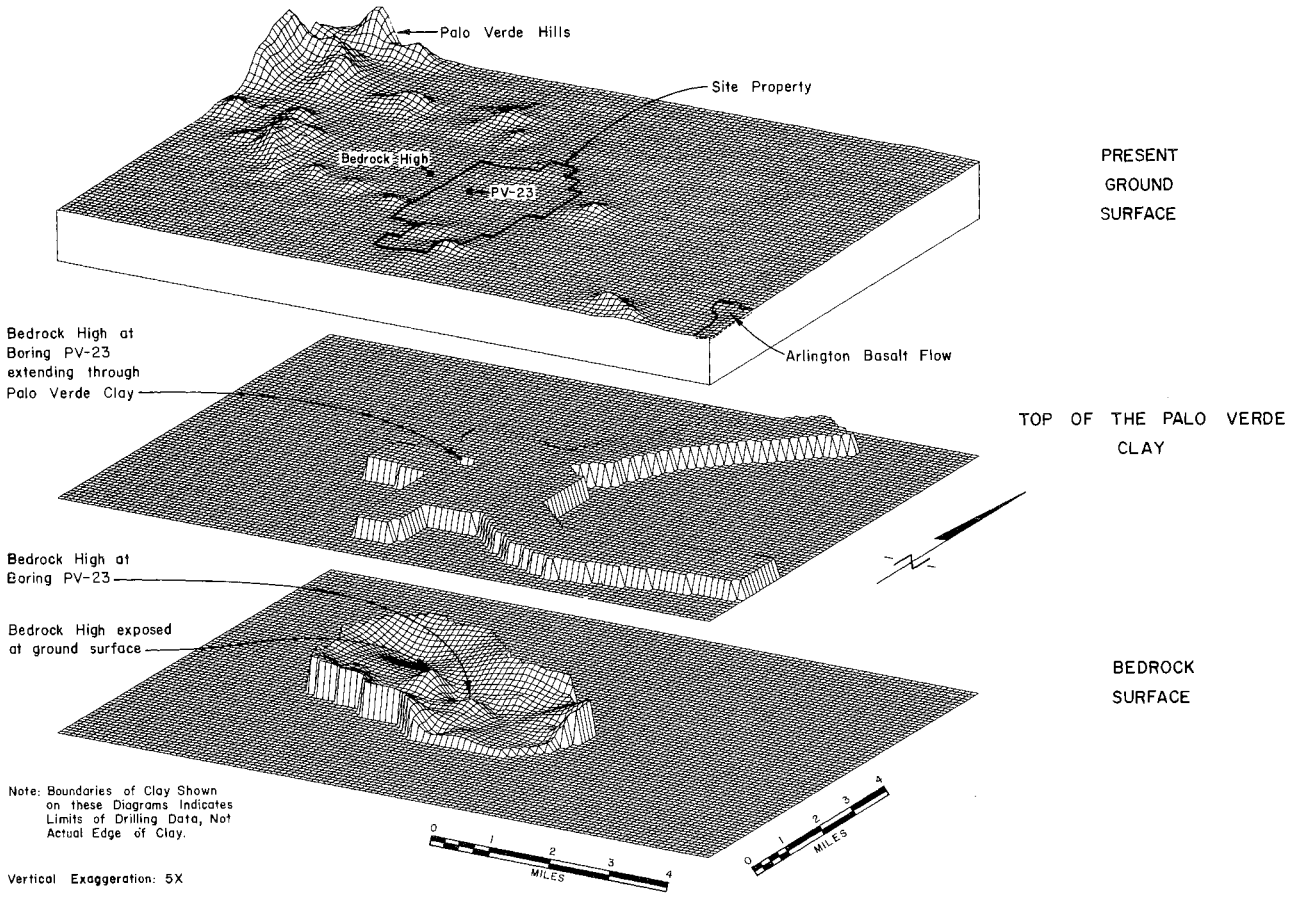

Figure 5. Isometric block diagrams of the present ground surface, top of Palo Verde Clay and bedrock surface in the plant site area.

Mineral Technology make detailed inspections of these excavations and check the critical components of the detailed mapping. All logs and other pertinent information will be assembled into a final report at the conclusion of grading. This data will be submitted as a part of Final Safety Analysis Report to the NRC, which, upon approval of the document, will issue the license to operate PVNGS.

REFERENCES CITED

Arizona Bureau of Mines, 1969, Mineral and Water Resources of Arizona: The University of Arizona, Bull. 180, 638p.

Arizona Public Service Company, 1975, Palo Verde Nuclear Generating Station Preliminary Safety Analysis Report, Vol. 2, Sec. 2.5, 185p.

Fugro, Inc., 1975, Geologic Investigation of Gillespie Dam Alternate Siting Area, Arizona Nuclear Power Project, report for NUS Corporation, 56p.

———, 1977, Inventory and Impact Report Salt River Project Transmission Line, Palo Verde to Kyrene, Maricopa County, Arizona, report for Wirth Associates, 57p.

Moore, Richard T., and Wilson, Eldred D., 1965, Bibliography of the Geology and Mineral Resources of Arizona: Arizona Bureau of Mines, University of Arizona, Bull. 173, 321p.

Scott, John D. and Moore, Richard T., 1976, Geotechnical Considerations in the Selection of the Palo Verde Nuclear Generating Station Site: Arizona Bureau of Mines, Fieldnotes, Vol. 6, Nos. 3–4, Dec. 1976.

ROAD LOG

MILES Interval	MILES Total	
0.0	0.0	Start at Broadway Road and Maricopa Freeway
2.9	2.9	Bridge over Salt River. The Salt River drainage basin comprises an area of 13,730 square miles and drains portions of the Sierra Ancha and Mogollon Rim on the north, the White Mountains on the east and the Superstition and South Mountains on the south. The average annual stream flow is about 350,000 acre-feet with a maximum flow recorded of 45,000 cubic feet per second (cfs). The South Mountains to the southwest expose Precambrian granite gneisses, schists, phyllites, and quartzite. The metamorphics are locally intruded by late Mesozoic granitics.
4.9	7.8	19th Avenue off-ramp and Maricopa Freeway
0.9	8.7	Buckeye Road (Highway 80) and Black Canyon Freeway

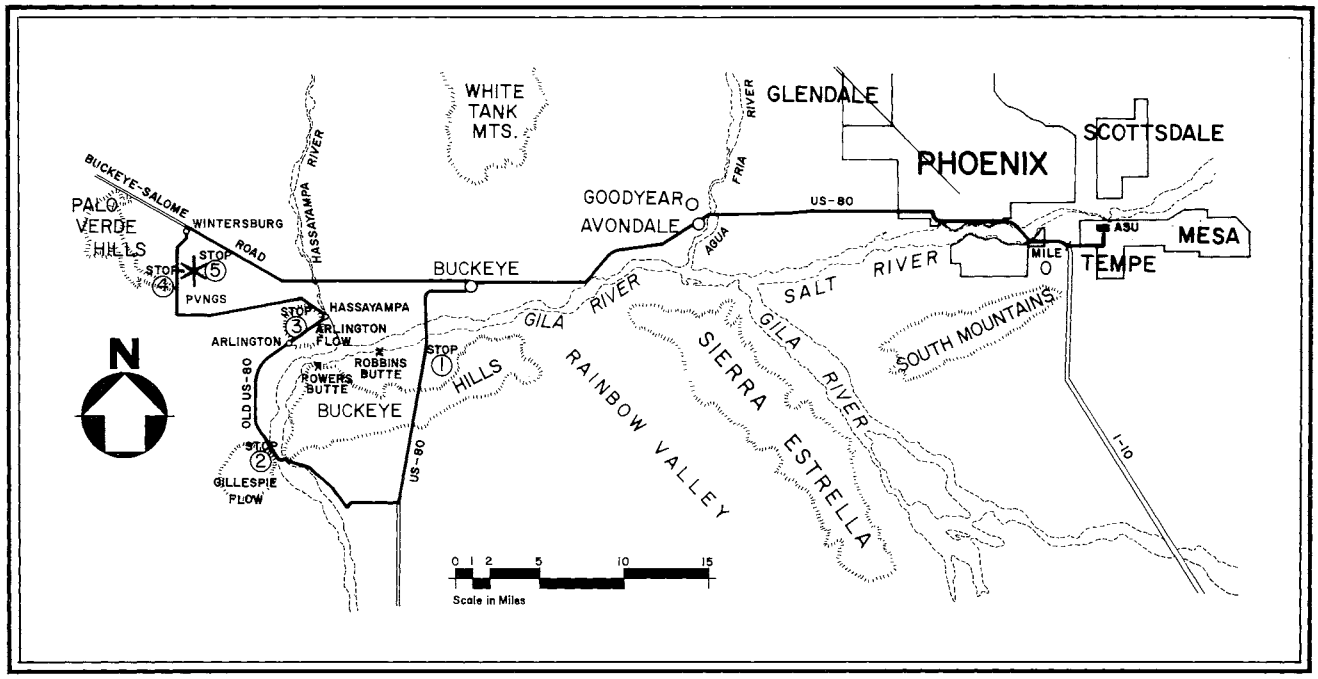

Figure 6. Location map showing route of travel.

3.5 12.2 On the south is a very good view of the Sierra Estrella Mountains, a northwest-trending range with a maximum relief of about 3,500 feet. The rock types exposed are similar to those exposed in the South Mountains.

9.2 21.4 Bridge over Agua Fria River. This southerly flowing tributary to the Gila River drains an area of about 2,000 square miles. Most of the runoff from the Hieroglyphic Mountains is retained by Lake Pleasant dam about 35 miles upstream of the mouth. The yearly average runoff is 1,100 cfs with a maximum recorded streamflow of 4,700 cfs.

4.0 25.4 To the north are the White Tank Mountains and the Caterpillar Tractor Company proving grounds. Gnessic rocks consisting of foliated granite and hornfelsic rocks intruded locally with pegmatitic veins make up the White Tank Mountains.

10.9 36.3 Town of Buckeye.

1.8 38.1 To the south, a view of the subdued terrain of the Buckeye Hills, an east-west trending complex of Precambrian gneiss, hornfels, mica schist (the mica is mined commercially by the Buckeye Mica Company,) granite, quartz monzonite, and quartz diorite. These rocks are intruded by late Mesozoic granitics. Mining and exploration for rare earth, uranium, gold, silver, and copper has occurred sporadically in this area.

1.5 39.6 Highway 80 and Olgelsby Road

2.5 42.1 Bridge over the Gila River. This river provides drainage for a large portion of Arizona and New Mexico, encompassing approximately 50,000 square miles. This area includes most of the Central Highlands Province and the Basin and Range Lowlands Province. Prior to construction of runoff control and irrigation diversion the greatest known flood discharge in this area was 250,000 cfs (1891). The greatest flood flow since construction was 45,800 cfs in 1941.

2.1 44.2 **STOP 1.** Overview of Gila River flood plain area with subdued knobs of Tertiary volcanics which protrude through the basin fill sediment (Power and Robins Buttes). The Buckeye Hills area is to the south, the Arlington basalt flow in the west middle distance, and the Palo Verde Hills and Saddle Mountain on the western horizon (fig. 7).

0.2 44.4 Road cuts in late Mesozoic granitics of the Buckeye Hills.

4.0 48.4 On the southeast is a view of Rainbow Valley and the Maricopa Mountains. Rainbow Valley was the site of the initial geologic field studies for one of the proposed nuclear power plant sites. After an intensive geologic mapping program supported by

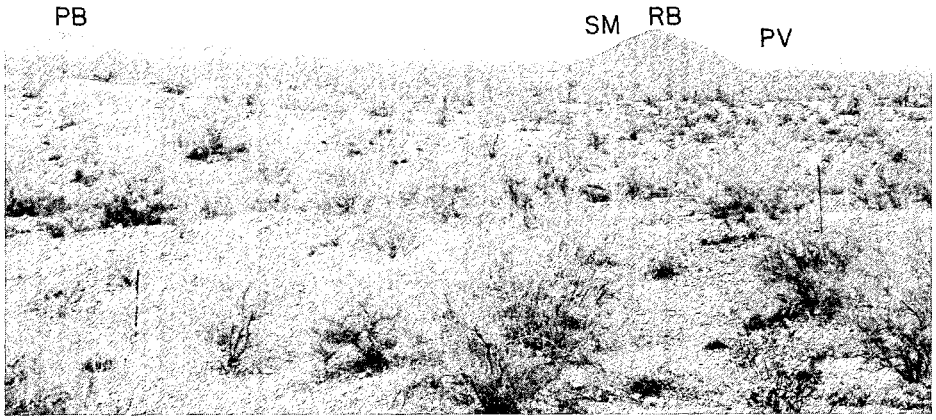

Figure 7. View from STOP 1 to the northwest: Robins Butte (RB) and Powers Butte (PB) in foreground; the Palo Verde Hills (PV) and Saddle Mountain (SM) in the distance.

drilling and geophysical surveys, the site was abandoned for more favorable sites at Gillespie Dam and Palo Verde. The Maricopa Mountains are predominantly Precambrian granitics with localized pegmatitic intrusions.

3.6 52.0 Patterson Road and Highway 80

3.2 55.2 Patterson Road and Old Highway 80

0.7 55.9 Towards the west is a good view of the Gillespie basalt flow. The Gillespie basalt forms a small flow along the west side of the Gila River in the vicinity of Gillespie Dam. It overlies portions of old alluvial fan deposits, old river terrace deposits, older alkali basalt, and granitic basement rock. The flow is dark gray to black and very dense with few vesicles except for occasional scoriaceous zones; it is slightly fractured and locally has columnar jointing. Petrographically, the unit is an olivine basalt, with olivine phenocrysts in a groundmass of matted plagioclase with intergranular calcic augite and opaque minerals. The basalt is 15–30 feet thick at its periphery and its surface is intensely calichified. The basalt is actually a composite of several flows and three or four flow fronts have been identified on the upper surface. Pillow lavas exposed in the northeast side of the basalt suggest that it flowed into the Gila River as it covered the old "40-foot" flood plain.

Ten radiometric dates have been obtained from the basalt. They range from 4.2 ± 0.4 million years for a sample near the bottom edge of the basalt to 1.3 ± 0.4 million years for a sample taken near the vent. Five of the dates fall between 3.3–3.5 million years and the average of all dates is 3.3 million years.

3.1 59.0 To the north can be seen typical examples of debris flows common to the volcanic terrain in this area. The underlying rock consists of several flows of dark gray alkalic basalt with abundant augitic phenocrysts. It dips about 10° to 30° to the west. Based on K-argon dating, it ranges in age from 19.1 ± 0.9 to 19.6 ± 0.4 million years.

1.0 60.0 Bridge over the Gila River; Gillespie Dam is to the north; the El Paso Natural Gas pipeline is to the south.

1.4 61.4 **STOP 2.** Borrow cut exposing Gila River gravel and sediments overlain by the Gillespie basalt flow. The sediments in this exposure are remnants of paired river terraces which border the modern flood plain and stand 40 to 80 feet above the modern channel. The deposit consists of material ranging from silty, fine sand to cobbles. Many of the clasts are well rounded and consist of distinctive rocks such as quartzite, rhyolite and metadiabase whose provenance is many miles upstream (fig. 8).

The deposits 80 feet above the present river channel represent the upper level of a major fluvial aggradation. These high terrace deposits are poorly preserved and strongly calichified. Old pediment-alluvial fan systems along the east side of the Gila Bend Mountains were graded to and interfingered with these deposits as they accumulated. Fine-grained basin-fill deposits overlie and/or interfinger with Gila River deposits at

Figure 8. View of borrow pit cut exposing Gila River gravels (GR) overlain by the Gillespie basalt flow (Gbf).

the 80-foot level. This suggests that at least the upper part of the basin-fill sequence in the western end of the Phoenix Basin (including the Palo Verde site area) accumulated after the Gila River entered the area.

1.6	63.0	Feed lot Arlington Cattle Company and El Paso Natural Gas substation.
5.8	68.8	**STOP 3.** Road cut exposing basin fill sediments overlain by the Arlington basalt flow. The flow, K-argon dated at 1.2 to 3.2 million years, unconformably overlies sands and silt sediments that have been traced continuously to the northwest where they underlie the plant site. A good paleosol has been recognized in this cut. Note the alteration zone at the contact between the flow and sediments (fig. 9).
2.3	71.1	Old Highway 80 and Salome Highway
1.0	72.1	On the east the gently undulating topography defines river terrace and overbank deposits of the Hassayampa River.
0.9	73.0	Salome Highway and Elliot-Ward Roads
6.6	79.6	On the north the southern site boundary of PVNGS.
1.1	80.7	Ward (Elliot Rd.) and Wintersburg Road
1.5	82.2	**STOP 4.** Road cut exposing Tertiary volcanic flow sequence (K-argon age of about 14 million years) and interbedded sequence of water-laid tuffs and sand. About six distinctive flows can be differentiated at this

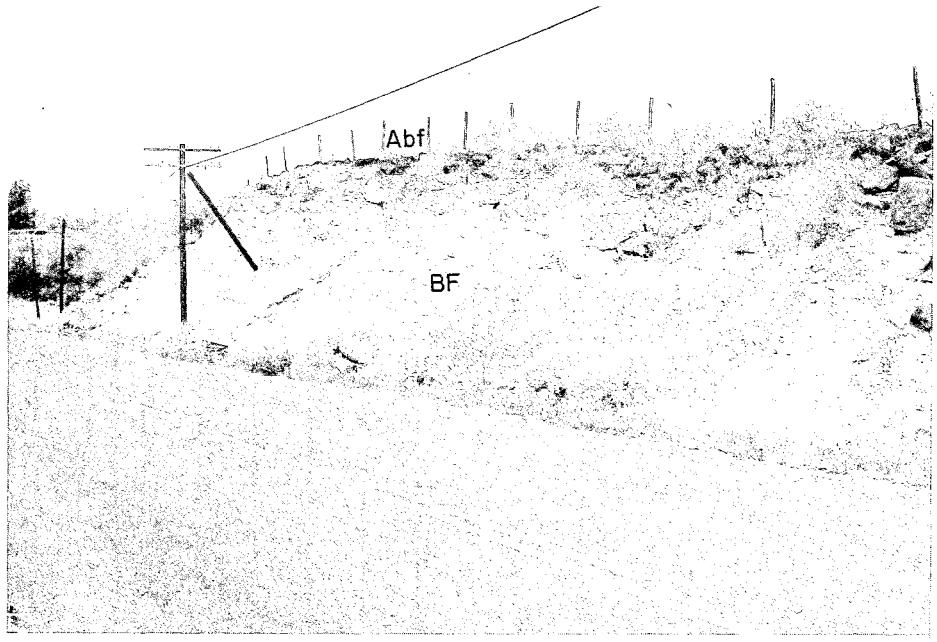

Figure 9. View of road cut exposing basin-fill sediments (BF) which are overlain by the Arlington basalt flow (Abf).

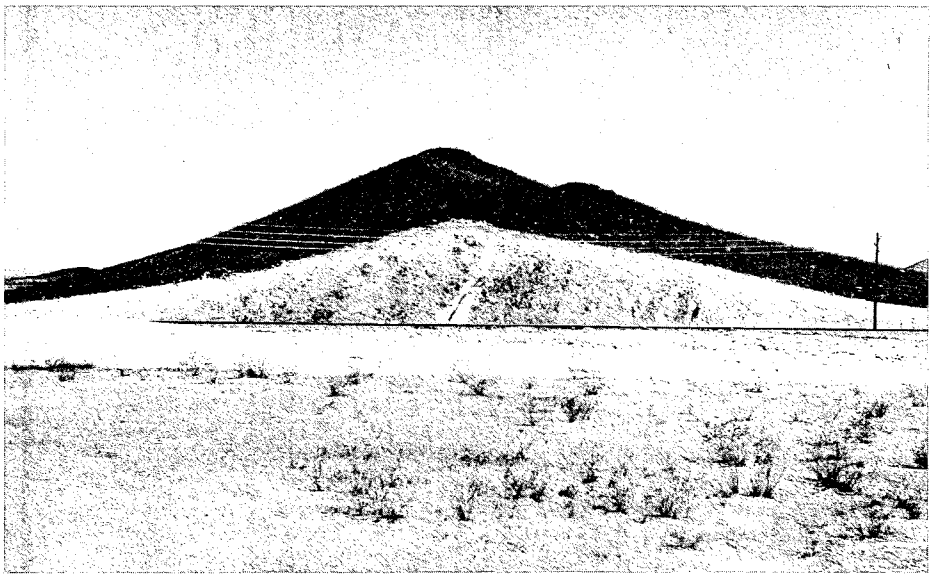

Figure 10. View of road cut adjacent to Wintersburg Road exposing a Tertiary volcanic flow sequence with sedimentary interbeds.

exposure as a result of alteration at contacts and the both massive and vesicular nature of the rock. Some of these flows were probably extruded into a body of water as evidenced by the glassy texture in portions of the exposure. The flows and sediments are striking to the northwest and dip to the south at about 45° to 55° (fig. 10).

1.4 83.6 Meteorological tower.

0.2 83.8 **STOP 5.** Main entrance, PVNGS.

RETURN LOG

0.0 0.0 Main gate

2.3 2.3 Wintersburg Road and Salome Highway

4.0 6.3 Baseline-Salome Highway Intersection

1.5 7.8 On the north and south is the Hassayampa River flood plain. Terrace and overbank deposits are quite extensive above the active channel. The Hassayampa River uncontrolled drainage area is about 2,000 square miles and drains portions of the Vulture and Bradshaw Mountains to the north. The yearly average discharge is 3,070 cfs with a maximum recorded streamflow of 6,500 cfs.

6.8 14.6 Baseline and Olgelsby Roads

Return to ASU via Highway 80 and Freeway

APPENDICES

BACKGROUND OF THE SITE SELECTION PROCESS; SCREENING THE REGIONAL SITE SELECTION PROCESS; SYNOPSIS OF THE NRC SITING CRITERIA; SEISMICITY OF ARIZONA; SUMMARY OF NEW GEOLOGIC INFORMATION RESULTING FROM PVNGS STUDIES.

BACKGROUND OF THE SITE SELECTION PROCESS

Experience has shown that the most effective way of identifying the best of a number of nuclear power plant sites is the systematic examination of a large region. This method provides the greatest effectiveness and flexibility in selecting optimum sites relative to all criteria critical to safety. This type of regional approach was utilized in the Palo Verde site selection and involved a screening, in distinct phases, of the entire state of Arizona. Each phase reduced the area under consideration using selected geologic, hydrologic, environmental and land-use criteria.

The first phase consisted of regional studies which divided the state in terms of seismotectonic characteristics based on selected geologic and seismologic criteria such as: physiographic provinces, natural geologic and structural provinces, complexity of geologic structure, distribution of Tertiary and Quaternary volcanic rocks, major tectonic lineaments, distribution of Quaternary faults, and distribution of historic and instrumented earthquake epicenters (fig. 11). In general, this regional screening showed that the most seismically active and geologically complex parts of Arizona for nuclear siting were 1) in the Southwest corner of the state, near Yuma, which is within the influence of the

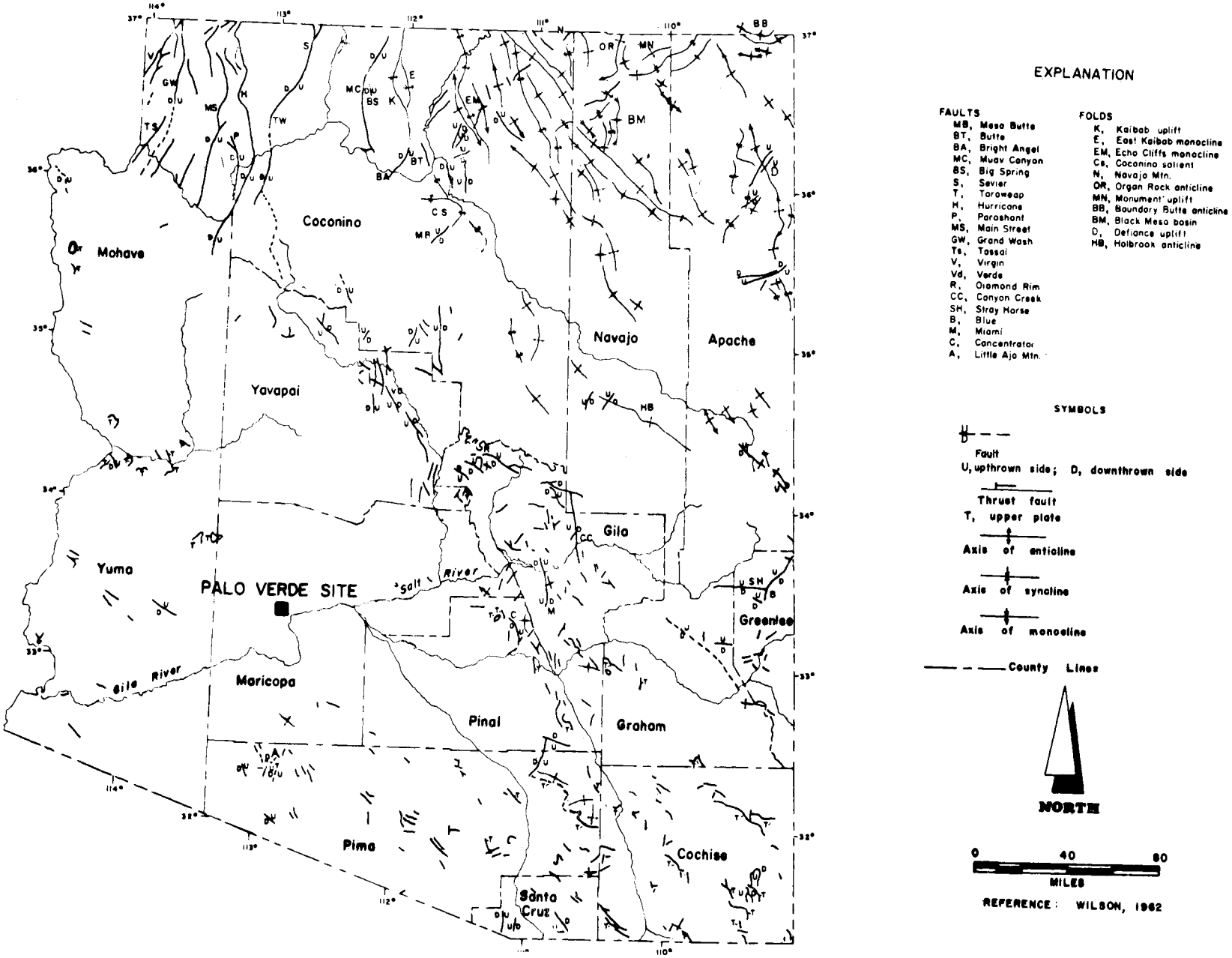

Figure 11. Generalized tectonic map of Arizona.

active San Andreas fault zone, and 2) a broad band coinciding roughly with the central mountains or Transition Zone, which extends diagonally across the state from near the Grand Canyon to Bisbee. In addition to identifying the most restrictive area for siting, the regional study rated all the major areas in the state in terms of potential for satisfying the stringent NRC criteria. The most satisfactory areas for demonstrating a suitable site were in the region west of Phoenix and a limited area on the Colorado Plateau. Since land access and availability were severely restricted on the Colorado Plateau, the area west of Phoenix was selected for the more detailed Phase II and III investigations, and eleven candidate valleys were identified for the second study phase.

Phase II of the screening studies evaluated and ranked the eleven candidate valleys using geotechnical and environmental criteria. Of prime consideration were 1) presence of sufficient quantities of water for plant operation, 2) absence of Quaternary faults or lineaments which might be considered capable of generating earthquakes and/or ground displacements, 3) presence of suitable topographic and foundation conditions, 4) presence of stratigraphic units of Quaternary or late Tertiary age at or near ground surface which would be useful in evaluating the long term geologic stability of the site and site area. In geologically complex regions such as the western United States, the Quaternary (most recent) stratigraphy becomes critically important to any effort to document conclusively that a site has been tectonically stable for a considerable length of time. Phase II investigations relied on extensive literature search, aerial reconnaissance, studies of satellite imagery and aerial photography, and consultation with experts in local geology. At the conclusion of this phase, three basic candidate valleys were identified with 28 potential siting areas divided among them.

Phase III screening reduced the three valleys and 28 candidate site areas to a number of top-rated site areas for further consideration. The prime objective was to have enough potential sites to identify a prime and alternate site having a high likelihood of satisfying the NRC criteria. The geologic criteria used in the Phase III screening were similar to Phase II, however, the ranking criteria were quantified in more detail based on extensive literature search, detailed air photo analysis, ground and aerial reconnaissance, and analysis of all available subsurface and water well data. The ability to age-date the late Tertiary and Quaternary stratigraphic units at the site areas was also an important consideration at this phase.

A limited amount of surface and subsurface exploration was performed in the highest-rated candidate sites in order to confirm the suitable geotechnical characteristics. Typical investigations included: reconnaissance geologic mapping on specially flown low level stereo aerial photographs; seismic refraction and gravity surveys; several borings to 500 feet with samples for geologic and engineering analysis; age-dating of subsurface materials (when possible); backhoe trenches across lineations or faults. As a result of these limited confirmatory investigations, several sites were removed from further consideration; however, it also became apparent that the Palo Verde site had superior geologic characteristics to satisfy the NRC siting criteria.

SEISMICITY

Historic seismicity in Arizona has been moderate in a few parts of the State and almost nonexistent in other parts (fig. 12). Of the recorded epicenters within the State, the three largest have been between magnitude 5.0 and 5.9 and were in the north central part of Arizona between Flagstaff and the north state line. More epicenters have been located for earthquakes less than magnitude 5.0 and these smaller earthquakes form loose concentrations along the Central Mountains Province, trending diagonally northwest across the State, and at the southwest corner near Yuma.

The most notable of strong earthquakes felt in Arizona, but originating outside the State, occurred in 1887 in Sonora, Mexico. The estimated magnitude was 8 and shaking was felt as far north as Prescott and as far south as Mexico City—a radius of about 400 miles from the assumed epicenter. Surface ruptures were reported for 35 miles along north-trending faults on the east and west sides of the Sierra Teras Mountains. The rupturing reportedly had a maximum vertical displacement of 26 feet and extended to within 10 miles of the Arizona border.

In terms of the Safe Shutdown Earthquake, the maximum level of earthquake shaking was postulated from the 1887 Sonora earthquake (magnitude 8) relocated at a distance of 72 miles from the Palo Verde site. This conservative estimation was based on a hypothetical relocation of the epicenter from Sonora, Mexico about 250 miles northwest along major fault and mountain systems in the Transition zone province. The closest approach of mapped Quaternary faults in the Transition zone are east of Phoenix and about 72 miles east of the site. This relocated earthquake is larger than any historical event occurring within Arizona and is a conservative representation of the maximum level of shaking that the plant might experience within its design life.

SYNOPSIS OF THE NRC SITING CRITERIA

The NRC has developed specific geologic and siesmologic siting criteria which require, in general terms:

1) Establishment of the maximum level of earthquake shaking that might conceivably be experienced by the plant;
2) Determination of the potential for surface faulting within 5 miles of the site;

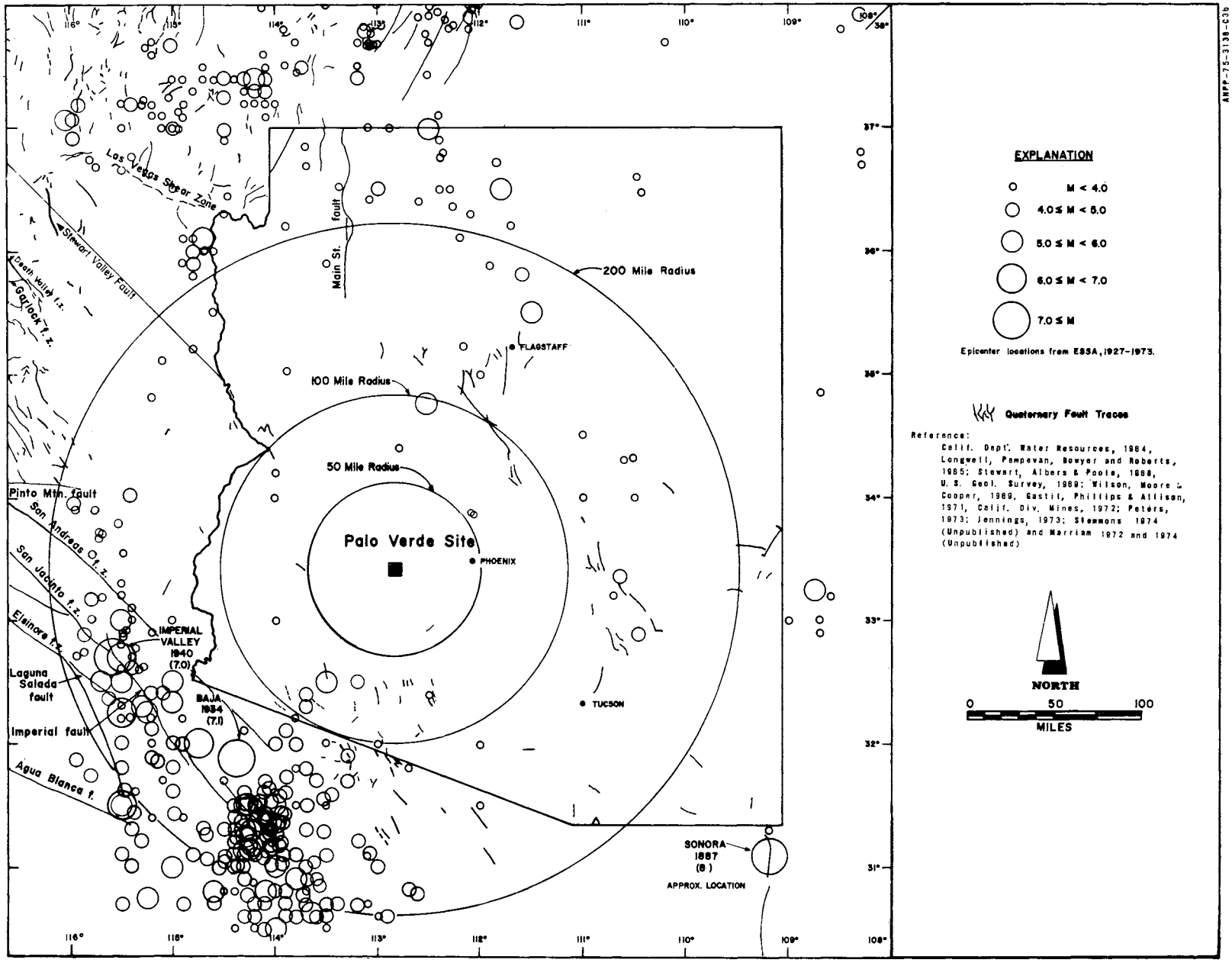

Figure 12. Earthquake epicenter map of Arizona and adjacent areas.

3) Effect of shaking or loading on the performance of foundation soils;
4) Impact of other geologic hazards at the site (subsidence, fissuring, collapse, etc.)

The maximum level of earthquake shaking that could conceivably be expected at the site is called the Safe Shutdown Earthquake (SSE). This is the level of shaking used to design the critical components of the plant. Under SSE conditions, the plant is designed to shut down operation without an accident if such shaking occurred. The SSE is a maximum credible seismic event that is conservatively determined after a complete study is made of the seismology, structural geology and tectonics of a 200-mile radius of the site.

The NRC criteria requires that the potential for surface faulting be precluded within a 5-mile radius of the site. To accomplish this, any faults within a 5-mile radius must be demonstrated to:

a) have not moved once within the last 35,000 years, or
b) have no multiple movements within the last 500,000 years, or
c) have no logical connection to a fault beyond the 5-mile radius which might be considered capable of movement
d) have no demonstration of active seismicity.

As a result, it becomes highly important that a potential nuclear site has consistent Quaternary stratigraphy relatively close to ground surface to determine minimum age on faults within the 5-mile radius and, in some cases, even beyond.

A comprehensive analysis of the foundation soils is required by the NRC for Preliminary Safety Analysis Studies to preclude differential settlements, excessive consolidation, liquefaction during the Safe Shutdown Earthquake, or any other foundation phenomena that might endanger the integrity of the plant. The foundation studies also include such considerations as subsidence due to decreases in groundwater level, differential settlements or collapse of soils, and the effects of man-made hazards such as mining or withdrawal of oil. Besides immediate impacts of such conditions, all of these investigations must also consider possible long-term changes over the projected 40-year life of the plant.

SUMMARY OF NEW GEOLOGIC INFORMATION RESULTING FROM PVNGS STUDIES

GENERAL GEOLOGY

- Detailed geologic mapping of the Palo Verde Hills, Gillespie Dam area; southcentral Gila Bend Mountains; southcentral Vulture Mountains; and Rainbow Valley north of the Maricopa Mountains.
- Petrographic analysis of early and pre-Tertiary igneous and metamorphic rock; late Tertiary and early Quaternary volcanics and volcanic-derived sediments within the study area.
- Refinement of the seismo-tectonic character of southern Arizona.
- Refinement of the late Tertiary and Quaternary geologic history of the western portion of the Phoenix basin.
- Definition of small desert basin depositional history and stratigraphy.
- Reevaluation of the geothermal characteristics of the Palo Verde Hills region.

GEOPHYSICS

- Detailed seismic information and reflection surveys within a 25 mile radius of PVNGS.
- Reconnaissance and detailed gravity and magnetic surveys near Gillespie Dam, Vulture Mountain and PVNGS.

AGE DATING

- Redefinement of volcanic rock ages in the vicinity of PVNGS using K-argon method. Rock making up the Palo Verde Hills, previously identified as being Quaternary age, was K-argon dated in excess of 13 million years b.p.
- Absolute ages of the Gillespie and Arlington basalt flows were established as being 3.4 to 1.4 million years b.p.
- Paleomagnetic analysis of several hundred samples of basin sediments in the vicinity of PVNGS; because of this analysis supported by the radiometric dates, we know that the Palo Verde basin fill is older than 0.7 million years.

GEOMORPHOLOGY

- Geomorphological studies were performed to differentiate alluvial deposits southwest of the Gillespie flow and establish their age relative to the Gillespie basalt.
- Geomorphic analysis of terrace levels on the Gila River from Hassayampa south to Gila Bend. The study was acccomplished through the use of leveling surveys on terrace benches and showed no evidence of deformation or displacement of the 40 foot terrace across the prominent Gila River lineament.

GROUNDWATER

- Identification, modeling, and analysis of a significant perched water zone in the Palo Verde site area. The zone apparently developed as a result of the infiltration of irrigation waters and the retarding of its downward migration by the Palo Verde Clay acting as an aquitard.

ENGINEERING

- Detailed engineering analysis of desert basin sediments to establish their potential for liquifying under seismic loads.
- Refinement of available subsidence data relative to salt bodies and massive groundwater withdrawal.

Specific details concerning the items listed may be obtained by consulting the references cited.

Interleaf. Spheroidal weathering of coarse-grained granite bedrock in a semiarid environment. Granite Delles, Prescott, Arizona. (Photograph No. 3739 taken August 31, 1975 by Troy L. Péwé.)

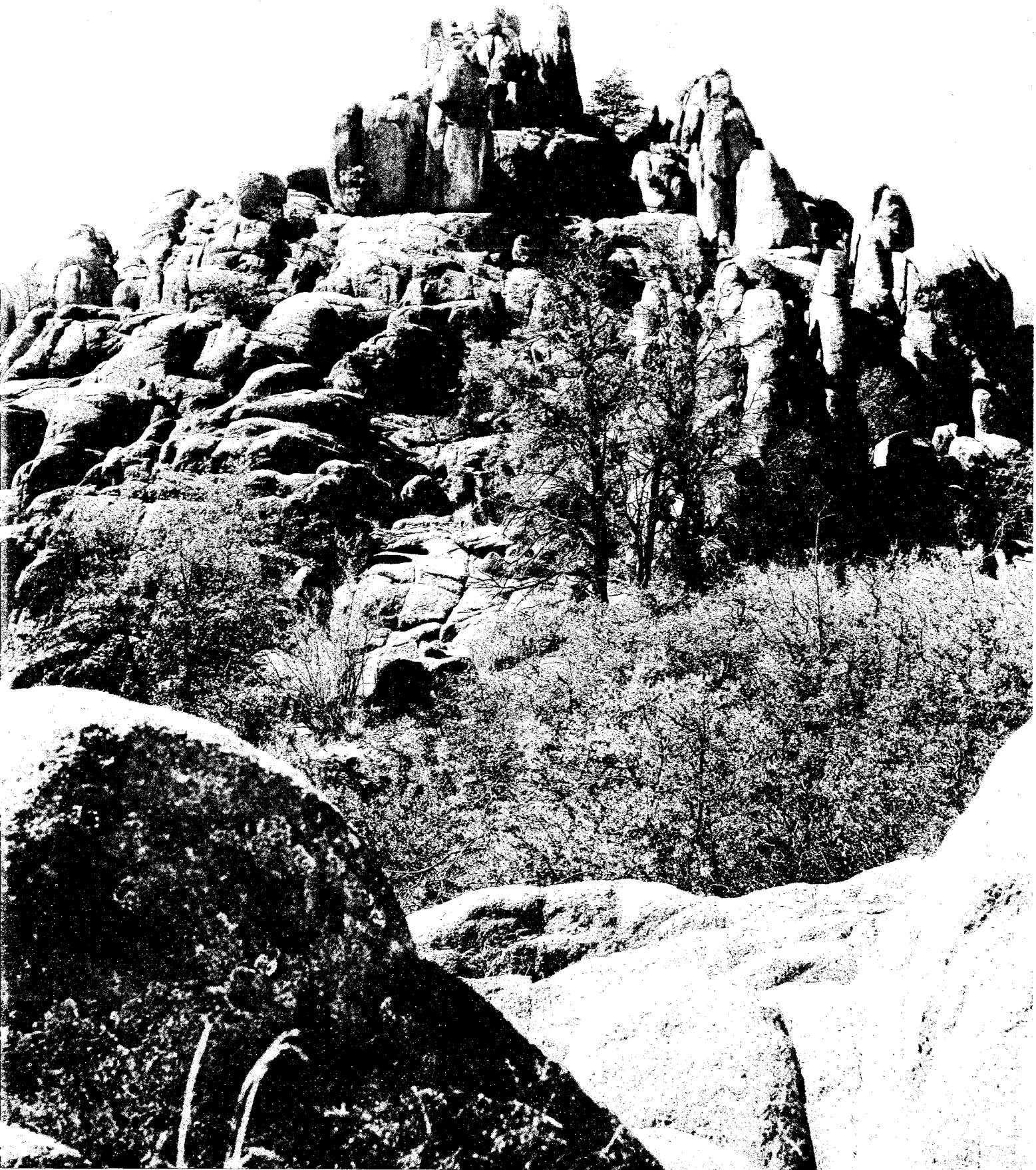

PALEOZOIC BIOSTRATIGRAPHY AND PALEONTOLOGY ALONG THE MOGOLLON RIM, ARIZONA

This one-day field trip permits examination of Devonian, Pennsylvanian, and Permian stratigraphy and biostratigraphy. Pennsylvanian and Permian fossil localities will also be visited.

The field trip guide consists of three separate articles. These involve, in order, paleontology, stratigraphy, and a road log. The road log from Payson to Pine, on pages 34–36 of the New Mexico Geological Society Thirteenth Field Conference Guidebook (1962), might also prove useful.

PALEONTOLOGY OF THE NACO FORMATION IN THE KOHL RANCH AREA, ARIZONA

by
Stanley S. Beus
Northern Arizona University
and
Douglas C. Brew
University of Minnesota

This trip will traverse part of the Basin and Range Province northeast of Tempe and end up in the transition zone between the Basin and Range and Colorado Plateau provinces below the Mogollon Rim. The total distance is about 230 miles.

We will examine outcrops of Devonian through Permian age, and collect Devonian, Pennsylvanian and Permian fossils. The major collecting site will be in the Naco Formation near Kohl Ranch, discussed below. Possible localities are indicated in figure 1.

GENERAL STRATIGRAPHY

The Naco formation of central Arizona is a predominantly marine sequence of interbedded limestones and terrigenous sedimentary rocks of Pennsylvanian age. The formation is separated from the underlying Mississippian Redwall Limestone by a conspicuous regional disconformity produced by deposition of Pennsylvanian sediments on an ancient Late Mississippian-Early Pennsylvanian karst topography (Huddle and Dobrovolny, 1945, 1952; Brew, 1970; Mckee and Gutschick, 1969). The Naco Formation is 1,200 feet thick in east-central Arizona, where it ranges in age from Middle through Late Pennsylvanian (?Atokan through Virgilian). The Naco thins northwestward, however, and wedges out, grading laterally and upward into the Pennsylvanian-Permian Supai Formation (Jackson, 1951, 1952; Brew, 1970; see fig. 1).

Brew (1970) recognized three members in the Naco Formation of central Arizona that were informally designated the alpha, beta, and gamma members. The lowermost, or alpha member, typically consists of a basal, unbedded reddish-brown cherty mudstone, siltstone, or conglomerate overlain by stratified mudstone, silstone, and sandstone that locally contain fossiliferous limestone lenses. The lower unbedded portion is generally interpreted to represent a regolith formed in situ via solution of the Redwall Limestone, whereas the upper portion consists predominantly of insoluble residues reworked by marine or perhaps both nonmarine and marine agencies (Huddle and Dobrovolny, 1945, 1952; Brew, 1970; McKee and Gutschick, 1969). The alpha member is gradationally overlain by the beta member, a richly fossiliferous sequence of ledge-forming limestones interbedded with less resistant calcareous shales and mudstones. The beta, in turn, grades into the overlying gamma member, a succession of reddish-brown clastics and interbedded limestones produced by the interfingering of marine units and continent marginal and terrestrial redbeds of the southeastward-building Supai delta (Brew, 1970).

The contact of the Naco Formation with the overlying Supai Formation is gradational and time-transgressive. Although the absence of fossils in the basal Supai beds precludes precise age determination, in central Arizona the contact has been tentatively assigned a late Middle Pennsylvanian age (late Desmoinesian). In east-central Arizona, Winters (1963, p. 15) and Brew (1970, p. 134) considered the Naco-Supai contact to be coincident with the Pennsylvanian-Permian boundary.

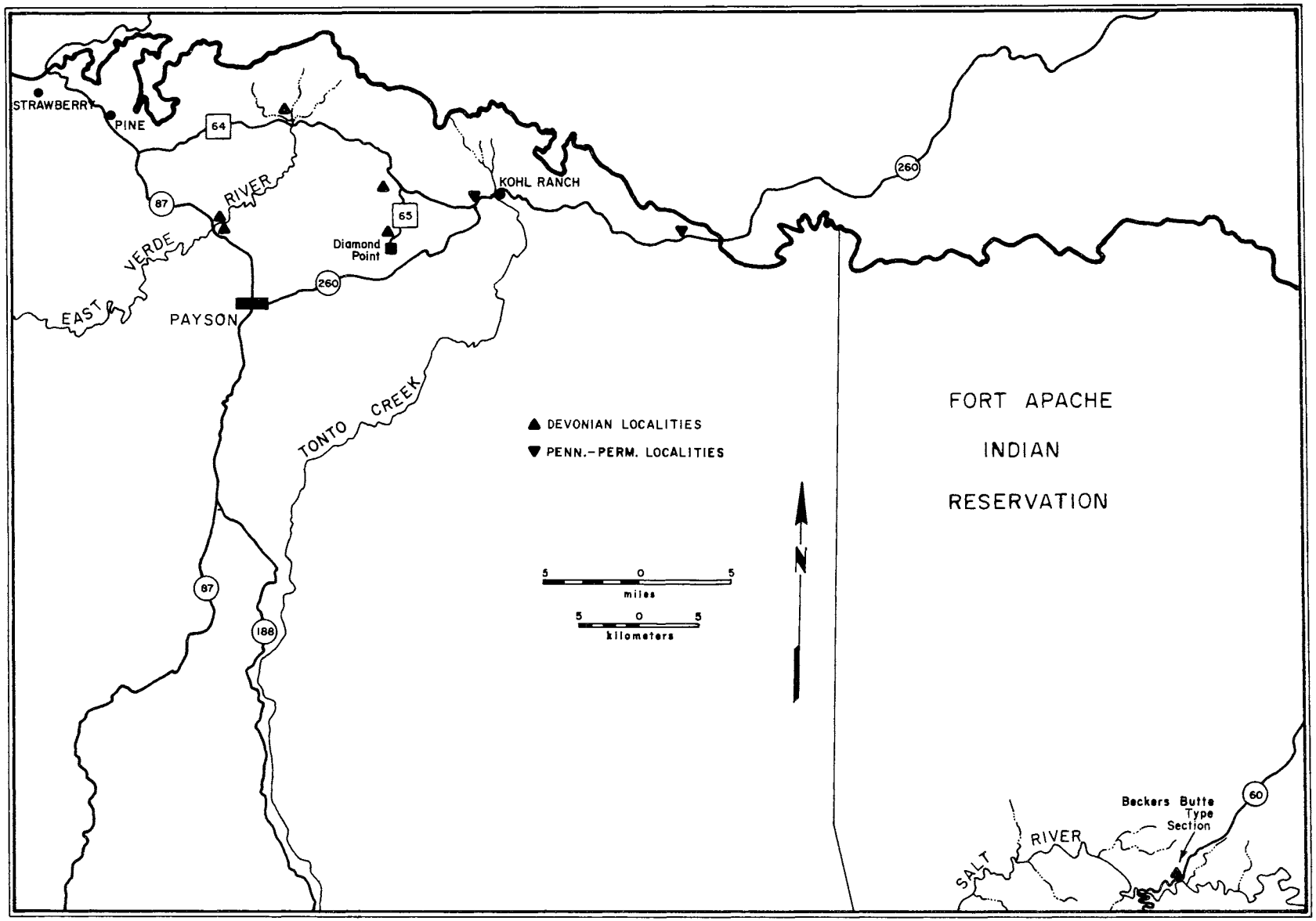

Figure 1. Selected Paleozoic stratigraphic and fossil localities below the Mogollon Rim, central Arizona.

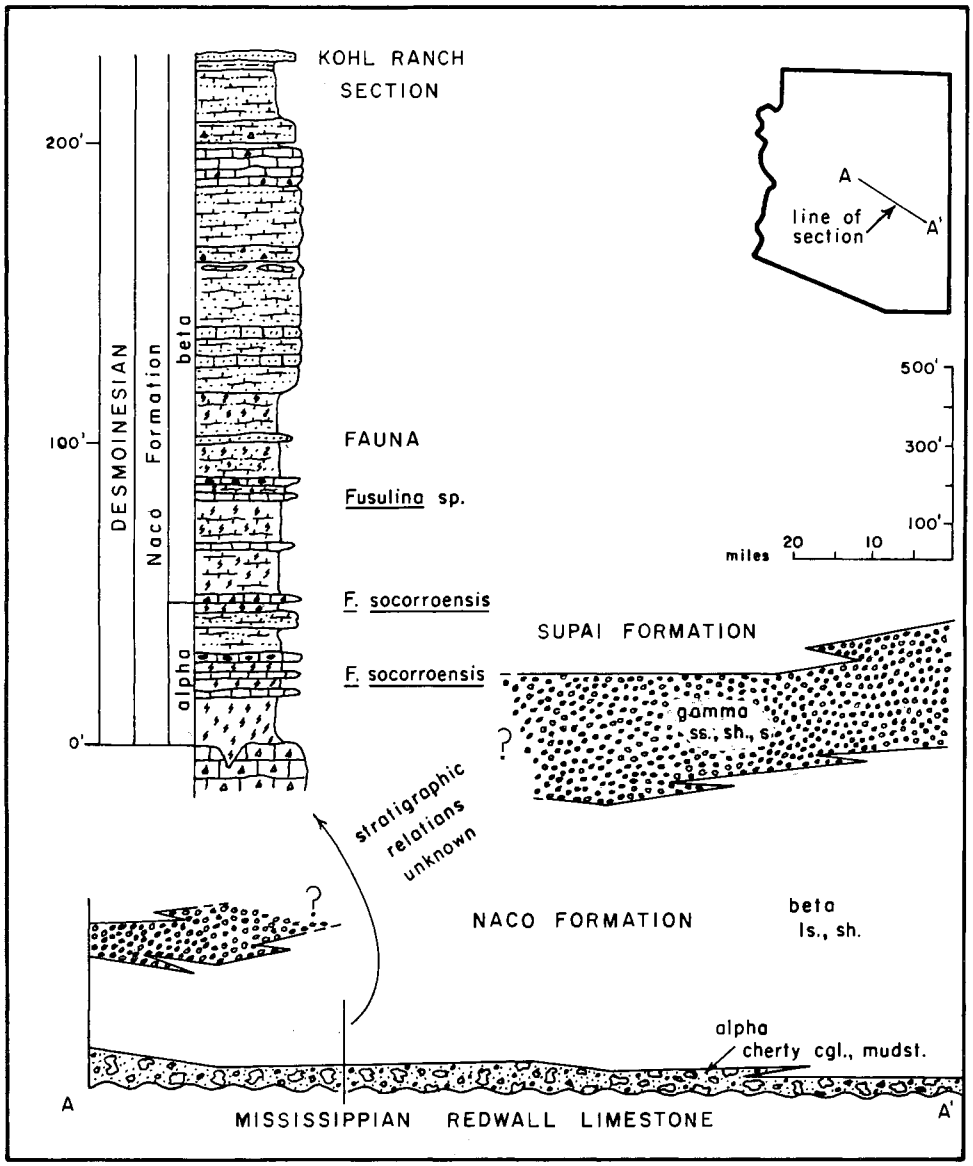

Figure 2. Diagrammatic cross section of the Naco Formation in east-central Arizona. Kohl Ranch columnar section is shown in detail. (Data from Brew, 1965, unpub. Ph.D. dissertation, Cornell University.)

PALEONTOLOGY

Pennsylvanian invertebrate faunas are rich and varied in the Naco Formation. The Kohl Ranch locality has been a favorite collecting site for paleontology classes and amateur collectors for many years, and is probably one of the most prolific fossil localities in the state. As such, it has been rather thoroughly depleted of the larger and rarer elements of the fauna, but continues to yield more common species in abundance.

The Kohl Ranch locality occurs in a light brownish-gray calcareous siltstone and mudstone of the beta member of the Naco. Although the locality is not from a measured stratigraphic section, the fossiliferous horizon appears to fall within the stratigraphic interval from bed 18 through bed 23 of the Kohl Ranch section of Brew (1965, unpublished Ph.D. Dissertation, Cornell University, p. 139–140), which is located approximately 1.2 miles to the east. The Kohl Ranch section is shown graphically in figure 2 and the probable stratigraphic position of the faunule is indicated on the section.

The common elements from this locality were described by Brew and Beus (1976) and Webster and Lane (1970). The more abundant species are illustrated in figures 3 and 4. The following species have been recognized at the Kohl Ranch locality:

Coelenterata
- *Paraconularia kohli*

Gastropoda
- *Straparollus (Amphiscapha) subrugosus*
- *Bellerophon (Bellerophon) crassus*
- *Platystoma* sp.
- Loxonemid Gen. and sp. indet.

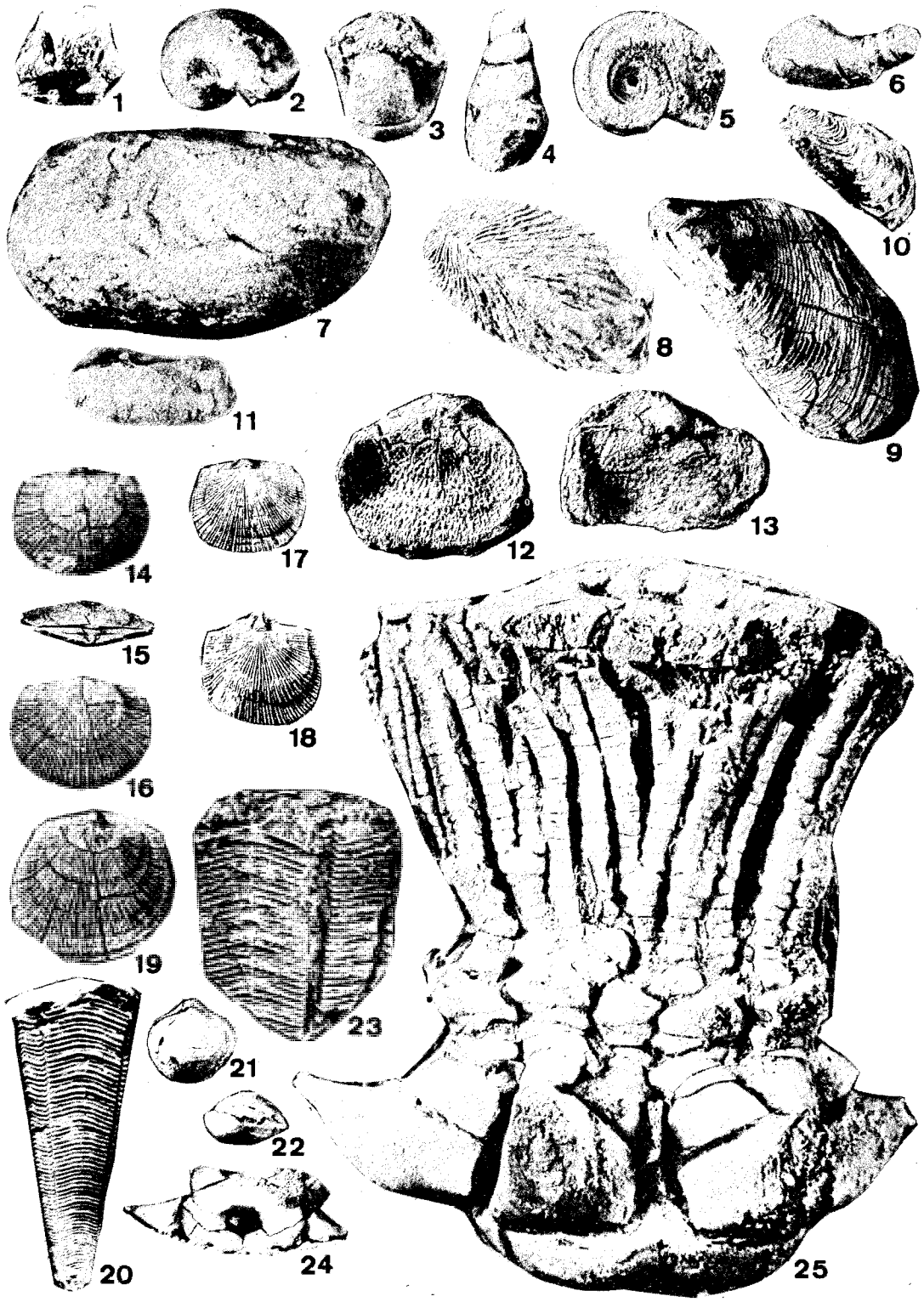

Figure 3. Common fossils from Kohl Ranch (used by permission of the S.E.P.M.)

Explanation of Figure 3

(All specimens × 1 unless otherwise indicated)

Nos. *1–3*—*Bellerophon (Bellerophon) crassus* (Meek and Worthen). *1, 3,* apertural view, NAU 563, 560; *2,* umbilical view NAU 561 (all ×2).

4—Pseudozygopleurid gastropod, side view, NAU 552.

5—*Straparollus (Amphiscapha) subrugosus* (Meek and Worthen). Umbilical view, NAU 558 (× 2).

6—*Phestia* sp., side view, NAU 571 (×2).

7—*Wilkingia terminale* (Hall). Side view, NAU 582.

8–10—*Myalina (Myalina) nacoensis* n. sp. *8,* dorsal view, NAU 572 (×2); *9,* left side view, holotype NAU 578; *10,* left side view, paratype, NAU 577.

11—*Permophorus subcostatus* (Meek and Worthen). Left side view of internal mold, NAU 558.

12, 13—*Juresania nebrascensis* (Owen). Brachial views, NAU 592, 576.

14–19—*Derbyia crassa* (Meek and Hayden). *14–16,* brachial, posterior and pedicle view, NAU 594; *17–19,* brachial view, NAU 597, 595, 596.

20, 23—*Paraconularia kohli* n. sp. Side view, holotype, ASUX-61; paratype, NAU 579 (×2).

21, 22—*Cleiothyridina orbicularis* (McChesney). Side view and brachial view, NAU 154.

24, 25—*Eirmocrinus jeani* n. sp. Holotype, NAU 591, viewed from base (×1) and anterior (×2).

Bivalvia

Phestia Sp.
Myalina (Myalina) nacoensis
Permophorus subcostatus ?
Wilkingia terminale

Brachiopoda

Derbyia crassa
Echinaria semipunctata
Juresania nebrascensis
Antiquatonia portlockiana
Linoproductus prattenianus
Cleiothyridina orbicularis
Composita subtilita
Anthrocospirifer occiduus
Leptalosia sp.
Chonetinella sp.

Bryozoa

Ramose, fenestrate and encrusting forms, 6-8 species

Crinoidea

Sciadiocrinus brewi
Eirmocrinus jeani
Delocrinus sp.
2 sp. indet.

The age of assemblage is Desmoinesian based on the age ranges of the above species and the age of underlying fusulinid-bearing beds.

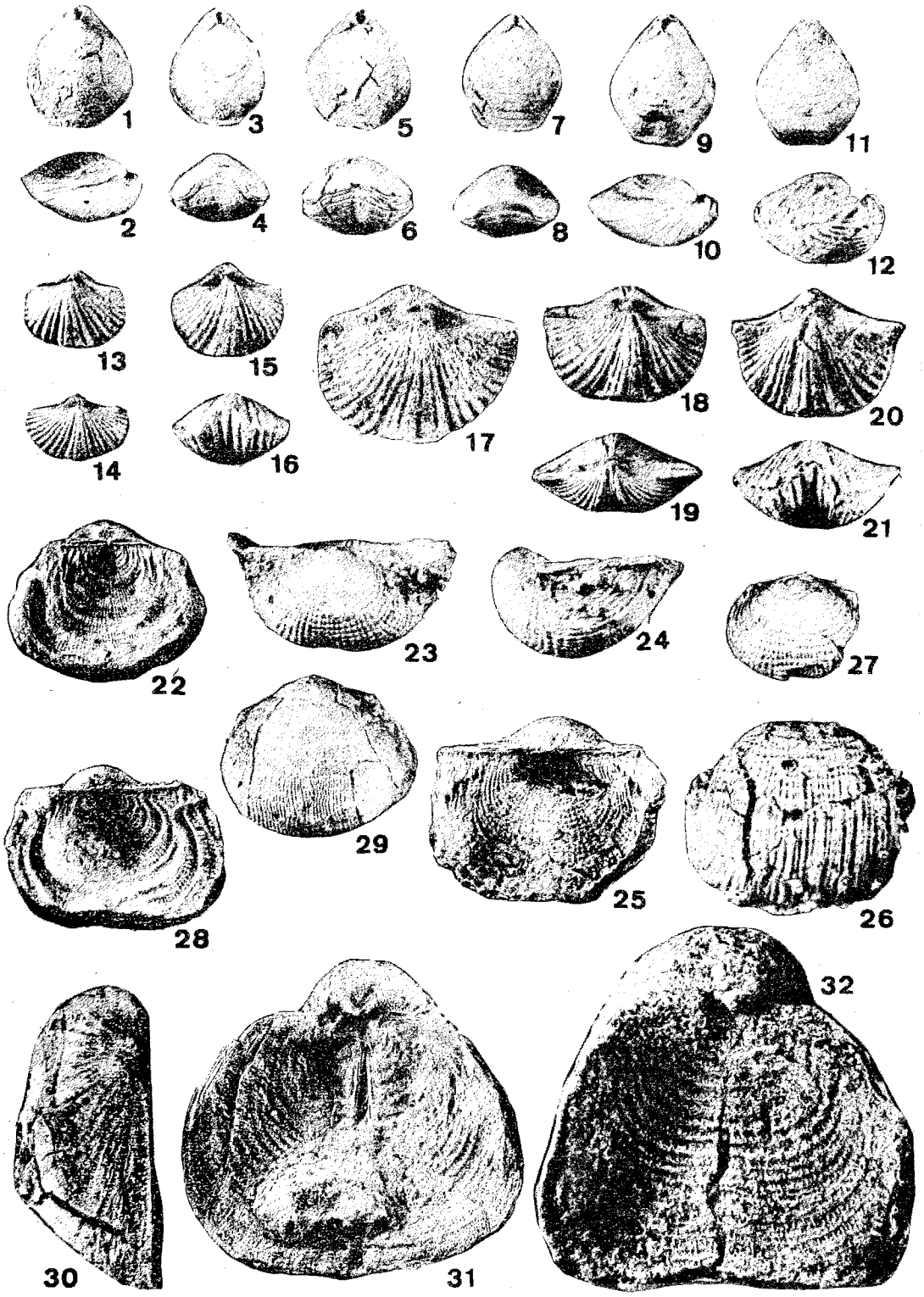

Figure 4. Additional common fossils from Kohl Ranch (used by permission of the S.E.P.M.)

Explanation of Figure 4

(All specimens ×1 unless otherwise indicated)

Nos. *1–11*—*Composita subtilita* (Hall). *1, 2,* Brachial and side view, NAU 547; *3, 4,* brachial and anterior view, NAU 615; *5, 6,* brachial and anterior view, NAU 548; *7,* brachial view, NAU 546; *8–11,* anterior, brachial, side and pedicle view, NAU 549.

12–21—*Anthracospirifer occiduus* (Sadlick). *12, 20, 21,* Side, brachial and anterior view, NAU 569; *13, 14,* brachial view, NAU 656, 564; *15, 16,* brachial and anterior view, NAU 566, *17,* brachial view, NAU 568; *18, 19,* brachial and posterior view, NAU 570.

22, 28, 29—*Linoproductus prattenianus* (Norwood and Pratten). *22, 29,* brachial and pedicle view, NAU 585; *28,* brachial view, NAU 583.

23–27—*Antiquatonia portlockiana* (Norwood and Pratten). *23–26,* Posterior, side, brachial, pedicle view, NAU 573; *27,* pedicle view, immature specimen, NAU 581.

30–33—*Echinaria semipunctata* (Shephard). *30, 31,* Side and brachial view, NAU 587; *32,* brachial view, NAU 586.

REFERENCES CITED

Brew, D.C. 1970. The Naco Formation (Pennsylvanian) in central Arizona: Plateau, 42(4): 126–138.

——and S.S. Beus. 1976. A Middle Pennsylvanian fauna from the Naco Formation near Kohl Ranch, central Arizona. Jour. Paleontol. 50: 888–906.

Huddle, J.W. and E. Dobrovolny. 1945. Late Paleozoic stratigraphy and oil and gas possibilities of central and northeastern Arizona. U.S. Geol. Survey Oil and Gas Inv. Prelim. Chart 10.

——1952. Devonian and Mississippian rocks of central Arizona. U.S. Geol. Survey Prof. Paper 233D, p. 67–112.

McKee, E.D. and R.C. Gutschick. 1969. History of the Redwall Limestone of northern Arizona: Geol. Soc. America Mem. 114, 726 p.

Webster, G.D. and N.G. Lane. 1963. Carboniferous echinoderms from the southwestern United States. Jour. Paleontol. 44: 276–296.

Winters, S.S. 1963. Supai Formation (Permian) of eastern Arizona. Geol. Soc. America Memoir 89, 99 p.

Stratigraphic and Paleomagnetic Relations Between Basal Cambrian and Devonian Strata in Central Arizona

by
D. P. Elston and S. L. Bressler
U.S. Geological Survey
Flagstaff, Arizona

ABSTRACT

In central Arizona basal Paleozoic arkosic cross-bedded sandstone is unconformably overlain by sandstone and carbonate of Devonian age. The basal sandstone, Tapeats-like in character, is shown from paleomagnetic directions and mixed polarities to be temporally equivalent to the Tapeats Sandstone (Early and Middle Cambrian) of the Grand Canyon of northern Arizona.

Strata of the Beckers Butte Member (late Givetian or early Frasnian) of the Martin Formation, directly overlie the Tapeats and form a thin stratigraphic interval that is present discontinuously across much of central Arizona. The lower unit consists of carbonate-cemented sandstone, and sandy carbonate. The upper unit consists of thin beds of aphanitic dolomite. The Beckers Butte is recognized for a distance of about 180 km, from the area of the Salt River Bridge on the southeast to exposures on the Verde River, about 25 km northwest of Jerome. Paleomagnetic directions of the Beckers Butte and overlying strata of the Martin Formation are identical with the reversed polarity paleomagnetic direction of the Temple Butte Limestone (late Givetian? to Frasnian) of the Grand Canyon. The Beckers Butte is unconformably overlain by the fetid dolomite unit of the Jerome Formation, a relationship seen from exposures along the highway just west and east of the bridge across the East Verde River.

INTRODUCTION

The age and stratigraphic relationships of basal Paleozoic sandstone and carbonate strata in central Arizona has long been a matter of concern and of some speculation. Arkosic cross-bedded sandstone exposed along the Mogollon Rim long ago was considered equivalent to the Tapeats Sandstone (Early and Middle Cambrian, McKee and Resser, 1945) of the Grand Canyon of northern Arizona (Ransome, 1916), and such an assignment has since been made by other workers (Huddle and Dobrovolny, 1945; Titley, 1962; Elston and Bressler, 1977; Hereford, 1977). Teichert (1965), in a regional study of Devonian strata of central Arizona, recognized the Tapeats Sandstone at Jerome, Arizona, but assigned highly similar basal arkosic cross-bedded sandstone southeast of Jerome and the Black Hills to the Devonian, although he found no significant lithologic differences between the Tapeats of Jerome and the Tapeats-like strata of the Mogollon Rim region to the southeast. The purpose of this report is to call attention to stratigraphic evidence for the existence of a profound unconformity at the top of the arkosic sandstone (Tapeats) of central Arizona, and to review evidence that allows recognition of a thin basal Devonian unit (the Beckers Butte Member of the Martin Formation) from its type section near the Salt River Bridge on the southeast, to northwest of Jerome. The stratigraphic evidence is supported by paleomagnetic data.

STRATIGRAPHY

REGIONAL RELATIONS

Regional stratigraphic relations extending from the area of the Salt River Bridge on the southeast to Jerome on the northwest are shown in figure 1. Four sections that serve as keys to understanding the regional relationships are depicted in generalized form. They are sections at or near: 1) Salt River Bridge, 2) Roosevelt Dam, 3) East Verde River Bridge, and 4) Jerome. The sections are shown to call attention to stratigraphic relations between units, and to facies changes within the Beckers Butte Member of the Martin Formation. A datum is drawn at the base of the fetid dolomite unit of the Jerome Member of the Martin Formation. Detailed descriptions of these measured sections are reported in Teichert (1965, sections 3, 36, 32, and 41), who has also described the stratigraphy from a number of intermediate exposures.

TAPEATS SANDSTONE

Teichert (1965, p. 26) recognized the arkosic sandstone at Jerome as Tapeats (Cambrian) from the presence of *Corophoides* burrows. However, farther to the east, Teichert included Tapeats-like arkosic sandstone in the Beckers Butte (Devonian), although such sandstone does not occur in the type section of the Beckers Butte near the Salt River Bridge (fig. 1). About 2 km south of the Salt River Bridge (fig. 1), Tapeats-like sandstone occupies a

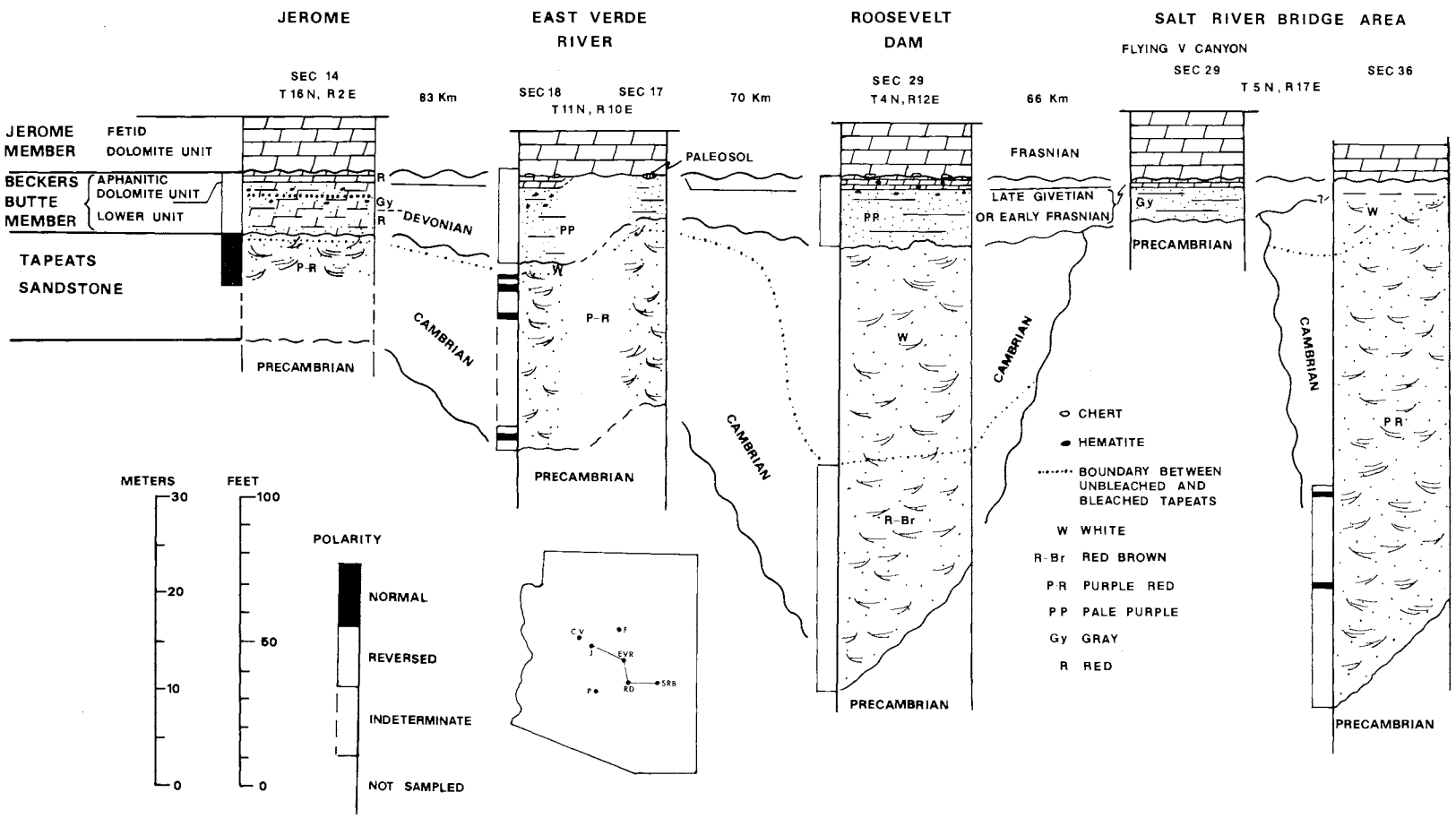

Figure 1. Stratigraphic relations and polarities for basal Cambrian and Devonian strata in central Arizona.

swale eroded into Precambrian strata. If strata typical of the Beckers Butte are present at this locality, they lie in a very narrow covered interval separating arkosic sandstone from the overlying fetid dolomite unit of the Martin. In exposures at Roosevelt Dam and near the East Verde River Bridge, Teichert also included thick sections of basal Paleozoic arkosic sandstone in the Beckers Butte.

Attention is called to the existence of an interval of white sandstone at the top of the Tapeats of Jerome and the Tapeats-like beds of the Mogollon Rim. An original dark red to purple coloration seen in underlying beds apparently has been removed, presumably by pre-Late Devonian weathering. Very locally east of the East Verde River Bridge, a pale purple coloration, similar to the color of overlying sandstone of the Beckers Butte, is irregularly superimposed at the top of the bleached sandstone. The zone of bleaching is regionally thickest on the east and southeast, thinner at the East Verde River, and very thin in the Jerome area on the northwest (fig. 1). The bleaching clearly predates deposition of the Devonian strata in central Arizona, and is interpreted to reflect bleaching as the Tapeats lay exposed at a surface of erosion some tens or hundreds of millions of years before deposition of the Devonian strata. Where strata of the Beckers Butte overlie the arkosic sandstone, material of the bleached zone that locally includes pebbles has been reworked into the basal part of the overlying sandstone.

Lithologic consistency, stratigraphic position, and evidence for a substantial stratigraphic break at the top of the arkosic sandstone, together argue for a general correlation of the basal Paleozoic arkosic sandstone of central Arizona with the Tapeats Sandstone of Jerome and the Grand Canyon. This conclusion is supported by paleomagnetic data (Elston and Bressler, 1977) and by the recent discovery of *Corophoides* by Hereford (1977) in the Tapeats Sandstone south of the Salt River Bridge.

BECKERS BUTTE MEMBER OF MARTIN FORMATION

The Beckers Butte Member of the Martin Formation was named by Teichert (1965, p. 16) for exposures along U.S. Highway 60, near Beckers Butte and Flying V Canyon, about 2 km northeast of the Salt River Bridge. At the type section, there is no arkosic sandstone reminiscent of the Tapeats, and the member is a simple two-fold unit consisting of gray to brown carbonate-cemented sandstone overlain by a narrow interval of thin bedded aphanitic dolomite. Thin, dark gray shale interbeds in the aphanitic dolomite unit contain a psilophyte flora, which Canwright (1968) in a re-evaluation considers to be late Givetian or early Frasnian in age, somewhat younger than the age originally reported by Teichert and Schopf (1958).

Proceeding westward from the Salt River Bridge, Teichert recognized both units of the type Beckers Butte at Roosevelt Dam, to which he also appended underlying arkosic sandstone of the Tapeats (fig. 1). At Roosevelt Dam, the sandstone unit of the Beckers Butte rests on an irregular erosion surface developed on the Tapeats, and conglomerate material of the Tapeats is reworked into the basal Beckers Butte sandstone. The carbonate-cemented sandstone is characterized by more parallel bedding than the Tapeats, and is mottled pale purplish, unlike the darker and redder hues of the Tapeats beneath the bleached zone. Unlike gray carbonaceous beds at the type locality near Flying V Canyon, the upper aphanitic dolomite unit is purplish red, reflecting a facies change. Chert nodules are present at the top of the aphanitic dolomite unit, a situation that also prevails in the exposure west of East Verde River Bridge (fig. 1).

The section exposed immediately west of the East Verde River Bridge is virtually identical to the section exposed just south of Roosevelt Dam. However, Teichert inexplicably assigned the upper, aphanitic dolomite unit of the Beckers Butte to the fetid dolomite unit of the Jerome Member (1965, fig. 12). Farther to the west and northwest he also failed to recognize the thin aphanitic dolomite unit as separate from the fetid dolomite unit. Thus, from the East Verde River crossing westward, the boundary between the Beckers Butte and Jerome Members was drawn by Teichert at a contact between sandstone below and dolomite above, unlike the stratigraphic relations he defined and recognized near the Salt River Bridge and at Roosevelt Dam.

Our studies call for a revision of the above stratigraphic inconsistencies. At the East Verde River, a two-fold subdivision of the Beckers Butte similar to that seen at Roosevelt Dam is recognized, and the Tapeats Sandstone is removed from the Beckers Butte. This two-fold subdivision is extended northwest to Jerome, and beyond to exposures along the Verde River northwest of Jerome. At the localities shown in figure 1, a thin but distinctive aphanitic dolomite unit underlies the fetid dolomite unit of the Jerome Member, and overlies carbonate-cemented purple sandstone or sandy red or gray dolomite, which in turn overlies the Tapeats Sandstone. The contact between the lower and upper units of the Beckers Butte is sharp, and could be disconformable, although no evidence exists for a large hiatus in deposition. The contact between the aphanitic dolomite unit and the overlying fetid dolomite unit of the Jerome Member also is sharp, and in the area of the East Verde River Bridge can be demonstrated to be unconformable, reflecting an appreciable but perhaps not large hiatus in deposition.

Exposures near the East Verde River Bridge. The Tapeats Sandstone and the Beckers Butte Member of the Martin Formation are exposed short distances west and east of the bridge that crosses the East Verde River (State Highway 87), about 7 km northwest of Payson, Arizona. A complete section of the Beckers Butte is exposed along the

highway west of the river, and should be examined before exposures along the highway east of the bridge are examined. Dark purple-red cross-bedded and cross-laminated arkosic sandstone typify the Tapeats. The upper part of the Tapeats is marked by a white, bleached interval that is about 1.5–2 m thick. Pale purple mottled, carbonate-cemented sandstone of the lower unit of the Beckers Butte Member of the Martin Formation disconformably overlies the Tapeats. The main bedding is characteristically parallel-bedded, within which cross-laminations and small scale cross-bedding occur. The upper aphanitic dolomite unit sharply overlies the lower sandstone unit, and is 1 m thick. Flattened nodular chert occurs at the undulating contact with the overlying fetid dolomite unit of the Jerome Member of the Martin Formation (see Teichert, 1965, p. 31, fig. 12). Hematite nodules are present in the aphanitic dolomite unit and in the lower part of the fetid dolomite unit. Hematite nodules also are found in the Beckers Butte Member at Roosevelt Dam and Jerome (fig. 1).

East of the bridge across the East Verde River, the fetid dolomite unit rests on an erosionally truncated section of the Beckers Butte. The aphanitic dolomite unit and beds of the upper part of the lower sandstone unit of the Beckers Butte are missing. Additionally, a prismatic-weathering red paleosol or regolith, a few centimeters thick, locally can be observed to separate the Beckers Butte and Jerome Members (fig. 1). (Indiscriminate sampling of this regolith should be avoided because of the scarcity of material, and the exposure should be preserved so that future generations of geologists can observe this rare fossil soil.) The contact of the base of the Beckers Butte with the underlying Tapeats Sandstone is perfectly exposed in the road-cut. It is here that a very pale purple coloration, similar to the color of the overlying Devonian sandstone, can be seen to be locally superimposed at the top of the white, bleached zone that marks the top of the Tapeats Sandstone.

The abrupt truncation of a significant part of the Beckers Butte in the area of the East Verde River may reflect a small structural adjustment, one that occurred at about the boundary between Middle and Late Devonian time. The presence of this unconformity can serve to explain the absence of the Beckers Butte at places in central Arizona, an absence that could be due either to erosion or to nondeposition. Some of the sections measured by Teichert (1965) show conglomerate and dolomite beds in the interval that can be assigned to the Beckers Butte. Conglomerates interbedded with dolomitic sandstone strata may simply reflect local sources from nearby hills of Precambrian rocks, which persisted in central Arizona throughout much of Paleozoic time. The possibility exists that some strata locally overlying the Tapeats and underlying strata that are more or less typical of the Beckers Butte could be considerably older than Middle Devonian, but such remains to be demonstrated.

Exposures near Jerome. Strata overlying the Tapeats Sandstone and underlying the fetid dolomite unit of the Martin Formation consist of red-brown and gray sandy dolomite, overlain by thin beds of red aphanitic dolomite that weather gray. The entire unit has been called the "dolomite facies" of the Chino Valley Formation (Cambrian?) by Hereford (1975), whose Cambrian (?) age assignment has since been changed to Devonian (Hereford, 1977) for reasons mostly summarized in this report, and largely devolving from an informal field conference held February 1976. The two-fold subdivision of the "dolomite facies" at Jerome was not recognized by Hereford, and no detailed stratigraphic correlation of these rocks can be made either with the "conglomerate facies" or with the slightly farther removed "lithic sandstone facies" of the Chino Valley Formation in the Chino Valley area. In contrast the two-fold character of the Beckers Butte is recognizable across central Arizona. Changes in lithology and color can be attributed to more or less gradual changes in facies.

On stratigraphic and paleomagnetic grounds, the interval between the Tapeats Sandstone and the fetid dolomite unit of the Jerome Member of the Martin Formation at and near Jerome is assigned to the Beckers Butte Member of the Martin Formation, a name that has clear priority. Formal revision of the stratigraphic nomenclature in the Chino Valley area is the subject of another paper.

PALEOMAGNETIC DIRECTIONS AND POLARITIES

Plots of the mean directions for Cambrian and Devonian strata of northern and central Arizona are shown in figure 2. The directions are thermally cleaned directions that are reported and discussed in Elston and Bressler (1977). The normal polarity directions (declination ~270°) for the Tapeats Sandstone of northern and central Arizona are virtually identical, as indicated by overlap of cones of confidence drawn at the 95 percent confidence level. Both the normal and reversed polarity directions for the central Arizona Tapeats are shifted toward the reversed polarity Devonian direction. The greater scatter of directions seen in the Tapeats of central Arizona (reflected by the larger cones of confidence) results from secondary overprints. One overprint was impressed during the Devonian when the Tapeats lay exposed before deposition of the Beckers Butte. This resulted in a "streaking" of some normal and reversed polarity directions toward the Devonian reversed polarity direction, implying a secondary magnetization shortly before deposition of the Beckers Butte. A second much younger overprint reflects recent exposure and weathering, and results in some directions that are "streaked" between the normal polarity present field direction and the normal and reversed polarity Tapeats directions. In spite of the

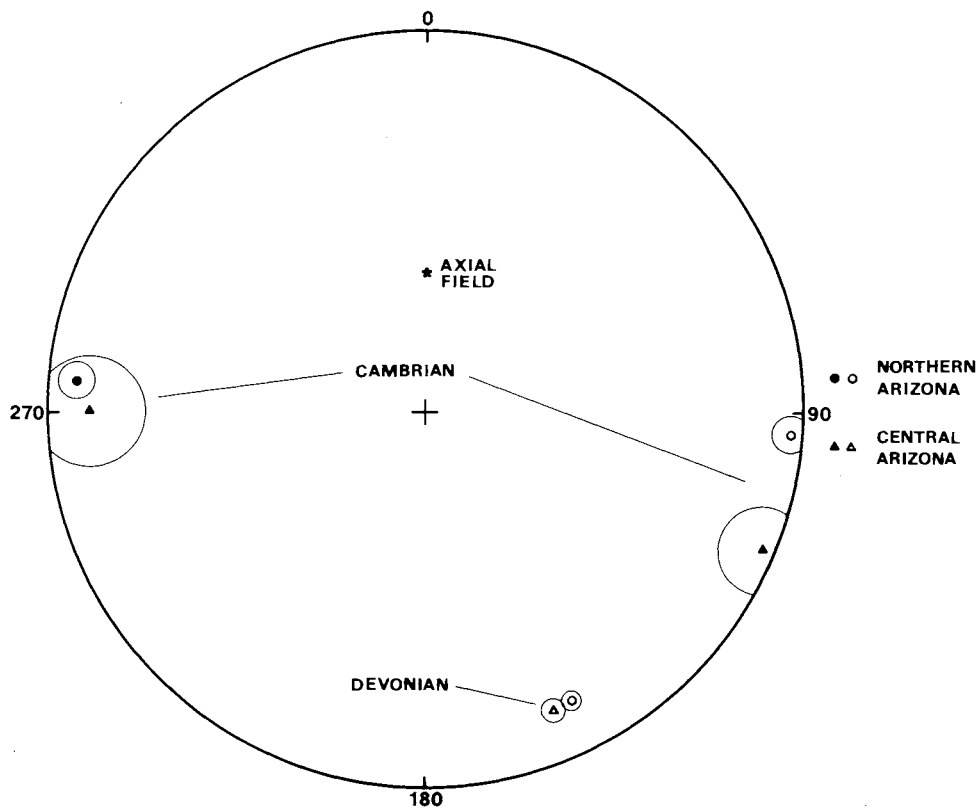

Figure 2.—Equal-area stereographic projection showing mean directions of magnetization for Cambrian and Devonian strata from northern and central Arizona. Open (closed) symbols on upper (lower) hemisphere. Circles about mean directions indicate radius of cone of confidence at the 95% level ($\alpha 95$). The number of samples, mean declination, mean inclination, and $\alpha 95$ for each unit are as follows: *Northern Arizona*—Cambrian Tapeats Sandstone—Normal polarity; n = 62, D = 275.1°, I = 8.0°, $\alpha 95$ = 4.7°; Reversed polarity, n = 67, D = 93.1°, I = −3.6°, $\alpha 95$ = 4.7; Devonian Temple Butte Limestone, n = 76, D = 153.2°, I = −15.7°, $\alpha 95$ = 1.8°; *Central Arizona* —Tapeats Sandstone Normal polarity, n = 30, D = 270.5°, I = 11.8°, $\alpha 95$ = 14°; Reversed polarity, n = 44, D = 111.5°, I = 4.2°, $\alpha 95$ = 12°; Devonian Beckers Butte Member of Martin Formation (East Verde River), n = 29, D = 156.9°, I = −15.5°, $\alpha 95$ = 2.9°.

overprints, distinct normal and reversed polarity directions are obtained from the Tapeats of central Arizona (fig. 2), and the means of these directions lie close to the normal and reversed polarity directions obtained from the Tapeats of the Grand Canyon.

It can here be noted that the polarity zonation of the Tapeats Sandstone of the Grand Canyon is marked by an interval of reversed polarity in the upper part of the formation, and that overlying strata of the Bright Angel Shale also appear to be entirely of reversed polarity (Elston and Bressler, 1977). The lower two-thirds of the Tapeats of the Grand Canyon is of mixed polarity (Elston and Bressler, 1977, fig. 2). The existence of mixed polarities in the Tapeats of central Arizona (fig. 1) thus indicate that much of the central Arizona Tapeats is temporally equivalent to the middle and lower parts of the Tapeats of the Grand Canyon.

In contrast to the mixed polarity directions seen in the Tapeats Sandstone, a single reversed polarity direction is obtained from Devonian strata of both northern and central Arizona (fig. 2). Following thermal cleaning, the paleomagnetic directions are essentially identical. (Although only data from the East Verde River Bridge section are shown in figure 2, similar directions have been obtained from other sections of the Beckers Butte.) The Devonian direction lies far from either the normal or reversed polarity Cambrian Tapeats direction, which has allowed a Devonian "streaking" of the Tapeats directions to be clearly identified on plots that show the directions of individual samples. The very tight grouping of directions seen from samples of Devonian strata of both northern and central Arizona reflects the lack of porosity of the rocks and the lack of percolation of ancient and recent ground waters, and thus a general lack of secondary magnetizations.

The paleomagnetic data, in summary, show distinctive directions and polarities between rocks of Cambrian and Devonian age in both central and northern Arizona. The change in paleomagnetic direction in central Arizona corresponds to the stratigraphic position of the unconformity at the top of the Tapeats Sandstone. Very locally, remagnetization of the uppermost Tapeats below its contact with the Beckers Butte has occurred. Such remagnetization is documented in the uppermost Tapeats exposed east of the East Verde River Bridge, where a Devonian paleomagnetic direction has been obtained from the uppermost part of the "bleached" Tapeats that now exhibits a pale purple color, presumably imposed at the time of deposition of the Beckers Butte.

SUMMARY

Stratigraphic relations and paleomagnetic data indicate that the basal Paleozoic Tapeats-like sandstone of central Arizona is temporally equivalent to the Tapeats Sandstone (Early and Middle Cambrian) of the Grand Canyon.

Basal-most Devonian strata that directly overlie the Tapeats in central Arizona are those of the Beckers Butte Member of the Martin Formation. The upper unit of the Beckers Butte consists of thin beds of aphanitic dolomite, which at the type section near the Salt River Bridge contain flora of late Middle or early Late Devonian age. Sandstone, carbonate, and locally conglomerate of the lower unit, and the upper thin aphanitic dolomite unit of the Beckers Butte are separated from overlying beds of Martin Formation by an unconformity marking a brief but appreciable hiatus in deposition. The Beckers Butte is discontinuously preserved across central Arizona, from the area of the Salt River Bridge on the southeast, to exposures along the Verde River northwest of Jerome, a distance of more than 180 km. Paleomagnetic directions from the Beckers Butte and from overlying strata of the Martin Formation are entirely of reversed polarity, and are identical to paleomagnetic directions obtained from the Temple Butte Limestone (Late Middle ? and early Late Devonian; Walcott, 1883; Noble, 1914; D. Schumacher, 1975, written communication) of the Grand Canyon of northern Arizona. Paleontologic and paleomagnetic data thus suggest that deposition of Devonian strata in northern and central Arizona began at about the same time.

REFERENCES CITED

Canright, J. E., 1968, Spores and Associated Macrofossils from the Devonian of Arizona: Geoscience and Man, Volume I, American Assoc. of Stratigraphic Palynologists, Proceedings of the First Annual Meeting, p. 83–88.

Elston, D. P., and Bressler, S. L., 1977, Paleomagnetic Poles and Polarity Zonation from Cambrian and Devonian Strata of Arizona: Earth and Planetary Science Letters, v. 36, p. 423–433.

Hereford, Richard, 1975, Chino Valley Formation (Cambrian?) in northwestern Arizona: Geol. Soc. America Bull., v. 86, p. 677–682.

———, 1977, Deposition of the Tapeats Sandstone (Cambrian) in central Arizona: Geol. Soc. Amer. Bull., v. 88, p. 199–211.

Huddle, J.W., and Dobrovolny, E., 1945, Late Paleozoic stratigraphy of central and northeastern Arizona: U.S. Geol. Survey Oil and Gas Inv. Prelim. Chart 10.

McKee, E. D., and Resser, C. E., 1945, Cambrian history of the Grand Canyon region: Carnegie Inst. Washington Pub. 563, 232 p.

Noble, L. F., 1914, The Shinumo quadrangle, Grand Canyon district, Arizona: U.S. Geol. Survey Bull. 594, 100 p.

Ransome, F.L., 1916, Some Paleozoic sections in Arizona and their correlation: U.S. Geol. Survey Prof. Paper 98-K, p. 113–116.

Teichert, Curt, 1965, Devonian rocks and paleogeography of central Arizona: U.S. Geol. Survey Prof. Paper 464, 105 p.

———, and Schopf, J. M., 1958, A Middle or Lower Devonian psilophyte flora from central Arizona and its paleogeographic significance: Jour. Geology, v. 66, no. 2, p. 208–217.

Titley, S.R., 1962, Geology along the Diamond Rim and adjoining areas, Gila and Navajo Counties, Arizona, *in* Weber, R.H., and Peirce, H.W. eds., New Mexico Geological Society Guidebook, Thirteenth Field Conf., p. 123–128.

Walcott, C.D., 1880, The Permian and other Paleozoic groups of the Kanab Valley, Arizona: Am. Jour. Sci., 3rd Ser., v. 20, no. 26, p. 221–225.

ROAD LOG FROM TEMPE TO PAYSON AND DIAMOND POINT VIA HIGHWAYS 87 AND 260

Prepared by
Department of Geology
Arizona State University
Tempe, Arizona

MILES Interval	MILES Total	
0.0	0.0	Start at parking lot north of Geology/Physics Building on campus of Arizona State University. Leave parking lot and drive east on University Drive.
0.3	0.3	Turn north on Rural Road.
0.2	0.5	**STOP 1.** At 9 o'clock we see Tempe Butte with Sun Devil Stadium nestled on its eastern end. This landmark is not a geologic "butte" but represents a fault block which has been tilted toward the south. The steep upper one-third of the section exposed on the north-facing slope is middle to late Tertiary porphyritic andesite flows. Beneath this volcanic sequence is a thicker unit consisting of thin to thick amygdaloidal andesitic flows intertonguing with thin beds of fine- to medium-grained tuffaceous clastic sedimentary rocks. The basal portion of the north slope is made of partly tuffaceous siltstones and sandstones which exhibit ripple marks, mudcracks, scour marks, sole markings, current lineation features and imprints of palm fronds. These sediments were deposited on the floodplain of an ancient stream which flowed generally northeast, just about the reverse of the modern Salt River. The sandstones yielded part of a tooth believed to be from *Procamelus*, a Middle Miocene to middle Pliocene North American cameloid. Within the sedimentary sequence outcrops a thin, tightly-convoluted layer of yellowish clay which is believed to have been deposited as a volcanic ash in a lake or pond. On the north side of the Salt River floodplain one can find a sequence of clastic deposits very similar in appearance of the lower part of the Tempe Butte section. The presence here of a distinctive tightly-convoluted, yellowish claystone layer suggests that this sequence of sedimentary rocks may be the same sequence that is exposed on the south limit of Salt River. Such repetition is probably the result of normal

faulting with the north block being displaced downward. Such a hypothetical fault probably lies beneath the alluvial fill of the Salt River; this fill is only about 12 feet deep in the vicinity of Tempe Butte.

0.2 0.7 Aqueduct across the main channel of the Salt River. Exposed on the surface of the river bed is a lag gravel which lies on top of the sandy gravel alluvium of the Salt River. The road across this part of the floodplain is often flooded during periods of intensive or extended precipitation.

0.3 1.0 **STOP 2.** At 10 o'clock we can see the unique morphology of the Papago Buttes. Camelback forms a suitable background. The Papago Buttes are not buttes either in a geologic sense but represent highly dissected remnants of a complexly faulted structure which probably formed after Middle Miocene time. The ? *Procamelus*-bearing sediments of Tempe Buttes were apparently caught up in the same faulting episode which isolated the Papago Buttes blocks. The arkosic conglomerates and breccias comprising the main rock type of the "buttes" were apparently derived by rather rapid erosion of the Precambrian granitic and metamorphic rocks which are now exposed in the subdued hills and slopes along the eastern flanks of the "buttes" and often between them. Fragments of the weathered and eroded source rock were transported by streams and mudflows and were quickly deposited on rather steep slopes then existing. The arkosic sediments dip toward the west. Other "buttes" of the area are made up of dacitic ash-flow tuffs of probable mid-Tertiary (Miocene?) age; these rocks form bold outcrops much like the coarse arkosic sediments. The undulating surface of a pediment cut into bedrock radiates outward in all directions from the Papago Buttes.

Cut into the arkosic and tuffaceous sediments are rock shelters called "taffoni." These small, spherical to ellipsoidal pockets and cavelets form by cavernous weathering a little-understood process which probably is the result of hydration of feldspars and biotite to form clays and salts. The rock shelters reach exceptional sizes in which ceiling heights are 50 feet, depths are 25 feet and lengths are 150 feet; however, average measurements are much smaller. Small shelters tend to be spheroidal and aligned along joint and bedding planes. Once these pockets reach a diameter of about 8 feet, they begin to grow transverse to joints and bedding.

Wind is known to be a factor in cavernous weathering (Jennings, 1968), but contrary to popular belief, windblown particles do *not* cut the taffoni (Péwé, 1974). Apparently the primary roles of wind are (1) to remove thin spalls broken from bedrock by cavernous weathering, and (2) to direct precipitation moisture into the rock shelters. In this part of the Phoenix Basin the dominant wind direction is from the east; on the Papago Buttes taffoni are most common on east- and south-facing slopes. However, pockets and niches are rare on steep slopes no matter what their orientation.

0.4 1.4 Road goes up scarp of the second highest terrace of the Salt River terrace system.

1.9 3.3 Intersection of Scottsdale Road and East McDowell Road. Turn right and proceed east.

4.1 7.4 Alma School Road.

0.7 8.1 Turn left onto Arizona Highway 87.

0.3 8.4 A gravel pit complex from which stream-washed, sandy gravels of the Salt River are being extracted for commercial purposes can be seen on the right.

0.8 9.2 Remnants of an ancient Hohokam irrigation system can be seen near the dissected scarp of the second highest terrace of the Salt River, the Mesa Terrace (Péwé, 1978). These people dug and maintained this network from the 10th through 13th centuries A.D. A total of about 125 miles of canals were built in the Salt River Valley. Each canal had to lie at just the right slope to provide water movement, but not erosion. The extensive system developed by these early peoples is testimony to their ingenuity and industry.

2.0 11.2 Silty-sandy slopewash covers the gravels of the second highest terrace. Ahead are Sawik Mountain and Mt. McDowell.

1.2 12.4 As we drop off the surface of the second highest terrace onto the next lower level we can see to our immediate right that we are driving across sandy deposits of low-angle alluvial fans. These fans are derived from our left by the natural dissection of the two highest terraces of the Salt River, the Sawik and Mesa Terraces. The light brown, sandy

fan deposits contrast sharply in color and grain size with the underlying gravelly alluvium.

1.2 13.6 Beeline Drag Strip on the right. Across the Salt River to the south we can see the graded profile of a pediment against the skyline. This is one of a series of coalescing pediments which grade to the floodplain of the Salt River and to the Phoenix Basin. Periodic uplifts of the Mazatzal Mountains to the east caused pediment dissection and formation of terraces along the Salt River. Evidence for at least four episodes of uplift are the four major terraces along the Salt River; these surfaces converge in a downstream (west) direction (Péwé,1971, 1978).

1.0 14.6 Crossing of the Arizona Canal. This irrigation system was constructed after Granite Reef Dam was completed in 1908; waters of the Salt River are diverted into this canal 3.6 miles to our east at Granite Reef Dam. An earlier version of the Arizona Canal was begun in 1883. This system drew its water directly from the bed of the river without benefit of a diversion dam.

1.5 16.1 Road climbs up the low-angle surface of an alluvial fan derived by the dissection of Salt River terraces. Ahead is Mt. McDowell. The basal rock of this prominent landmark is Precambrian quartz monzonite. Overlying this granitic material outcrops a rather thick sequence of reddish Tertiary(?) arkosic conglomerates and breccias. A series of thin basalt flows is sandwiched between the arkosic sediments and a thick sequence of mid-Tertiary dacite ash-flow tuffs that comprise most of Mt. McDowell. The entire sedimentary section dips toward the southwest. Mt. McDowell is a horst block surrounded on all sides by faults.

0.9 17.0 First outcrop of the Mt. McDowell arkose along Highway 87.

0.3 17.3 To the right you can see part of the basalt flow unit outcropping on the lower flanks of Mt. McDowell. To the left at 10 o'clock the Precambrian metamorphic-igneous terrain of the McDowell Mountains appears a drab gray compared to the colorful sedimentary sequence of Mt. McDowell proper.

1.2 18.5 First roadside outcrop of the Precambrian quartz monzonite basement rock in the Mt. McDowell area.

0.8 19.3 Junction of Highway 87 with Shea Blvd.

1.6 20.9 Highway 87 now descends to the Verde River floodplain. The road crosses a typical gullied surface of the pediment (Péwé, 1978) cut into Precambrian quartz monzonite and Tertiary valley-fill sediments.

0.5 21.4 Junction of Highway 87 with access road to Fort McDowell Indian Reservation. Ahead across the Verde River you can see a very prominent high-level surface (Pope, 1974). This terrace is made up entirely of Cenozoic valley-fill sediments which have been reworked by the Verde River to form a surface equivalent in elevation and age to the Mesa terrace of the Salt River. The bold vertical cliffs of the Verde River terrace are supported by a 30- to 40-foot thick caliche zone which is very old and partially silicified.

0.4 21.8 Crossing of the Verde River. The waters of this perennial stream are derived from faults at the head of numerous tributaries draining the Mogollon Rim area (Feth and Hem, 1962).

0.7 22.5 To the right we can see part of the highest terrace of the Salt River.

0.4 22.9 The road traverses Tertiary valley-fill deposits. The glacis surface to our right is being cut into these rather soft sediments and is graded to a low terrace of the Salt and Verde Rivers.

0.6 23.5 Note the well-developed, typical caliche beds and zones in the valley-fill sediments. These features suggest that the climate during formation of this sequence was little different from the present arid climate of this area.

0.9 24.4 To the right front is Stewart Mountain, a mass of Precambrian quartz monzonite surrounded by Tertiary valley fill.

1.1 25.5 Ahead Four Peaks stands boldly against the sky. Amethyst is commercially mined from this area.

7.7 33.2 **STOP 3.** Desert Vista turnoff. To our southeast on the skyline we see a rough, mountainous terrain dominated in the center by Weaver's Needle. These highlands are famous in Arizona's history and legends. The Goldfield and Superstition Mountains comprise the right portion of the mountains; the Cauldron Complexes form topographic lows in the center between us and Weaver's Needle; Geronimo Head lies on the north (left) end of the complex. This middle Tertiary volcanic terrain has been described by Sheridan (this guidebook) and Sheridan,

Stuckless, and Fodor (1970). Structurally the area is made up of at least two highly-faulted cauldrons surrounded by a higher, relatively flat-lying, unfaulted volcanic plateau made up in large part by pyroclastic ash-flow tuffs derived from the cauldrons. Weaver's Needle is often described as a classic volcanic neck, but is now known to be an erosional remnant of ash-flow tuffs which formerly extended completely around the Superstition cauldron.

The oldest rocks in the Superstition-Goldfield Mountains area are Precambrian granites. These igneous rocks are unconformably overlain by reddish, arkosic conglomerates such as we have seen cropping out on the lower flanks of Mt. McDowell. Overlying the arkosic sediments is the volcanic sequence which you see before you. This volcanic sequence can be divided into three distinct episodes: (1) an early stage of dome and lava flow formation by latites and basalts; (2) a thick sequence of more silicic rhyodacite to rhyolite welded ash-flow tuffs comprising several cooling units and associated with the collapse of the central cauldrons; and (3) a late stage emplacement of rhyolite-rhyodacite domes on the cauldron margins followed by flooding of the cauldron center by thin basalts at the end of the volcanic cycle.

To the north from Geronimo Head the Precambrian granitic and metamorphic rocks of the Mazatzal Mountains form a distinctively different topography than that which we have been discussing.

1.1 34.3 Directly ahead is an excellent example of spheroidally-weathered blocks of coarsely crystalline intrusive granitic rocks. To the left (northwest) we can see a small mesa capped by a lava flow. Sugarloaf Mountain rises just beyond the mesa.

1.2 35.5 **STOP 4.** At this locality spheroidal weathering is especially well exhibited. Evidence that most of this type of weathering is accomplished beneath the ground surface is seen in roadcuts which we will see later. There unweathered "core stones" surrounded by weathered "gruss" are exhibited. The piles of rounded blocks you see in this area represent residual accumulations of these core stones left when this gruss is stripped by erosion.

0.7 36.2 Here a north-south trending dike stands about 30 feet above the surrounding quartz monzonite. This is a classic example of differential weathering.

1.7 37.9 A large basalt dike in quartz monzonite is seen in the left roadcut.

0.8 38.7 Crossing of Mesquite Creek.

0.2 38.9 Crossing of Rock Creek. Note the Tertiary volcanics outcropping in this area.

1.4 40.3 In this area the Tertiary basin-fill deposits are overlain by later volcanic flows. These flows commonly form planar surfaces capping many of the hills and form conspicuous dipslopes.

5.1 45.4 Note the conspicuous fault in the left road cut. This is a normal fault with a block of Precambrian quartz monzonite uplifted into contact with Tertiary basin-fill deposits.

0.6 46.0 Spheroidal weathering in this area indicates that the bedrock is coarsely jointed, intrusive granitic rocks.

3.3 49.3 Entrance to Sunflower store and cafe. To the northwest Mt. Ord rises to 7,128 feet elevation as the high, rounded mountain with the towers on top. This landmark is composed of early Precambrian pyroxenite that intruded still older schists. The pyroxenite has in turn been intruded by later Precambrian quartz monzonite.

0.1 49.4 Basalt lava flow and volcanic ash are exposed in the left roadcut.

0.4 49.8 Road passes down onto the floodplain of Sycamore Creek. This stream eventually empties into the Verde River to the west.

6.8 56.6 **STOP 5.** In the roadcuts on either side of the road the Tertiary basin fill is cut by a high-angle normal fault. At first glance this feature appears to be a dike; the zone of disturbance is bounded by discolored zones and varies in width from 25 feet on the south side of the road to 8 feet on the north side. Closer inspection reveals that the tannish-gray "dike" is in reality a highly comminuted gouge zone containing numerous fragments of Precambrian igneous and metamorphic rocks. There is no evidence that the heat associated with intrusion of an igneous dike has affected these small fragments. The material we see is quite soft and dike rock would be quite hard. Evidence of solution activity along and within the fault zone is the discolored border zone, the light color of the

gouge, its uniform appearance, and the presence of small veinlets of calcite within the gouge. The presence and shape of the drag fold within the basin-fill sediments indicates this break is not a thrust fault.

0.3 56.9 In the right roadcut a dike cuts across the basin fill.

0.3 57.2 In the left exposure, flow-banded dacite outcrops. Tertiary clastic sediments are seen in the right roadcut.

0.7 57.9 Highly contorted, Precambrian slate-phyllite can be seen to the left along the highway. Greenstone (altered basalt) is intercalated with these rocks.

0.7 58.6 **STOP 6.** Canyon of Slate Creek. These rocks are typical of the metamorphic sequence which forms the core of the Mazatzal Mountains (Wilson, 1939). They were formed from sediments during the episode of extensive and intensive mountain building termed the "Mazatzal Revolution." Damon and Giletti (1961) used rubidium-strontium dating to show that this orogeny occurred between 1.2 and 1.5 billion years ago. Many geologists correlate the low-grade metamorphic rocks you see here with the higher-grade Vishnu-Brahma Schist Complex found in the Inner Gorge of the Grand Canyon. Both metamorphic units were extensively intruded by granitic masses during the last stages of the Mazatzal Revolution. Slates, phyllites, and schists containing talc and chlorite minerals can be found at this site. On the ridges to the northeast resistant beds of Precambrian quartzite in near vertical attitude stand above the softer surrounding slates and phyllites.

1.9 60.5 In the left bank, Tertiary basin-fill material is in normal fault contact with Precambrian phyllite.

2.9 63.4 Tertiary terrestrial deposits are faulted against a block of altered and sheared quartz monzonite of Precambrian age in the left roadcut.

0.2 63.6 The Tonto Basin can be seen to the right front across the dissected basin fill.

1.6 65.2 The conglomerate-filled channel exposed in the right bank records an ancient cycle of dissection of the older gravels in this area.

0.2 65.4 Directly west from here differential weathering has exposed a very resistant bed of the Precambrian Deadman Quartzite along the lower flank of the Mazatzal Mountains. This unit is one of the last units deposited before the inception of the Mazatzal Revolution and so is one of the youngest rocks incorporated in that deformation.

0.9 66.3 Directly north of here the very light-colored, Pliocene lake beds of the Payson Basin can be seen. The Payson Basin is one of a series of structural troughs which trend northwest to southeast across Arizona and lie in the Transition Zone between the Colorado Plateau and the Basin and Range Physiographic Provinces. The Verde Basin lies to the northwest and the Tonto Basin lies to the southeast (Royse and Wadell, 1970; Lance, Downey, and Alford, 1962). The Payson Basin is bounded on the southwest by the Mazatzal Mountains and on the northeast by the Sierra Ancha Mountains. Similarly to the Verde Basin, the Payson Basin apparently developed in middle to late Tertiary time and we can speculate that this depression also may be the result of block faulting. Much evidence of faulting is seen in the area, but no bounding faults have been found.

The sedimentation history of the Payson Basin is as complex as that of the Verde Basin. Pedersen (1969) has determined that an early stage of extensive alluvial-colluvial fan development around the basin margins was contemporaneous with deposition of fluvial silts and sands along the basin axis. As the basin was filled by these clastic sediments, small, local lakes developed in topographic lows and silty clays and limestones were deposited in them. Remains of freshwater mollusks have been found in the calcareous deposits (Taylor, 1968).

Deposition of the fluvial and lacustrine deposits was followed by an alluvial stage characterized by development of broad alluvial fans. Later these fan surfaces were altered by stream dissection and the pan-pediment or terrace surfaces you see cut into the relatively soft basin-fill material developed during this erosion.

0.8 67.1 Part of the carbonate-silt facies of the lacustrine sequence of the Payson Basin is exposed in the roadcuts on either side of the road. The limestone beds here reach one foot or more in thickness and form resistant, vertical outcrops.

0.4 67.5 Junction of Highways 87 and 188.

3.7 71.2 Crossing of Rye Creek. To the left across

the floodplain of Rye Creek one can see part of the fine-grained facies of the early basin-fill stage interbedded with fluvial gravels. Rye Creek flows to the southeast from its source near the East Verde River and its course may be aligned along an ancient drainage system that was later modified by volcanism and perhaps stream piracy to form three aligned stream systems in this area: the Verde River, the East Verde River, and Rye Creek (Pedersen, 1969).

1.6 72.8 The "town" of Rye.

2.9 75.7 In the left roadcut the Tertiary basin-fill deposits are offset by a normal fault which also displaced the altered, older Precambrian diabase.

0.7 76.4 Roadcut through the same diabase unit.

4.6 81.0 We are now driving through the juniper-pinyon woodland of Merriam's Upper Sonoran Life Zone. Until now we have been passing through desert-grasslands and chaparral of this same zone.

0.3 81.3 To the north we can see the Mogollon Rim on the skyline capped by the Coconino Sandstone. This gigantic scarp extends northwest to southeast across central Arizona and marks the southern boundary of the Colorado Plateau Physiographic Province. The Mogollon Rim is separated from us by a lesser scarp termed the Diamond Rim; we will discuss the significance of this feature later. The Mogollon Rim is a retreating scarp being cut by erosion into the upper Paleozoic sedimentary rocks to the north; the rim began its retreat from a fault scarp termed the Diamond Rim fault.

0.8 82.1 First outcrop of the beautifully cross-bedded, Middle Cambrian Tapeats Sandstone along the highway (fig. 1). This sedimentary unit formed during the advance of the Cambrian sea that progressively lapped onto Mazatzal Land, a hypothetical highland in this part of central Arizona that persisted intermittently at least through the Paleozoic (Stoyanow, 1936). This sea entered the area from the west. This Cambrian basal sandstone shows evidence of reworking of the purplish, arkosic debris covering the low-angle weathered surface then existing. The lower Tapeats is purplish in color, fine grained, and arkosic in composition.

0.2 82.3 Entering Payson. This settlement lies at 4,887 feet elevation along the lower limit of ponderosa pine, the characteristic plant of Merriam's Transition Life Zone.

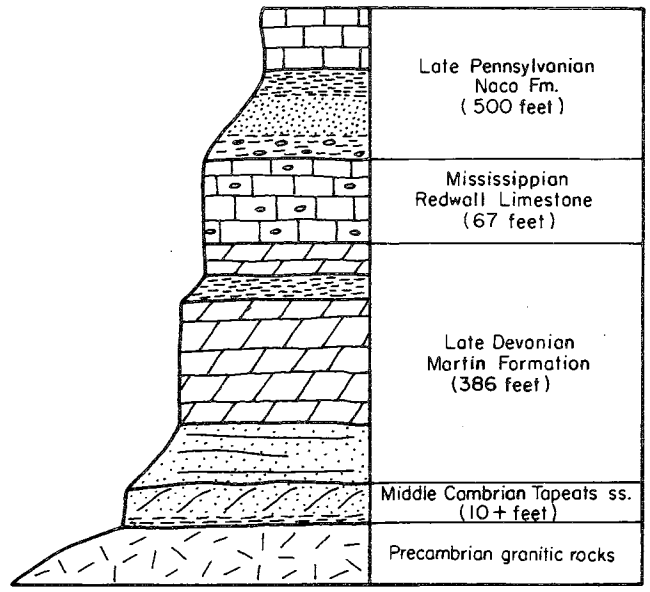

Figure 1. Stratigraphic section in the Payson area, Arizona.

1.6 83.9 Junction of Highways 87 and 160. Turn right and proceed east toward Heber and Snowflake.

1.1 85.0 In the roadcuts here and for several miles to the east, weathered quartz monzonite outcrops. These Precambrian granitic rocks are thought to be part of an extensive igneous-metamorphic complex which includes the Bradshaw Granite of the Bradshaw Mountains to the west and the Ruin Granite in the Superior area to the southeast. To our south and southeast the terrain is underlain by older Precambrian metasediments and altered volcanics which have been described by Gastil (1958). Resistant quartzite units within this sequence support many of the linear ridges and higher mountains of the area.

0.7 85.7 To the northeast we can see Diamond Point, one of the highest points along the Diamond Rim. This landform is the site for a fire lookout tower. The Diamond Rim is a resequent fault-line scarp that probably began its retreat from the vicinity of the Diamond Rim fault to its present position during Miocene time (Titley, 1962). Diamond Rim fault is a west-northwest-trending normal fault system which northwest of Payson has brought the Tapeats Sandstone and the Martin Fm and Redwall Limestone down into

fault contact with Precambrian granitic rocks. These and later Paleozoic units have been stripped almost entirely from the Precambrian basement complex in the area of our present location (Huddle and Dobrovolny, 1952; Kottlowski and Havenor, 1962; Teichert, 1965; and McKee and Gutschick, 1969).

0.9 86.6 Star Valley.

6.4 93.0 To the left and just below Diamond Rim, the purplish, bold outcrops are of Middle Cambrian Tapeats Sandstone. In this area Diamond Rim is capped by more than 200 feet of the Devonian Martin Formation (Teichert, 1965).

1.3 94.3 Little Green Valley.

3.5 97.8 Outcrop along the highway of the Early to Middle Mississippian Redwall Limestone. Note the collapse breccia structures characteristic of this unit in this area. Many faults in this area complicate the structure.

0.7 98.5 Control road to Diamond Point. Proceed straight ahead.

0.5 99.0 **STOP 7.** Kohl Ranch fossil locality in shaly limestones and sandy mudstones of the Naco Formation. Organic remains of crinoids (stem fragments and plates), bryozoans (branching, fan-shaped and crustose), gastropods, pelecypods, productid and spiriferid brachiopods and conularids can be found here in the roadcuts on the other side of the fence (see the introduction).

0.5 99.5 Return to Control road. Turn right and proceed west.

4.4 103.9 Turn left onto the road to Diamond Point Lookout and proceed south.

3.4 107.3 **STOP 8.** Parking site below Diamond Point Lookout. Take walk down the dipslope of the Martin Formation (or perhaps the Redwall Limestone) for about one mile to Scout Cave. Observe the small karat sinks, tarantulas, and rattlesnakes along the route.

Scout Cave has been dissolved in the upper member of the Martin Formation (Hassemer, 1962) or perhaps in the Redwall Limestone by groundwaters percolating along a prominent joint system that trends about N78°W. This cavern system consists of a main passage about 550 feet in length and a side passage 345 feet long. The entrance slope is covered with angular, blocky rubble that collapsed from the former cave ceiling and exposed this underground cavern system. The room at the base of the entrance slope is the largest room in the cave. Flowstone features can be seen on the south wall of this room. UNDER *NO* CIRCUMSTANCES IS ANYONE TO PROCEED BEYOND THE ENTRANCE ROOM. DO NOT ENTER ANY SIDE PASSAGES!!!

REFERENCES CITED

Damon, P. E., 1969, Correlation and chronology of ore deposits and volcanic rocks: U. S. Atomic Energy Comm., Annual Progress Report no. 000-689-120, 90 p.

———, and Giletti, B. J., 1961, The age of the basement rocks of the Colorado Plateau and adjacent areas: New York Acad. Sci., Annals, v. 91, art 2, p. 443–453.

Feth, J. H., and Hem, J. D., 1962, Springs along the Mogollon Rim in Arizona, *in* Weber, R. H., and Peirce, H. W., Eds., Guidebook of the Mogollon Rim region, east-central Arizona: 13th Field Conf., New Mexico Geol. Soc., p. 129–134.

Gastil, Gordon, 1958, Older Precambrian rocks of the Diamond Butte Quadrangle, Gila County, Arizona: Geol. Soc. America Bull., v. 69, p. 1495–1514.

Hassemer, Jerry, 1962, Scout Cave (Gila County, Arizona): Cave Crawler's Gazette, v. 3, no. 8, p. 102–103.

Huddle, J. W., and Dobrovolny, E., 1952, Devonian and Mississippian rocks of central Arizona: U. S. Geol. Survey Prof. Paper 233-D, p. 67–112.

Jennings, J. N., 1968, Tafoni, *in* Fairbridge, R. W., Ed., The encyclopedia of geomorphology, New York, Reinhold Book Corp., p. 1103–1104.

Kottlowski, F. E., and Havenor, K. C., 1962, Pennsylvanian rocks of the Mogollon Rim area, Arizona, *in* Weber, R. H., and Peirce, H. W., Eds., Guidebook of the Mogollon Rim region, east-central Arizona: 13th Field Conf., New Mexico Geol. Soc., p. 77–83.

Lance, J. F., Downey, J. S., and Alford, M., 1962, Cenozoic sedimentary rocks of Tonto Basin, *in* Weber, R. H., and Peirce, H. W., Eds., Guidebook of the Mogollon Rim region, east-central Arizona: 13th Field Conf., New Mexico Geol. Soc., p. 98–99.

McKee, E. D., and Gutschick, R. C., 1969, History of the Redwall Limestone of northern Arizona: Geol. Soc. America Mem. 114, 726 p.

Pedersen, E. P., 1969, Sedimentology and stratigraphy of basin-fill sediments of the Payson Basin, Gila County, Arizona: MS Thesis, Arizona State Univ., 136 p.

Péwé, T.L., 1971, Guidebook to the geology of the lower Salt River Valley: unpub., 21 p.

Péwé, T.L., 1974, Geomorphic processes in polar deserts: *in* Smiley, T.L. and Zumberge, J. H., Polar deserts and modern man: Univ. of Ariz. Press, Tucson. p. 33–52.

Péwé, T. L., 1978, Guidebook to the Terraces of the lower Salt River Valley in relation to the late Cenozoic history of the Phoenix Basin: this volume.

Pope, C. W., 1974, Geology of the lower Verde River Valley, Maricopa County, Ariz: unpub. MS thesis, Dept. of Geol. Ariz. State Univ., 104 p.

———, Stuckless, J. S., and Fodor, R. V., 1970, A Tertiary silicic cauldron complex at the northern margin of the Basin and Range Province, central Arizona, USA: Bull. Volcanologique, v. 34, no. 3, p. 649–662.

Royse, C. F., and Wadell, J. S., 1970, Geology of the Verde Valley, Yavapai County, Arizona, *in* Smith, C. T., Ed., Guidebook to Four Corners, Colorado Plateau, Central Rocky Mountain region: Nat. Assoc. Geol. Teach., p. 35–39.

Stoyanow, A. A., 1936, Correlation of Arizona Paleozoic formations: Geol. Soc. America Bull., v. 37, p. 459–540.

Taylor, D. W., 1968, Summary of North American non-marine Blancan mollusks: Malacologia, v. 4, p. 1–72.

Teichert, Curt, 1965, Devonian rocks and paleogeography of central Arizona: U. S. Geol. Survey Prof. Paper 464, 181 p.

Titley, S. R., 1962, Geology along the Diamond Rim and adjoining areas, Gila and Navajo Counties, Arizona, *in* Weber, R. H., and Peirce, H. W., Eds., Guidebook of the Mogollon Rim region, east-central Arizona: 13th Field Conf., New Mexico Geol. Soc., p. 123–128.

Wilson, E. D., 1939, Pre-Cambrian Mazatzal Revolution in central Arizona: Geol. Soc. America Bull., v. 50, p. 1113–1164.

BARRINGER METEORITE CRATER, COCONINO COUNTY, ARIZONA

Eugene Shoemaker
California Institute of Technology
David Roddy
United States Geological Survey
Carleton Moore
Arizona State University
Robert Dietz
Arizona State University

A one-day field trip will visit Barringer Meteorite Crater. Participants will depart from Tempe in the evening and spend the night in Flagstaff. The field trip will depart from Flagstaff to the Crater and will return to Flagstaff and Phoenix on the same day. At the Crater participants may choose from a number of guided or self-guided options to visit this interesting geologic feature. In addition to the road guide included here participants will be provided with a "Guidebook to the Geology of Meteor Crater, Arizona" prepared for the 37th Annual Meeting of the Meteoritical Society. It has been reprinted and is available from the Center for Meteorite Studies, Arizona State University, Tempe, Arizona 85281.

Access to the Crater is by the courtesy of the Barringer Crater Company and Meteor Crater Enterprises, Inc. Visitors must receive permission to enter nonpublic areas of the Crater.

SYNOPSIS OF THE GEOLOGY OF METEOR CRATER

by Eugene M. Shoemaker

REGIONAL SETTING

Meteor Crater lies in north-central Arizona in the Canyon Diablo region of the southern part of the Colorado Plateau (fig. 1). The climate is arid and the exposures are exceptionally good.

In the vicinity of the crater, the surface of the Plateau has very low relief and is underlain by nearly flat-lying beds of Permian and Triassic age. The crater lies near the anticlinal bend of a gentle monoclinal fold, a type of structure characteristic of this region. The strata are broken by wide-spaced northwest-trending normal faults, generally many kilometers in length but with only a few meters to about 30 meters of displacement. Two mutually perpendicular sets of vertical joints of uniform strike occur in the region of the crater. One set is subparallel to the normal faults and the other controls the trend of secondary stream courses (fig. 1).

Basaltic cinder cones and flows of late Tertiary and Quaternary age lie at distances of about 11 to 29 km (7 to 18 miles) to the south, west, and northwest of the crater.

PRE-QUATERNARY STRATIGRAPHY

Rocks exposed at Meteor Crater range from the Coconino Sandstone of Permian age to the Moenkopi Formation of Triassic age. Drill holes in and around the crater have intersected the upper part of the Supai Formation of Pennsylvanian and Permian age, which conformably underlies the Coconino.

The Supai Formation consists of interbedded red and yellow fine-grained argillaceous sandstone and subordinate siltstone. It is more than 300 meters (1,000 feet) thick in this region (Pierce, 1958, p. 84), but not more than 100 meters or so (a few hundred feet) have been penetrated by drill holes at the crater. The Coconino Sandstone (McKee, 1933) consists of about 210 to 240 meters (700 to 800 feet) of fine-grained saccharoidal, white, cross-bedded sandstone. Most of the Coconino sandstone is an unusually clean quartz sandstone; in the lower part of the formation the quartzose sandstone is interbedded with red sandstone beds of Supai lithology. Only the upper part of the Coconino is exposed at the crater. The Coconino is overlain conformably by 2.7-meter- (9-foot-) thick unit of white to yellowish- or reddish-brown, calcareous, medium- to coarse-grained sandstone interbedded with dolomite referred to the Toroweap Formation of Permian age (McKee, 1938).

The Kaibab Formation of Permian age, which rests conformably on the Toroweap Formation, includes 79.5 to 81 meters (265 to 270 feet) of fossiliferous marine sandy dolomite, dolomitic limestone, and minor calcareous sandstone. Three members are recognized (McKee, 1938). The lower two members, the Gamma and Beta Members, are chiefly massive dense dolomite; the upper or Alpha Member is composed of well-bedded limestone and dolomite with several continuous thin sandstone interbeds. The Kaibab is exposed along the steep upper part of the wall of the crater, and a large area west of Meteor Crater is a stripped surface on the Alpha Member (fig. 1).

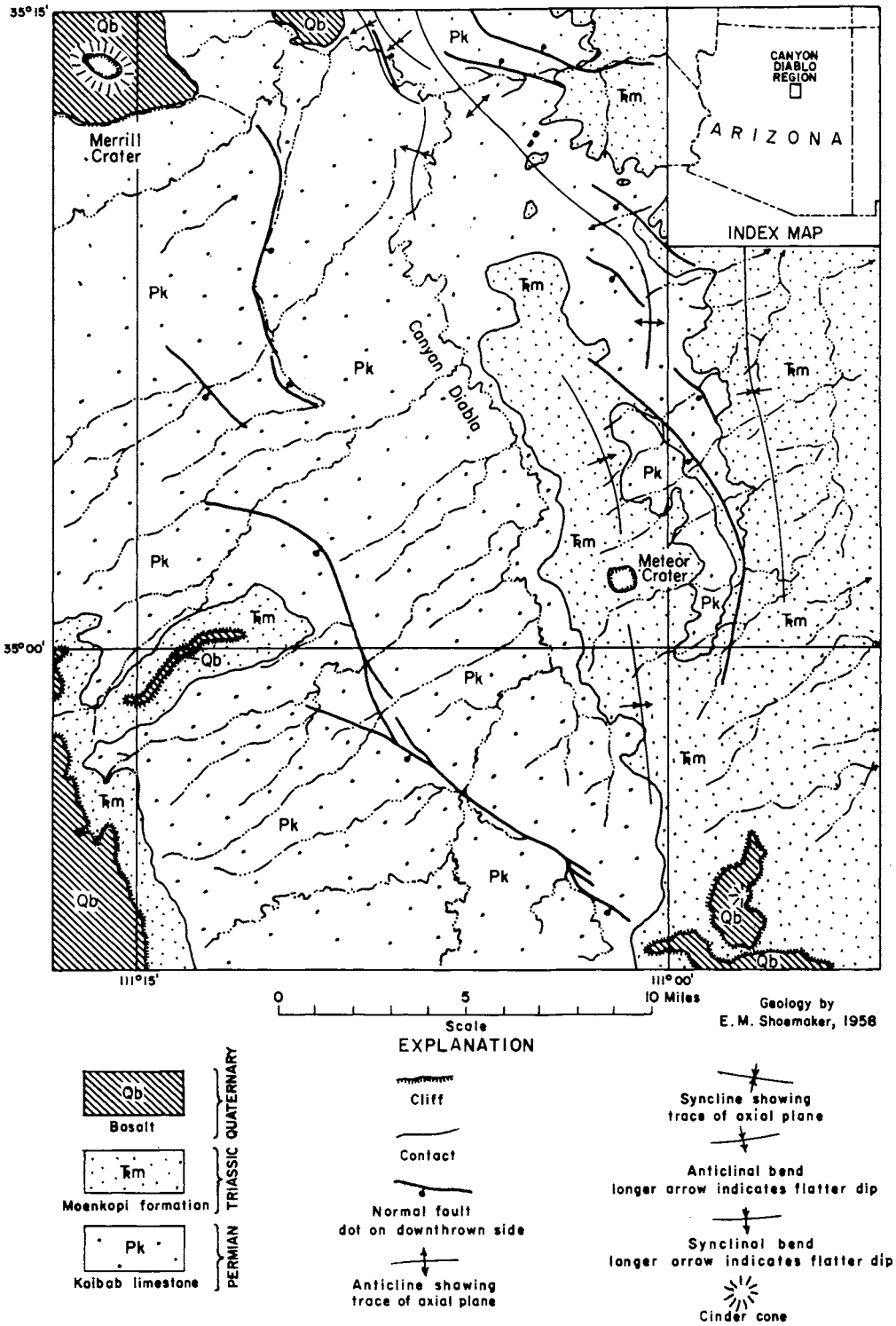

Figure 1. Sketch geologic map of Canyon Diablo region, Arizona.

In the vicinity of the crater, and to the east, beds of the Moenkopi Formation (McKee, 1954) of Triassic age form a thin patchy veneer resting disconformably on the Kaibab. Two members of the Moenkopi are present in the vicinity of the crater. A 3- to 6-meter (10- to 20-foot) bed of pale reddish-brown, very fine-grained sandstone (McKee's lower massive sandstone), which lies from 0.3 to 1 meter (1 to 3 feet) above the base, constitutes the Wupatki Member. Above the Wupatki are dark, reddish-brown fissile siltstone beds of the Moqui Member. About 9 to 15 meters (30 to 50 feet) of Moenkopi strata are exposed in the wall of the crater.

QUATERNARY STRATIGRAPHY AND STRUCTURE OF THE CRATER

Meteor Crater is a bowl-shaped depression 180 meters (600 feet) deep, about 1.2 km (¾ mile) in diameter, encompassed by a ridge or rim that rises 30 to 60 meters (100 to 200 feet) above the surrounding plain. The rim is underlain by a complex sequence of Quaternary debris and alluvium resting on disturbed Moenkopi and Kaibab strata (fig. 2).

The debris consists of unsorted angular fragments ranging from splinters less than 1μ in size to great blocks more than 30 meters across. Because of the striking lithologic contrast among the older formations from which the debris is derived, it is possible to distinguish and map units or layers in the debris by the lithic composition and stratigraphic source of the component fragments.

The stratigraphically lowest debris unit of the rim is composed almost entirely of fragments derived from the Moenkopi Formation. Within the crater this unit rests on the edge of upturned Moenkopi beds (fig. 3) or very locally grades into the Moenkopi Formation; away from the crater wall the debris rests on the eroded surface of the Moenkopi. A unit composed of Kaibab debris rests on the Moenkopi debris. The contact is sharp where exposed within the crater, but, at distances of 0.8 km (half a mile) from the crater, there is slight mixing of fragments at the contact. Patches of a third debris unit, composed of sandstone fragments from the Coconino and Toroweap Formations, rest with sharp contact on the Kaibab debris. No fragments from the Supai Formation are represented in any of the debris.

The bedrock stratigraphy is preserved, inverted, in the debris units. Not only is the gross stratigraphy preserved, but even the relative position of fragments from different beds tends to be preserved. Thus most sandstone fragments from the basal sandstone bed of the Moenkopi Formation occur near the top of the Moenkopi debris unit, fragments from the Alpha Member of the Kaibab limestone occur at the base of the Kaibab debris unit, and brown sandstone fragments from the 3-meter- (9-foot-) thick Toroweap Formation occur just above the Kaibab debris unit.

Pleistocene and Holocene alluvium rests unconformably on all the debris units, as well as on bedrock. The Pleistocene alluvium forms a series of small, partly dissected pediments extending out from the crater rim and also occurs as isolated patches of pediment or terrace deposits on the interstream divides. It is correlated on the basis of well-developed pedocal paleosols with the Jeddito Formation of Hack (1942, pp. 48–54) of Pleistocene age (Leopold and Miller, 1954, pp. 57–60; Shoemaker, Roach, and Byers, 1962) in the Hopi Buttes region, some 80 km (50 miles) to the northeast. Holocene alluvium blankets about half the area within the first 0.8 km (half-mile) of the crater and extends along the floors of minor stream courses (fig. 2). It includes modern alluvium and correlatives of the Tsegi and Naha Formations of Hack (1942) of Holocene age (Shoemaker, Roach, and Byers, 1962) in the Hopi Buttes region.

Both the Pleistocene and the Holocene alluvium are composed of material derived from all formations represented in the debris and also contain meteorite fragments, lechatelierite (Merrill, 1907, 1908, pp. 472–478; Rogers, 1928, pp. 82–84, and 1930), other kinds of fused rock (Nininger, 1954, 1956, p. 117–134), and less strongly shocked rocks with coesite and stishovite (Chao, Shoemaker and Madsen, 1960; Chao and others, 1962). Oxidized meteoritic material and fragments of relatively strongly shocked Coconino Sandstone are locally abundant in the Pleistocene alluvium where it occurs fairly high on the crater rim. Unoxidized meteoritic material occurs in two principal forms: (a) large crystalline fragments composed mainly of two nickel-iron minerals, kamacite and taenite (Merrill and Tassin, 1907), and (b) minute spherical particles of nickel-iron (Tilghman, 1906, pp. 898–899, 907; Nininger, 1949, 1951a, b, pp. 80–81). The bulk of the meteoritic material distributed about the crater is apparently in the form of small particles. The total quantity of fine-grained meteoritic debris about the crater, which occurs not only in the Pleistocene and Holocene alluvium but also as lag and dispersed in colluvium, has been estimated by Rinehart (1958, p. 150) as about 12,000 tons.

Beds ranging from the Coconino Sandstone to the Moenkopi Formation are exposed in the crater walls. Low in the crater the beds dip gently outward. The dips are generally steeper close to the contact with the debris on the rim, and beds are overturned along various stretches totalling about one-third the perimeter of the crater. Along the north and east walls of the crater, the Moenkopi can locally be seen to be folded back on itself, the upper limb of the fold consisting of a flap that has been rotated in places more than 180° away from the crater (fig. 3). At one place in the southeast corner of the crater, the flap grades outward into disaggregated debris, but in most places there is a distinct break between the debris and the coherent flap.

Rocks now represented by the debris of the rim have been peeled back from the area of the crater somewhat like the

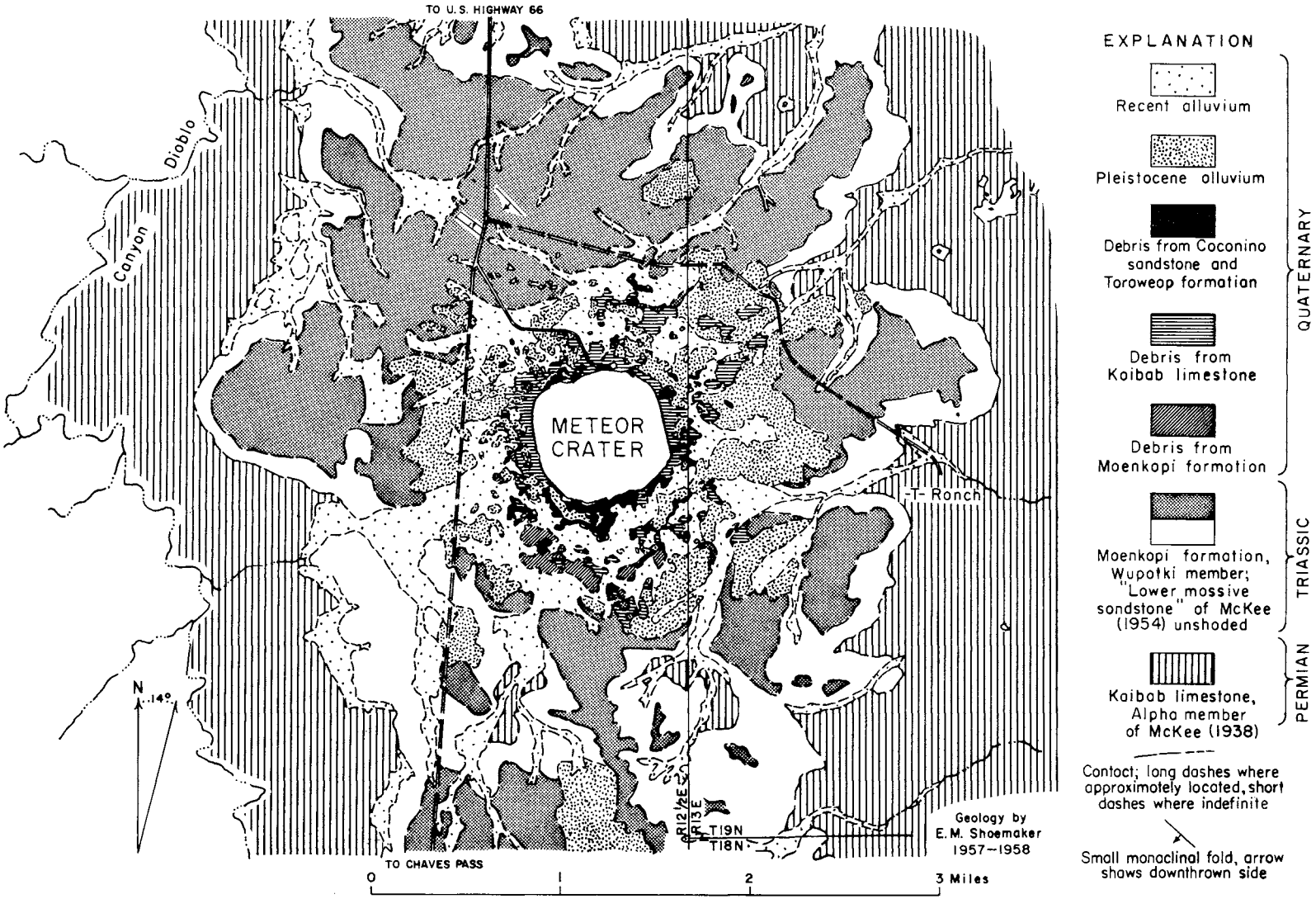

Figure 2. Geologic map of area around Meteor Crater, Arizona.

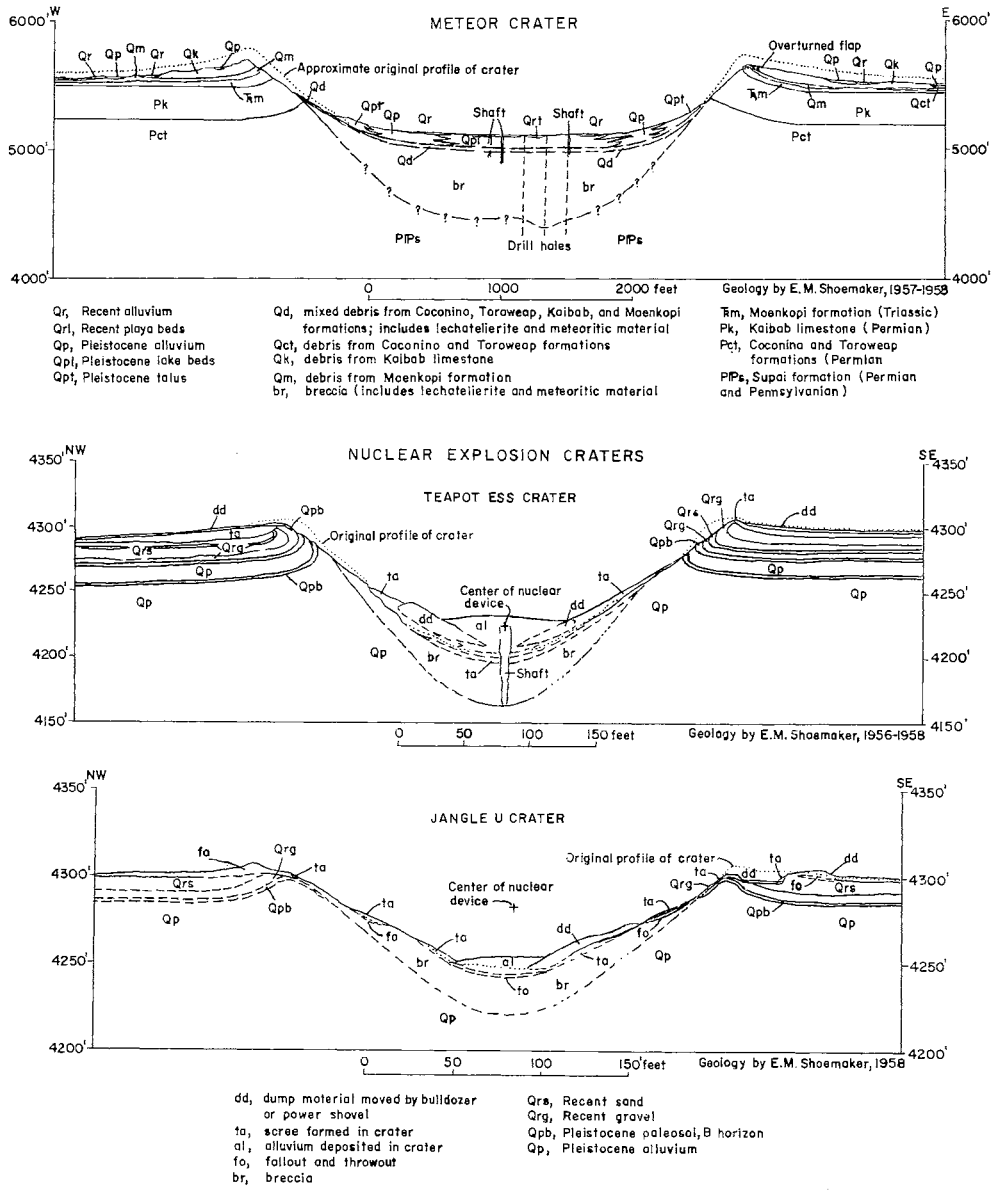

Figure 3. Cross sections of Meteor Crater, Arizona, and nuclear explosion craters.

petals of a flower. The axial plane of the fold in three dimensions is a flat cone, with apex downward and concentric with the crater, that intersects the crater wall. If eroded parts of the wall were restored, more overturned beds would be exposed.

The upturned and overturned strata are broken or torn by a number of small, nearly vertical faults with scissors-type displacement. A majority of these tears are parallel with the northwesterly regional joint set, and a subordinate number are parallel with the northeasterly set. Regional jointing has controlled the shape of the crater, which is somewhat squarish in outline; the diagonals of the "square" coincide with the trend of the two main sets of joints. The largest tears occur in the "corners" of the crater. In the northeast corner of the crater a torn end of the overturned flap of the east wall forms a projection suspended in debris. A few normal faults, concentric with the crater wall, occur on the southwest side. A number of small thrust faults occur on the north and west sides of the crater. Relative displacement of the lower plate is invariably away from the center of the crater. Crushed rock is locally present along all types of faults; it has been designated authigenic breccia, to distinguish it from another type of breccia under the crater floor.

The floor of the crater is underlain by Quaternary strata, debris, and breccia. Pleistocene talus mantles the lowest parts of the crater walls and grades into Pleistocene alluvium along the floor. The Pleistocene alluvium, in turn, interfingers with a series of lake beds about 30 meters (100

feet thick) toward the center of the crater. Up to 1.6 meters (6 feet) of Holocene alluvium and playa beds rest unconformably on the Pleistocene. Where exposed in shafts, the lowermost Pleistocene lake beds contain chunks of pumiceous, frothy lechatelierite.

A layer of mixed debris underlies the Pleistocene talus and lake beds and rests on bedrock and on breccia. This layer is composed of fragments derived from all formations intersected by the crater and includes much strongly shocked rock and oxidized meteoritic material. The material from all the different sources is thoroughly mixed. Where intersected by a shaft in the crater floor, it is about 10.5 meters (35 feet) thick and almost perfectly massive, but exhibits a distinct grading, from coarse to fine, from base to top. The average grain size, about 2 cm, is much less than in the debris units of the rim or in the underlying breccia; the coarsest fragments at the base rarely exceed 0.3 meter (1 foot) in diameter. I believe that this unit was formed by fallout of debris thrown to great height. It has not been recognized outside the crater, probably because it has been entirely eroded away. Its constituents have been partly redeposited in the Pleistocene and Holocene alluvium.

Where exposed at the surface, the breccia underlying the mixed debris is composed chiefly of large blocks of Kaibab, but the breccia exposed in shafts under the central crater floor is made up chiefly of shattered and twisted blocks of Coconino. Extensive drilling conducted by Barringer (1905, 1910, 1914) and his associates (Tilghman, 1906) has shown that, at a depth of 100 to 200 meters (300 to 650 feet), much finely crushed sandstone and some fused and other strongly shocked rock and meteoritic material are present. Some drill cuttings from about 180 meters (600 feet) depth contain fairly abundant meteoritic material. In cuttings examined by the writer the meteoritic material is chiefly in the form of fine spherules dispersed in glass, similar to the impactite described by Nininger (1954) and by Spencer (1933, pp. 394–399) from the Wabar and Henbury meteorite craters. Cores of ordinary siltstone and sandstone of the Supai were obtained at depths of 210 meters (700 feet) and deeper. The lateral dimensions of the breccia are not known because the drilling was concentrated in the center of the crater. Some of the meteorite-bearing or allogenic breccia was evidently encountered in a hole drilled from 1920 to 1922 on the south rim of the crater (Barringer, 1924). (See log of hole in Hager, 1953, pp. 840–841.)

MECHANISM OF CRATER FORMATION

Nearly all the major structural features of Meteor Crater, Arizona, are reproduced in a crater in the alluvium of Yucca Flat, Nevada, formed by the underground explosion of a nuclear device. The Teapot Ess crater (fig. 3), about 90 meters (300 feet) across and originally about 30 meters (100 feet) deep, was produced in 1955 by a 1.2 kiloton device detonated at a depth of 20 meters (67 feet) below the surface (Johnson, 1959, p. 10). Beds of alluvium exposed in the rim are peeled back in an overturned syncline, just as the bedrock is peeled back at Meteor Crater. The upper limb of the fold is overlain by and locally passes outward into debris that roughly preserves, inverted, the original alluvial stratigraphy. Shock-formed glass and other strongly shocked materials, some containing coesite, are present in the uppermost part of the debris. A thin layer of debris formed by fallout or fall-back is also present in the crater. The floor and lower walls of the crater are underlain by a thick lens of breccia containing mixed fragments of alluvium and dispersed glass. Some of the fragments are strongly sheared and compressed. The breccia was formed by complex movement of material within the crater; locally, the original bedding of the alluvium is roughly preserved in the breccia.

A crater with the structure of Teapot Ess crater is formed chiefly by two mechanisms, which operate in succession. First, the alluvium, as it is engulfed by a compressional shock caused by the explosion, is accelerated in all directions radially outward from the detonated device, and an expanding cavity is formed underground. When the shock reaches the free surface of the ground, it is reflected as a tensional wave. Momentum is trapped in the material above the cavity, and it continues to move up and outward, individual fragments following ballistic trajectories. Kinetic energy is also imparted to the fragments from expanding gases in the cavity. Ejected fragments close to the crater maintain their approximate relative positions, inverted during flight. Along low-velocity trajectories, their range is largely a function of the angle at which they are thrown out, which in turn varies continuously with their original position relative to the nuclear device. The margin of the crater is determined primarily by the radial distance, in plan, at which the reflected tensional wave is just strong enough to lift and separate the alluvium. The position at which this occurs is just inside of and concentric with the hinge of the overturned flap, i.e., the intersection of the axial plane of overturning with the surface of the ground. The reflected tensional wave starts a fracture at the surface but does not appreciably change the momentum of most of the material thrown out. Beds are sheared off along a roughly conical surface that starts at the surface slightly inside the hinge and is propagated downward to join tangentially the lower part of the hole expanded behind the shock front. Material brecciated by very strong shock initially has the form of a roughly spherical shell around the hole, but most of the upper hemisphere is thrown out, and the lower hemisphere is sheared out in the form of a concavo-convex lens. Overturning of the beds in the upper crater wall may be looked on as drag along the conical shear zone.

It is essential that the shock originate deeper than a certain minimum distance below the surface, relative to the total energy released, in order to produce the overturned

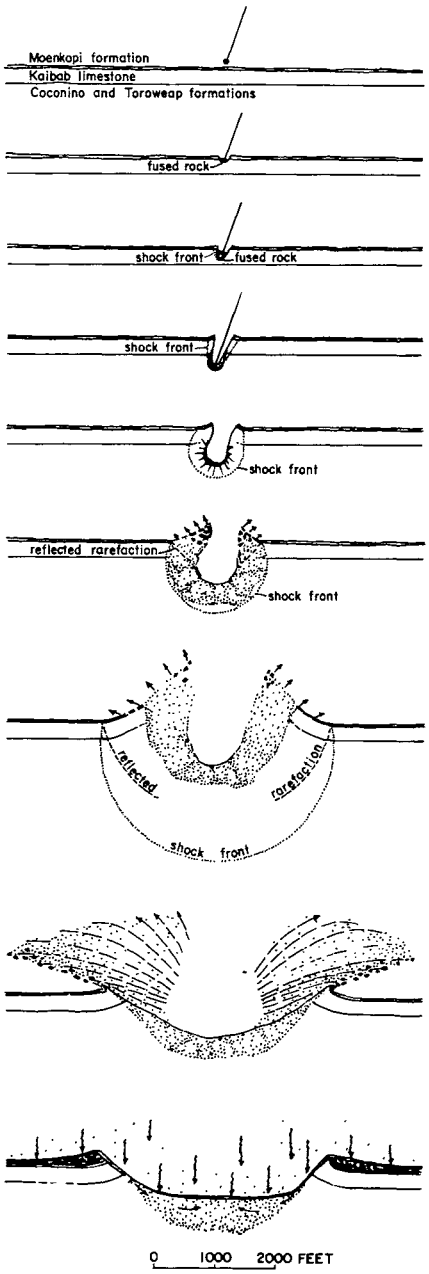

1. Meteorite approaches ground at 15 km/sec.
2. Meteorite enters ground, compressing and fusing rocks ahead and flattening by compression and by lateral flow. Shock into meteorite reaches back side of meteorite.
3. Rarefaction wave is reflected back through meteorite, and meteorite is decompressed, but still moves at about 5 km/sec into ground. Most of energy has been transferred to compressed fused rock ahead of meteorite.
4. Compressed slug of fused rock and trailing meteorite are deflected laterally along the path of penetration. Meteorite becomes liner of transient cavity.
5. Shock propagates away from cavity, cavity expands, and fused and strongly shocked rock and meteoritic material are shot out in the moving mass behind the shock front.
6. Shell of breccia with mixed fragments and dispersed fused rock and meteoritic material is formed around cavity. Shock is reflected as rarefaction wave from surface of ground and momentum is trapped in material above cavity.
7. Shock and reflected rarefaction reach limit at which beds will be overturned. Material behind rarefaction is thrown out along ballistic trajectories.
8. Fragments thrown out of crater maintain approximate relative positions except for material thrown to great height. Shell of breccia with mixed meteoritic material and fused rock is sheared out along walls of crater; upper part of mixed breccia is ejected.
9. Fragments thrown out along low trajectories land and become stacked in an order inverted from the order in which they were ejected. Mixed breccia along walls of crater slumps back toward center of crater. Fragments thrown to great height shower down to form layer of mixed debris.

Figure 4. Diagrammatic sketches showing sequence of events in formation of Meteor Crater, Arizona.

syncline in the rim. A crater formed near the Teapot Ess crater by a nuclear device of the same yield, but detonated at 5.4 meters (18 feet) depth rather than 20 meters (67 feet) (fig. 3, Jangle U crater), has an anticline under the rim, not a syncline. An explosion at such a depth (shallow relative to the yield of the device) produces a crater more through radial expansion of the cavity behind the shock and less by ejection of material than in the case of Teapot Ess crater. The greatest expansion of the hole occurs at the surface because of upward relief of stress at the free surface, which manifests itself in concentric anticlinal buckling.

The structure of Meteor Crater would be produced by a very strong shock originating about at the level of the present crater floor (120 meters (400 feet) below the original surface). A minimum scaled depth of penetration of the meteorite or of a major part of the energy associated with the meteorite is indicated by the overturned synclinal structure of the rim. A closer estimate of the depth for the apparent origin of the shock can be obtained from the base of the breccia under the crater floor by scaling from Teapot Ess crater. Some limits may also be set on the mechanics of impact by the fact that the shock was strong enough to fuse

Coconino Sandstone, at a depth of some 90 meters (300 feet) or more below the surface, and that part of the meteorite itself was fused by shock on impact, as shown by the dispersal of spherical particles of meteoritic material in some of the fused rock.

Not all meteorite craters exhibit overturned synclines in the rim, as at Meteor Crater, which indicates that the scaled depth of penetration on impact is not always so great. The rim of the main meteorite crater at Odessa, Texas, for example, is underlain by an anticline similar to that of the Jangle U crater (compare with Hardy, 1953; Sellards and Evans, 1941).

The reconstructed sequence of events in the formation of Meteor Crater, based on theoretical analysis (Shoemaker, 1960), is illustrated in figure 4. The crater was formed by impact of meteoritic iron bolide about 30 meters (100 feet) across. On the basis of scaling from the Sedan Crater in Nevada, the energy released by impact was 4 to 5 megatons TNT equivalent. This event occurred a few tens of thousands of years ago, as shown by the mid-Wisconsin age of the oldest sedimentary deposits on the rim and in the interior of the crater.

REFERENCES CITED

Baker, A. A., and Reeside, Jr., J. B., 1929, Correlation of the Permian of Southern Utah, northern Arizona, northwestern New Mexico, and southwestern Colorado: Bull. Amer. Assoc. Petrol. Geol., v. XIII, p. 1413–1448.

Barringer, D. M., 1905, Coon Mountain and its crater: Acad. Nat. Sciences, Philadelphia Proc., v. 57, p. 861–886.

Barringer, D. M., 1910, Meteor Crater (formerly called Coon Mountain or Coon Butte) in northern central Arizona: Published by the author, 24 p.

Barringer, D. M., 1914, Further notes on Meteor Crater, Arizona: Acad. Nat. Sciences Philadelphia Proc., v. 66, p. 556–565.

Barringer, D. M., 1924, Further notes on Meteor Crater in northern central Arizona (No. 2): Acad. Nat. Sciences Philadelphia Proc., v. 76, p. 275–278.

Chao, E.C.T., 1967, Shock effects in certain rock-forming minerals: Science, v. 156, p. 192–202.

Chao, E.C.T., Fahey, J. J., Littler, Janet, and Milton, D. J., 1962, Stishovite, SiO_2 A very high pressure new mineral from Meteor Crater, Arizona: Jour. Geophys. Res., v. 67, p. 419–421.

Chao, E.C.T., Shoemaker, E. M., and Madsen, B. M., 1960, First natural occurrence of coesite: Science, v. 132, p. 220.

Colton, H. S. (revised 1967), The basaltic cinder cones and lava flows of the San Francisco Mountain volcanic field: Mus. of Northern Arizona Bull. No. 10, Northland Press, Flagstaff, Ariz., 58 p.

Damon, P. E., 1965, Correlation and chronology of ore deposits and volcanic rocks: Ann. Prog. Rept., COO-689-50 Contract AT (11-1)-689, U.S. Atomic Energy Comm., p. 36–43.

Damon, P. E., Shafiqullah, M., and Leventhal, J. S., 1974, K-Ar chronology for the San Francisco volcanic field and rate of erosion of the Little Colorado, *in* Geology of Northern Arizona for the Geological Society of America, Rocky Mt. Section Meeting, Flagstaff, Arizona, pt. I, p. 221.

Darton, N. H., 1910, A reconnaissance of parts of northwestern New Mexico and northern Arizona: U.S. Geol. Survey Bull. 435, p. 21.

Fairchild, H. L., 1907, Origin of Meteor Crater (Coon Butte), Arizona: Bull. Geol. Soc. America, v. 18, p. 493–504.

Hack, J. T., 1942, The changing physical environment of the Hopi Indians: Peabody Museum Nat. History Papers, v. 35, p. 3–85.

Hager, Dorsey, 1953, Crater mound (Meteor Crater), Arizona, a geologic feature: Am. Assoc. Petroleum Geologists Bull., v. 37, p. 821–857.

Johnson, G. W., 1959, Mineral resource development by the use of nuclear explosives: Calif. Univ., Lawrence Radiation Lab. Rept. 5458, 18 p.

Kennedy, G. C., Wasserburg, G. J., Heard, H. C., and Newton, R. C., 1962, The upper Millphase region in the system SiO_2–H_2O, Am. Jour. Sci., v. 260, p. 501.

Kieffer, S. W., 1970, 1. Shock metamorphism of the Coconino Sandstone at Meteor Crater, Arizona; 2. The specific heat of solids of geophysical interest: Ph.D. thesis, California Institute of Technology, Pasadena.

Kieffer, S. W., 1971, Shock metamorphism of the Coconino Sandstone at Meteor Crater, Arizona: Jour. Geophys. Res., v. 76, p. 5449.

Kieffer, S. W., Phakey, P. P., Christie, J. M., Shock processes in porous quartz (in prep).

Kluth, C. F., and Kluth, M. J., 1974, Geology of the Elden Mountain area, *in* Geology of Northern Arizona for the Geological Society of America, Rocky Mt. Section Meeting, Flagstaff, Arizona, pt. II, p. 521.

Leopold, L. B., and Miller, J. P., 1954: A post-glacial chronology for some alluvial valleys in Wyoming: U.S. Geol. Survey Water-Supply Paper 1261, 90 p.

McKee, E. D., 1933, The Coconino Sandstone—its history and origin, *in* Contributions to Paleontology: Carnegie Inst. Washington Pub. 440, p. 78–115.

McKee, E. D., 1938, The environment and history of the Toroweap and Kaibab Formations of northern Arizona and southern Utah: Carnegie Inst. Washington Pub. 492, 221 p.

McKee, E. D., 1951, Triassic deposits of the Arizona-New Mexico border area: *in* New Mexico Geol. Soc. Guidebook, 2nd Field Conf., San Juan Basin, p. 85–92.

McKee, E. D., 1954, Stratigraphy and history of the Moenkopi Formation of Triassic age: Geol. Soc. America Mem. 61, 133 p.

Merrill, G. P., 1907, On a peculiar form of metamorphism in siliceous sandstone: U.S. Nat. Mus. Proc., v. 32, p. 547–550.

Merrill, 1908, The Meteor Crater of Canyon Diablo, Arizona: its history, origin, and associated meteoritic irons: Smithsonian Inst. Misc. Coll., v. 50, p. 461–498.

Merrill, George Perkins, and Tassin, Wirt, 1907, Contributions to the study of Canyon Diablo meteorites: Smiths. Misc. Col. 50, p. 203–215.

Moore, R. B., Wolfe, E. W., and Ulrich, G. E., 1974, Geology of the eastern and northern parts of the San Francisco volcanic field, Arizona, *in* Geology of northern Arizona for the Geological Society of America, Rocky Mt. Section Meeting, Flagstaff, Arizona, pt. II, p. 465.

Nininger, H. H., 1949, Oxidation studies at Barringer crater. Metal-center pellets and oxide droplets: Am Philos. Soc. Yearbook, p. 126–130.

Nininger, H. H., 1951a, Condensation globules at Meteor Crater: Science, v. 113, p. 755–756.

Nininger, H. H., 1951b, A resume of researches at the Arizona meteorite crater: Sci. Monthly, v. 72, p. 75–86.

Nininger, H. H., 1954, Impactite slag at Barringer crater: Am. Jour. Sci., v. 252, p. 277–290.

Nininger, H. H., 1956, Arizona's meteorite crater: Denver, Colo., World Press, Inc., 232 p.

Noble, L. F., 1914, The Shinumo Quadrangle: U.S. Geol. Survey Bull. 549, p. 1–100.

Opdyke, N. D., and Runcorn, S. K., 1960, Wind direction in the western United States in the late Paleozoic: Geol. Soc. America Bull. v. 71, p. 959–971.

Peirce, H. W., 1958, Permian sedimentary rocks of the Black Mesa basin area: New Mexico Geol. Soc. 9th Field Conference, Guidebook of the Black Mesa Basin, Northeastern Ariz., p. 82–87.

Peirce, H. W., and Scurlock, J. R., 1972, Arizona well information: Ariz. Bur. Mines Bull. 185, 195 p.
Read, C. B., 1950, Stratigraphy of the outcropping Permian rocks around the San Juan Basin, *in* New Mexico Geol. Soc. Guidebook of the San Juan Basin, New Mexico and Colorado, p. 62–66.
Reiche, Parry, An analysis of cross-lamination the Coconino Sandstone: The Jour. of Geology, v. XLVI, no. 7, p. 905–932.
Rinehart, J. S., 1958, Distribution of meteoritic debris about the Arizona meteorite crater: Smithsonian Inst. Contrib. Astrophys., v. 2, p. 145–160.
Rogers, A. F., 1928, Natural history of the silica minerals: Am. Mineralogist, v. 13, p. 73–92.
Rogers, A. F., 1930, A unique occurrence of lechatelierite or silica glass: Am. Jour. Sci., 5th Ser., v. 19, p. 195–202.
Schuchert, C., 1918, On the carboniferous of the Grand Canyon of Arizona: Amer. Jour. Sci., v. XLV (4th Ser.), p. 347–361.
Shoemaker, E. M., 1960, Penetration mechanics of high velocity meteorites, illustrated by Meteor Crater, Arizona: Internat. Geol. Con., 21st Session, pt. 18, Copenhagen, p. 418–434.
Shoemaker, E. M., Roach, C. H., and Byers, F. M., Jr., 1962, Diatremes and uranium deposits in the Hopi Buttes, Arizona, *in* Petrologic Studies, a volume to honor A.F. Buddington: Geol. Soc. America, p. 327–355.
Smiley, T. L., 1958, The geology and dating of Sunset Crater, Flagstaff, Arizona, *in* Guidebook of the Black Mesa Basin, northeastern Arizona, New Mexico Geol. Soc. 9th Field Conf., p. 186–190.
Spencer, L. J., 1933, Meteoric iron and silica-glass from the meteorite craters of Henbury (central Australia) and Wabar (Arabia): Mineralog. Mag., v. 23, p. 387–404.
Tilghman, B. C., 1906, Coon Butte, Arizona: Acad. Nat. Sciences Philadelphia Proc., v. 57, 887–914.
von Engelhardt, W., and Stoffler, D., 1967, Stages of shock metamorphism in crystalline rocks of the Rees Basin, Germany, *in* French, B., and Short, N., eds., Shock Metamorphism of Natural Minerals, Baltimore, Md.

ROAD GUIDE FROM FLAGSTAFF TO METEOR CRATER

by
Eugene M. Shoemaker,
Susan W. Kieffer,
and Robert L. Sutton

MILES Interval	Total	
0.0	0.0	Butler Street interchange, U.S. Interstate Highway 40 (I-40), heading east toward Meteor Crater and Winslow. Just north of U.S. Route 66 in Flagstaff, at 9:00 below the horizon, is Switzer Mesa, which is capped by Pliocene basalt flows dated at 5.80 ± 0.34 m.y. (Damon and others, 1974). The relatively straight margins of Switzer Mesa suggest that basaltic lava once flowed down a graben valley and that subsequent erosion produced the present "reverse topography." This filled graben is one of many straight-walled valleys and escarpments formed in the pre Plio-Pleistocene deposits by pervasive normal faulting. Cropping out below the protective lava cap of Switzer Mesa is part of the lower Wupatki Member of the Moenkopi Formation of Early Triassic age (McKee, 1951). San Francisco Mountain, including Humphreys Peak, and Elden Mountain are visible at 10 and 11 o'clock, respectively, on the left. San Francisco Mountain, a largely andesitic strato-volcano, probably attained a total eruptive elevation of more than ~4,500 m (15,000 feet). The volcano may have been modified by either summit collapse or explosive eruption. More recent fluvial and glacial erosion have also modified the form of the volcano. Humphreys Peak, elevation 3,851 m (12,633 feet), is the highest mountain in Arizona. Elden Mountain (2,835 m; 9,299 feet) is a dacite dome, complex in detail because part of it (north) appears to be laccolithic, tilting and exposing pre-Kaibab Paleozoic rocks as old as Devonian, while another part (the south end, visible from the road) was extrusive (Kluth and Kluth, 1974). Large viscous flow lobes with marked jointing can be seen from the highway on the south and east sides of the mountain.
0.6	0.6	The road cut exposes the top of the Alpha Member of the Kaibab Formation of Permian age (McKee, 1938). The top of the Kaibab is an ancient karst surface. The upper 20 to 30 meters (65 to 100 feet) of the Kaibab Formation appear to have been modified by solution.
0.4	1.0	The road crosses a southeast-trending escarpment bordering a small valley ("park") which is probably a graben.
1.9	2.9	Route 89 north toward Page and Grand Canyon exists here. Continue west on I-40.
0.4	3.3	Proceed slowly! About 100 meters ahead of you, a fault-line scarp is visible. The downthrown block is on the west and forms the small depression which you are traversing. On the left at 9:00 o'clock is Sheep Hill, a cinder cone of the Tappan age-group (Moore and others, 1974). As you approach the fault-line scarp, a quick glance to the rear at about 5:00 o'clock will reveal a basalt flow in the depression below I-40. This flow emanated from the base of Sheep Hill. The east margin of this depression is sometimes occupied by an ephemeral lake, Bill Fill Lake.

0.1	3.4	In the escarpment directly east of Big Fill Lake and in the road cut, the jumbled beds of the karst horizon of the Alpha Member of the Kaibab Formation are again exposed. A distinctive red bed sequence may be seen below the top of the Kaibab; this unit thins toward the east and is not present at Meteor Crater. The entire Kaibab Formation pinches out 30 miles beyond Meteor Crater.
0.1	3.5	Many quarries are dug into the cinder cones, such as Sheep Hill (at 9:00 o'clock), Wildcat Hill (11:00 o'clock), and Turkey Hill. The cinders are used in road metal and in cinder blocks. There are more than 400 cinder cones in the San Francisco volcanic field.
2.5	6.0	Turn off to Walnut Canyon National Monument.
0.2	6.2	The red beds in the Alpha Kaibab Formation are again exposed in the road cut north of eastbound I-40.
2.2	8.4	Cosnino road exit.
0.6	9.0	Normal fault, downthrown to the west.
0.7	9.7	From this section of the road, the view to the south is of a stripped surface developed on top of the Kaibab Formation. Topography in this area accurately reflects the bedrock structure, except where it is moderately dissected by gullies.
0.3	10.0	At about 8 o'clock, below the horizon, Sunset Crater is visible as a bright-rimmed cinder cone, devoid of vegetation. It lies just to the right of, and below, O'Leary Peak. The most recent eruption in the volcanic field occurred in 1064 A.D. at Sunset Crater. The date is based on dendrochronology (Smiley, 1958).
1.2	11.2	Along the highway good exposures of thin grey beds within the Alpha Member of the Kaibab Formation are visible beneath 1 to 3 m of the jumbled rocks in the karst horizon. The Kaibab here is mostly silty dolomite and dolomitic sandstone with some chert. Marine fossils (brachiopods such as Derbya; productids; cephalopods; invertebrates; a few fish teeth) are abundant in many beds.
0.1	11.3	At 10:30 o'clock is a large cinder quarry (the Darling pit) at Cinder Mountain, owned by the Santa Fe Railroad.
0.4	11.7	Walnut Canyon
0.3	12.0	A lava flow of the Tappan age-group (Moore and others, 1974), is visible in the road cut. For the next 2.5 miles a cinder blanket of variable thickness covers the land surface. The cinders probably came from four cinder cones just south of the highway.
0.4	12.4	Winona exit. The basaltic cinder cone on the right has a rootless lava flow on its northwestern flank. This cone is probably the source of the lava flow at mile 12.0. A last view of Sunset Crater silhouetted in front of O'Leary Peak may be obtained by looking back to the left (about 8 o'clock?).
1.2	13.6	The road drops back to the stripped surface on the Kaibab, thinly strewn with cinders. To the left, just beyond the Santa Fe railroad tracks, is the margin of a basaltic lava flow.
1.0	14.6	Looking ahead, the road rises over a gentle anticline, reflected as a swell on the stripped surface on top of the Kaibab Formation.
0.4	15.0	Three miles to the north at 9:30 o'clock, Piper Crater, a basaltic cinder cone, is superposed on the south side of Rattlesnake Crater, an older maar-type vent. Merrill Crater is east of Piper Crater at 10 o'clock.
2.1	17.1	Merriam Crater is located in the distance at 9:00 o'clock.
1.2	18.3	The small cinder cone at 3:00 o'clock is the nearest Quaternary volcanic feature to Meteor Crater.
0.7	19.0	The eastward gradient of the highway steepens noticeably as it comes over the crest of the anticline mentioned at mile 14.6. From here, the road descends into Padre Canyon. The Hopi Buttes volcanic field can be seen in the distance (about 80 km; 50 mi) at 10 to 11 o'clock, across the Little Colorado River valley). On the skyline to the right is Anderson Mesa, capped by basalt flows dated at 6.2 ± 1.2 m.y. (Damon, 1965).
0.9	19.9	Padre Canyon and Twin Arrows Trading Post.
1.3	21.2	As one looks out across the broad stripped surface on the Kaibab, it should be kept in mind that in this region of the Colorado Plateau, the topography reflects the structures beneath. A broad anticline is visible in the distance ahead. Normal faults which have been crossed are controlled by a regional pattern of jointing. Two orthogonal sets of joints which trend predominantly northeast and northwest are parallel to important regional structures in this part of the Colorado Plateau (Colton, 1936).
1.7	22.9	The long ridge between about 2 and 3 o'clock is an irregular basalt-capped ridge

which extends toward Meteor Crater and will be seen end on from road to Meteor Crater.

2.4 25.3 For the next 2 miles the highway traverses an anticline where an oil test well was drilled to Precambrian strata in 1962, about half a mile north of the highway (NE¼ NW¼ sec. 12, T. 20N., R.11E.). The well was converted for watering stock. Following are subsurface thicknesses of Paleozoic formations penetrated by this well (Peirce and Scurlock, 1972, p. 159):

	Feet	Meters
Kaibab (Permian)	283	86.3
Coconino (Permian)	890	271.3
Supai (Permo-Pennsylvanian)	1370	417.7
Naco (Pennsylvanian)	515	157.0
Molas (Pennsylvanian)	12	3.7
Redwall-Zones A, B, C (Mississippian)	110	33.5
Martin (Devonian)	380	115.8
Precambrian, depth	3560	1085.4
Precambrian, elevation	2175	663.1
Total depth of well	3630	1106.7

The Toroweap Formation, a marine unit between the Kaibab and the Coconino Formations in the Grand Canyon, was not recognized in this well as it is readily confused with the Coconino (McKee, 1938). Approximately the lower 73 m (240 ft) of Coconino in this well are correlated with the DeChelly Sandstone, which thickens toward the Defiance Plateau (Pierce and Scurlock, 1972).

0.2 25.5 The escarpment crossed by the road is a fault-line scarp on the flank of the anticline. The bedrock is downthrown to the east and exhibits reverse drag.

0.2 25.7 Crest of anticline.

1.5 27.2 A good view is obtained here of the rim of Meteor Crater in the distance at 1:00 o'clock. The Hopi Buttes volcanic field has become more prominent on the left horizon at about 11 o'clock.

1.9 29.1 The road rises over the crest of another anticline. East and West Sunset Buttes are visible in the distance to the right of Meteor Crater.

0.5 29.6 A fault-line scarp bounding the drainage at 1:30 to 3:00 o'clock at a distance of about one half mile is along a normal fault downthrown to the west.

1.1 30.7 Canyon Diablo.

0.7 31.4 Weathered outcrops of massive sandstone beds in the Wupatki Member of the Moenkopi sandstone (Triassic) form characteristic knobby or biscuit-like outcrops just above the Kaibab limestone.

2.8 34.2 Meteor Crater exit from I-40.

0.6 34.8 **STOP 1.** The first stop is at Indian Country Road intersection. To the east may be seen an abandoned stone building located just north of the old alignment of U.S. Highway 66. This building once housed H. H. Nininger's meteorite collection. It was operated as a museum, open to the public at a fee, where visitors heard lectures by Nininger and could study the collection and purchase specimens. The operation of this museum was the source of Nininger's livelihood for many years. Visitors could climb the stone tower and look off to the north to get a view of Meteor Crater without deviating from their route on Highway 66.

The museum is built just above a low escarpment which trends northwest-southeast and can be traced by eye for a distance of about two miles. The escarpment is along a small normal fault which offsets the lower beds of the Moenkopi at this place. The throw on the fault is about 9 meters (30 feet). On the upthrown side may be seen outcrops of the lower Massive Sandstone unit of the Wupatki Member of the Moenkopi Formation, which are the lowermost beds of the Moenkopi at this place. Erosional remnants of the Lower Massive Sandstone form a line of small knobs trending off to the southeast. About 3 meters (10 feet) of siltstone and very fine sandstone of the Moqui Member of the Moenkopi Formation are preserved locally above the Lower Massive Sandstone. Nininger's old museum is built of pieces of Moenkopi sandstone from both the Wupatki and Moqui Members. Some of these pieces are beautifully ripplemarked.

A water well, 100 meters (300 feet) away, at 11 o'clock, brings water up from the middle of the Coconino Sandstone at a depth of 200 meters (600 feet). The Coconino Sandstone is the principal aquifer in this part of northern Arizona. Here the water table slopes gently to the north, in the same direction as the average regional dip of the beds. Meteor Crater is located on the southern flank of the Black Mesa basin; the beds dip generally about one degree to the northeast.

0.5 35.3 The road drops into a shallow valley where Wupatki sandstone is well exposed.

Interleaf. Upturned edges of stratified rock on west side of interior of Meteor Crater, Arizona; San Francisco Peaks in distance. (Photograph No. PK 14,092 by Troy L. Péwé, January 2, 1970.)

0.9 36.2 The road drops to the level of the Moenkopi-Kaibab contact. A few scattered blocks of Kaibab Limestone may be seen to the side of the road.

0.9 37.1 **STOP 2.** Here the road comes over the crest of a rise, and the visitor obtains a first good overall view of the crater rim. At this point, the road is on the Moqui Member of the Moenkopi, about 5 meters (15 feet) above the base of the Moqui Member.

To the left and behind the rim of Meteor Crater may be seen the lava-capped mesas known as East Sunset Butte and West Sunset Butte. Both buttes are capped by basalt, which rests on the Chinle Formation of Upper Triassic age. The flanks of the buttes visible from the vantage point along the road are mantled with landslide debris which supports a pygmy forest of pinyon and juniper. In places along the flanks of the buttes, not visible from this point, a complete section of the Moenkopi Formation and a partial section of the Chinle Formation are exposed. Three cinder cones are visible on the buttes which mark the vents from which the basaltic lavas were erupted.

To the right of Meteor Crater, from about 12 o'clock to about 3 o'clock, the skyline is formed by basalt-capped mesas of the Mormon Mountain volcanic field. The basalts in this field are Miocene and Pliocene in age. One of the basalts capping Anderson Mesa, at 3 o'clock, is dated at 6.2 ± 1.2 m.y. (Damon, 1965). The two highest points visible in the volcanic field are Hutch Mountain, at about 1:30, and Mormon Mountain, at about 2 o'clock.

The high point between Hutch Mountain and Mormon Mountain is the end of a long, northeast-trending ridge that extends directly toward the viewer from the more distant part of the volcanic field. The ridge is capped by a single lava flow, most of which has now been destroyed by landsliding on both sides of the ridge. Red beds of the Chinle Formation and Moenkopi Formation may be seen exposed in parts of the landslide blocks on the near end of the ridge.

Between 3 o'clock and 5 o'clock lie the volcanoes of the San Francisco volcanic field. The largest volcano is San Francisco Mountain. A circle of peaks surround the eroded core of this volcano, the highest of which is Mt. Humphreys. At 3,851 meters (12,633 feet), Mt. Humphreys is the highest point in Arizona. The San Francisco stratovolcano is composed mainly of andesite lava flows and ashes. Rhyolites and dacites occur as domes perches on the flank of the older stratovolcano. The largest of these domes forms Mount Elden, which is the prominent toe extending to the left of the main mountains. Domes which have been dated range in age from 2.71 ± 0.13 m.y. to 0.212 ± 0.011 m.y. (Damon and others, 1974).

To the right of the San Francisco peaks is an extensive field of Pleistocene basaltic cinder cones. This is the main locus of basaltic activity, at the present time, in the San Francisco volcanic field. The youngest cinder cone in this field, not visible from this vantage point, is Sunset Crater, which has been dated by dendrochronological methods at A.D. 1064 (Smiley, 1958). The nearest prominent reddish colored cinder cone is Merrill Butte, which lies about 27 km (17 miles) airline distance. At the extreme right of the volcanic field is a large symmetrical cinder cone called Merriam Crater. The cinders on the side road, extending to the west, and also used as aggregate in the asphalt capping of the Meteor Crater road, have been excavated from basaltic cinder cones.

1.9 39.0 **STOP 3.** AT JUNCTION OF BAR-T-BAR RANCH ROAD. Low buttes on each side of the road are formed by beds of the Moqui Member of the Moenkopi Formation. An excavation around the flank of the butte, on the right side of the road, is a fossil quarry excavated by the University of California. Materials recovered from this quarry include an extensive collection of footprints and fossils of ganoid fishes and amphibians. On the basis of regional studies of the stratigraphy of the Moenkopi Formation and on fossils obtained from this and other nearby quarries, the beds at this horizon can be placed near the base of the Middle Triassic. The fossils were found in freshwater dolomite and siltstone beds in the floor of the quarry. These beds are no longer exposed.

0.7 39.7 **STOP 4.** This stop is just beyond a broad curve in the road at a point where road heads nearly due east. To the north of the road, at 9

o'clock, the skyline is formed by a ridge of siltstone and sandstone of the Moqui Member of the Moenkopi. The south slope of the ridge is mantled with late Pleistocene colluvium containing abundant fragments of sandy dolomite from the Kaibab Formation. These fragments have been derived by reworking of a blanket of ejecta that surrounds the crater. At one time this ejecta blanket extended beyond the ridge of Moenkopi, but the more distant parts of that blanket have now been eroded away during the time elapsed since the crater was formed. The colluvium extends to the south into a shallow drainage where it is overlain by a thin deposit of Holocene alluvium. The outer eroded edge of the ejecta blanket lies essentially at this position, and is concealed beneath late Pleistocene and Holocene alluvial deposits.

The difference in elevation between the crest of the Moenkopi ridge and the lowest outcrop in the ejecta blanket, near the drainage, provides a minimum estimate of the relief on the precrater surface. It is clear that the ridge of Moenkopi is an erosional feature that predated the crater and had a precrater relief of at least 15 meters (50 feet).

On the near side of the drainage is a surface that climbs gradually toward the crater rim and which is underlain by late Pleistocene alluvium. The road bed is built on this alluvial unit. The age of this and other alluvial deposits at Meteor Crater has been determined by correlation of pedocal paleosols developed on them. A well-defined sequence of Pleistocene and Holocene deposits has been studied in the Hopi Buttes region, about 80 km (50 miles) to the northeast. (The nearest of the Hopi Buttes are just visible on the northeast horizon.) There the deposits have been dated by means of vertebrate fossils, C-14 analysis, and on the basis of artifacts contained in the youngest alluvial units. A well-developed paleosol, corresponding to the youngest Pleistocene soil in the Hopi Buttes, is exposed in a shallow borrow pit in the alluvium 50 meters (170 feet) to the south of the road. This Pleistocene alluvium rests directly on the preserved part of the ejecta blanket.

The ejecta blanket surrounding Meteor Crater is stratified and can be divided into three distinct mappable units:

1) a unit composed of fragments of the Moenkopi Formation at the base,
2) a unit composed of fragmental debris from the Kaibab Formation, and
3) a unit composed of fragments of the Coconino Sandstone at the top.

Exposures of the Kaibab debris unit can be seen between 10 o'clock and 3 o'clock. At 3 o'clock the Kaibab debris rises high on the crater rim. Low mounds with large, light-colored blocks, lying 100 to 300 meters (300 to 1,000 feet) from this vantage point, between 10 o'clock and about 1 o'clock, are exposures of the Kaibab debris unit that protrude through the surrounding Pleistocene alluvium. This part of the crater rim is essentially a stripped surface on the top of the Kaibab debris unit. The gently hummocky topography of the rim reflects the original configuration of the contact between the Kaibab debris unit and the overlying Coconino debris unit, which has been largely stripped away.

At 2 o'clock, on the horizon, is the chimney of a building now destroyed by fire. This building was the headquarters for the exploration activity of the old Standard Iron Company and the latter-day Barringer Crater Company. During the 1930's and 1940's, after exploration had ceased, the building also served as a visitor center and a small museum for the public visiting the crater. This building is constructed on a high-level pediment surface that is cut into the rim units of the crater. The pediment is capped by relatively coarse alluvial and colluvial debris derived from still higher parts of the rim. The pediment can be traced as a cut surface between about 1:30 and 3 o'clock. The easternmost edge of the pediment lies just to the left of a powder magazine, which has been dug in a brilliant white deposit beneath the pediment gravels. This white deposit is a remnant of the Coconino Sandstone debris unit, which is preserved in a pocket beneath the pediment gravels.

The difference in elevation between the highest recognizable pediment on the crater rim and the upper edges of the latest Pleistocene alluvial deposits at this locality provide a minimum estimate for the amount of

Interleaf. Upturned edges of stratified rock on southwest side of interior of Meteor Crater, Arizona. (Photograph No. PK 14,093 by Troy L. Péwé, January 2, 1970.)

dissection of the rim by erosion that has occurred since the crater has formed. On the northeast flank of the crater rim this difference is about 12 meters (40 feet). The total amount of degradation of the rim is, of course, substantially greater than this. A conservative but realistic estimate of the total reduction in rim elevation by erosion would be 15 to 20 m (50 to 75 feet). In places the rim crest may have been eroded down as much as 30 m (100 feet). In most places the Coconino debris unit has been entirely stripped away.

0.2 40.0 **STOP 5.** BY TRAILER INSTRUCTION SIGN AND JUST BEYOND ROAD TO WATER WELL. At approximately 1 o'clock may be seen a tongue-shaped mass of light-colored rocks, extending to the crest of the crater rim. This mass is a remnant of the Coconino Sandstone debris layer preserved in a depression on the top of the Kaibab debris layer. Kaibab debris underlies the grassy slopes surrounding the Coconino debris remnant. A water well at 7:30 extends slightly below the water table at a depth of about 200 meters (600 feet). This well provides the water for the museum and the visitor center on the crater rim and for the residences of the museum staff.

0.2 40.2 **STOP 6.** IN LOWER PARKING LOT. Exposures in cuts at the southeast corner of parking lot provide an excellent introduction into the nature of the rim debris units. A part of the Kaibab debris unit is exposed in this cut. The debris consists of angular to subangular fragments ranging in size from 1 micron or less up to blocks more than a meter across. The size frequency distribution of this material follows a rather well-known fragmentation law. The cumulative mass of the debris is a simple power function of the particle size. The exponent of this power function is such that about 50 percent of the total mass falls in the largest three phi intervals. As one examines the debris in the cut, about 50 percent of the volume of the material consists of easily recognized fairly coarse blocks set in a matrix of finer crushed material. In general, the fines are only recognizable in fresh exposures such as this. The effect of weathering is to wash away the fines, leaving the surface mantled with the coarser debris. When seen on a natural outcrop, the debris unit appears to be composed almost entirely of the coarser blocks.

THE ERUPTIVE MECHANISM OF THE PERIDOT MESA VENT, SAN CARLOS, ARIZONA

by
K. H. Wohletz*
Arizona State University
Tempe, Arizona
*Present address: University of California, Los Alamos Scientific Laboratory, Los Alamos, NM 87545

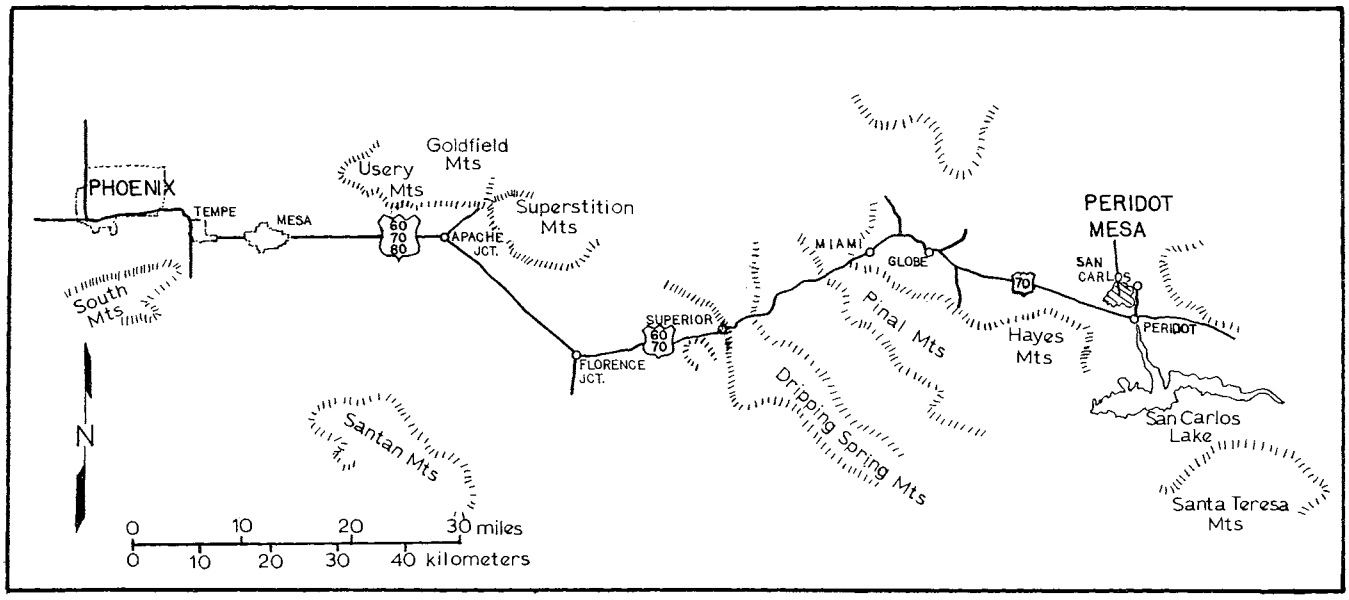

Figure 1. Location map of Peridot Mesa and road log for the field trip.

INTRODUCTION

The Peridot Mesa Vent belongs to the San Carlos volcanic field located in San Carlos Valley and Ash Flat, Arizona (fig. 1). This field has received little attention but Bromfield and Schride (1956) suggest an age of Pliocene or Pleistocene for the lavas which have not been dated radiometrically. The volcanic field is comprised of several diatreme-like vents of which Peridot Mesa is the best studied. The vents erupted tuff rings of pyroclastic surge tephra and flows of lava of entirely a basaltic composition. The flows are generally thin (less than 10 m) and overlie as well as interbed with Tertiary lake beds and Gila-type conglomerate. The lavas are flat-lying and form uplifted plateaus and terraces that have been dissected by erosion. The lavas are widely noted for the abundant four-phased lherzolite nodules that are contained in the flows and bombs around at least several of the vents.

This study is primarily directed at the Peridot Mesa Vent although petrologic data from nearby vents is also examined. Both the physical and the petrologic aspects of the vent are of great interest and will be discussed as two parts in this report.

The author would like to acknowledge M. F. Sheridan for his help in unraveling the eruptive history of the vent, and M. Prinz whose unpublished studies of the nodules have drawn much attention to the locality, and Luween Smith of the Los Alamos Scientific Laboratory for help in drafting.

DESCRIPTION

STRATIGRAPHY

Peridot Mesa is a basalt flow that caps grus and lake beds of Pliocene age. Upon closer inspection the lava flow is found to be of several parts: a lower unit of pyroclastic-surge beds which are overlain by a welded scoria and a massive nodule containing flow that is of coarser texture within the vent (fig. 2). Cinders, bombs, and spatter are abundant near the vent.

The grus, a reddish-tan friable material, is a Tertiary surface and a relative basement high. It has limited exposure and in most areas is overlain by Pliocene lake beds that

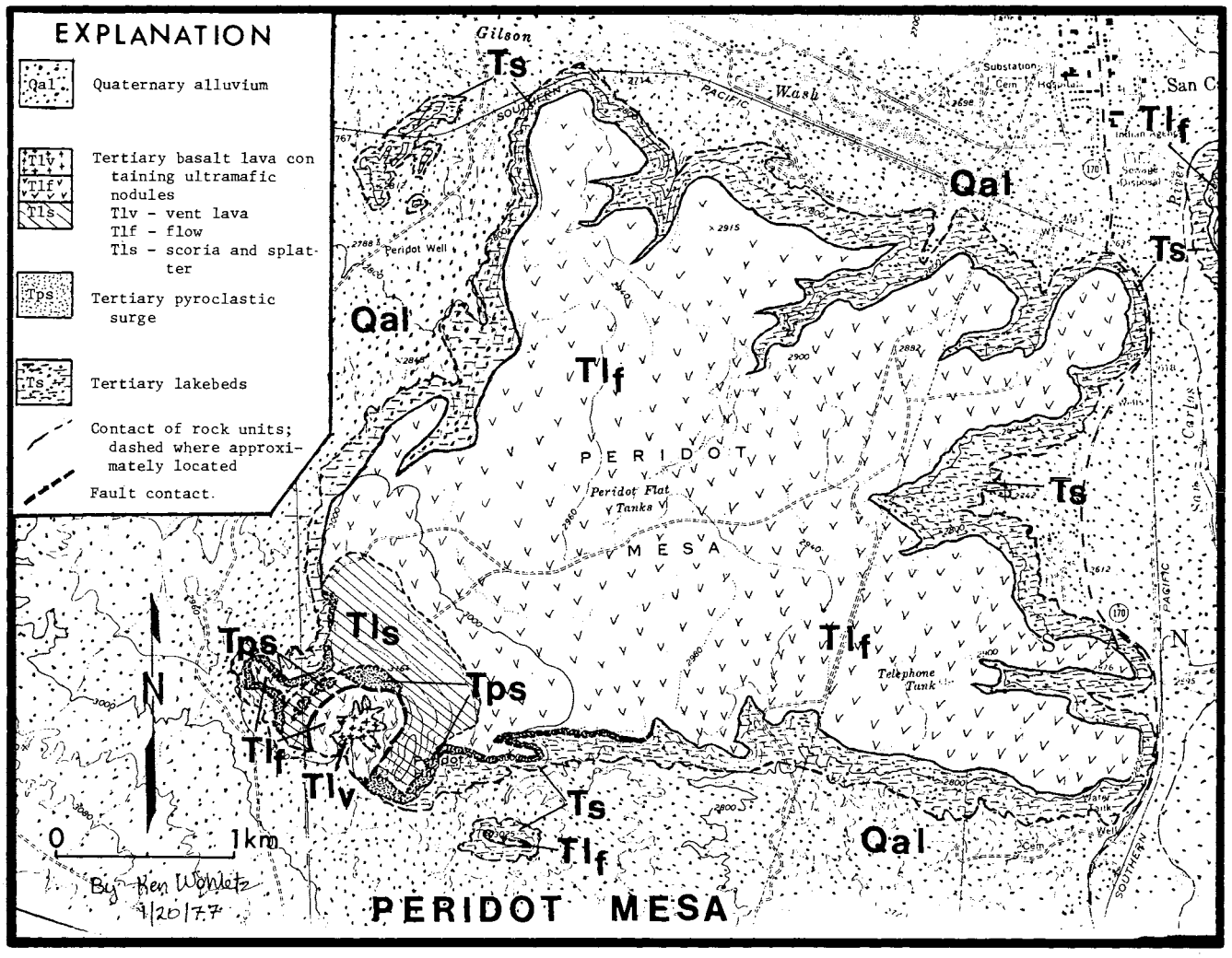

Figure 2. Geologic map of the Peridot Mesa area.

form extensive flat-lying deposits along the Gila and San Carlos rivers. The lake beds are white and are very distinct from interbeds of basalt that exist in the area. The lake beds are normally graded, often cross bedded, and are composed of silts and sands.

The Pyroclastic-surge deposit (Sparks, 1976; Wohletz and Sheridan, in press) is of great importance in understanding the eruptive history of the vent. It overlies the lake beds and grus and is 10 to 15 m thick at the vent decreasing in thickness away from the vent where it pinches out at a distance of 1,200 to 1,500 m. The surge deposit is light tan and is composed of dominantly reworked lake-bed silts and sands with lithic fragments of granite, basalt and peridotite. About 5 to 10 percent of the deposit is accretionary lapilli and palagonite, found mostly near the vent. Surge beds average in thickness from 1 to 5 cm and show three main bed forms: inversely graded planar beds, massive beds, and sandwave beds consisting of dunes, antidunes, ripple-drift laminations, and cross laminations. Sandwave beds are most common near the vent whereas planar beds dominate in distal portions of the deposit. Massive beds are common throughout the deposit.

A thin (less than 1 m) scoriaceous agglutinate (welded scoria) overlies the surge and grades into massive lava above. Caliche has filled vesicles in both the scoria and the lava. The lava flow is just 2 to 3 m thick at its lateral extremities but thickens to 15 to 20 m along its central axis. In its thickened portions near its terminus, columnar jointing is well developed in the upper portions of the flow. Near the vent cinders and air-fall lapilli interbed with the surge and scoria units. The lava within the vent is coarse-grained and apparently occurring as intruded masses and foundered blocks within a breccia matrix. Although the bulk of the nodules occupy a distinct zone within the flow, there is no

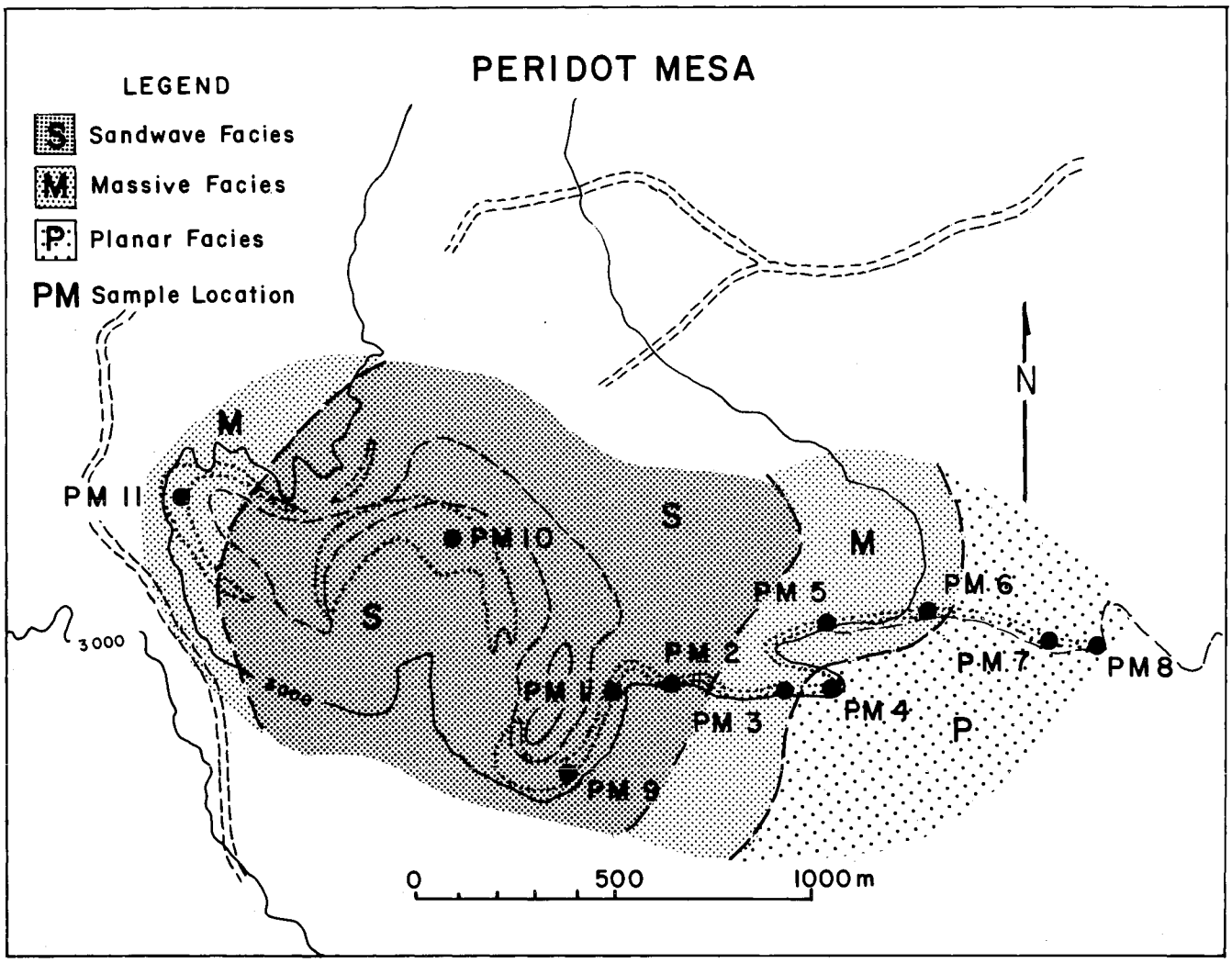

Figure 3. Pyroclastic surge facies map of Peridot Mesa.

evidence that the nodules accumulated at the bottom of the magma reservoir prior to eruption with the result of them being the last extruded materials. On the basis of their overall occurence throughout the lava, the spatter, and to some degree the surge, nodules were probably suspended in the magma.

STRUCTURE

The vent is best described as a diatreme. It is surrounded by a tuff ring made up of surge beds and air-fall lapilli and cinders. The tuff ring is breached on its southeastern side forming a crater of approximately 550 m in diameter. The tuff ring is armored with spatter. A circular fault exists within the tuff ring apparently displacing the inner portion of the vent 5 to 10 m downward. The lava flow is "rootless" in that it begins outside the tuff ring probably having formed from a lava fountain. The flow trends northeast following a paleo-valley.

PYROCLASTIC-SURGE FACIES

The surge deposit shows a bed-form facies distribution (fig. 3) that is discussed by Wohletz and Sheridan (1976; in press). A sandwaves facies is where sandwave and massive beds dominate; a massive facies is where sandwave and planar beds interfinger with massive beds; and a planar facies is where planar and massive beds dominate. The facies distribution was studied by measurement of 11 stratigraphic sections at various distances from the vent. The sections were classified to a facies by a Markov analysis of bed-form transitions (Wohletz and Sheridan, in press). This facies distribution suggests that the surge was erupted as a highly inflated cloud containing a lean mixture of particles and entrapped gases. As it moved away from the vent, particles moving in a viscous mode of transport, saltated along the substrate depositing dominantly sandwave type beds. As the cloud moved farther away from the vent, gases escaped and the cloud deflated until prior to

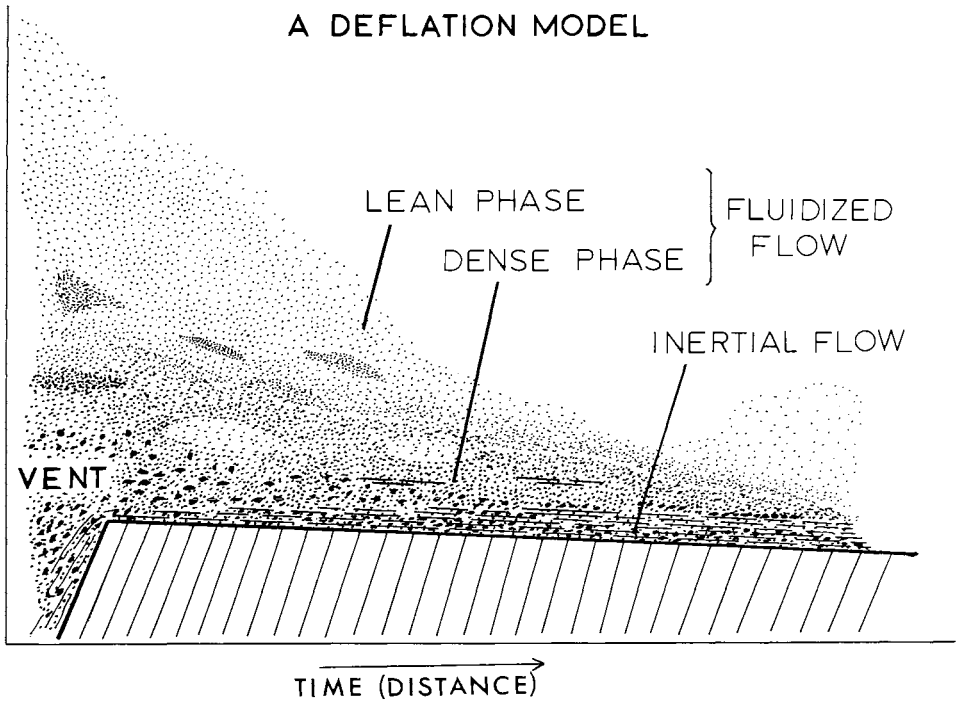

Figure 4. Schematic diagram illustrating the deflation (loss of gas) of a pyroclastic surge with increasing time (distance) from the vent. This diagram is an integration of a number of surge-cloud profiles that likely exist at various stages of surge transport.

its dissipation, particles moved as a dense inertial flow depositing dominantly planar beds. At intermediate distances from the vent, the surge cloud, not wholly deflated, deposited massive, planar, and sandwave beds. Massive beds appear to be the result of deposition from partially deflated zones within the cloud where inertial and viscous flow modes interact. For a more complete description of this model see Wohletz and Sheridan (in press). Figure 4 illustrates the surge model.

ERUPTIVE HISTORY

Eruptive activity began with explosive vent-clearing activity and emplacement of pyroclastic surges. Surges have been shown by Moore (1967) and Waters and Fisher (1971) to be the results of explosive phases of activity. Due to the existence of accretionary lappilli, palagonite, and lake beds, water was likely abundant in the first phases of eruption, producing steam explosions (phreatomagnatic) as it contacted hot magma. Beside expanding steam, CO_2 is a volatile likely to have contributed to the explosive nature of eruption as McGetchin (1968) suggests for mantle-derived magmas in Colorado Plateau diatremes. Pyroclastic explosions forming surges occurred before much magma made its way to the surface as evidenced by materials blasted out of the vent that are dominantly lake-bed material. Surge deposits along with fall deposits formed a tuff ring around the vent.

Following the phreatomagmatic/volatile-fluids eruption stage, less explosive magma was extruded producing a lava fountain. Spatter from the fountain "armored" the earlier-formed tuff ring and remobilized to form a "rootless" lava flow. The flow followed topography down a depression trending to the NE carrying numerous nodules that had also been blasted out by vigorous fountaining.

The final stage of activity was marked by cessation of fountaining, passive emplacement of the last volumes of magma as a plug within the vent, and collapse of vent as the volcanic neck foundered.

CONCLUSIONS

The eruptive sequence at Peridot Mesa casts light on the eruptive mechanism and therefore the composition of some mantle-derived magmas. The explosiveness of the eruptions, the structure of the vent, and the existence of dense ultramafic nodules that were supported or suspended in the lava suggest that the magma was volatile-rich and moved at high velocities to the surface. At some point in time, volatiles (CO_2, H_2O) must have exsolved from the magma and reached the surface prior to the rest of the magma. The eruption scenario at the Peridot Mesa diatreme is likely to be much like that proposed by McGetchin (1968). The sequence of events is illustrated in Figure 5 and is summarized as follows: (A) a crack is propagated to the surface by a supercritical, CO_2-H_2O-rich fluid by hydraulic fracture; (B) the fluid flows through the fracture, blasting away a vent at the surface, producing pyroclastic surges; (C) a Venturi-like vent structure develops allowing magma to flow to the surface at increased velocities and entraining

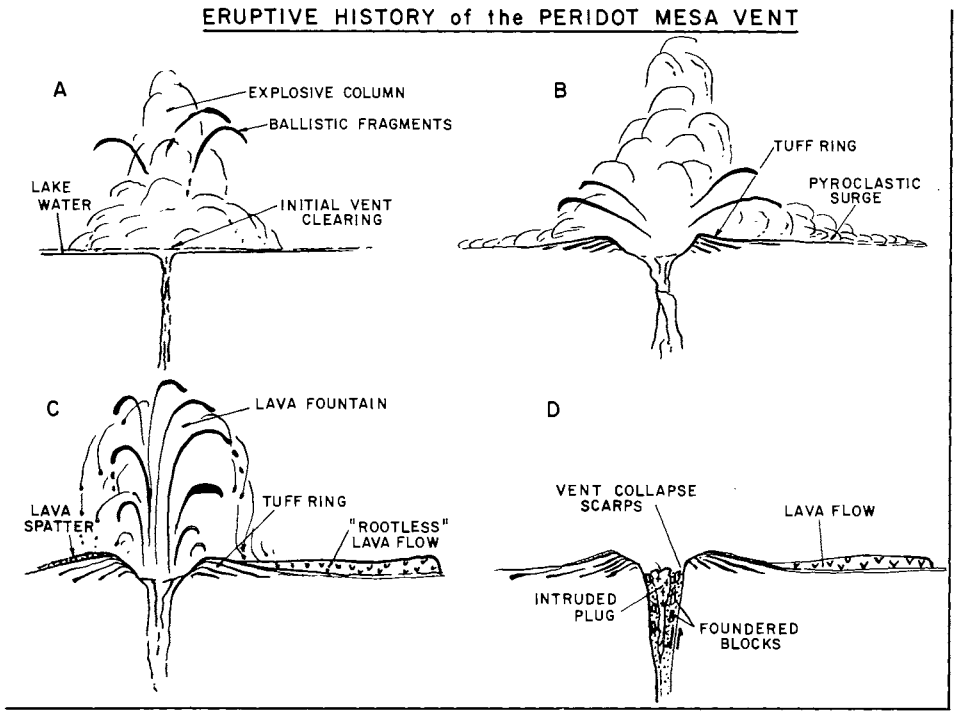

Figure 5. Illustration of four stages of the eruptive history of the Peridot Mesa vent: (A) Explosion of volatiles initiating a vent; (B) pyroclastic-surge stage developing a tuff ring and widening the vent; (C) lava fountaining stage producing a "rootless" lava flow; and (D) collapse of the vent after cessation of lava extrusion.

ultramafic nodules to produce a lave fountain; (D) when the magma in the reservoir is expended, pressure in the vent decreases and the material in the vent neck collapses downward.

REFERENCES CITED

Bromfield, C.S., and Schride, A.F., 1956, Mineral resources of the San Carlos Indian Reservation, Arizona: U.S. Geol. Sur. Bull. 1027-N, p. 613–691.

McGetchin, T.R., 1968, The Moses Rock dike: Geology, petrology and mode of emplacement of a kimberlite bearing breccia dike, San Juan County, Utah: Pasadena, PhD thesis, Calif. Inst. of Technol.

Moore, J.G., 1967, Base surge in recent volcanic eruptions: Bull. Volcanol., V. 30, p. 337–363.

Sparks, R.S.J., 1976, Grain size variations in ignimbrites and implications for the transport of pyroclastic flows: Sedimentology, V. 23, p. 147–188.

Waters, A.C., and Fisher, F.V., 1971, Base surges and their deposits: Capelinhos and Taal Volcanos: Jour. Geophys. Res., V. 76, P. 5596–5614.

Wohletz, K.H., and Sheridan, M.F., 1976, A model for base-surge deposits (abs.): Geol. Soc. America Abstracts with Programs, V. 8, no. 5, p. 645–646.

Wohletz, K.H., and Sheridan, M.F., in press, A model of pyroclastic surge: Geol. Soc. America Memoir on ash flows.

THE SAN CARLOS ALKALINE ROCK ASSOCIATION

by
John R. Holloway
and
Christina Cross

Arizona State University

Several volcanic features occur in close proximity to the Peridot Mesa tuff ring and flow (see fig. 1). The features were noted and briefly described in a doctoral dissertion by Marlowe (1961). They are apparently related in time and major-element chemistry. The following paragraphs give a brief description of the features:

Peridot Mesa Basanite. The profusion of ultramafic nodules contained in this lava make it the best known of the volcanics in the area. The published work on the area is concerned mainly with the nodules and megacrysts in the basanite (Mason, 1968; Prinz and Nehru, 1969; Frey and Prinz, 1971). An average of several analyses collected

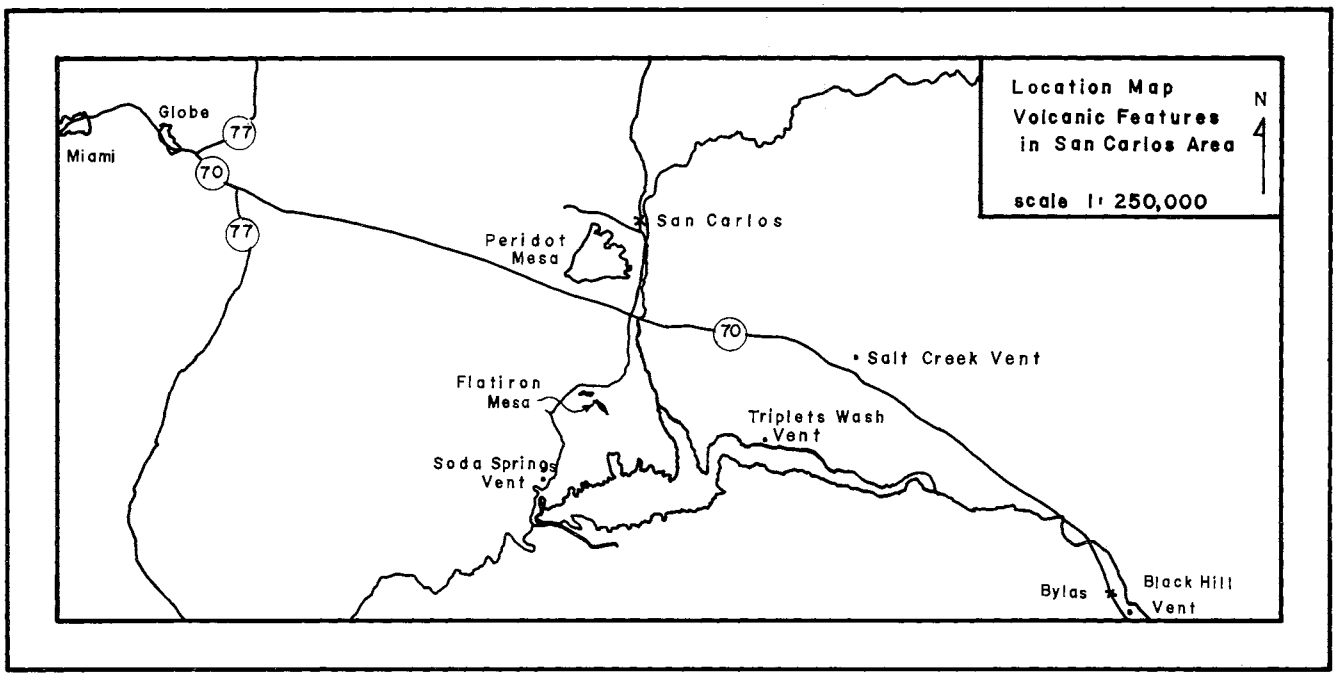

Figure 1. Location map of alkaline volcanics in the San Carlos area.

along the length of the flow is given in Table 1 (column 1). That average is very similar to analyses published by Prinz and Nehru (1969). The composition of the flow is remarkably uniform except for two-fold variations in potassium, rubidium and barium. The cause of the alkali metal variations is unknown; it may be due to alteration but the rocks appear fresh in thin section. Thin sections of the basanite reveal fragments of olivine and pyroxene from the lherzolite nodules, thus the analyses probably show higher Mg/Fe than initially present. Nevertheless, the Mg/Fe ratio in the basanite is easily high enough to be in equilibrium with upper mantle olivine.

The nodules range up to 50 cm in diameter and commonly are 10 cm in diameter. The most abundant type of nodule is spinel lherzolite consisting of olivine, orthopyroxene, spinel, and chromian diopside. Other nodule types include harzburgite, websterite, clinopyroxenite, orthopyroxenite and gabbro. Clinopyroxene-rich bands up to 10 cm thick are present in many of the spinel lherzolite nodules. In addition to the polycrystalline nodules, there are megacrysts of black, vitreous clinopyroxene and spinel, and plagioclase. Fragments of kaersutite up to 2 cm long have been found in the vent area. Geochemical evidence suggests that the polycrystalline nodules are accidental inclusions in the host basanite, but that the megacrysts are probably cognate.

Soda Springs Vent. Described by Cross and Holloway (1974).

A small (~100 meter) tuff ring or eroded plug consisting of mugearite (#2, Table 1) with trachytic texture containing numerous megacrysts of ferro-kaersutite (#3, Table 1) and anorthoclase, (#4, Table 1) and rare titanomagnetite and ferrobiotite. The composition of the megacrysts is consistent with their formation by cotectic crystallization from the host magma. Calculations suggest the mugearite is produced by fractional crystallization of kaersutite from the Peridot Mesa basanite. A K-Ar determination done on an anorthoclase megacryst yields an age of 5.28 ± 0.13 m.y.

Table 1. Chemical Composition of Rocks and Minerals from the San Carlos Area, Arizona. (in weight percent)

Oxide	1	2	3	4	5
SiO_2	46.0	52.3	38.7	62.6	47.0
TiO_2	2.77	2.02	4.56	0.08	2.32
Al_2O_3	15.2	18.2	13.6	21.1	15.2
Fe_2O_3*	13.3	11.1	17.3	0.43	11.6
MgO	8.15	2.76	8.56	n.d.	8.24
CaO	7.68	5.82	10.0	1.60	8.58
Na_2O	4.73	4.54	2.56	7.80	3.48
K_2O	1.89	2.89	1.14	3.50	1.99
P_2O_5	0.90	0.96	n.d.**	n.d.	0.62
Total	100.7	100.6	96.4	97.1	99.0

* Total iron calculated as Fe_2O_3
** n.d. = not determined

1. Average of 7 analyses of the Peridot Mesa basanite.
2. Representative analysis of Soda Springs mugearite.
3. Ferro-kaersutite megacryst from Soda Springs.
4. Anorthoclase megacryst from Soda Springs.
5. Alkali Basalt from Black Hill.

Flatiron Mesa. This is a flow remnant which is identical to Peridot Mesa basanite in texture and composition. Its topographic position would allow it to be a remnant of the Peridot Mesa flow. No ultramafic nodules have been found in it.

Triplets Wash. Apparently the remnant of a small volcano, the lavas here are highly altered and no detailed investigations have been carried out on this area.

Salt Creek. Probably a diatreme, all exposed rocks are pyroclastic. It has a roughly circular outline of about 400-meter diameter.

Black Hill. An eroded volcano consisting of massive flows and dikes with minor tuff. Chemically the lavas are alkali basalts (#5 Table 1), intermediate in composition between the Peridot Mesa basanite and the Soda Springs mugearite.

In addition to the above localities, several smaller remnants of flows and vents have been found in the San Carlos area. All of the volcanics appear to be of roughly equivalent age and all have alkaline affinities. They would thus appear to have a common origin. The abundance of ultramafic nodules whose mineralogy indicates an upper mantle source (Frey and Prinz, 1971), and the Fe/Mg ratio of the basanite would allow it to be in equilibrium with olivine in the mantle. Consequently it would appear that the basanite is the parental magma for the other volcanics, the latter being produced by fractional crystallization of the basanite.

REFERENCES CITED

Cross, C. and J. R. Holloway, 1974, A megacryst-bearing alkali basalt, San Carlos, Arizona: Geol. Soc. Am. Abstracts with Programs 6, 437.

Frey, F. A. and M. Prinz, 1971, Ultramafic nodules from San Carlos, Arizona: Mineralogy and Chemical Composition: Geol. Soc. Am. Abstracts with Programs 3, 537–574.

Marlowe, J. I., 1961, Late Cenozoic geology of the lower Safford basin on the San Carlos Indian Reservation, Arizona: Ph.D. thesis, University of Arizona.

Mason, B., 1968, Kaersutite from San Carlos, Arizona, with comments on the paragenesis of this mineral: Mineral. Mag. 36, 997–1002.

Prinz, M. and C. E. Nehru, 1969, Comments on Kaersutite from San Carlos, Arizona with comments on the paragenesis of this mineral, by Brian Mason: Mineral. Mag. 37, 333–337.

FIELD GUIDE

Leaders: J. Holloway and K. H. Wohletz

GENERAL STATEMENT

The trip begins at Arizona State University, Tempe, Arizona and is designed to return there at the end of one full day. The purpose of the trip is to examine the volcanic vent and peridotite nodules of great beauty at Peridot Mesa, and other volcanic rocks near San Carlos, Arizona. It is most important for those interested in this trip to note that Peridot Mesa is on the San Carlos Apache Indian reservation and that access is limited. Prior permission for access must be obtained through the Chairman of the San Carlos Council, San Carlos, Arizona. The trip proceeds from Tempe in the Salt River Valley on US 60–70 east towards Apache Junction where the valley is bordered on the north and east by the Goldfield Mountains and Superstition Mountains. These mountains are part of a large silicic volcanic field (Sherian and others, 1970; Sheridan, 1968). From Apache Junction, the field trip proceeds along US 60–70 to Florence Junction along the border of the Basin and Range Province to the west with the transition zone of the Colorado Plateau to the east. From Florence junction, US 60–70 continues to Superior, Miami, and Globe, passing through exposures of the Apache Leap Tuff (Peterson, 1968), and the Schultze Granite, a pluton surrounded by porphyry copper mines. From Globe the trip continues along the Gila River on US 70 to the San Carlos River where the town of San Carlos is located at the foot of Peridot Mesa. In this area there are several diatreme-like vents whose basaltic lavas contain abundant peridotite nodules. Much of the following road log is updated from an earlier log in the Arizona Geological Society Guidebook III (1968).

ROAD LOG

MILES Interval	MILES Total	
0.0	0.0	Leave loading dock at A.S.U. Physical Science Building. Turn right on University Drive, then right on Rural Ave., and then left on Apache (US 60–70) to Apache Junction.
16.4	16.4	East of the Bush Highway three main structural blocks can be seen in the volcanic complex to the northeast. The Goldfield Mountain front to the north is underlain by basement granite. Above the granite is a band of non-welded rhyolite ash-flow tuff, the Geronimo Head Formation of 17 m.y. age, which forms a conspicuous light-colored outcrop. The ash-flow tuff is in turn overlain by a black, glassy dacite lava. The elevation of the Goldfield front is approximately 1,000 m on the west and 800 m on the east; the volcanic sequence thickens to the east. To the east of the Goldfield Mountains is the Superstition mountain block. This mass of ash-flow tuffs and lavas has an

elevation of 1,600 m of which at least 650 m are part of the Superstition volcanic sequence. Whereas the Goldfield volcanics are dipping to the northeast, the ash-flow tuffs and lavas of the Superstition Mountains are horizontal.

Between these two main mountain masses is an area with an elevation of 600–700 m, which is underlain by steeply dipping lavas, ash-flow tuffs, and epiclastic volcanic breccias (lahars). The lahar units suggest volcanotectonic subsidence. The dips of the lahars and the outcrop distribution outline at least two caldera margins.

7.4 23.8 Apache Junction. Continue on US 60–70–80 which curves toward the southeast. For the next 15 miles the highway parallels the trend of the Superstition Mountains, which lie to the east and northeast. This range, the locality of the fabled Lost Dutchman Gold Mine, is composed chiefly of volcanic rocks of Tertiary age: ash flows, air-fall and water-laid tuffs, mud flows and lava flows and plugs that range from rhyolitic to basaltic in composition. Volcanic activity in the Superstitions began 29 m.y. ago with eruptions of dominantly quartz latite lava to form a ring of stratovolcanoes and domes. At 25 m.y. the eruption of vast quantities of ash formed what is now called the Superstition Tuff. During the eruption of ash, caldera collapse occurred, ponding ash to thicknesses over 1,000 m within the caldera. The prominent layered cliffs making up the summit of the Superstition mountains represents the resurgent dome of the caldera composed of the Superstition Tuff (showing at least 9 cooling units) which ponded in the caldera. Parts of the caldera ring domes form the rampart-like cliffs on the northern part of the mountains.

7.2 31.0 Roadcut through a rhyodacite lava, part of a caldera moat-filling dome. Hills on the low lands west of the Superstition Mountains are all silicic lava flows and dikes. The road here parallels the trend of a major Basin and Range fault to the west which displaces basement rock over 1,000 m downward on the western side.

9.3 40.3 Florence Junction. The hills just north of the highway are eastward-tilted blocks of remnants of quartz latitic ash flows.

2.5 42.8 The rugged hills to the north are composed mainly of volcanic rocks of the Superstition Mountain complex. The volcanic rocks overlie tilted and faulted Pinal Schist, granitic rocks, and sedimentary rocks of the Apache Group, all of Precambrian age.

1.4 44.2 To the north (~8 o'clock), glimpses may be caught of a pointed mountain, Weavers Needle, which is a historic landmark used in location of the Lost Dutchman Gold Mine.

0.5 44.7 Dromedary Peak at 2 o'clock. Faulted and sheared remnants of an ash flow resting on Pinal Schist.

1.3 46.0 Pinal Schist in roadcuts.

1.3 47.3 At 12 o'clock is Picketpost Mountain, a prominent landmark of the region.

2.5 49.8 Roadcuts in alkali olivine basalt of probable Tertiary age, very similar to the 30 m.y. basalt that underlies all of the Superstition complex.

For the next several miles, there are excellent views of Picketpost Mountain. At its base are rhyolitic lava flows which are overlain by a thick series of light-colored tuffs that make up most of the steep flanks. The mountain is capped by quartz latite lava flows that emerge from a vent on the eastern flank of the mountain. This lava has been K-Ar dated at 18.0±0.3 m.y. (Damon, et al., 1966).

2.0 51.8 Entrance to Boyce Thompson Arboretum, a center for the study of desert biology and ecology, recently acquired by the University of Arizona. The basin over which we are driving is filled by alluvium and the Gila Conglomerate. At the east boundary of the basin is the Concentrator Fault, trending north to northwest, with its west side down. East of the fault lie eastward-dipping sedimentary rocks of late Precambrian and Paleozoic ages that have been intricately faulted by both north- and east-trending fault systems. Many of the east-trending faults are mineralized, and one of them formed the Magma vein, the location of one of the major copper mines of Arizona. The pre-Tertiary rocks are overlain by the thick sequence of quartz latitic ash flows (dacite) that make up the towering cliffs of Apache Leap. The ash flow has been K-Ar dated at 19.6±0.6 m.y. (Creasey and Kistler, 1962; Damon and Bikerman, 1964).

To the southwest, toward the base of

Picketpost Mountain, several light-colored pits mark areas where high-grade perlite has been mined from the rhyolitic lava flows.

2.6 54.4 Town of Superior. Road forks. Keep to right on main highway. Proceeding to the east out of Superior, the road crosses the Concentrator fault, the east side of which is the uplifted block. The lower parts of the cliffs consist stratigraphically of: The Cambrian Balsa Quartzite resting with sedimentary contact on diabase, the Martin Limestone (Devonian), the Escabrosa Limestone (Mississippian), the Naco Limestone (Pennylvanian), and the Tertiary Whitetail Conglomerate. Important replacement copper mineralization occurs within the lowermost beds of the Martin and manganese mineralization occurs along faults in the Escabrosa (prominent white cliff former).

2.9 57.3 The upper parts of the cliffs east of Superior are the reddish colored quartz latite ash flows of the Apache Leap Formation. The ash flows overlie the Whitetail Conglomerate and consist of one well-developed cooling unit. For the next six miles the road goes upward through the cooling unit from the non-welded zone through a densely-welded block vitrophyre, a brown to gray densely welded, devitrified zone, and finally through light colored vapor phase zone of partial welding.

6.3 64.1 Near Pinal Ranch at the eastern fault boundary of the ash-flow sheet. For the next several miles, the highway passes through the Tertiary Schultze Granite stock. Much of the copper mining in this area is around the northern contact of the granite with Pinal Schist.

4.7 68.8 At 2 o'clock, Pinal Mountains. The higher part of the range consists of the Pinal Schist and Madera Diorite, the lower rounded hills consist of Schultze Granite. In the next few miles along the canyon of Bloody Tanks Wash, the granite shows spectacular jointing.

4.2 73.0 Enter town of Miami, Arizona. The town is built around the Miami copper mine of the Inspiration Consolidated Copper Company. Many smaller mining companies operate in the area.

6.4 79.4 Enter town of Globe, Arizona.

1.6 81.0 Intersection of Highways US 60 and 70. Keep to the right on US 70. The route now leaves the Pinal Mountains, which were a highland and drainage-divide area through much of late Cenozoic time. The Phoenix basin to the west received sediment from the mountains through most of late Cenozoic time. The route now enters the Safford basin, where nearly continuous deposition continued into early Quaternary time. The deposition was terminated by differential uplift. Because of this uplift and subsequent erosion, about 800 feet of lower Quaternary sedimentary deposits were removed from the area. Remnants of the deposits are exposed on the slopes of mesas and benches, which are predominant in Safford and Duncan basins. The cycle of erosion is continuing in this area at the present time; the gravels exposed in roadcuts here and for several miles to the east are late Pleistocene in age and were deposited in the earlier versions of the present stream channels.

0.06 81.6 At 12 o'clock, Hayes Mountains, altitude 5,300 to 5,700 feet. The lone peak to the north is capped by a basalt flow that is early Quaternary in age. The rugged peaks and slopes to the south are composed of granite of Precambrian age, and the southwestward-dipping rocks on the south skyline are Precambrian and Paleozoic quartzite overlain by Paleozoic limestone.

0.4 82.0 Drainage divide. To the northwest, the streams drain into Pinal Creek, which is tributary to the Salt River. To the southeast the drainage is into the Gila River.

1.2 83.2 On right: State Highway 77 to Tucson.

5.7 88.9 Entering hills and ridges, erosional remnants of sediment probably early Pleistocene in age. These sediments are termed informally the "upper unit of basin fill" and are the uppermost unit of Gilbert's (1875) Gila Conglomerate. Note the characteristic red-brown to brown color, fine-grain size, local calcareous beds and tuff beds, and the even near-parallel bedding. The upper unit of basin fill is well sorted; the bedding, grain size, and good sorting contrast with the lenticular bedding, coarse material, and poorly sorted gravel of middle to late Pleistocene age. Here, the mesas slope northward to Aliso Creek and are gravel-capped terraces of streams tributary to the creek.

1.0 89.9 At 9 o'clock, the low hills to the north are part of the Apache Mountains and are underlain by Precambrian and Paleozoic quartzite.

Near the southeast end are minor outcrops of grayish Paleozoic limestone.

3.5 93.4 Top of divide, approaching Safford basin.

At 10 o'clock to 11 o'clock, the Natanes Plateau is on the skyline. The volcanic rocks on the skyline are andesite to basalt flows of middle Tertiary age. The low platform in the middle foreground is capped by basalt of early Pleistocene age. The altitude of the platform is about 4,000 feet, and it formerly was buried by the upper unit of basin fill (early Pleistocene in age).

At 11 o'clock to 12 o'clock, the Gila Mountains—principally andesite flows and tuffs of middle Tertiary age.

At 3 o'clock, the upper unit of basin fill crops out beneath the flow that caps the northernmost peak of Hayes Mountains. The top of the peak (4,200 feet altitude) corresponds to the approximate top of the upper unit of basin fill in this area.

4.5 97.9 At this point, Peridot Mesa is in view from 9 o'clock to 11 o'clock. The vent tuff ring is the low rounded hill on the west side of the mesa with the lava flow extending out to the northeast. San Carlos Valley in the background consists of Tertiary lake beds and Gila-type conglomerate interbedded with numerous basalt flows.

4.0 101.9 Turn left off US 70 to Peridot, and continue north on State Route 170 towards the town of San Carlos. Just before reaching San Carlos, the road passes along the cliffs that form the terminus of the Peridot Mesa Lava flow. Note the lake beds beneath the flow.

3.8 105.7 San Carlos. From this point make a left turn on a road paralleling the mesa top.

0.5 106.2 Turn left on dirt road ascending to the mesa top. From this point on the trip will be described by your guides; the road is to be used only with proper permission.

4.3 110.5 Return to junction of US 70, but instead of returning to highway, continue south under bridge on road to San Carlos reservoir. For locations and descriptions of the following localities, refer to Appendix.

4.0 114.5 Flatiron Mesa lies directly south of the road. The flow capping the mesa is compositionally identical to the flow at Peridot Mesa.

4.0 118.5 Soda Springs. A small, black outcrop can be seen northwest of the road.

7.0 125.5 Return to junction of US 70.

27.0 152. 5 Black Hill (also called Black Point). Continue east on US 70 past the town of Bylas. Black Hill can be seen to the northeast of the highway. A small dirt road goes past the east side of the vent from the highway.

133.2 285.7 Return trip to Tempe.

STATE OF ARIZONA
BUREAU OF GEOLOGY AND MINERAL TECHNOLOGY

The Arizona Bureau of Geology and Mineral Technology was established in 1977 by an act of the State legislature. This act represents a reorganization of the Arizona Bureau of Mines which first was created in 1915 and placed under the authority of the Arizona Board of Regents. This authority has not changed. The Bureau continues its service in the fields of geology, metallurgy, and mining in response to public inquiries, state agency requirements, and various research grants. In order to carry out these functions, two basic branches now are recognized:

Geological Survey Branch

This branch is charged with the responsibility of acquiring, disseminating, and applying basic geologic data that are designed to (a) enhance our understanding of Arizona's general geologic and mineralogic history and to assist in determining the short and long range influences these have on human activity, and (b) assist in developing an understanding of the controls influencing the locations of metallic, nonmetallic and mineral fuel resources in Arizona.

Mineral Technology Branch

This branch conducts research and investigations into, and provides information about, the development of Arizona's mineral resources, including the mining, metallurgical processing, and utilization of metallic and nonmetallic mineral deposits. These activities are directed toward the efficient and safe recovery of Arizona's mineral resources as well as insuring that recovery and treatment methods will be compatible with the basic environmental needs of the state.

1-2/78AL20/3933